ΠΑΝΕΠΙΣΤΗΜΙΟ ΘΕΣΣΑΛΙΑΣ
ΠΟΛΥΤΕΧΝΙΚΗ ΣΧΟΛΗ | ΤΜΗΜΑ ΠΟΛΙΤΙΚΩΝ ΜΗΧΑΝΙΚΩΝ
ΤΟΜΕΑΣ ΓΕΩΤΕΧΝΙΚΗΣ ΚΑΙ ΓΕΩΠΕΡΙΒΑΛΛΟΝΤΙΚΗΣ ΜΗΧΑΝΙΚΗΣ

Διπλωματική Εργασία

ΕΚΤΙΜΗΣΗ ΑΠΟΚΡΙΣΗΣ ΥΠΕΡΑΚΤΙΑΣ ΑΝΕΜΟΓΕΝΝΗΤΡΙΑΣ ΜΕ ΠΛΗΡΗ ΚΑΙ ΑΠΛΟΥΣΤΕΥΜΕΝΗ ΤΡΙΔΙΑΣΤΑΤΗ ΑΝΑΛΥΣΗ

Μιχαήλ Κωμοδρόμος

Επιβλέπων Καθηγητής
Ευριπίδης Μυστακίδης, Καθηγητής Π.Θ.
Διευθυντής του Εργαστηρίου Ανάλυσης και Σχεδιασμού Κατασκευών

Βόλος,
Φεβρουάριος 2019

UNIVERSITY OF THESSALY
FACULTY OF ENGINEERING | SCHOOL OF CIVIL ENGINEERING
DEPARTMENT OF GEOTECHNICAL ENGINEERING

DIPLOMA THESIS

APPLICATION OF SIMPLIFIED AND FULL THREE DIMENSIONAL NUMERICAL METHODS TO THE ANALYSIS OF OFFSHORE WIND TURBINE

Michael E. Komodromos

Supervisor:
Euripidis Mystakidis, Professor.

Volos,
February 2019

Acknowledgements

At the fulfillment of my thesis, I would like to thank these individuals whose contribution and constant support have been of vital importance for the accomplishment of this goal.

First of all, I would like to express my gratitude to my supervisor Professor Euripidis Mystakidis. His guidance and valuable advice have been the stepping stone for me as a student and I feel sincerely grateful to have been a thesis candidate under his surveillance.

I would like to acknowledge Professor Panagiotis Dakoulas and Dr Apostolos Koukouselis for their beneficial comments on my work.

I am truly indebted to Professor Ioannis Anastasopoulos and PhD Researcher Maria Antoniou for providing me all the required data of their work in order to carry out the preprocessing of my simulation. Their cooperation has been an honor for me and an excellent chance of investigating an advanced simulation project.

I am grateful to my father, Professor Emilios Comodromos, for providing me fundamental knowledge inside or outside classes, whose example is a true motivation for me and a solid support on research (and not only) difficulties.

Finally, words are not enough to thank my family, friends and teammates who have constantly and truly supported me during this challenge and have been always present to soothe me in times of stress and anxiety. Special thanks to Sofia Faliaga, Alexis Giannoulis, Christine Fanouraki for their patience and devotion.

Εκτεταμένη Ελληνική Περίληψη

Μεταξύ των σημαντικότερων ζητημάτων που απασχολούν τα Ευρωπαϊκά κράτη είναι η εξασφάλιση της ενεργειακής τους αυτονομίας. Εξαιτίας πολιτικών και περιβαλλοντικών ζητημάτων τα οποία έχουν προκύψει τις τελευταίες δεκαετίες, ως η λύση στο πρόβλημα της ενεργειακής κρίσης προτείνεται η εκμετάλλευση ανανεώσιμων πηγών ενέργειας, η δε αιολική ενέργεια εμφανίζει σημαντικά πλεονεκτήματα και προσελκύει το ενδιαφέρον κατασκευής συναφών έργων. Η κατασκευή ανεμογεννητριών με σταθερά υψηλές απαιτήσεις σε επίπεδα ενεργειακής απόδοσης οδηγεί στη συνεχή αύξηση του μεγέθους των ανεμογεννητριών, δεδομένου ότι η απόδοση των ρευμάτων αέρα είναι κατά πολύ υψηλότερη σε μεγάλα ύψη. Είναι προφανές ότι ανεμογεννήτριες με ύψη της τάξης των 100 m και διάμετρο πτερυγίων της τάξης των 70 και πλέον μέτρων δεν μπορεί να κατασκευασθεί για ευνόητους λόγους σε αστικό περιβάλλον, ενώ συχνά το υφιστάμενο νομικό πλαίσιο δυσχεραίνει την κατασκευή τους ακόμη και σε περιοχές που θεωρούνται απομακρυσμένες. Η εναλλακτική λύση κατασκευής ανεμογεννητριών στη θάλασσα φαίνεται να κερδίζει συνεχώς έδαφος και η κατασκευή τους έχει δημιουργήσει νέα ερευνητικά πεδία και ειδικότερα έχει ανοίξει νέους ορίζοντες έρευνας στην κατασκευή υπεράκτιων έργων σε μέσου μεγέθους βάθη. Συγκεκριμένα στις ανεμογεννήτριες, ο κατασκευαστικός σχεδιασμός πρέπει να παρέχει ευστάθεια έναντι μεγάλων ροπών ανατροπής και πλευρικών φορτίσεων και αντίστοιχων μεγάλων μετακινήσεων , ενώ παράλληλα θα πρέπει να είναι συμβατός με τον οικονομικό σχεδιασμό που ορίζει ένα ορισμένο ποσοστό του συνολικού κεφαλαίου για την υλοποίησή του.

Οι απαιτήσεις ενός τέτοιου έργου είναι σίγουρα αυξημένες και απαιτούν προηγμένη δομοστατική και γεωτεχνική ανάλυση. Ο σχεδιασμός βάσης πακτωμένης στον πυθμένα, όπως ορίζεται από μοντέλα ανεμογεννητριών που εδράζονται σε βαθιά θεμελίωση ή σε βάσεις βαρύτητας, καλύπτουν τις ανάγκες στατικής λειτουργίας υπαρχόντων έργων ανεμογεννητριών σε μικρά βάθη, παρόλα αυτά δεν είναι εφικτό να εφαρμοστούν σε μεσαία ή μεγάλα βάθη άνω των 40 μέτρων επειδή ξεπερνούν τα οικονομικά κριτήρια. Επιπρόσθετα, σχεδιασμός ο οποίος έχει εφαρμοστεί σε υπάρχουσες πλωτές κατασκευές εγκατεστημένες σε τέτοια βάθη εξασφαλίζει τη ζητούμενη ευστάθεια αποκλειστικά μέσω τενόντων αγκυρωμένων στον πυθμένα, ο οποίος όμως δεν επαρκεί για έργα τέτοιας φύσης και κλίμακας. Συνδυάζοντας την τεχνολογία της βάσης στον πυθμένα και του συστήματος υποστήριξης μέσω τενόντων, έχει αναπτυχθεί το ο συνδυασμένος φορέας του Σχήματος 1. Ο πύργος της ανεμογεννήτριας εδράζεται σε επιφανειακή θεμελίωση, η οποία πρωτίστως μεταφέρει τα κατακόρυφα φορτία στο έδαφος και εξασφαλίζει επίσης σημαντική αντίσταση έναντι ολίσθησης. Επιπρόσθετα, πύργος υποστηρίζεται έναντι πλευρικών φορτίων και ροπών ανατροπής μέσω ενός συστήματος προεντεταμένων τενόντων

σταυροειδούς διάταξης, οι οποίοι είναι συνδέονται στο μέσο περίπου σώματος του πύργου και αγκυρώνονται σε βαθιά θεμελίωση (πάσσαλο μεγάλης διαμέτρου ή ομάδα πασσάλων) στον πυθμένα της θάλασσας.

Η ανάλυση αλληλεπίδρασης εδάφους και κατασκευής για την πρόβλεψη της απόκρισης της κατασκευής έναντι εξωτερικών φορτίσεων ανέμου και κυματισμού και εν γένει των μηχανισμών που συνεισφέρουν στην δυσκαμψία της μπορεί να πραγματοποιηθεί με τις παρακάτω μεθόδους:

- απλοποιημένη τριδιάστατη αριθμητική μέθοδο,
- πλήρη τριδιάστατη αριθμητική μέθοδο.

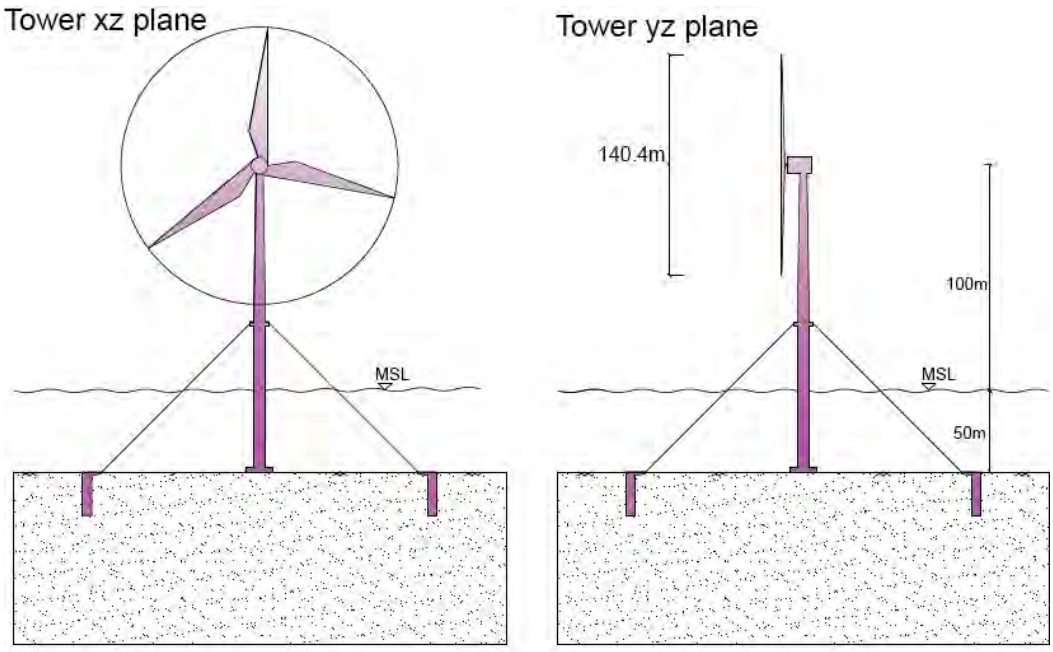

Σχήμα 1: Σχηματική παρουσίαση διάταξης ανεμογεννήτριας μεγάλου ύψους σε μέσο βάθος θάλασσας με χρήση τενόντων προέντασης και αγκύρωση σε βαθιά θεμελίωση.

Η απλοποιημένη τριδιάστατη αριθμητική μέθοδος αποτελεί μία τεχνική προσομοίωσης η οποία υποκαθιστά το περιβάλλον έδαφος με ελατήρια τα οποία είναι υπακούν σε μη γραμμικό καταστατικό νόμο τάσης τροπής και μπορούν να αποδώσουν με ικανοποιητική ακρίβεια τη μη γραμμική φύση του εδάφους. Η ανάλυση αυτού του τύπου εστιάζει κυρίως στην απόκριση των δομικών στοιχείων σε αλληλεπίδραση με το έδαφος, δίνοντας όμως περιορισμένη πληροφορία σχετικά με τη επιρροή της κατασκευής στο έδαφος. Η προσέγγιση αυτή πραγματοποιείται στο πλαίσιο απλουστεύσεων, οι οποίες σε ορισμένες περιπτώσεις δεν αντανακλούν πλήρως του μηχανισμούς που αναπτύσσονται στην πραγματικότητα. Παράλληλα απαιτεί υψηλές γνώσεις και εμπειρία σε θέματα προσομοίωσης στο πλαίσιο της μηχανικής συμπεριφοράς, ενώ είναι προσαρμοσμένη στις ανάγκες του σχεδιασμού των κατασκευών ο οποίος απαιτεί αναλύσεις αξιόπιστες σε

θέματα ασφάλειας και παράλληλα συμβατές με οικονομοτεχνικό σχεδιασμό και αυστηρό χρονοδιάγραμμα.

Σε θέματα προ επεξεργασίας και ορισμού του μοντέλου προσομοίωσης, η δήλωση των παραμέτρων του εδάφους καθίσταται εύκολη καθώς, πέρα από τις ελαστικές παραμέτρους για τις οποίες υπάρχει διαθέσιμη εκτενής βιβλιογραφία, ενώ όταν η μετελαστική συμπεριφορά περιορίζεται στην περίπτωση της ελαστικής-τέλεια πλαστικής συμπεριφοράς η προσομοίωση είναι ακόμη και εύκολα υλοποιήσιμη. Με την παραδοχή αυτού του απλοποιημένου καταστατικού μοντέλου είναι εφικτή η πραγματοποίηση αναλύσεων χωρίς την προϋπόθεση αποτελεσμάτων δύσκολων εργαστηριακών δοκιμών(τριαξονικών κτλπ). Περνώντας στη διαδικασία υπολογισμού, οι συνθήκες είναι επίσης ευνοϊκές. Η επίλυση του φορέα διαρκεί χρονικό διάστημα της τάξεως των λεπτών, ενώ τα παραγόμενα αρχεία αποτελεσμάτων δεσμεύουν μνήμη της τάξεως των Megabyte. Παρά την ραγδαία αύξηση της υπολογιστικής ισχύος και της διαθέσιμης μνήμης τα τελευταία χρόνια, τα μεγέθη παραμένουν πεπερασμένα και απαιτείται συνετή χρήση τους. Ακόμα η ταχεία επίλυση επιτρέπει τη διεξαγωγή παραμετρικού σχεδιασμού, ο οποίος εκ των πραγμάτων απαιτεί την πραγματοποίηση μεγάλου πλήθους επιλύσεων εντός ορισμένου χρονικού διαστήματος και είναι απαραίτητος για την εύρεση οικονομοτεχνικά βέλτιστων λύσεων. Απέναντι στο αδύναμο σημείο της μεθόδου αυτής, το οποίο είναι η παράβλεψη κάποιων μηχανισμών αλληλεπίδρασης, έρχεται η εφαρμογή των συντελεστών ασφάλειας να καλύψει την επικείμενη διαφοροποίηση, φέρνοντας μία πιο συντηρητική αλλά ταυτόχρονα μία πιο ασφαλή εκτίμηση του εξεταζόμενου αντικειμένου.

Η προσέγγιση με πλήρη τριδιάστατη ανάλυση αποτελεί την εναλλακτική ή και συμπληρωματική σε αρκετές περιπτώσεις λύση, η οποία πλέον στοχεύει στην κατά το δυνατό πιο πιστή αποτύπωση της απόκρισης του εξεταζόμενου φορέα. Το έδαφος προσομοιώνεται από τριδιάστατα στοιχεία εφοδιασμένα με καταστατικό νόμο ο οποίος ορίζει επικείμενη διαρροή βάση της τριδιάστατης εντατικής κατάστασης των στοιχείων και με νόμο πλαστικής ροής που ορίζει τη μετάβαση από την ελαστική περιοχή στην πλαστικότητα. Αυτό το πεπερασμένο πλήθος στοιχείων συγκροτεί ένα πλέγμα το οποίο αποδίδει με ακρίβεια το μέγεθος αλλά και την χωρική κατανομή των τάσεων, των τροπών και των μετακινήσεων του εδαφικού σκελετού, αλλά παράλληλα είναι σε θέση να αποτυπώσει και την έκταση που παίρνουν φαινόμενα πλαστικοποίησης. Η αλληλεπίδρασή του με τα δομικά στοιχεία λαμβάνει χώρα μέσω στοιχείων διεπιφάνειας τα οποία ενσωματώνονται στα σύνορα μεταξύ των σωμάτων, τα οποία στοιχεία έχουν την δυνατότητα να αποτυπώσουν με ακρίβεια μη γραμμικά φαινόμενα διεπιφανειών, όπως αποκόλληση ή διαφορική μετακίνηση-ολίσθηση. Λόγω της υπεροχής της πιστότητας των αποτελεσμάτων, αναλύσεις αυτού του τύπου στοχεύουν στην ανάλυση σε καθεστώς λειτουργίας (SLS) και όχι σε καθεστώς σχεδιασμού σε κατάσταση οριακής αντοχής (ULS). Ας

σημειωθεί ακόμη ότι η εφαρμογή συντελεστών σε προβλήματα μη γραμμικής συμπεριφοράς αποδίδουν λανθασμένη εικόνα, της απόκρισης και για το λόγο αυτό δεν επιτρέπεται η εφαρμογή τους. Αν και η παραπάνω μέθοδος οδηγεί σε πιο πιστά και πιο διευρυμένα αποτελέσματα σχετικά με την κατασκευή αλλά και το περιβάλλον έδαφος στο οποίο εδράζεται, συνοδεύεται από πολλά μειονεκτήματα τα οποία καθιστούν την χρήση της δύσκολη. Αφενός, προκειμένου να αποτυπωθεί η πλήρης δυναμική της μεθόδου, πρέπει να δοθούν ακριβείς παράμετροι, των οποίων η αποτίμηση απαιτεί χρονοβόρες και ακριβές εργαστηριακές δοκιμές. Αφετέρου, η διαδικασία επίλυσης διαρκεί μέρες, ίσως και βδομάδες, με μεγάλες απαιτήσεις σε υπολογιστική ισχύ και μνήμη αποθήκευσης, συνθήκες οι οποίες δεν επιτρέπουν ευρεία παραμετρική ανάλυση και εκτοξεύουν τη ζημιά ενός επικείμενου σφάλματος στη δήλωση των παραμέτρων. Τέλος, η διαδικασία συλλογής και ταξινόμησης των αποτελεσμάτων αποτελεί από μόνη της μια απαιτητική διαδικασία, καθώς τα παραγόμενα αποτελέσματα είναι τόσα πολλά λόγω του μεγάλου πλήθους των στοιχείων, ώστε να απαιτεί την σύνταξη ρουτινών ανάλυσης και συλλογής δεδομένων.

Έπειτα από τη διεξαγωγή και των δύο μεθόδων ανάλυσης στο παρόν έργο ανεμογεννήτριας, προκύπτει από τη σύγκριση των αποτελεσμάτων ενθαρρυντική εικόνα για την αξιοπιστία της απλοποιημένης τριδιάστατης ανάλυσης, πέρα από την εξασφάλιση της στατικής επάρκειας της κατασκευής. Εστιάζοντας στη συνεισφορά του συστήματος τενόντων στην πλευρική δυσκαμψία του συστήματος, σε πρώτο επίπεδο εξετάζεται η απόκριση των πασσάλων έναντι εξόλκευσης για το δυσμενέστερο σενάριο φόρτισης. Αν και οι μηχανισμοί οι οποίοι αναπτύσσονται για την αντίσταση έναντι εξόλκευσης είναι σύνθετοι και απαιτούν διευρυμένη ανάλυση, όπως και η κινηματική κατάσταση του σώματος του πασσάλου, ζητούμενη συνεισφορά του πασσάλου στο σύστημα μπορεί να αποτιμηθεί επαρκώς από την μετατόπιση στην κεφαλή του. Αποδεικνύεται ότι η απόκλιση στην εκτίμησή της από της δύο μεθόδους είναι της τάξεως των 3.17 χιλιοστών (Σχήμα 2), μέγεθος το οποίο επηρεάζει ελάχιστα τη δυσκαμψία των τενόντων, όπως επιβεβαιώνεται και από το ποσοστό απόκλισης 0.05% στην εκτίμηση των αξονικών τους δυνάμεων, γεγονός αντιπροσωπευτικό της εγκυρότητας της αντικατάστασης του περιβάλλοντος εδάφους από ελατήρια εφοδιασμένα με καμπύλες απόκρισης ‘t-z’ και ‘p-y’. Στη συνέχεια, εξετάζοντας την πλευρική μετατόπιση του πύργου στο επίπεδο όπου είναι προσαρτημένοι οι τένοντες, η απλοποιημένη μέθοδος εκτιμά μέγιστη μετατόπιση 45 χιλιοστών, ενώ η πλήρης δίνει το δυσχερέστερο σενάριο τω 250 χιλιοστών. Αν και η διαφορά είναι μεγάλη, η απόλυτη εκτιμώμενη μετατόπιση σε αυτό το επίπεδο σε σχέση με αυτήν που δίνεται στην κορυφή του πύργου είναι μία τάξη μεγέθους χαμηλότερη, επομένως η στατική λειτουργία των τενόντων ως περιορισμός της πλευρικής μετατόπισης στο σημείο πρόσδεσής τους παραμένει έγκυρη (Σχήμα 3). Στην κορυφή του πύργου, όπου εδράζεται η ανεμογεννήτρια, οι μέγιστες μετατοπίσεις εκτιμώνται 1534 και 1340 χιλιοστά από την απλοποιημένη και την πλήρη τριδιάστατη

ανάλυση αντίστοιχα με σχετική ποσοστιαία διαφορά 12%. Αν και η μεμονωμένη εικόνα της κορυφής φαντάζει ανεπίτρεπτη λόγω της μεγάλης απόλυτης τιμής της μετακίνησης, στην πραγματικότητα είναι εντός των ορίων στατικής λειτουργίας, καθώς αντιστοιχεί σε κλίση 0.01 ακτινίων, μέγεθος που δεν επιτρέπει την ανάπτυξη επικίνδυνων φαινομένων όπως καμπτικές ροπές δεύτερης τάξης.

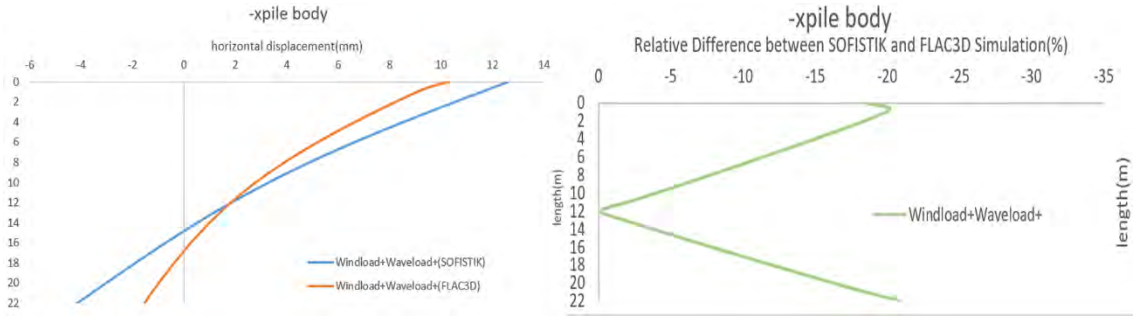

Σχήμα 2: Σύγκριση εκτιμήσεων μέγιστης οριζόντιας μετατόπισης πασσάλου από τις μεθόδους επίλυσης.

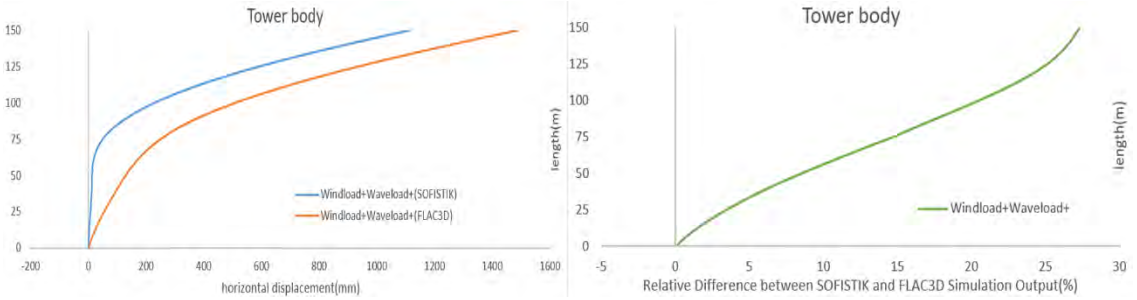

Σχήμα 3: Σύγκριση εκτιμήσεων μέγιστης οριζόντιας μετατόπισης πύργου έδρασης από τις μεθόδους επίλυσης.

Από την άλλη πλευρά, σε θέματα κατακόρυφης μετατόπισης, η απόκριση του πύργου διαφέρει σημαντικά από την μία μέθοδο στην άλλη. Αν και η απλοποιημένη μέθοδος είναι σε θέση να αποτιμήσει σωστά την περιστροφή της πλάκας θεμελίωσης και τις επιπλέον μετατοπίσεις λόγω αυτής, οι εκτιμήσεις της ισοδύναμης κατακόρυφης μετατόπισης στο σημείο σύνδεσης της πλάκας με τον πύργο παρουσιάζουν απόκλιση της τάξης των 2 εκατοστών (Σχήμα 4). Η απόκλιση αυτή οφείλεται στο γεγονός ότι κατά τη συμπίεση του εδάφους από την πλάκα, ανάγκη αποσυμπίεσης οδηγεί το έδαφος σε πλευρική μετατόπιση (φαινόμενο Poisson) και ανύψωση του εδάφους στην περιοχή κοντά στην πλάκα, με αποτέλεσμα να παρουσιάζεται αυξημένη καθίζηση (Σχήμα 5). Αυτά τα φαινόμενα αναδιάταξης της εδαφικής δομής είναι σύνθετα ζητήματα τριδιάστατης ανάλυσης και δεν μπορούν να αποτιμηθούν από ένα απλό ελαστικό τέλεια πλαστικό νόμο απόκρισης ελατηρίου. Από την εφαρμογή αυτήν πηγάζει η ανάγκη περαιτέρω έρευνας καμπυλών απόκρισης οι οποίες λαμβάνουν υπόψη φαινόμενα Poisson, αλλά και η σημασία της πλήρους τριδιάστατης ανάλυσης η οποία έχει τον ρόλο της επιβεβαίωσης ή της απόρριψης αποτελεσμάτων τα οποία δίνει η αντίστοιχη απλοποιημένη. Εξετάζοντας το γεγονός της

απόκλισης στο συγκεκριμένο ζήτημα με τεχνικό σκεπτικό, αυτή η επιπλέον μετατόπιση δεν επηρεάζει σημαντικά την κατασκευή καθώς δεν προκαλεί αποτόνωση της προέντασης των τενόντων, ενώ παράλληλα δεν παραβιάζει κάποιο κριτήριο λειτουργικότητας.

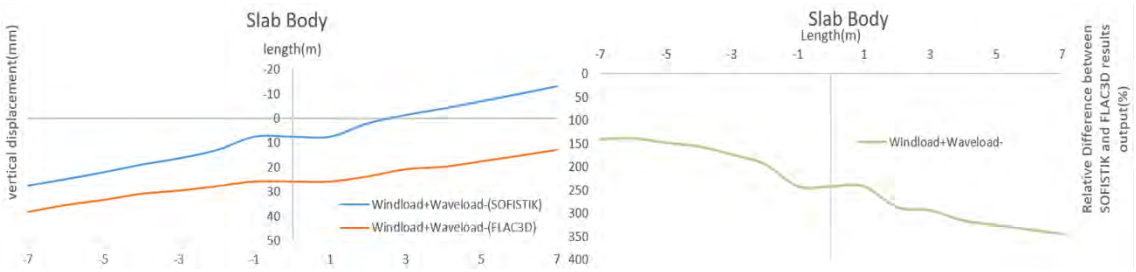

Σχήμα 4: Σύγκριση εκτιμήσεων μέγιστης κατακόρυφης μετατόπισης πλάκας θεμελίωσης από τις μεθόδους επίλυσης

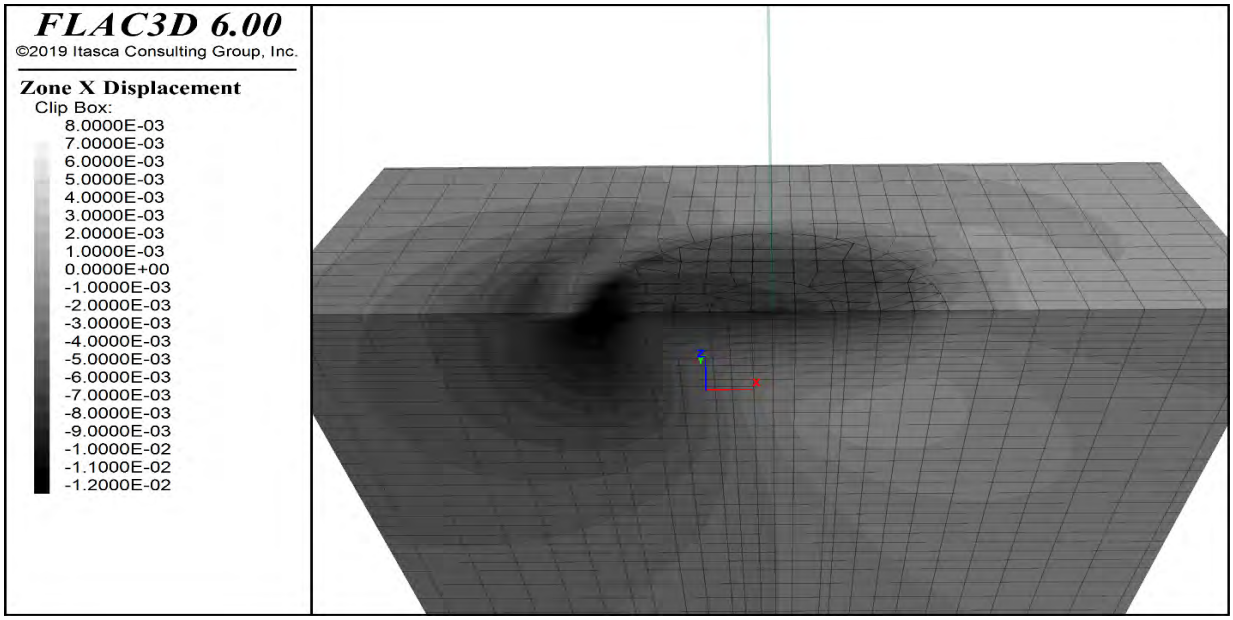

Σχήμα 5: Πλευρική μετατόπιση εδάφους υπό το κατακόρυφο φορτίο της πλάκας θεμελίωσης

Συμπληρωματικά με την παραπάνω σύγκριση, η οποία επικυρώνει τα αποτελέσματα της απλοποιημένης τριδιάστατης ανάλυσης, πραγματοποιείται μία δεύτερη διαδικασία ανάλυσης, η οποία εξετάζει αποκλειστικά την επιρροή της εξής παρέμβασης στη γεωμετρία των πασσάλων. Η παρέμβαση είναι η προσθήκη μίας δοκού προβόλου η οποία παρεμβάλλεται μεταξύ της κεφαλής του πασσάλου και της θέσης πρόσδεσης του τένοντα. Αυτή η απόσταση εκμεταλλεύεται την κατακόρυφη συνιστώσα της δύναμης του καλωδίου και προκαλεί μια ευεργετική ροπή η οποία δρα ενάντια στην δράση που τείνει τα περιστρέψει τον πάσσαλο παράλληλα με την εξόλκευσή του. Σύμφωνα με τις συγκρίσεις μεταξύ των δύο εκδοχών της γεωμετρίας, ταύτισης της κεφαλής του πασσάλου με το σημείο πρόσδεσης του καλωδίου(WC) ή διαχωρισμού των δύο με την προσθήκη προβόλου(NC),

παρατηρείται πως η παραπάνω παρέμβαση έχει σημαντική συνεισφορά στον περιορισμό των μετακινήσεων του εξεταζόμενου δομικού στοιχείου, ιδιαίτερα στο επίπεδο της κεφαλής του. Συγκεκριμένα η ευεργετική δράση της ροπής περιορίζει κατά 50% και 21% την πλευρική μετατόπιση της κορυφής και της άκρης του πασσάλου αντίστοιχα, μεταβάλλοντας την κινηματική από πασσάλου ελεύθερης κεφαλής σε πακτωμένης κεφαλής(Σχήμα 6). Ο περιορισμός της περιστροφής του πασσάλου και της ισοδύναμης πλευρικής μετατόπισης δεν προκαλεί εξίσου σημαντικές μεταβολές στη συνεισφορά του συστήματος των τενόντων στη συνολική δυσκαμψία του φορέα. Το ευεργέτημα εντοπίζεται στις συνθήκες αλληλεπίδρασης με το έδαφος. Κατά την κατάσταση NC η ζώνη πλαστικοποίησης εκτείνεται σε βάθος 9 μέτρων, ενώ η κατάσταση WC την περιορίζει στα 5 μέτρα(Σχήμα 7). Η σημασία του περιορισμού αυτού έγκειται στο γεγονός ότι εκτεταμένη πλαστικοποίηση οδηγεί σε ευαίσθητες καταστάσεις, στις οποίες μικρές μεταβολές των φορτίσεων μπορούν να οδηγήσουν σε δυσανάλογα μεγάλες αυξήσεις των μετακινήσεων, οι οποίες στην προκειμένη περίπτωση απειλούν με χαλάρωση των τενόντων και επικείμενη απώλεια της δύναμης προέντασης. Επιπλέον μία τέτοια κατάσταση είναι μη αναστρέψιμη, με αποτέλεσμα ο φορέας να χάσει την ικανότητα μελλοντικής απόκρισης όπως αυτή έχει σχεδιαστεί. Αποτυπώνεται λοιπόν ξεκάθαρα πως η προσθήκη ενός τέτοιου προβόλου είναι απαραίτητη για την αποφυγή μίας ενδεχόμενης κατάστασης ευαίσθητης σε μεταβολές φορτίου.

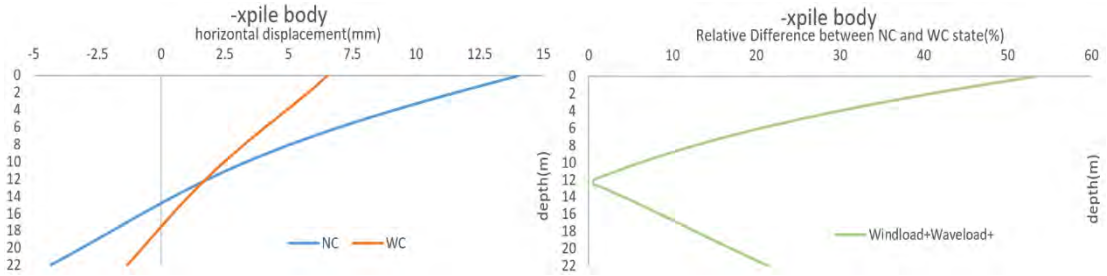

Σχήμα 6: Σύγκριση αποτελεσμάτων πλευρικής μετατόπισης μεταξύ συνθηκών ελεύθερης και πακτωμένης κεφαλής

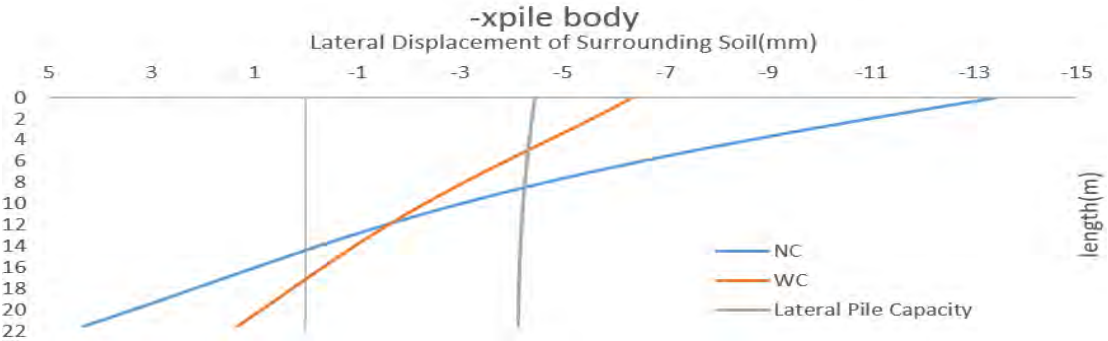

Σχήμα 7: Σύγκριση εκτίμησης ζώνης πλαστικοποίησης κατά μήκος του πασσάλου

CONTENT

FIGURE INDEX

1. INTRODUCTION

1.1. Wind Turbine as a trend in structures

According to major economic analysis conducted by Energy Information Agency, the macroeconomic growth which takes place in heavily populated regions of the world implies directly an augmentation of energy consumption, Fig. 1.1. Furthermore, the production and provision of goods and services demand energy, whose production is relied on combustion of fossil fuel (gas, coal and oil) at major percentage of 80%. The oil and gas reserves are in the hands of a small group of nations, several of which are considered political unstable or have testy relationships with large consuming countries, and therefore the international energy market operates under an oligopoly status. On top of that, the last decades there has been given scientific evidence that emissions of carbon dioxide into the Earth's atmosphere – primarily as a result of burning fossil – are proved to be the cause of rising global temperatures, suggesting for urgent action by all nations to prevent ecological degradation on a massive scale. Facing these two challenges that rule the subsistence and the development of nations, energy security prompt policymakers seek exemption from imported energy through renewable, carbon-free sources of energy.

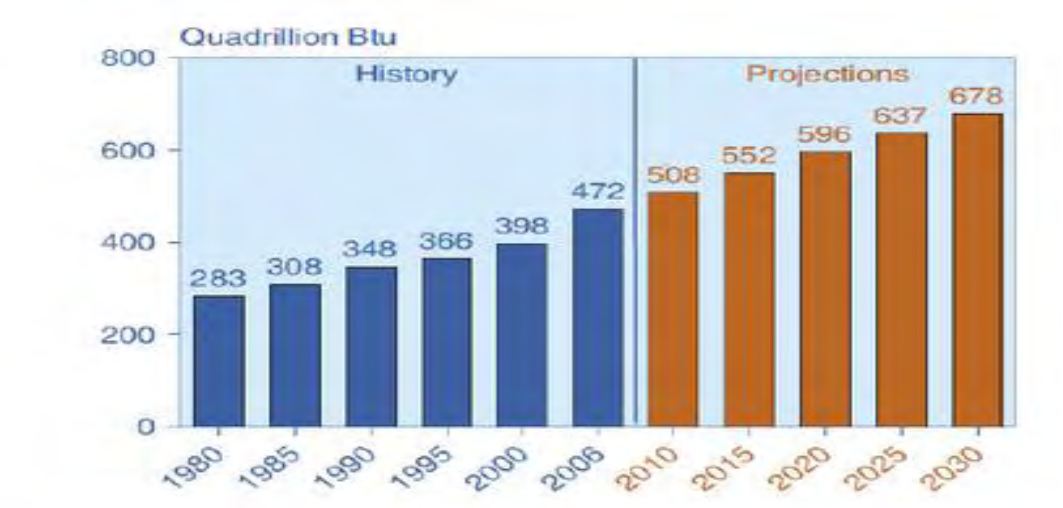

Figure 1.1 Illustration of Predictions of Future Energy Consumption (EIA 2008).

Among the most applied types of renewable energy, i.e. wind, solar and hydro produced electricity, wind has an outstanding rising as demonstrated in Fig. 1.2**.** According to the wind market, the cumulative installed capacity increases with a constant pace of 24% per year (%/yr) from the period starting in 2000 and closing in 2012. Specifically, by the end of 2012, the total installed capacity was estimated at 282 GW, an amount of energy which corresponds to the 2.6% of the global energy consumption. More recent results have shown

that in 2016 cumulative grid-connected wind capacity reached 466 GW (451 GW onshore wind and 15 GW offshore wind) and wind power accounted for almost 4% of global electricity generation, following by predictions of growth by 295 GW in the next four years and reach almost 750 GW by 2022.

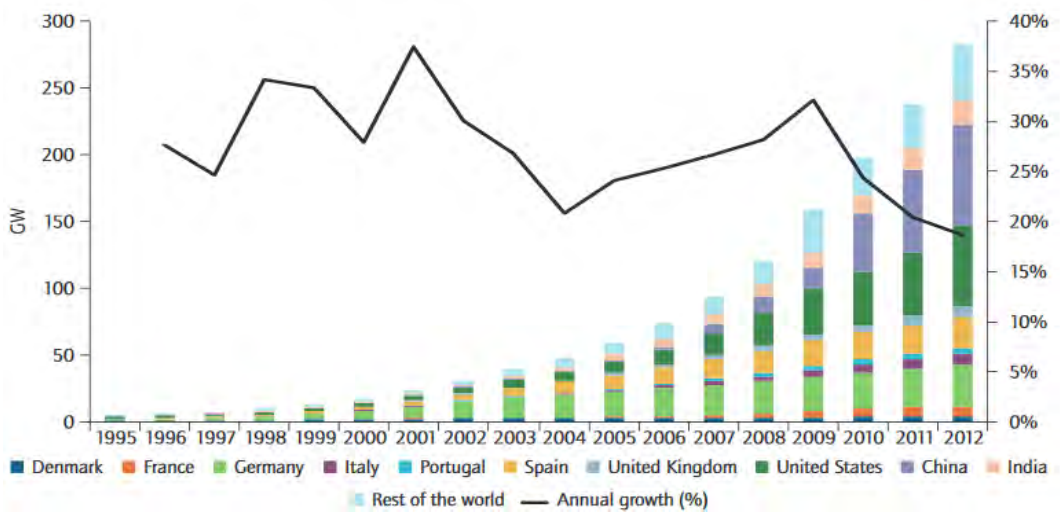

Figure 1.2 Global Cumulative Growth of wind power capacity(IEA International Energy Agency 2013).

So far, the majority of the wind turbines that create the statistics are installed onshore, yet recent engineering has suggested that the installation should be transposed offshore. Scientifically proven that the wind at sea is less turbulent, the offshore installation can be credited for longer lifetime of the turbine and higher performance, therefore less maintenance costs and higher energy production. In terms of settlement capacity, the sea is once more a convenient location, as there are no property limitations to the sea surface, less legislations enacted which adjust the construction and the operation of the wind turbine and less objections by the residents considering any possible imminent aesthetic or acoustic disturbance, facts that have delayed or even canceled the implementation of such onshore projects in the past.

As the demands of development increase, the scale in terms of size and serviceability enlarges, so do the challenge in structural and geotechnical design. Of primary concern to engineers is the evolution and improvement of the foundation and support structures applied on offshore wind turbines. The design must cope with critical overturning moments and lateral loading caused by the wave and wind multi-cycled loading under conditions of minimum vertical constant load. Various types of foundations have been developed to resist

the environmental loading by having the depth of the seabed at the installation point as basic parameter of their design.

1.2. Types of existing Offshore Wind Turbines

At shallow waters, at a maximum range of 30-40 meters, the dominant principle of the design is the fixity of the structure at the bottom of the sea. The most popular type of shallow foundation is the monopile (76% of existing shallow foundations), which is essentially an extended turbine tower driven into the seabed, followed by gravity based foundations (12% of existing shallow foundations), which exploit the sizeable submerged mass of the base to grant the required stability, rather than the resistance given by the soil through the penetration. Moving to transient depths of 40 to 50 meters' depth, the design proposes tripods and jacket structures, technology which is borrowed from the offshore oil drilling platforms although not applied to wind turbines vastly (Fig. 1.3).

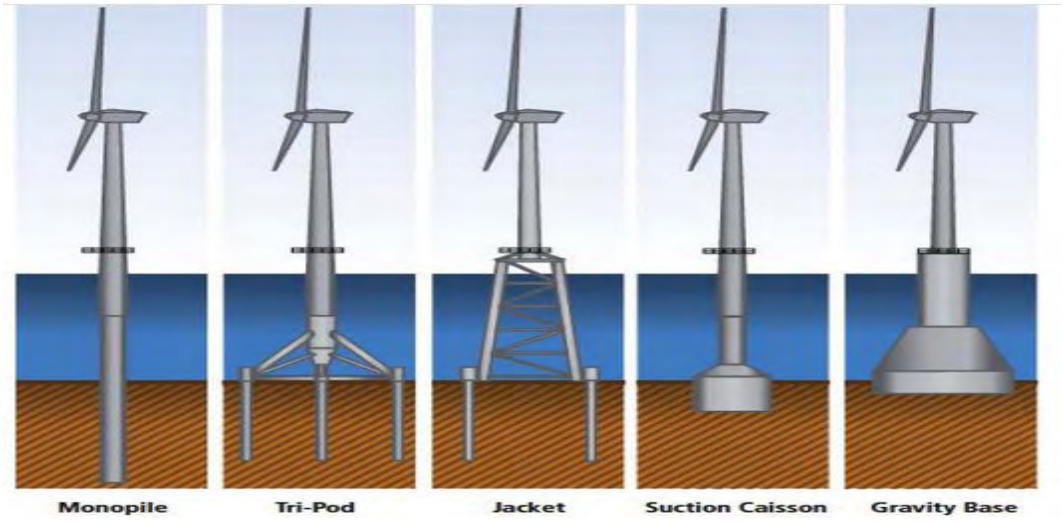

Figure 1.3 Schematic presentation of typically applied foundation of Wind Turbines(Wiser et al., 2011).

In order to surpass the limitations of the depth and the great cost of fulfilling such massive structures, which are coupled with fixed based wind turbines, new technology concepts indicate the floating wind turbines. Even if this type of foundation opens an array of additional design considerations, it provides access to the significantly greater resource area of the ocean and offer the opportunity to develop more uniform offshore installation techniques, as they would minimize variable seabed and water-depth considerations, resulting to vaster and more economic application. Moreover, the location which is distant from coast allows the relaxation of the criteria associated with sound and visual concerns and leads to turbines of higher performance.

The concept of floating wind turbines is realized by three major models, all based on cables anchored in the seabed, where variations are applied to the set-up and the attachment to the body of the wind turbine tower(Fig. 1.4). The ballast stabilized spar-buoy employs a buoyant structure stabilized by a large ballast placed on the lower portion of the structure; the floating structure is fixed to the seabed with mooring lines but relies on the ballast to remain upright and withstand wave and wind loading. In contrast, tension leg platforms consist of a buoyant structure located below the surface of the water that is fixed to the seabed and stabilized by taut or "tensioned" mooring lines. The buoyancy stabilized "barge" uses a large buoyant structure for both stability and floatation; the size of the buoyant structure is expected to provide the required stability.

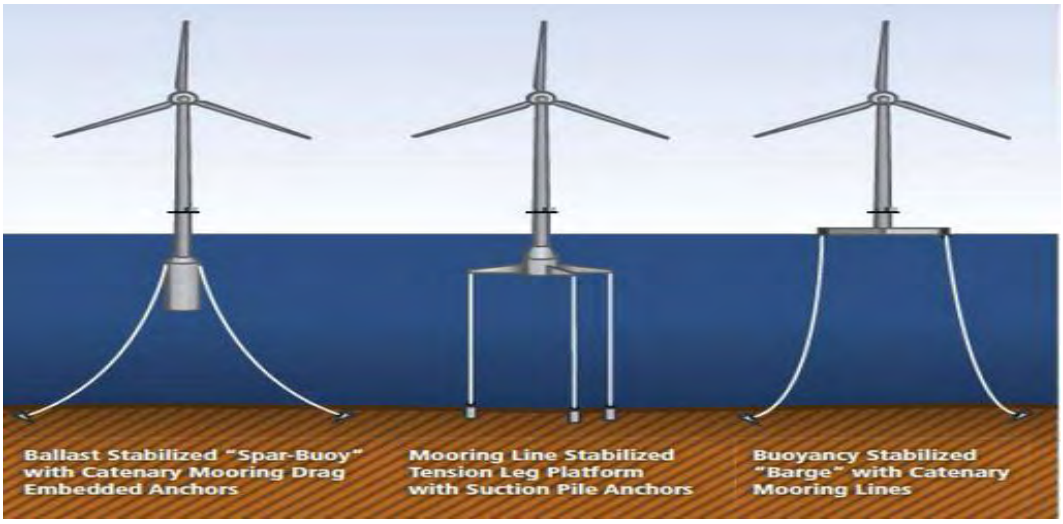

Figure 1.4 Floating Offshore wind turbine concepts(Wiser et al., 2011).

Following the pace of contemporary economical demands of construction, which indicates further exploitation of materials' post-elastic capacity and need of exact prevision of structure's behavior, alongside with the new scale of the structures in terms of loading and size which exceeds the ones implemented in the past, structural and geotechnical analysis are called to combine complex mechanisms into simulation. Within this framework and taking into account the constant demands in improving safety and economy in the design of offshore WT an alternative shape has been recently adopted mainly for WT of ultra-performance. Pretension cables are introduced at the level of WT mid-span to control the deflection of the tower. Further to the beneficial effect arising from the reduction of the lateral displacement and the stability against tilting this approach is, in general leading to lower bending moment development across the WT tower. Therefore the demands in cross section capacity could be essentially reduced. However, further to the pretension cables this

new layout is accompanied with large diameter piles serving as points of 'fixity' where the cables are anchored. Obviously the cable force is transferred to the soil through the soil resistance on the pile against lateral and vertical movement. It is evident that the disposition creates a strong soil-structure interaction involving

- the superstructure and the loads associated with
- the cables that further to the initial pretension they have to be in position to carry and transfer the variation of loads that the various environmental actions provoke
- the reaction piles and the mechanisms that are developing at their interface with the surrounding soil
- the shallow foundation and the mechanism of separation with the soil underneath in the case of tilting, or the soil yielding at the most compressive zones

The analysis of such a structure was the subject of a research work (Antoniou, 2014). With the aim of a profound investigation of the aforementioned mechanisms a full three-dimensional analysis was carried out using the F.E. code Abaqus (). It is well known that the efficiency of such analyses is associated with the 'inconvenient' of extreme computations demands. Therefore, a applicability of a rather simplified 3D analysis, the level credibility together with the associated methodology for the method to be efficient was the main issue that prompt the present research work. To achieve this goal a series of simplified 3D analyses was carried out consisting the first part of the numerical analyses carried out in this work.

Further to the above analysis it was considered that the results of a full 3D analysis are required for the sake of credibility that could be arise for the comparison of the results of the two methodologies. Therefore, a full 3D analysis using FLAC^{3D} was carried out consisting the second main part of the numerical analysis.

The third part was focused on the behavior of the reaction piles and the mode of soil-pile interaction that may be produced as a result of shifting the location of the applied load. The behavior from free-head to a rather fixed-head pile, may lead to an important reduce of both the displacement and the bending moment distribution on the piles. This third topic was investigated using the F.E. code Marc Mentat.

Prior to the presentation of the above topics a chapter providing a short theoretical review and brief description of the structure is given in the next chapter.

2. THEORETICAL BACKGROUND OF INTERACTION BETWEEN SOIL AND STRUCTURE

2.1. Shallow Foundation

A foundation is called shallow, Fig. 2.1, if its bearing capacity relies exclusively on the soil underneath it, without any additional resistance provided by its shaft surface, which is a dominant characteristic of deep foundations. The ultimate superstructure load transferred to the soil underneath, without the formation of excessive displacements, depends on several parameters which don't relate solely to the granulometry of the soil (clay or sand) but also to

- the capacity of water drainage (development of total or effective stress condition),
- the geometric shape of the foundation,
- the shaft loading of the foundation and
- the combination of the loads (horizontal, vertical forces and overturning moment).

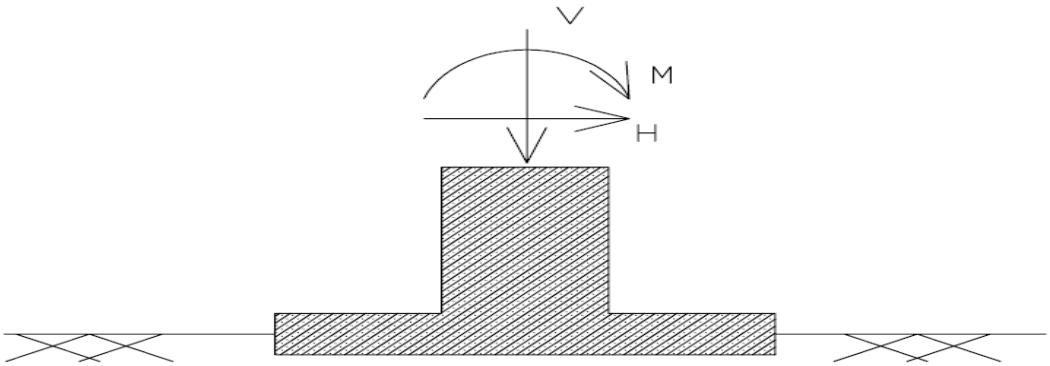

Figure 2.1 Schematic illustration of a shallow foundation under combined loading.

In the case studied, the soil is saturated and there's no capacity of water drainage, therefore phenomena of overpressure of soil water may probably occur leading to limitation of soil's resistance to its cohesion, excluding any contribution by internal friction. According to Eurocode 7, the characteristic ultimate resistance of a shallow foundation is given by the equation

$$R_{\mathrm{k}} = A'[(\pi + 2)\, c_{\mathrm{u}}\, b_{\mathrm{c}}\, s_{\mathrm{c}}\, i_{\mathrm{c}} + q] \quad (1)$$

where

R_{k} : the characteristic ultimate resistance,
A' : the active foundation surface,
c_{u} : the undrained shear strength of the soil,
b_{c} : the factor of influence determined by surface leaning,
s_{c} : the factor of influence considered by the shape of the foundation,
i_{c} : the factor of influence considered by the angle of the imposed loading,
q : the vertical loading at the surface of the surrounding soil.

Under a loading remaining below the bearing capacity of the soil, the stress is distributed to the soil having the form of bulbs under the foundation, which extend to wider area as the depth increases and gradually diminish in terms of magnitude(Fig. 2.2). Along with the stress development, soil deformation occurs, limited to the region under the shallow foundation forming a blear wedge.

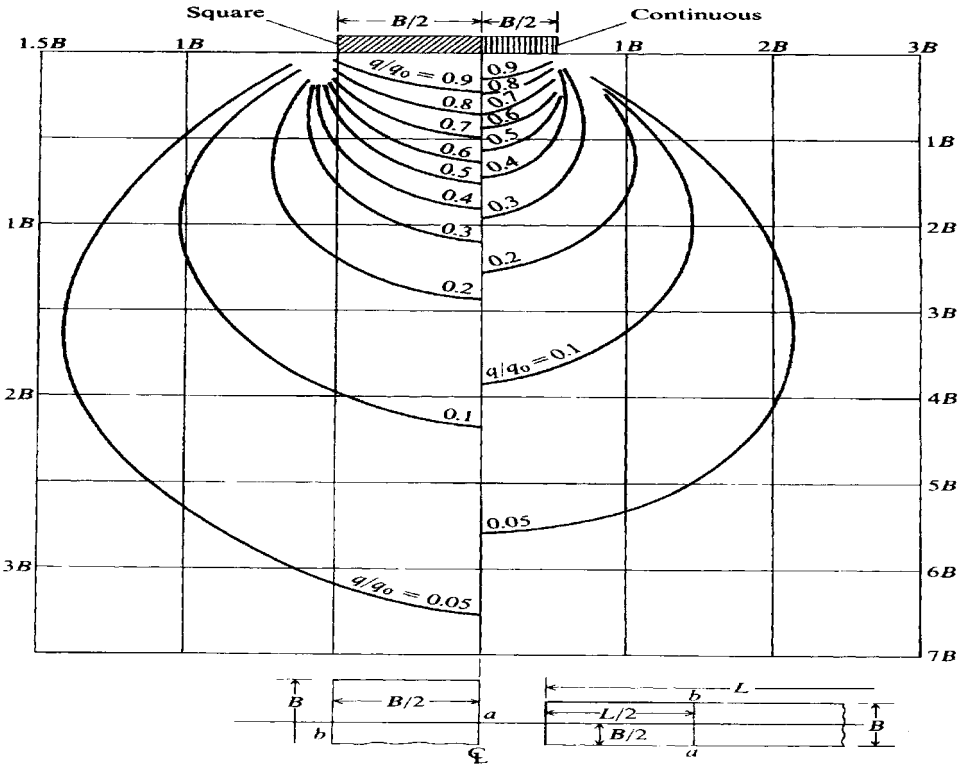

Figure 2.2 Development of soil stress under shallow foundation according to Boussinesq distribution(Bowles, 1996).

Failure Types of shallow foundations

At the time when the loading is about to exceed the bearing capacity of the soil a complete shear surface is formed apparently close to the soil surface, which provoke the elevation of the adjacent soil (Fig. 2.3). This type of shear surface is called general shear failure by Terzaghi (1943) and is characterized by a ductile behavior, without showing any sudden failure, but stiff at the same time, as the ultimate resistance is activated at settlement of of the order of 10% of the foundation's width. The aforementioned shape of failure is not valid in the case of very loose sandy soils or very soft sensitive clays, where a punching mechanism is developed.

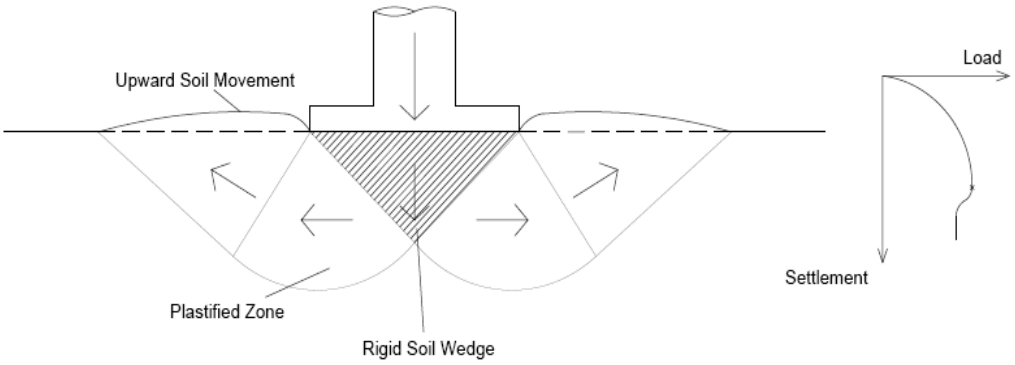

Figure 2.3 Failure surface of a shallow strip foundation at limit equilibrium.

2.2. Piles under axial loading

In structural analysis a pile is considered as beam element, given that its length is at least 10 times its width. Therefore every loading a pile is subjected to, is analyzed to vector components, parallel and perpendicular to the pile. The parallel component of the load is called axial and the perpendicular component is called lateral. While the pile utilizes the same resisting mechanism against lateral loading no matter its direction, the mechanism against axial loading differs a lot due to its direction. This fact drives to the necessity of characterizing the axial load as tensile if it tends to pull the pile out of the soil and as compressive if it tends to drive the pile deeper in the soil.

By isolating the phenomenon of an axially loaded pile in a compressive manner, there are three resisting mechanisms which stand out:

- Axial deformation of the pile
- Soil skin friction along the shaft surface of the pile
- Soil end- resistance at the tip of the pile

Out of the mechanisms above, it is essential to point out that the axial deformation and the skin friction are coupled, fact which is explained by the analytical approach of the problem.

Analytical Expression of the Compressive Axial Response

Shaft Resistance

Along the shaft surface of the pile, the resistance is calculated as the integral of the unit skin friction at the soil-pile interface. The differential equation which expresses the load transfer from pile head to the soil through the shaft surface is derived from the force equilibrium of the free body diagram of an infinitesimal length at global z-axis direction (Fig. 2.6).

$$Q_z = Q_z + dQ_z + \tau\, dz\, L_c \tag{2}$$

$$-\frac{dQ_z}{dz} = \tau\, L_c \tag{3}$$

where

Q_z : the axial force at the bottom of the pile,
τ : the soil skin resistance,
L_c : the pile circumference z,
dz : the pile segment.

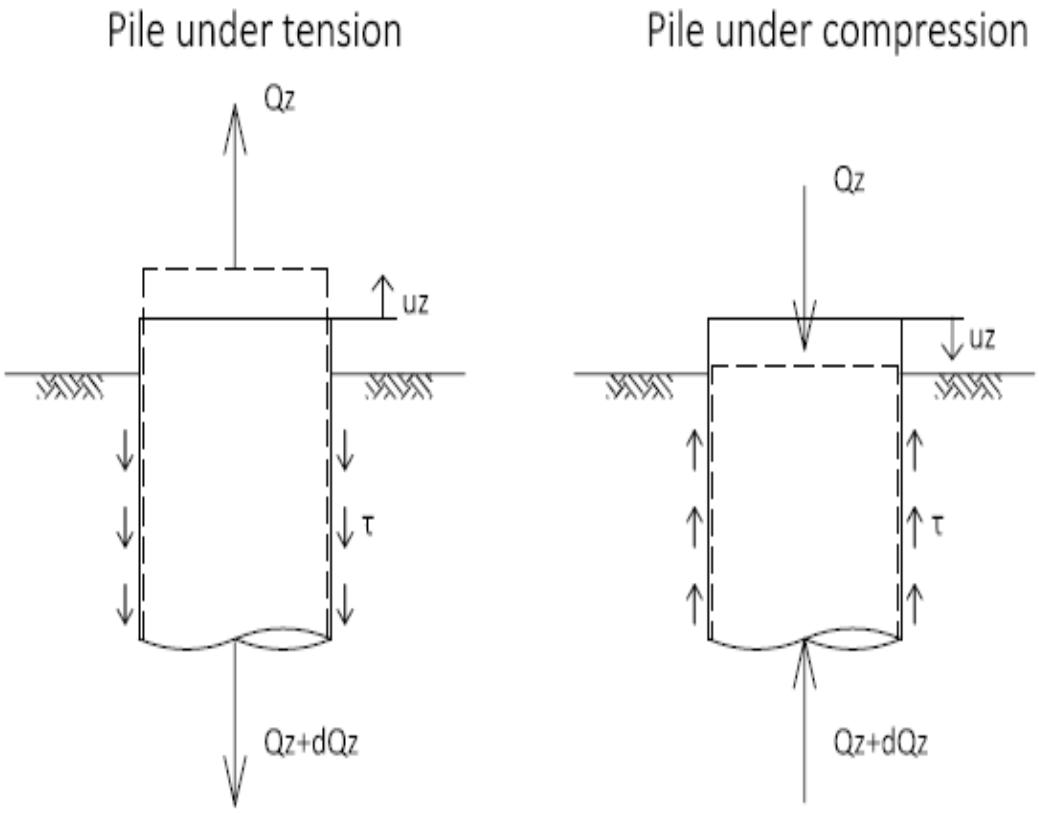

Figure 2.4 Schematic illustration of an one dimensional element under axial loading.

Continuum mechanics indicate that the differential equation which expresses the development of internal forces in the pile due to axial deformation is given as

$$Q_z = -EA\frac{du_z}{dz} \tag{4}$$

where

E : pile infinitesimal length modulus of elasticity at depth z
A : pile segment cross sectional area at depth z
u_z : pile segment displacement at depth z due to applied load

The differentiation of Eq. (2) with respect to z gives

$$\frac{dQ_z}{dz} = -EA\frac{d^2u_z}{dz^2} \tag{5}$$

and by combining the above result with Eq. (3) derives the equation which governs the interaction between pile and soil at the axial direction as follows:

$$EA\frac{d^2u_z}{dz^2} + \tau L_c = 0 \tag{6}$$

Ultimate Base Resistance

At the tip of the pile, the end bearing capacity is calculated as the integral of the normal stress at the area of the pile tip total cross sectional surface, mathematically expressed as

$$Q = qA_{toe} \tag{7}$$

where

q : unit end bearing capacity,
A_{toe} : cross sectional area of the pile toe.

It is obvious that the ultimate resistance is sensitive to any variations of the cross sectional area. For a hollow cross section, there are two distinct cases, the plugged and the unplugged condition, as shown in Fig. 2.5.

Plugged Condition

It is the case where the open tube pile is compacted with soil such that it behaves like a solid full cross section against the soil. The ultimate resistance is given by the equation

$$Q_{plugged} = qA_{plugged} \tag{8}$$

where

$A_{plugged}$: full (or plugged) cross sectional area at the pile toe
q : unit end bearing resistance

Unplugged Condition

This condition occurs considering the load transfer mechanism of the pile to consist of two individual components, the normal resistance of the soil against the pile cross sectional area and the internal skin friction from the soil moving inside the pile shaft. The ultimate resistance is given by the equation

$$Q_{unplugged} = qA_{unplugged} + \tau_{internal}A_{s,int} \quad (9)$$

where

$A_{unplugged}$: unplugged cross sectional area at the pile toe,
$\tau_{internal}$: internal skin friction.
$A_{s,int}$: surface area of the pile segment inside the shaft interior, in contact with soil

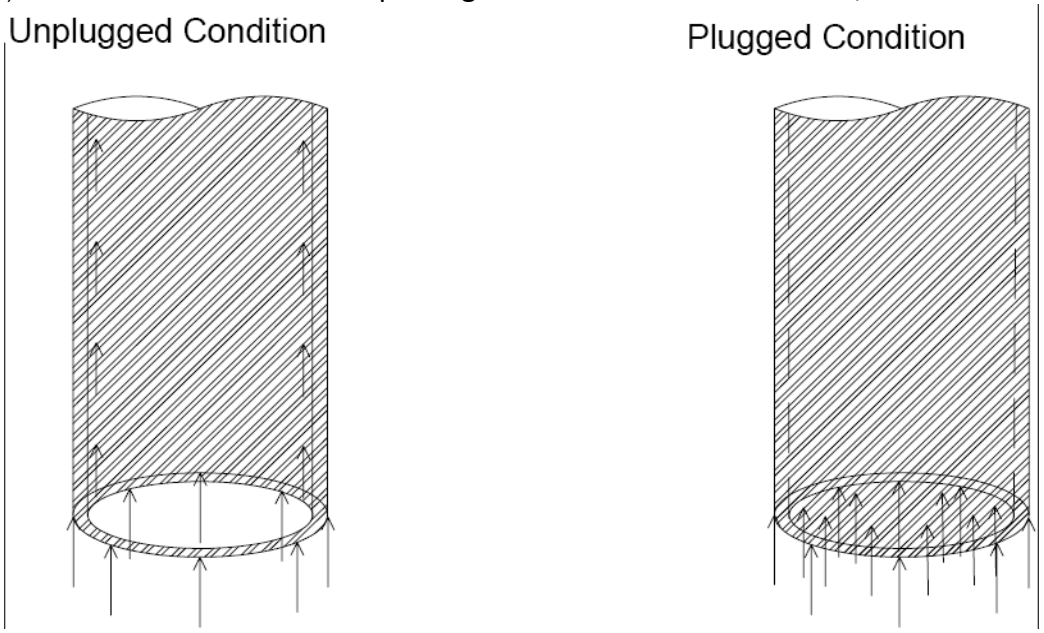

.Figure 2.5 Plugged and Unplugged condition of the pile toe.

The determination of the pile plugged condition is briefed to the check if the internal resisting force is sufficient to lift the dead load of the plugged soil volume.
In the case where the pile is loaded axially in a tensile manner, a phenomenon called extrusion, the resisting mechanisms change radically. The outstanding mechanisms are

- Axial deformation of the pile
- Soil skin friction along the shaft surface of the pile
- Pile and soil attached dead weight

The shaft resistance remains as it was in the previous, compressive loading due to the isotropic consideration of the soil, tending to keep the pile inside the soil with the vector pointing down. However, the end tip of the pile loses its interaction with the soil underneath, which is a reasonable fact as soils in general are characterized by little or none tensile

interface interaction due to small tensile strength. Finally, as the action of extrusion is by definition an action at the opposite direction of that of gravity, the dead load of the pile and the soil which is attached to it is a fundamental parameter of the overall resistance of the pile against extrusion.

2.3. Piles under lateral loading

Opposed to a lateral loading, the piles respond the same way, no matter the direction of the loading, whether is right or left. To approach and comprehend the parameters that dominate the problem, there are three basic mechanisms that determine the overall resistance of a pile against lateral loading:

- the bending stiffness of the pile,
- the shear stiffness of the pile,
- the normal resistance of the surrounding soil.

Furthermore, it is essential to point out that the deflection mechanism is practically limited to the upper part of the pile, in contrast with the axial loading which activates the whole length of the pile. Additionally, it is easily comprehended that in the case of lateral loading the soil and pile interaction is mainly limited to the face of the resisting zones (Fig 2.6).

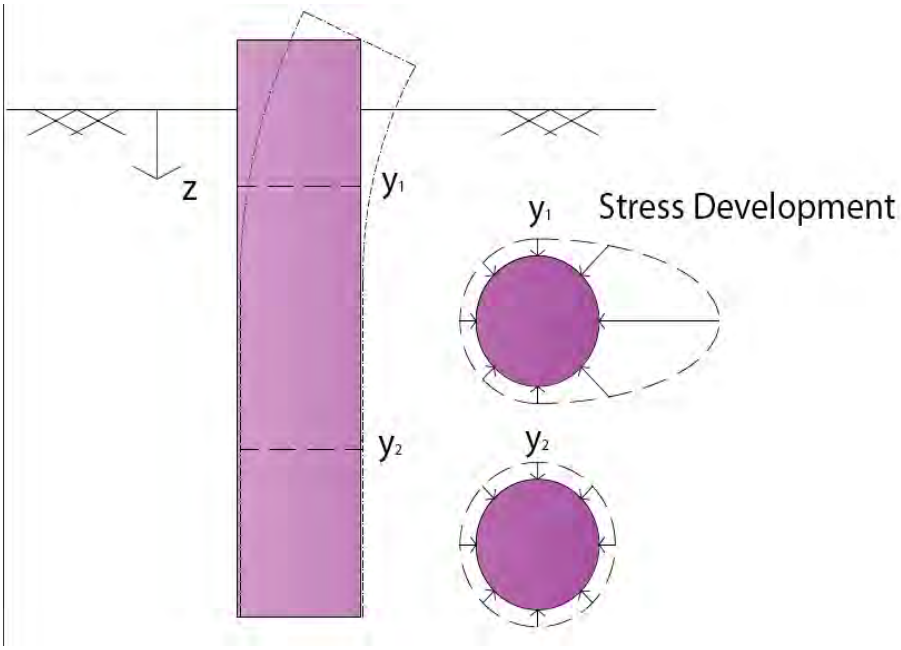

Figure 2.6 Development of soil resistance in form of the pile as a function of pile deflection.

Analytical Expression of the lateral response

The first approach of this rather complex problem was the beam on elastic half space, governed by the following differential equation, expressed in conventional form (Hetenyi,1946)

$$E_p I_p \frac{d^4 y}{dx^4} + P_x \frac{d^2 y}{dx^2} + E_{py} y = 0 \tag{10}$$

where

y : lateral deflection of the pile,
$E_p I_p$: flexural stiffness of pile,
P_x : axial load on the pile head,
E_{py} : soil reaction modulus (mainly varying with deflection).

The integration of the above equation provides that given the shear force along the pile and is given by:

$$E_p I_p \frac{d^3 y}{dx^3} + P_x \frac{dy}{dx} = V \tag{11}$$

where

V : shear force

A further integration leads to the relationship providing the bending moment along the pile as follows:

$$E_p I_p \frac{d^2 y}{dx^2} = M \tag{12}$$

where

M : bending moment

Finally a third integration give the slope along the pile:

$$\frac{dy}{dx} = S \tag{13}$$

The above formulation is extremely useful in the case of three-dimensional analysis (see later the analysis with FLAC^{3D}) where the pile is simulated using brick elements that only stress results are available. However, it could be possible to estimate the bending moment from Eq. (12), having estimated slope from Eq. (13) and curvature by a further differentiation.

Mode of equilibrium for piles under lateral loading

Under lateral loading, the mode of equilibrium of a pile is determined by two major parameters. The first parameter is the boundary condition on pile head -concerning its ability to rotate (free head pile) or not (fixed head pile)-, which governs the response of the pile and the soil reaction. The second is the type of failure that takes place in case of excessive imposed lateral force, which focus on whether it is going to be the pile by the formation of plastic hinges (long pile failure), or the surrounding soil by the excessive displacements produced (short pile failure). Combining the cases above, there have been produced by Broms (1964) four principal figures that describe the mechanism of a pile in limit equilibrium (Fig 2.7). It has been scientifically proved that the condition where the pile head is restrained provides the highest resistance against lateral loading (Fig 2.8).

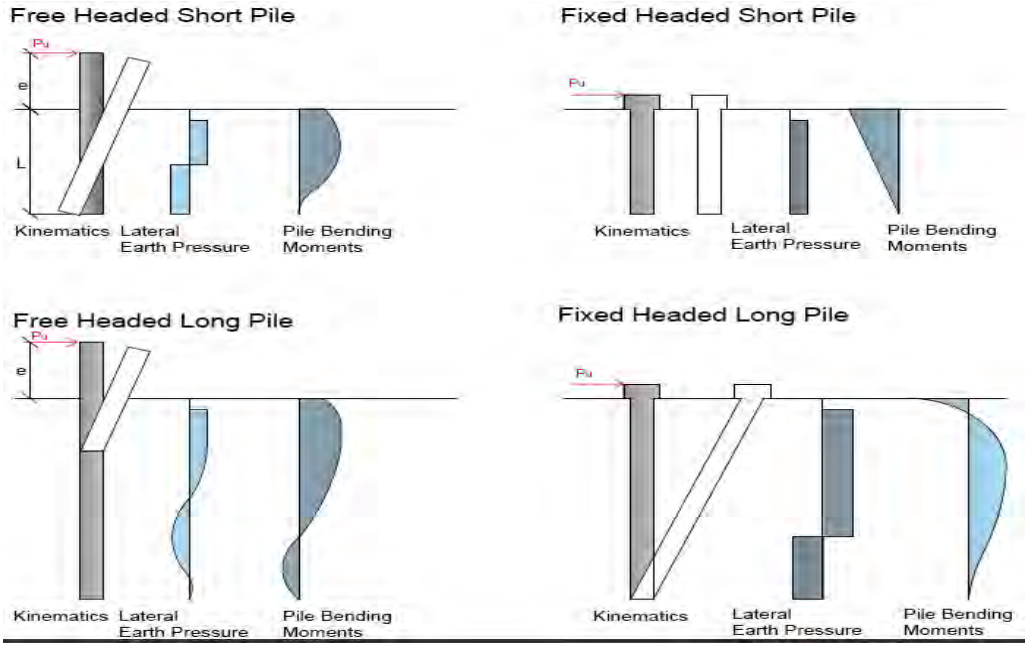

Figure 2.7

Dominant modes of failure and corresponding limit equilibrium condition.

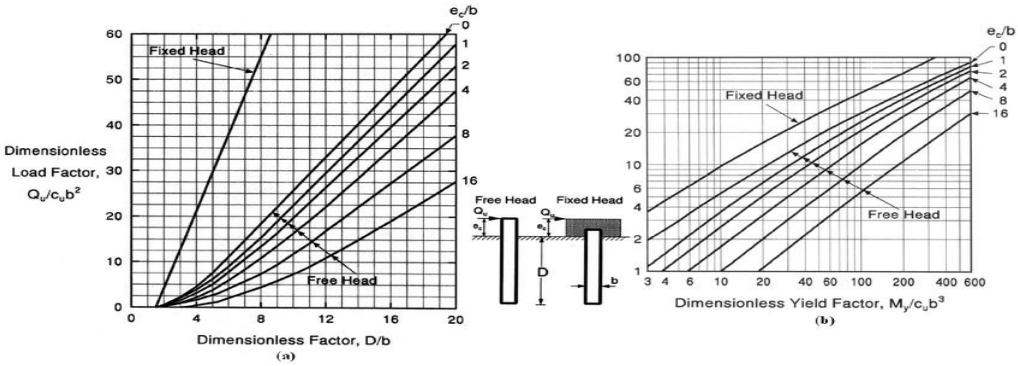

Figure 2.8 Ultimate capacity of piles embedded to cohesive soil (Broms,1964).

2.4. Mohr-Coulomb Constitutive Law in Numerical 3D Analysis

Any disturbance of the initial field stress of the soil which may be implied by the enforcement of a structure brings a new order to the stress distribution at the soil. In order to predict the effect of this new order of stresses to the soil and afterwards to the superstructure, continuum mechanics have utilized the constitutive laws, which are mathematical transformations that link the stresses with the imminent strains and displacements. In the case of clay, the study of the material turns out to be complex as soils in general exhibits nonlinear behavior from a relatively low level of stresses. Dealing with the nonlinearity, criteria have been conceived to define the state that the soil is.

Mohr-Coulomb failure criterion is the most popular criterion as it relates the two shear strength parameters, the angle of internal friction and the cohesion, to the surface of failure in one, two and three dimensional problems. In the case of clayey soils under undrained conditions, where the internal angle of friction becomes equal to zero, the model takes the well-known form of Tresca, depending only on the undrained shear strength. The Mohr Coulomb criterion provides a closed surface in the space of principle stresses, where every possible stress condition is represented by a unique point. This enclosed surface contains all the possible stress conditions which correspond to the elastic phase of the material(elastic domain). When a stress path reaches the bound surface the material yields, and in the case of perfect plasticity this corresponds to the point of failure as well.

It is essential to point out that soil yield, or commonly failure, in terms of geotechnical engineering is the condition when the soil displays excessive strains and loses the ability to recover to its initial form. Such phenomena are unavoidable in geotechnical construction and occur near the boundaries between the structure and the soil where there is concentration of stresses. The duty of an engineer is to constraint this phenomenon and don’t let it violate any serviceability or ultimate limit state, providing viable design satisfying the required safety level at the minimum possible cost.

The simplest expression of the Mohr-Coulomb corresponds to the fundamental equation at point and is given by Eq. (14). The surface of failure that corresponds to this equation is given in Eq. (2.9). It is worthy noticing that the slope of the surface in the negative axis of the normal stress is generally taken lower than in the compression to reflect the fact that the resistance in tension is lower than that provided by Eq. (14), and in some cases a zero value is applied.

$$\tau = \sigma_{\mathrm{n}} tan\varphi + c \tag{14}$$

where

τ : shear strength,
σ_{n} : imposed normal stress,
φ : internal friction angle,
c : cohesion.

When applied the Mohr-Coulomb model Eq. (14) must be rewritten as a function of planar stresses. In the case of principal stress it takes the form of the following equation:

$$f^{s}(\sigma_1, \sigma_3) = -\sigma_1 + \sigma_3 N_{\varphi} - 2c\sqrt{N_{\varphi}} = 0 \tag{15}$$

where

$$N_{\varphi} = \frac{1 + sin\varphi}{1 - sin\varphi}$$

Tension failure criterion is an additive curve to the above envelope which expresses the tensile strength of the material and closes the shear surface at the positive stress direction. It is expressed by the follow condition

$$f^{\mathrm{t}} = \sigma^{\mathrm{t}} - \sigma_3 = 0 \tag{16}$$

where

σ^t : tensile strength , $\sigma^t \leq \frac{c}{tan\varphi}$

The fit union of the above envelopes is presented at the two dimensional diagram displayed at figure 2.10.

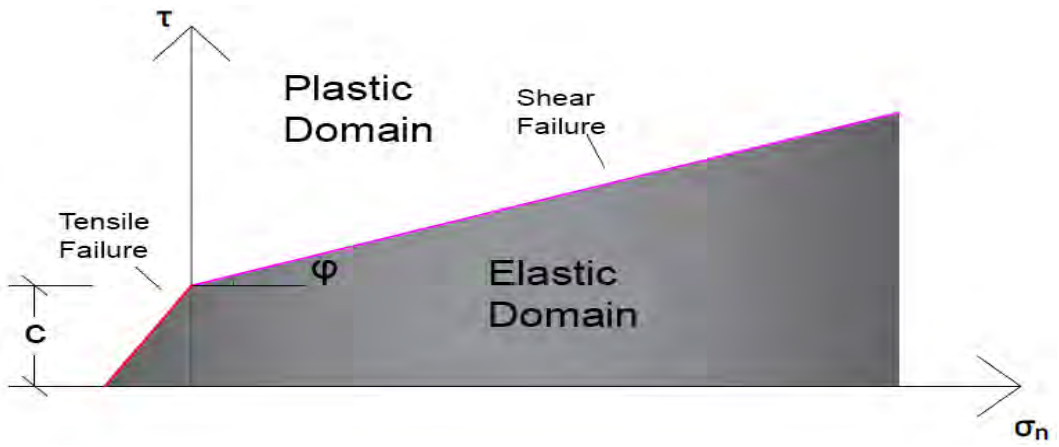

Figure 2.9 Schematic illustration of Mohr-Coulomb failure criterion.

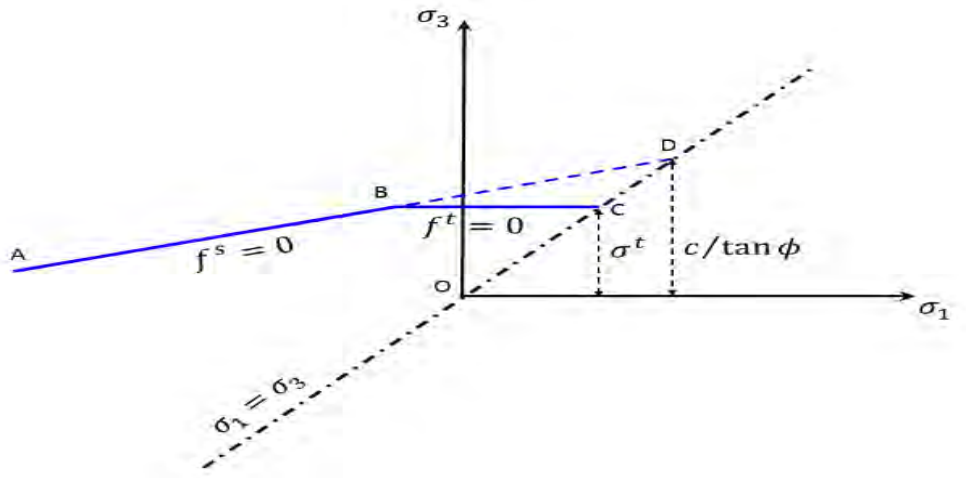

Figure 2.10 Planar aspect of union between the shear and tension failure envelope(FLAC[3D] User's Manual).

Expanding the failure line by revolving around the hydrostatic axis and extracting the hexagon located inside the produced circle, the enclosed surface is provided, as shown in the three dimensional diagram below.

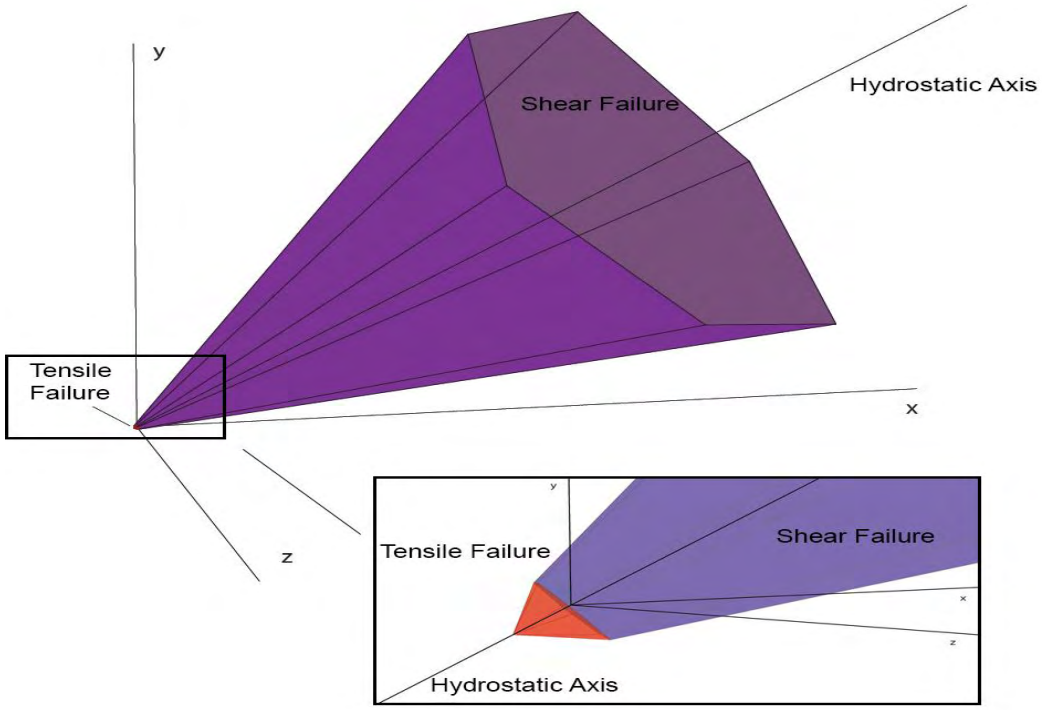

Figure 2.11 Illustration of Mohr Coulomb failure envelope in the three dimensional stress space.

In the case if clayey soils under undrained conditions the angle of internal friction is zero and therefore the failure envelope depends only on the undrained shear strength. The mean

stress value, first invariant of stresses, does not affect the failure surface and therefore it takes the shape associated to Tresca failure criterion, Fig. 2.12.

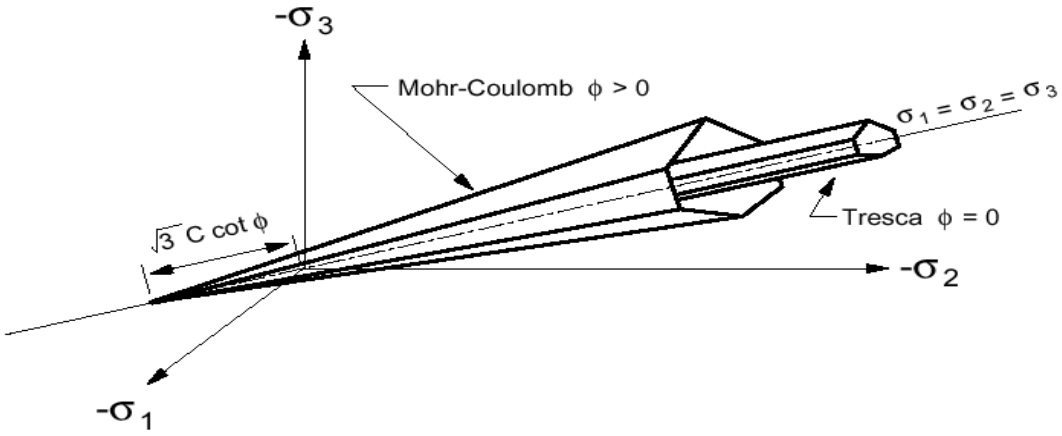

Figure 2.12 Illustration of Mohr Coulomb and Tresca failure envelope in the three dimensional stress.

2.5. Soil replacing by spring elements

Performing three dimensional numerical analysis in soil and structure interaction requires solving potentiality and very advanced technology in the finite element meshing and processing. Even if the previous preconditions are fulfilled, still there is the problem of the extent time which is required to produce results, which incommodes or even counts out the possibility of running parametric analysis as every project is limited by time deadlines. Specifically, in the study of piles and soil interaction, the problems mentioned above are surpassed by substituting the action of the soil with springs equipped with laws of response (Fig. 2.12). Every spring is practically substituting the contribution of a certain surface at the shaft or the tip of the pile. Although this method was initially developed due to insufficiency of computational power back in 60s, it is still commonly used today as it produces results which are close enough to reality to design with safety and basically it allows to perform a series of analyses that arises from the demands of multiple load conditions required by the design codes . The laws which define the response of the springs attached to the piles are decoupled and classified into two major genres according to their direction, perpendicular or parallel to pile axis. The springs which are parallel to the axis of the pile are equipped with the ‘t-z’ curves of behavior and the rest which are perpendicular to the pile axis are governed by the ‘p-y’ curves of behavior. Additionally, the bottom node is equipped with an extra spring which carries the soil resistance at the pile tip, whose response is determined by the ‘Q-z’ curve.

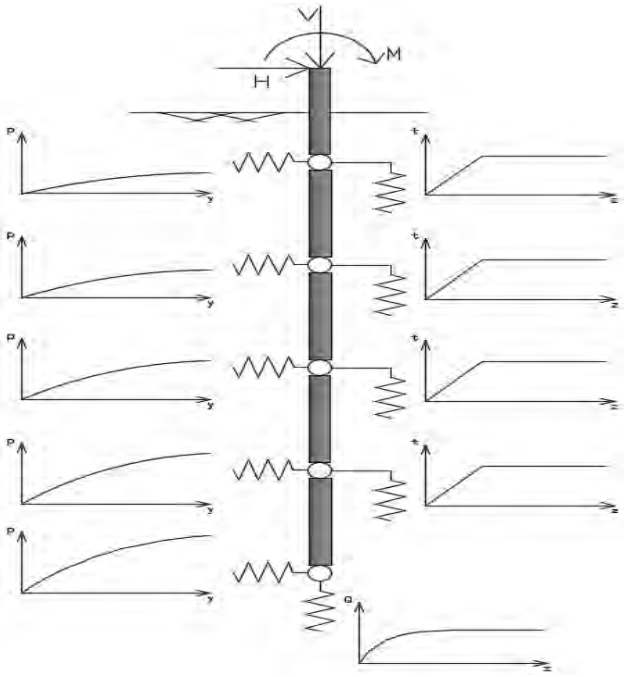

Figure 2.13 Illustration of finite element mesh of a pile under axial loading by replacing the soil resistance with spring elements.

Short reference to '*t-z*' curves

Various forms of the '*t-z*' relationships with parabolic, hyperbolic or multilinear shape have proposed to replace the soil resistance at the pile shaft. In the present research work the development of the shaft resistance as a function of pile displacement is considered according to the guidelines of the American Petroleum Institute (API, 2003). The relationship is given in tabular form, Table 2.1, and it has a rather parabolic shape. It is worthy noticing the reduction associated with the post peak behavior, which however should be justified by the results of laboratory tests.

Soil Displacement/Pile Diameter (z/D)	Unit Skin Friction/ Ultimate Unit Skin Friction (τ/τ_{ult})
0	0
0.0016	0.3
0.0031	0.5
0.0057	0.75
0.0080	0.9
0.0100	1
0.0200	0.7 to 0.9*
∞	0.7 to 0.9*

* The residual strength of API Clay is assumed to be 0.9 times the ultimate unit skin friction

Table 2.1 API Clay Skin Friction (t-z) Load Transfer Curve.

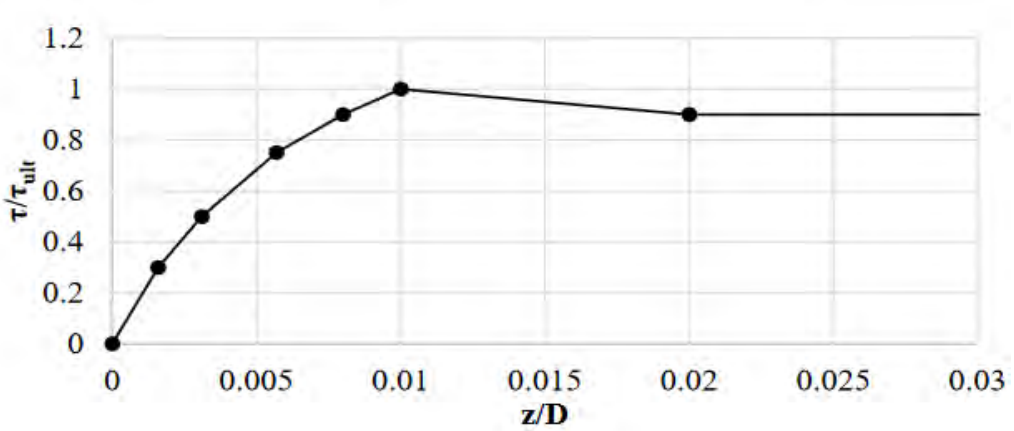

Figure 2.14 Load-transfer curve of pile shaft from clayey soils according to API (2003).

It is implied that the springs are within the elastic phase as long as there's no violation of a strain limit. Referring to the ultimate friction resistance of the clay, the following formula is recommended

$$\tau_{\mathrm{ult}} = a\, c_{\mathrm{u}} \tag{17}$$

where

a : dimensionless reduction factor,
c_{u} : undrained shear strength of soil at calculation point.

The factor a mentioned above is defined

$$a = \begin{cases} a = 0.5\psi^{-0.5}, \psi \le 1.0, \alpha \le 1.0 \\ \alpha = 0.5\psi^{-0.25}, \psi > 1.0, \alpha \le 1.0 \end{cases} \tag{18}$$

where

ψ : c_u/σ_v
σ_{v} : effective overburden pressure at calculation point

Short reference to '*p-y*' curves

Considering the lateral resistance of the soil to pile movement, springs laterally attached to the piles are utilized, equipped with '*p-y*' curves of hyperbolic form, as defined in the following equation of Comodromos E. and Papadopoulou M.(2013)

$$p = \frac{y}{\frac{1}{K_{\mathrm{i}}} + \frac{y}{p_{\mathrm{ult}}}} \tag{19}$$

where

K_{i} : spring stiffness, defining the initial stiffness of the '*p-y*' relationship,
p_{ult} : soil's ultimate lateral resistance, which is the cut off to plasticity, reducing the ultimate resistance to 80% of its magnitude for further displacement.

The stiffness which is given to the springs is an equivalent produced by the combination of all those parameters that contribute to the soil and pile interaction system, having the initial elastic modulus of the soil in dominant position and giving the cross sectional properties of the pile in minor influence, as displayed by its mathematical formation

$$K_{\mathrm{i}} = \frac{1.3E_{\mathrm{i}}}{1-\nu^2}\left(\frac{E_{\mathrm{i}}D^4}{E_{\mathrm{p}}I_{\mathrm{p}}}\right)^{1/12} \tag{20}$$

where

E_{i} : clay's initial modulus of elasticity
ν : soil's Poisson ratio
E_{p} : pile's material modulus of elasticity
I_{p} : pile's cross section moment of inertia
D : pile's diameter

The ultimate soil resistance is provided by the following equation.

$$p_{\mathrm{ult}} = N_{\mathrm{p}}c_{\mathrm{u}}D \tag{21}$$

where

N_{p} : bearing capacity factor.

3. STRUCTURE OVERVIEW

3.1. Introduction

The project studied is the NOWITECH 10 MW reference wind turbine founded at 50 meters water depth via a guyed support system. Combining the technology of the shallow foundation and the cable support system, a next generation wind turbine structure is developed, which satisfies the serviceability criteria of small rotation and deals with the wave and wind loading in a vast range of cycles (Fig. 3.1). The system is consisted of a solid slender tower with the rotor on top which reaches the seabed and is installed with a shallow foundation, actually touching the bottom. The shallow foundation transfers all the vertical loads of the structure to the soil and provides the lateral resistance against the horizontal wave and wind loading by exploiting the shear resistance which is activated at the interface between the soil and the foundation by the friction. In order to the stabilize the structure against the overturning moments caused by the horizontal action of waves and wind, the tower is supported by four prestressed cables, attached at the middle of the tower's height which lies above the wave highest altitude and anchored to the seabed via four tubular steel piles. The installation of the cables functions as a lateral displacement constraint, targeting on relocating the start of the cantilever beam static system up to the convenient height of 75 meters from the sea floor. Besides the fact that the required resistance against overturning moment and lateral displacement is gained without the need of constructing massive tower cross sections, this intervention efficiently moderates the deflection of the top, phenomenon which is highly possible to violate serviceability criteria.

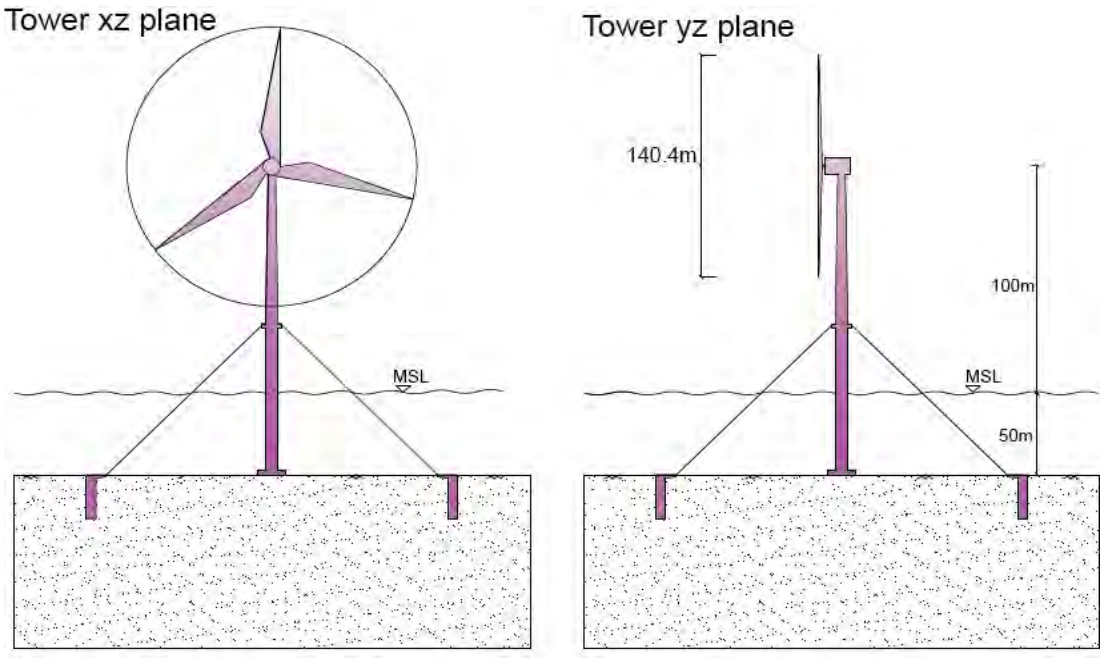

Figure 3.1 Structure layout.

3.2. Short description of the Superstructure Review

The wind turbine simulated and studied carries a three bladed rotor of energy capacity production of 10 MN which has certain functional requirements and is placed at the top of the tower, 100 meters above the sea level (Table 3.1). The tower that supports the rotor and its nacelle is totally made of steel, geometrically defined by a tubular cross section of initially constant diameter of $D_b = 6$m which at the middle height starts to reduce linearly to the minimum diameter of $D_t = 3.6$m while moving upwards, forming a conical frustum looking up (Fig. 3.2). The overall length of the tower reaches the 150 m, from which the initial 50 meters of the bottom are submerged into the ocean.

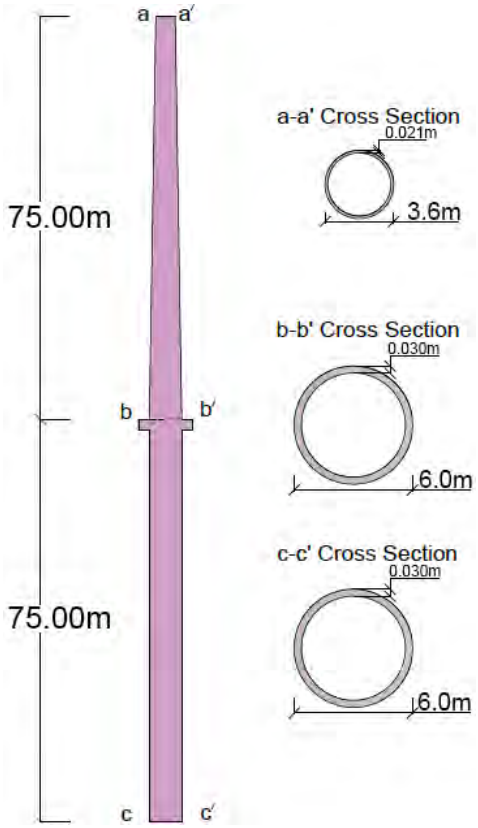

Figure 3.2 Tower cross section at characteristic locations.

At the middle of the tower's height, there is a platform which projects 3 meters from the solid body of the structure and functions as the attachment point of four prestressed cables that placed radially by the tower (Fig. 3.3) and are anchored to the seafloor by four steel tube anchor piles. These cables are consisted of four galvanized steel spiral strands, composed of a multitude of wires knitted helically around a core wire and carry pretension load of 7100 kN, property which gives the possibility of interacting with the massive lateral forces with which the tower is imposed, without any development of large displacements.

According to API regulations, the cable members that are loaded with pretension are obliged to have the double potential ultimate strength than the maximum load that are imposed to and obviously remain in constant tension. Analyzing the forces provoked by the pretension at still conditions, the vertical and horizontal compound of magnitude 5021 kN (Fig. 3.4) stands out in both directions creating a constant resistance against overturning of 377 MN.m and an additive vertical force of 20084 kN, with a potential of maximum overturning resistance 2477 MN.m.

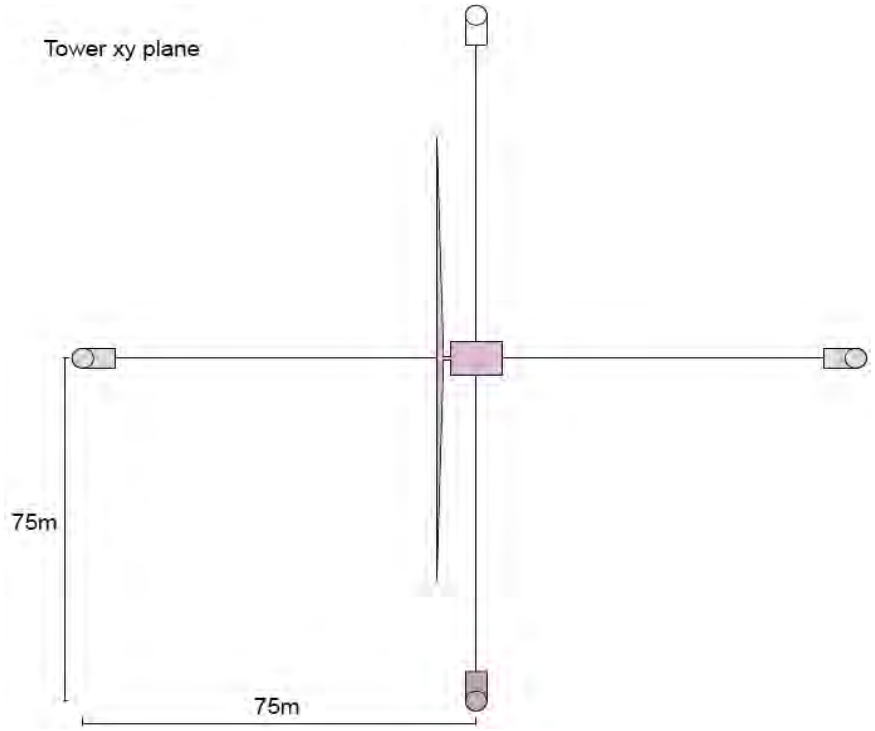

Figure 3.3 Cable Set-Up.

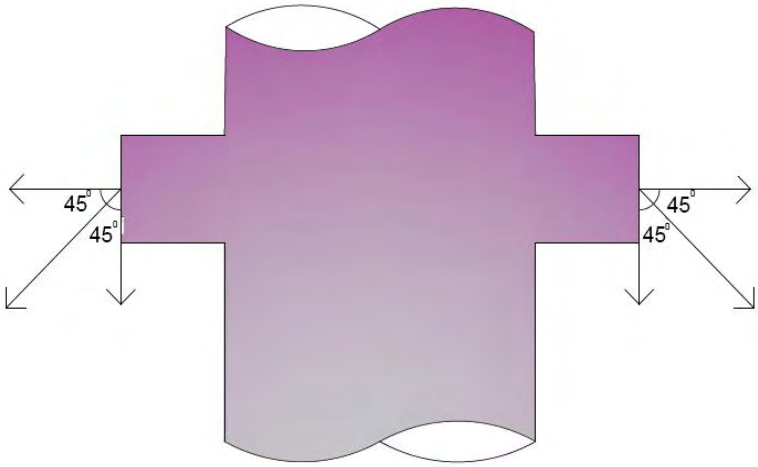

Figure 3.4 Cable disposition and components of vertical and horizontal forces.

3.3. Soil properties and foundation layout

The soil stratum introduced to the simulation is estimated as a 40 m deep homogenous clayey soil, with undrained shear strength of s_U = 60 kPa, Poisson's ratio equal to v=0.49, corresponding to saturated condition and submerged unit weight γ'=10 kN/m^3. The assumption made to determine the initial elastic stiffness of the studied soil is to be directly derived from the undrained shear strength, by the linear relationship

$$E_{\mathrm{i}} = 1800\, S_{\mathrm{u}} \tag{22}$$

The selection of this rather large factor is due to undrained conditions that rule the response of the clay, which imply zero volume change, therefore a stiffer deformation response. Additionally, the internal friction angle between the participle is considered negligible, condition also compliant to the undrained condition along with the tension capacity, which is conservatively declared negligible.

The tower is founded on a circular steel basis of total diameter 14 meters placed on the sea floor, without any further embedment in the soil. It is designed to receive the circular cross section of the tower as its core and expand its footing surface to an annular ring (Fig. 3.5). In order to eliminate the strains in the plane of the slab and render the connection of the tower and the slab rigid, eight steel stiffeners are fitted to enforce the bending stiffness of the slab (Fig. 3.5). Additionally, by the time its estimated weight reaches the magnitude of 57215 kN, it consists approximately the 63% of the total structure's weight, acquiring the beneficial influence of the ballast against overturning, technique borrowed from naval engineering.

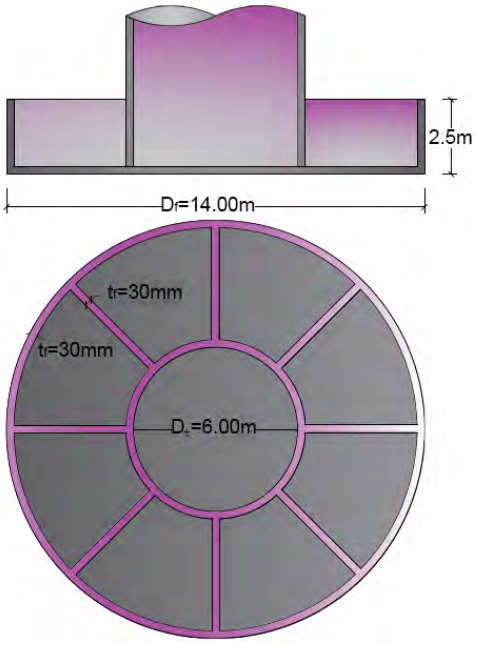

Figure 3.5 Presentation of the foundation: cross section at the top, horizontal view at the bottom.

Along with the foundation, the system interacts with the soil through the piles that consist the anchor mechanism of the cables. These tubby piles of diameter D_p = 5 meters, thickness t_p= 0.02 meters and total embedded length L_p=22 meters (Fig. 3.6)are placed radially around the tower at distance L=75 meters. The core of these hollow elements is filled with soil and behaves as a solid component of the pile, contributing to their response against pull out and lateral forces.

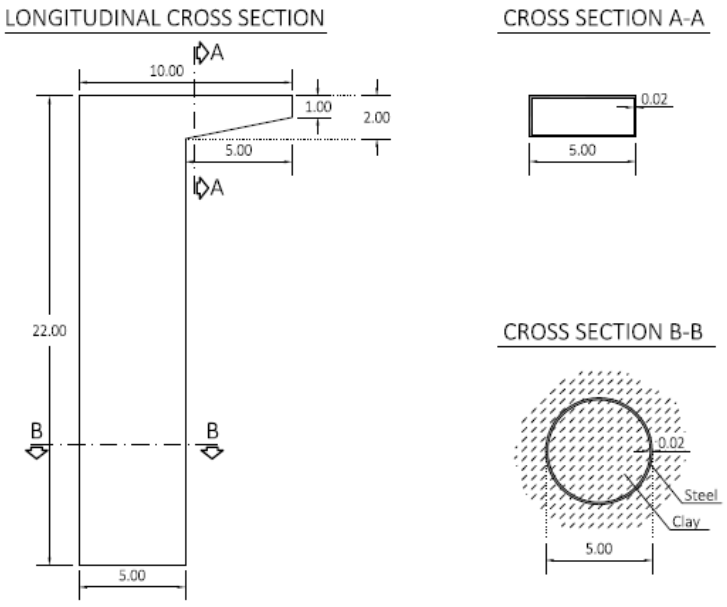

Figure 3.6 Pile element geometry.

Following the stress path to the soil, the resisting mechanism of the piles is examined. The dead load of the piles is the sum of the weight provided by the steel tubular cross section along the whole length of the pile and by the soil which is plugged inside the tube. The ultimate shaft resistance force by the contribution of the friction resistance of the interface between steel and clay is determined as the integral of the interface friction stress on the surface of the pile. The shear strength attributed to the interface elements between the piles and the soil is equal to the soil shear strength multiplied by reduction factor a as proposed by API(2003). This reduction is made because the variation of the initial field that takes place at the drive of the pile is reason to disturb the skeleton frame of the soil and harm its cohesion.

A rough estimation of the axial capacity that a pile can carry out is leads to a maximum force of 17133 kN, which is way than enough, as such action corresponds to factor of safety of 1.37.

3.4. Environmental Loading

Wave Loading

Like every periodic phenomenon, the wave loading is characterized by its dynamic nature. Nevertheless, since the offshore structure is robust enough that its stiffness and mass provide a natural frequency which differs massively from the loading frequency of the waves, this load may be adequately represented by its static equivalent.

By the time the structural member doesn't actually modify the incident's wave, condition practically standing for a ratio of wavelength to the member diameter lower than 5, the computation of the forces exerted by waves on cylindrical objects, such as the tower of the wind turbine, is given as the sum of the drag and the inertia force as expressed by the Morison's equation

$$F(x,z,t) = F_{\mathrm{d}}(x,z,t) + F_{\mathrm{i}}(x,z,t) \tag{23}$$

Decomposing the equation above, the drag and inertia force are given respectively

$$F_{\mathrm{d}}(x,z,t) = C_{\mathrm{D}}\frac{w}{2g}AU|U| \tag{24}$$

and

$$F_{\mathrm{i}}(x,z,t) = C_{\mathrm{M}}\frac{w}{g}V\frac{\delta u}{\delta t} \tag{25}$$

where

C_{D} : drag coefficient[-]
w : weight density of water [kN/m^3]
g : gravitational acceleration [m/s^2]
A : projected area normal to the cylinder axis per unit length (diameter for circular cylinders) [m]
V : displaced volume of the cylinder per unit length (circular surface for circular cylinders)[m^2]
D : effective diameter of circular cylindrical member including marine growth [m]
U : component of the velocity vector (due to wave current) of the water normal to the axis of the member [m/s]
$|U|$: absolute value of U [m/s]
C_{M} : inertia coefficient
$\delta u/\delta t$: component of the local acceleration vector of the water normal to the axis of the member [m/s^2]

According to the API(2003) recommendations, the drag and inertia coefficients are expressing the contribution of the harshness of the surface which is hit by the waves. For the unshielded circular cylinders, shape corresponding to current project, the following values are given

Smooth: C_D =0.65,C_m =1.6

Rough: C_D =1.05,C_m=1.2

Finally, the computation of the horizontal wave kinematics (velocity and acceleration of water particles) can be performed utilizing the linear wave theory, also known as the Airy theory, which is expressed by the equations

Wave Velocity:

$$\dot{u}(x,z,t) = \hat{\zeta} 2\pi f \frac{\cosh k(z+d)}{\sinh kd} \cos(kx - 2\pi f t), 0 \le z \le -d \quad (26)$$

Wave Acceleration:

$$\ddot{u}(x,z,t) = \hat{\zeta} (2\pi f)^2 \frac{\cosh(z+d)}{\sinh kd} \sin(kx - 2\pi f t), 0 \le z \le -d \quad (27)$$

where

ζ : wave's amplitude (Hwave/2)
k : wave number ($2\pi/\lambda$)
f : wave frequency [1/s]
λ : wave length [m]
d : water depth [m]
x : horizontal position in the wave direction
t : time [s]

These parameters defining the force to be applied to the superstructure by the waves vary with the area studied and can be found at statistic data base which refers to the last 100 years Wave Height, Associated Wave period and Storm Water Depth. Finally it is crucial to mention that in order to use the velocity derived by the linear wave theory to produce wave force data, the following transformation must be applied

$$U = u + U_c \quad (28)$$

where

u : velocity derived by the linear wave theory
U_c : current wave velocity, extracted by statistical data base

At the current study, *U*c is determined as 2 m⁄s, value typical for the North Sea.

Wind Loading

Like the wave loads, the loads caused by the wind are dynamic in nature, but by the time the frequency of the load doesn't reach the natural frequency of the structure, the response can be assumed static. The relationship of the wind and the equivalent drag force on the object is a function of the wind speed and its given by the equation

$$F = \frac{\rho}{2} u^2 C_s A \tag{29}$$

where

F : drag force caused by the wind [kN]
ρ : mass density of the air, approximately 1.225 $\left[\frac{\text{kg}}{\text{m}^2}\right]$
u : wind speed $\left[\frac{\text{m}}{s}\right]$
C_s : shape coefficient [-]
A : surface area of the rotor [m2]

According to API (2003), the recommended shape coefficient for a cylindrical section is 0.5. An important advantage of the OWT is the fact that the rotor operates in a certain band of wind speed, ranging from 3 m/s to 25 m/s. The lower and the upper speed values are called cut-in and cut-out speed respectively in rotor terminology. Below the cut-in speed, the function of the turbine is not sufficient anymore and above the cut-out speed, there's serious danger of severe damage to the rotor mechanical parts and the nacelle which encloses them. To avoid the scenario of exposure to high speed wind, the turbine is designed in such way that whenever the blades surpass to upper limit of speed, are forced to slow down, keeping the structure within safety boundaries.

Seismic Loading

By the time the tower o of the wind turbine rests on a shallow foundation which primarily takes vertical loads and deals in a minor degree with the restrain of horizontal displacements or rotations, it can be concluded that the shallow foundation is actually a partial pinned support. According to classic statics, the pinned connection that allows rotations relieves the structure from any concentration of massive moments. Moreover, the superstructure is a slender and tall entity governed by minimum natural frequencies which differ adequately from the frequencies exerted during the seismic loading, fact that excludes the danger of imminent resonance. The consideration of the above facts leads to the judgement that the structure isn't sensitive in seismic phenomena, therefore such case is not examined.

Loadcases Declared

Regarding the loading scenario and their impact on the foundation bearing capacity and stiffness, the simulation doesn't focus on the dynamic nature of the external loading. Such approach is not simplistic and doesn't lose in producing fair results, by the time the

frequency which characterizes the dynamic nature of both waves and wind differs from the natural frequency of the structure so that they will never match. Besides that the case of resonance is not possible, the frequencies of each phenomenon are distant as the period indicating the switch in the direction of the wind is of order of minutes, in contrast with the period indicating the switch in the direction of the wave which to corresponds up to 10 seconds. Exploiting this distance between periods of external loading, the analysis is massively simplified, targeting in analyzing structure's response to extreme loading scenarios, while the wind direction is determined constant during the whole analysis.
In order to keep track of the causes of stress which the structure receives and cover every possible combination of extreme loading condition, there are four load cases pointed out(Fig. 3.7):

- Still Conditions(Dead Load and Pretension Actions)
- Wind Action (Windload+)
- Wind and Wave acting at the same direction(Windload+Waveload+)
- Wind and Wave acting at the opposite direction(Windload+Waveload-)

Both of the environmental loading are simulated as horizontal concentrated point loads, with the wind acting at the top of the tower at 150 meters above the foundation and the alternative wave force acting at the level of the sea, at 41 meters above the foundation.

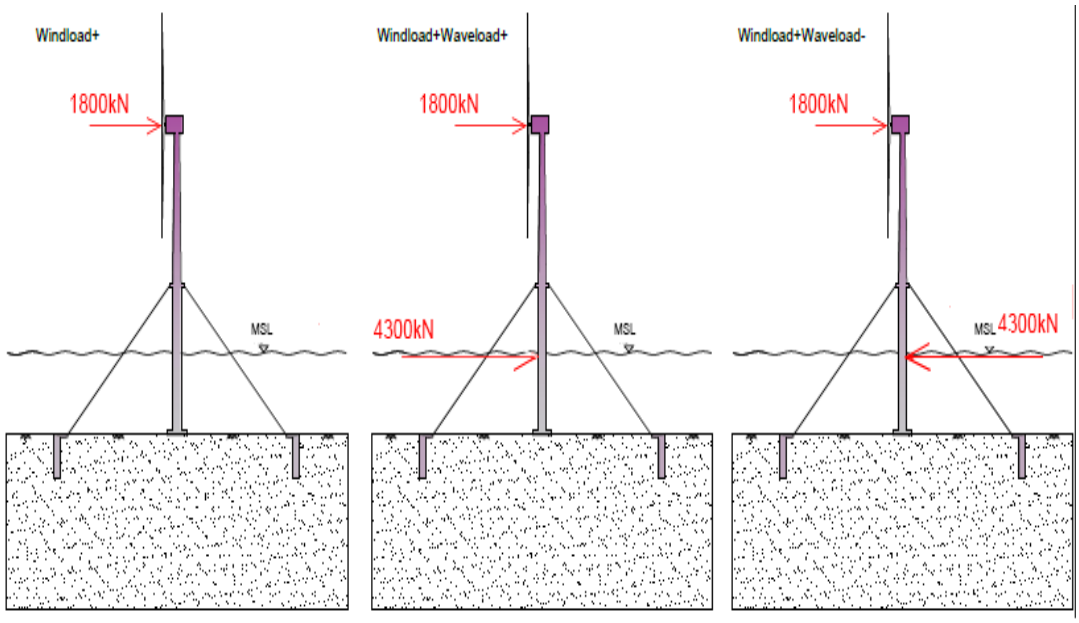

Figure 3.7 Loadcases corresponding to the load combinations carried out in both simplified and full three dimensional analysis.

4. SIMPLIFIED THREE DIMENSIONAL ANALYSIS

4.1. Simulation of Project

Structural Elements

Initially, the studied project is simulated using the F.E. commercial code SOFiSTiK. Aiming to form a general idea of the response of the structure to the environmental loads in terms of safety, a simplified three dimensional analysis has been performed (Fig. 4.1).

This first attempt, which substitutes the resisting action of the soil with springs attached to the elements that interact with the soil, produces results which represent the overall response of the structure and may vary from the reality, fact anticipated by the application of increment factors. Concerning the superstructure, which is entirely made of structural steel, the simulation uses beam elements defined in three dimensional space by two nodes which define their length and their orientation. Assuming elastic response, these linear elements are equipped with geometric cross sectional properties that are summarized in Table B.1 (appendix B) and the material properties that define elastic perfectly plastic behavior based on Von Mises yielding criterion (Table B.2). In order to keep track of the beam kinematics and developed actions these linear elements are divided in segments of 0.5 meters length.

The same way are simulated the piles under the following assumptions. Even if the geometry of the embedded piles doesn't match the geometry that defines beam elements, by the time pile diameter to pile length ratio is relatively high, corresponding to stubby structural components, the production of beam elements resultants is enough to give to provide information about the areas where there is stress concentration or the way that stresses vary. It must be clarified that such simulation is not sufficient to design the cross section of the piles. Furthermore, additional weight and bending stiffness which is contributed by the plugged soil is not included, which is a fact in favor of safety as it stands for the in unfavorable case where the hollow pile doesn't cooperates with the soil as a coupled body(unplugged). Considering the cables, they are modeled with cable elements, defined in three dimensional space by two nodes. These elements are an order simpler than beam elements, which are used in tower and piles, as they are able to carry only axial tensile loads. Apart from the properties that define elastic perfectly plastic behavior, they are also equipped with a pretension force that ensures that they will be constantly in condition of tension.

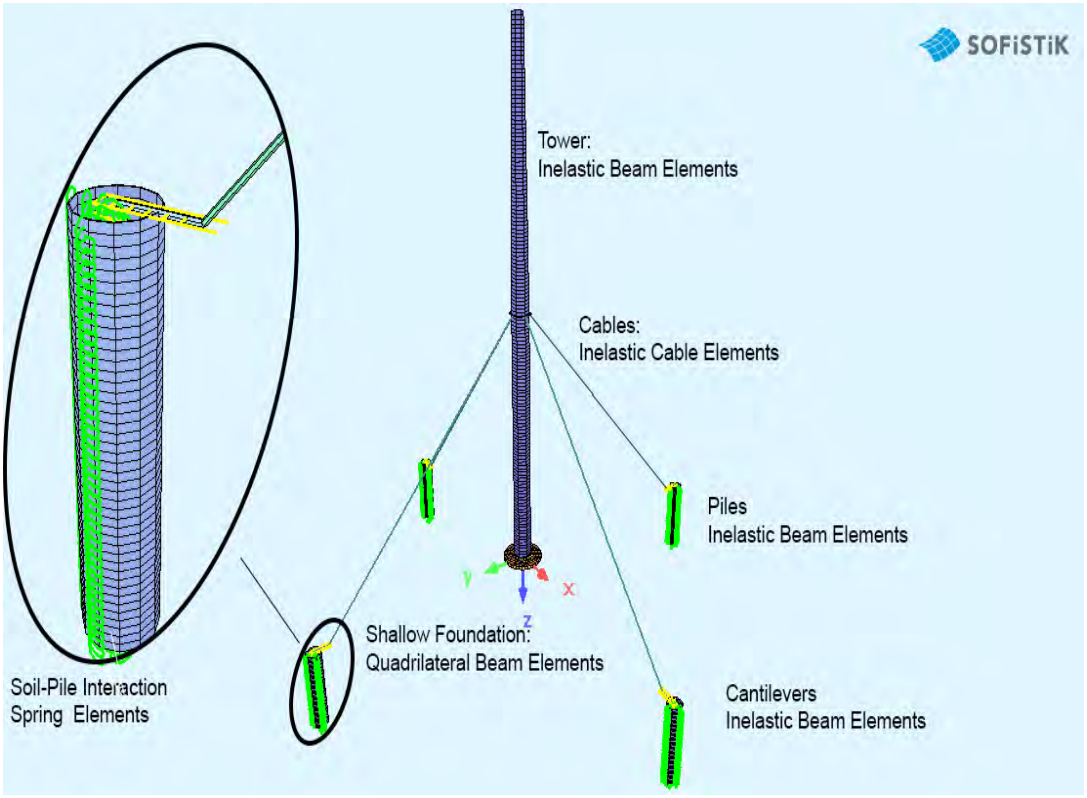

Figure 4.1 Schematic presentation of the finite element layout adopted by the simplified analysis using the F.E. code SOFiSTiK.

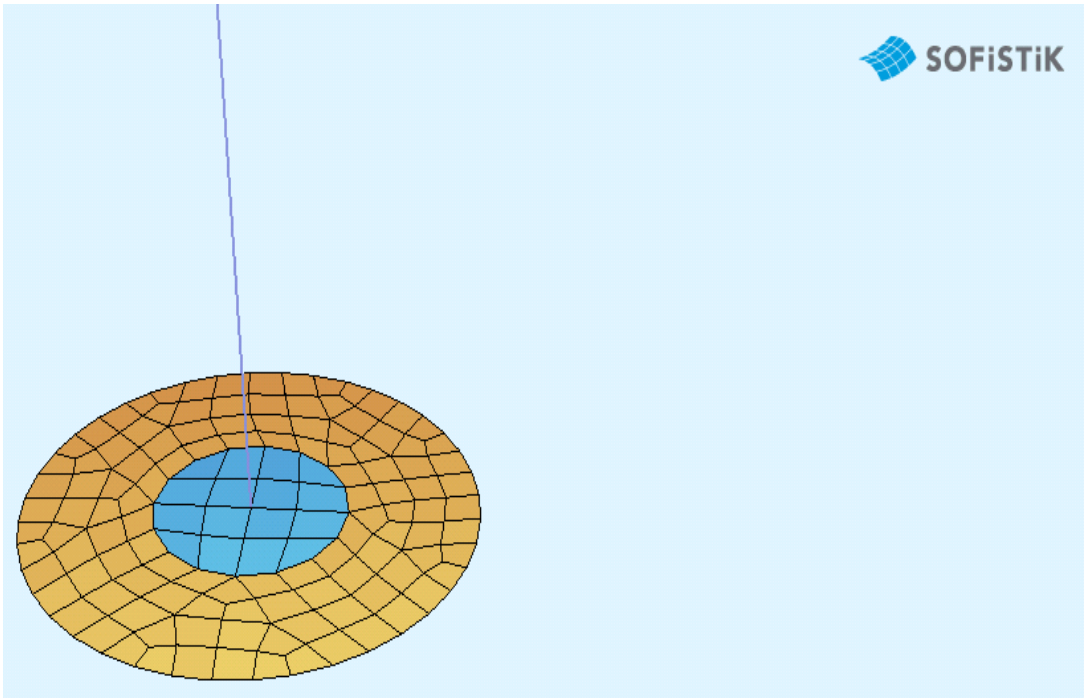

Figure 4.2 Illustration of the shallow foundation of the Wind Turbine by shell elements with two different groups accounting for geometrical variations form edge to center.

Finally, the circular slab of the shallow foundation is modeled by quadrilateral shell elements whose plane is defined by four nodes. In order to simulate the foundation the best way possible, two kinds of shell elements are established; an inner solid circle of 6 meters diameter and 2 meters thickness and an annular ring of 14 meters external diameter and 1 meter thickness which environs the inner (Fig. 4.2). Once again, based on the fact that the foundation is made of steel, elastic perfectly plastic behavior is assumed (Table B.2).

Soil Substitution

Every interface in contact with the soil is equipped with springs that substitute the supporting action. Regarding to the position of the interface and the nature of the loading changes the constitutive law that defines the behavior of the spring. The simplest application of the soil substitution at the current thesis is the shallow foundation bedding approach. The plane elements that composite the shallow foundation are declared with support characteristics (Table B.3) that define elastic perfectly plastic behavior in compression and zero tensile strength, which allows the possibility of instant detachment. The declared constant that determines the predicted stiffness is calculated after analytical settlement to the soil beneath the foundation slab. The springs are imported automatically to the nodes that define the element in both normal and tangential direction, with spring elastic constant that is calculated depending on each element surface area by Eq. 30.

$$K_{\text{elastic}} = C\,A \tag{30}$$

where

K_{elastic} : stiffness attributed to nodal springs (kN/m)
C : soil modulus of reaction resulting from a simplified settlement analysis (kN/m^3)
A : surface area corresponding to the node (m^2)

Continuing to the simulation of the interaction between soil and piles, the approach becomes harsher and the sorting of cases is required. The first step of the analysis is the exclusive study of the pile surface, divided into shaft and base. Nevertheless, since the current study investigates the case of pile extrusion, attention is given to the shaft surface, for the base of the pile has minimum to none interaction with the soil below.

The springs which provide lateral and axial support to the pile are equipped with 'p-y' and 't-z' curves of response, whose form has already been cited in chapter 2.5. The actual curves are calculated and displayed indicatively after inserting the actual input data of the problem for specific depths of the pile, in order to give a clarified sense of their form and the variation caused by depth (Figs 4.3 and 4.4).

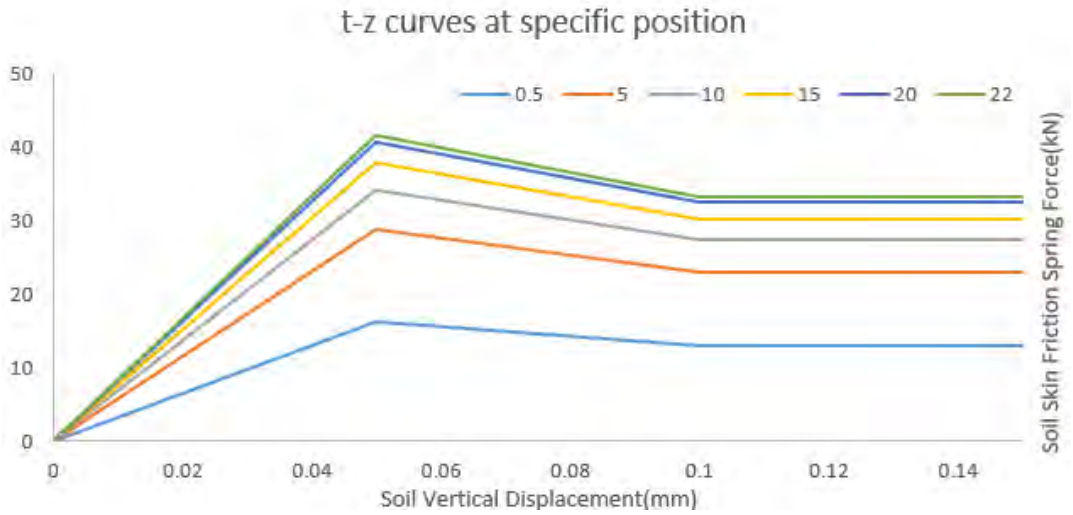

Figure 4.3 Actual shaft friction response curve '*t-z*' at specific depth.

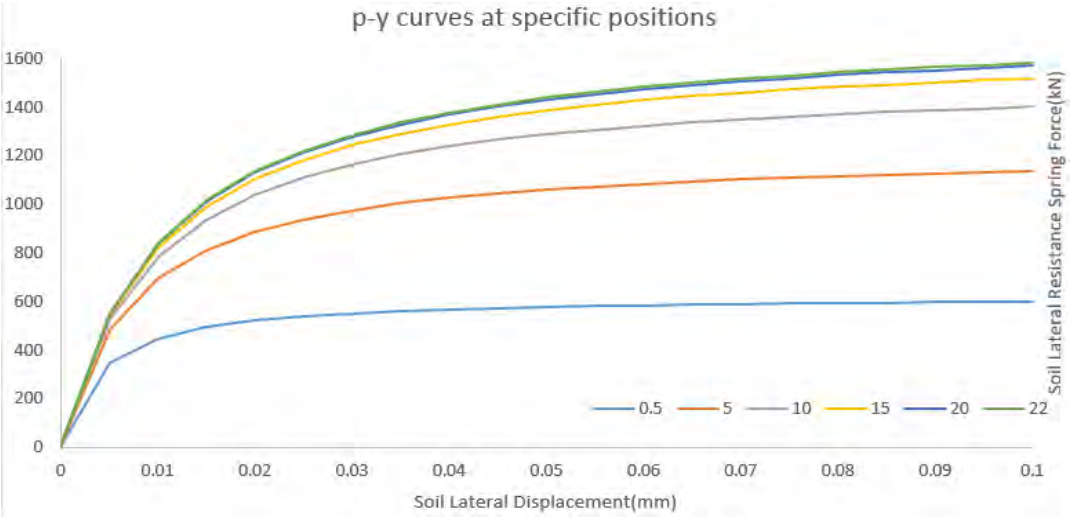

Figure 4.4 Actual lateral resistance response curve '*p-y*'.

4.2. Structure Response

Tower

Decomposing the structure as displayed in the simulation, the attention is focused on the positions where constraints are placed or loads are imposed. Confirmed by the analysis output(figure A.1 and A.2), the points of interest are which are primarily examined through this thesis are

- The level of installation of the rotor, 150 meters height
- The level of cables attachment, 75 meters height
- The level of sea surface, 41 meters height
- The level of shallow foundation, 0 meters height

Supposing that the wind is acting without the involvement of waves, the results are bearable (Table B.4). The curvature changes sign at the level of the sea (Fig. A.1), although at this stage of the analysis the waves are inactive. Studying the path of the horizontal displacement, it is concluded that two peaks are formed, a negative at the level of the sea and a positive at the level of installation of the rotor. The constraints imposed are also tested, showing functionality in safe boundaries by limiting the lateral displacement sufficiently and providing the structure the stability required, preventing primarily dangerous eccentricity and resisting the overturning moments. In terms of vertical displacement along the body of the tower, the interest is limited by serviceability and ultimate limit state, with the exception of the displacement of the base, which may imply frailty of the soil beneath. Therefore such scenario is not displayed in the exclusive action of wind.

Referring to the axial forces, the results are reasonable as they are directly formed by the involved vertical forces. Such forces are the dead load and the pretension that form the axial stress, dominant in conditions of calmness. So are the shear forces, which are successfully absorbed by the cables and the shallow foundation without any critical displacement occurring. Therefore, the bending moments, which are dominant due to the large distance that the structure offers for their amplification, consist an obstacle to the cooperation between the tower and the shallow foundation. Despite the precautions taken by the design of the foundation, which target to the free rotation of the base, in order to avoid the concentration of moments on the base, which would imply the concentration of normal stresses and further settlements, such concentration has occurred and it is considerable (Fig. A.2).

By adding the action of waves in the same direction as that of wind, it is estimated that such action is beneficial to the horizontal kinematics of the structure, as eliminates the deflection and the tilt that it causes. Still the action is limited to percentages up to 8% (Fig. 4.5), if the comparison is made with the maximum displacement as base, rendering the wave action of less importance than the wind to the structure and base kinematics. What is pointed out as the significant contribution is the fact that it relieves the base from the bending moment imposed by the wind, with overall variation 130% ,net reduction of 80%, of the initial moment (Fig. 4.8).

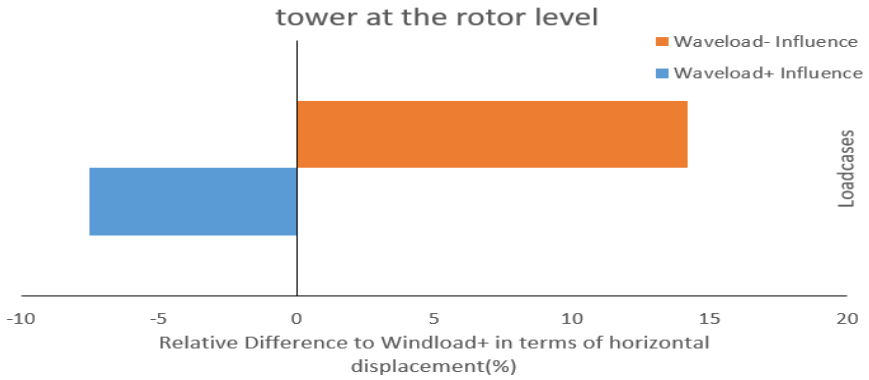

Figure 4.5 Wave Influence at horizontal displacement of top(%).

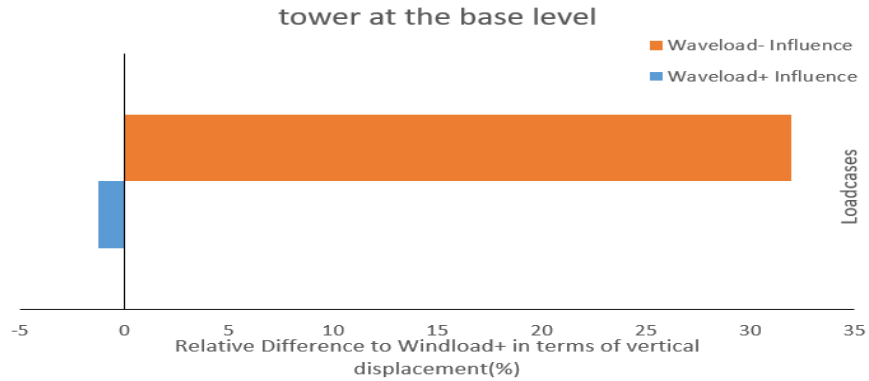

Figure 4.6 Wave Influence on vertical displacement of base(%).

Finally, by reversing the action of waves to be opposite to that of wind, the worse loading scenario comes in surface for the superstructure. This pair of external forces creates a powerful moment that the structure is summoned to carry, with serious impact to the deflection of the structure and the cooperation of the shallow foundation with the soil beneath. It provokes further displacement at the top of the tower at the order of 14% (Fig. 4.5) and gives the variation of the bending moments a slightly different form to that provoked by exclusive wind action (Fig. 4.8). Still, these changes are foreseen and none of them mentioned violates any serviceability criterion. The unexpected is the fact that such

horizontal action of waves has serious impact at the vertical response of the shallow foundation, which provokes augmentation of the vertical displacement by 35%(Fig. 4.6).

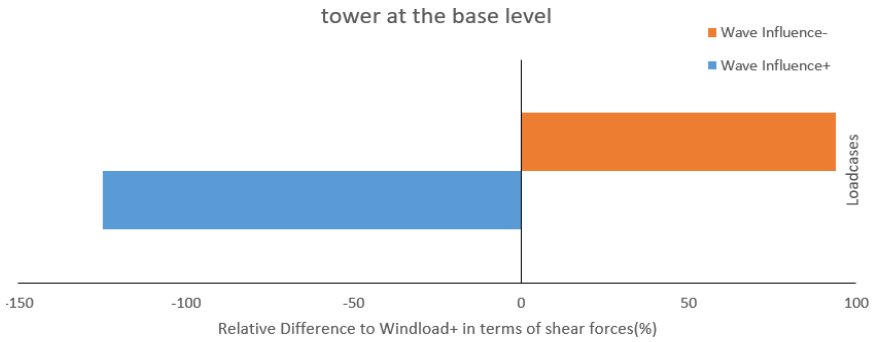

Figure 4.7 Wave Influence on shear force of base(%).

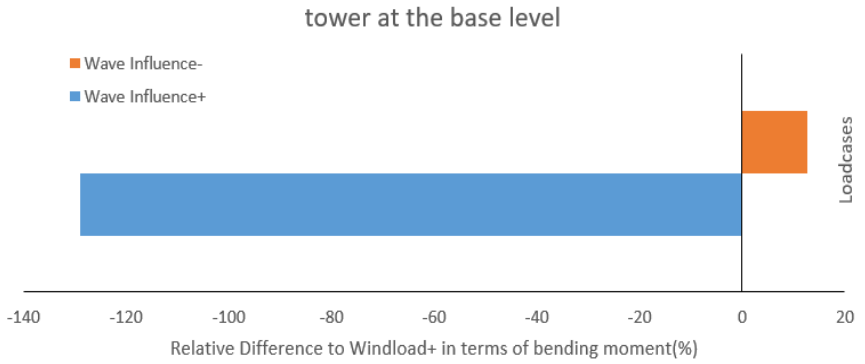

Figure 4.8 Wave Influence on bending moment of base(%).

According to the results produced, the worst loading scenario in terms of lateral deflection is the case where wind and wave act in opposite directions. Still, none of the results displayed in terms of displacement violates any safety criterion. Specifically, even if the maximum magnitude is 1514 mm, it is actually a result in the margin of acceptance of serviceability criterion which indicates a maximum tolerance 0.01 rad of tilt[Lombardi et al]. Moreover, focusing on the interaction between the wind and the wave forces, it is estimated that the wind is dominant over the wave as it defines the bending moments of the tower which are an order of magnitude larger than any other resultant. By the time the interaction between wind and structure is controlled by the torsional rotation of the blades, the WT can be in constant surveillance and can operate with safety, no matter how puissant the wave force turns out to be.

Shallow Foundation

Focusing on the base of the tower, it is pointed out that the two major conditions that it is summoned to face are

- the vertical dead and pretension load that need to be transferred to the soil without excessive deflection

- the imminent moment which may imply rotation that complicate the interaction with the soil with harming influence to the overall response

As it is concluded, the axial force which is transferred down to the foundation is relatively constant, whose possible variation is due to the increase or relief of the pretension, therefore such variation can be assumed as a matter of minor importance.

Due to the touching conditions of the interface between the soil and the circular slab, the shallow foundation consists the member which is sensitive to large rotations as a result of the differential vertical displacements taking place along its length. Soil yielding is expected, but due to its substitution with springs, the phenomenon cannot be studied in depth, except from the fact that it has taken place and the irreversible large displacement it may provoke. In addition, partial detachment is expected between the slab and the soil. Such phenomenon would be a serious sign of instability and a threat to the superstructure itself. Practically, if it surpasses the percentage of 33% of the total length, it would reduce the active interacting surface significantly and may lead to high concentration of stresses at the touching interface between the slab and the soil beneath it.

Thanks to the cables attachment, operating as a lateral displacement constraint in terms of statics, the shallow foundation is minimum exposed to actions that tend to laterally dislocate it. Displayed by the output of the analysis (Fig. 4.9), the absolute values of horizontal displacement are negligible to the horizontal displacements overall, yet the resistance provided is sufficient.

On the other hand, the transfer of the vertical loads and moments to the soil consist a much more complex matter. In agreement with the static analysis that gives greater moment in the case where wind and water are of opposite direction, the slab shows excessive differential vertical displacement and absolute settlement magnitude in the position of tower attachment.

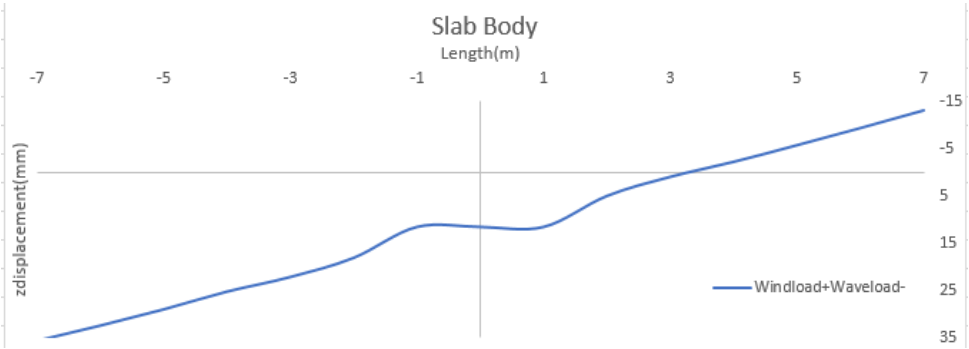

Figure 4.9 Horizontal displacements of the foundation slab.

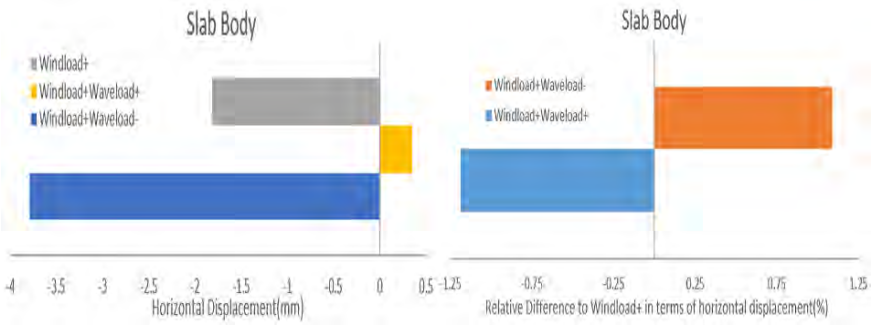

Figure 4.10 Maximum Vertical Displacement of the foundation slab.

Specifically, the settlement of 11.53 mm corresponds to 31% of maximum vertical deflection expressed so far at the top of the tower(figure 4.10), which is the maximum vertical deflection along the tower (Fig A.1).

Studying this matter by soil's prospect, the interaction between it and the slab is driven to its limits. Displayed in the Fig. 4.11, there is constant plastification of the soil due to vertical loading. The region of that zone fluctuates regarding with the bending moments that are transferred to the base by the superstructure. According to the results that have been displayed, the most favorable situation is when the environmental loads are of the same direction and the worst is when they are opposite. It has been expected that accompanied by the vast plastification zone goes extended detachment. Specifically, the detachment taking place in the worst loading scenario starts at the tip of the slab and expands to 4 meters to the interior of slab. Such region corresponds to the 28.5% of the total length of the slab which is acceptable in terms of stability. Therefore, this detachment region implies sensitivity to further rotations and operates at its limit. Since the normal stresses gives limited output as it has reached its extremity, further information is provided by the displacements in figure 4.10.

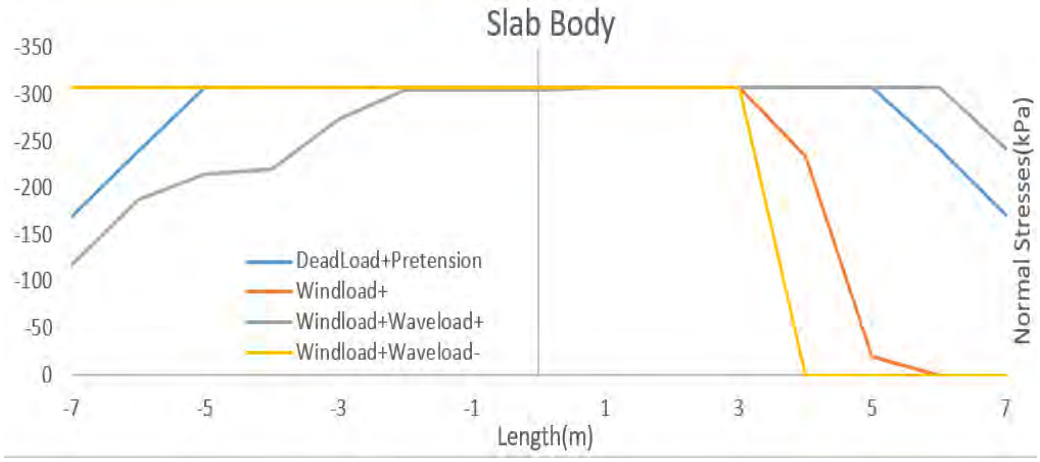

Figure 4.11 Normal stresses distribution along the foundation slab.

Cables

Operating as a lateral displacement constraint in terms of statics, the cables are the basis of the control of the deformation of the tower and consist an essential element of the structural system. Working at pairs, the amount of extra tensioning to the one side implies the same amount of relief to the other. As proven in the results (Fig. 4.12), the cables are sufficient carrying the largest tension imposed, of magnitude 11377 kN, tracked in the loadcase when both wind and wave act at the same direction, with an over sufficient factor of safety of 6.16. Additionally, the pretension of the cables is also capable to keep them in constant tension, having the lowest axial force of magnitude 2581 kN, which corresponds to the 36.25% of the initial pretension force.

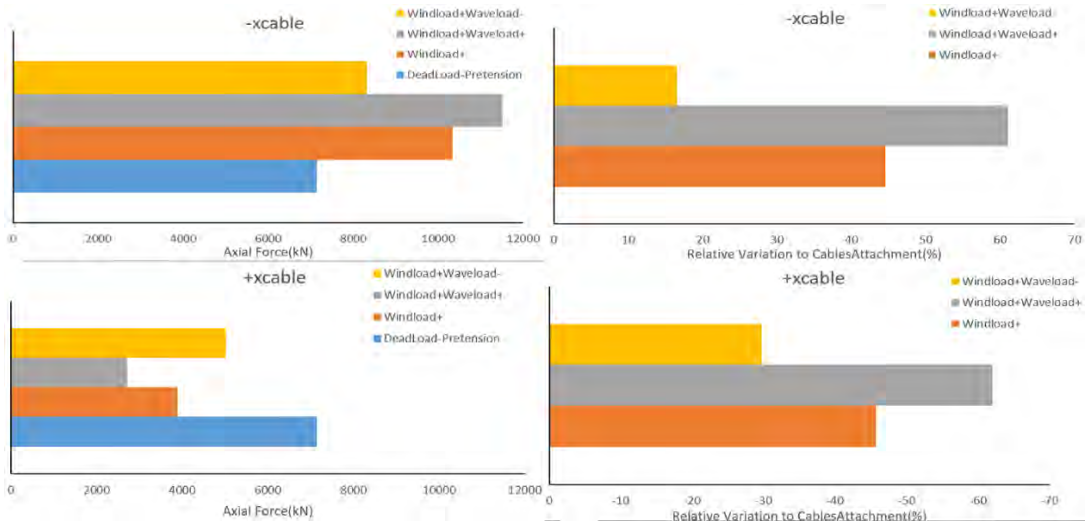

Figure 4.12 Cable axial forces and relative comparison.

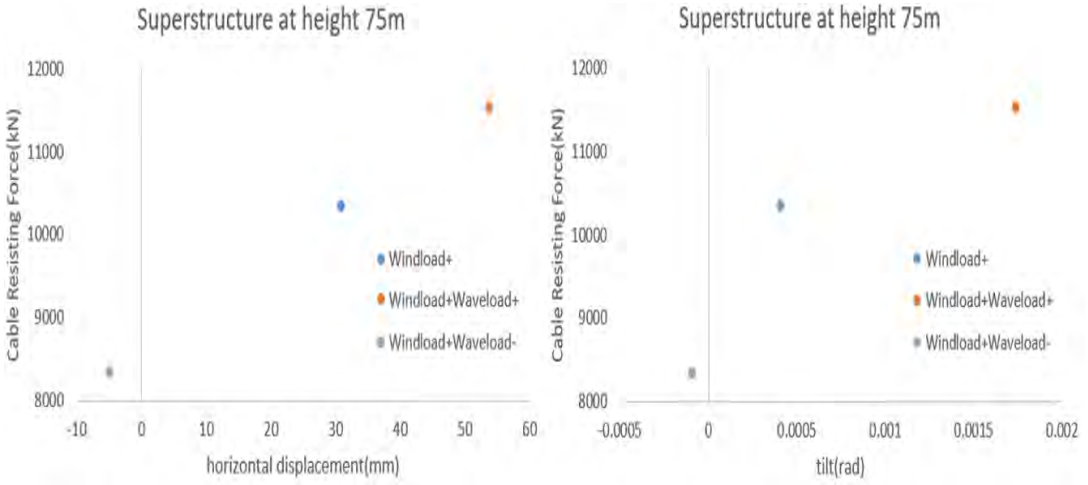

Figure 4.13 Superstructure horizontal displacement and tilt at cable attachment level.

Besides the importance of cables ultimate axial load, equal importance has their capacity of restraining the tower at the level of 75 meters from diverging laterally, which is actually a matter of provided stiffness. Shown by the results output focused at height of 75 meters, the lateral deflection leads to tilt which minimum in comparison with the rest of the positions along the tower length (Fig. 4.13), proof of the sufficient stiffness granted by the cables.

4.3. Lateral Pile Response

The forces carried by the cables are directly transferred to the anchor piles and then to the soil around them. The piles are in continuous state of extrusion, even in condition of calmness due to the requirement of transferring the pretension force to the soil. By previous study of the variation of the axial force of the cables, it is concluded that the extreme loading scenario for both sides of piles is the one when wind loading has the same direction with the wave loading. Three positions are pointed out to describe the vertical kinematics of the short piles response

- Horizontal displacement of the head
- Horizontal displacement of the tip
- Neutral position about which the pile rotates

The most extreme displacements in terms of magnitude and variation due to different loading imposition take place at the head of the pile (Fig. A.4). On the stressed side, it is concluded via relative comparison that in the worst loadcase, the displacement has increased about 55% from the initial state(3.6mm to 6.6 mm), following closely the variation of the cable force whose augmentation is about 60% (7147kN to 11511kN). Such close analogy in the variation of stress and displacement implies elastic behavior of the soil, which is expected at the small strains, as described by the p-y theory. On the relieved side, the stress path is opposite, following the direction of unloading, where the variation of displacements path a steeper gradient due to smaller displacements than the loaded one. Alongside with the head is transposed the tip of the pile, following the body of the pile preserving a constant ratio to the head displacement of 0.2, indicating a constant position of rotation at 18 m depth as the $^{4}/_{5}$ of the total body length.

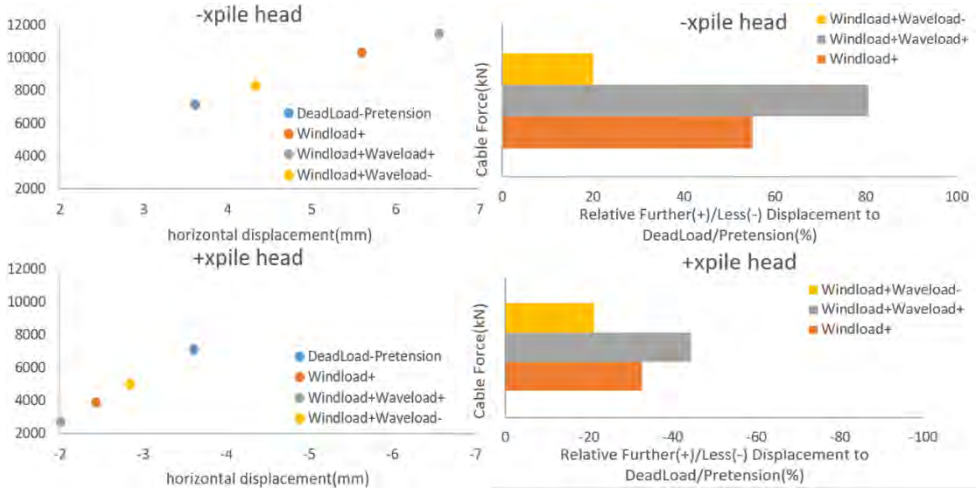

Figure 4.14 Lateral Head Deflection of pair of opposite piles.

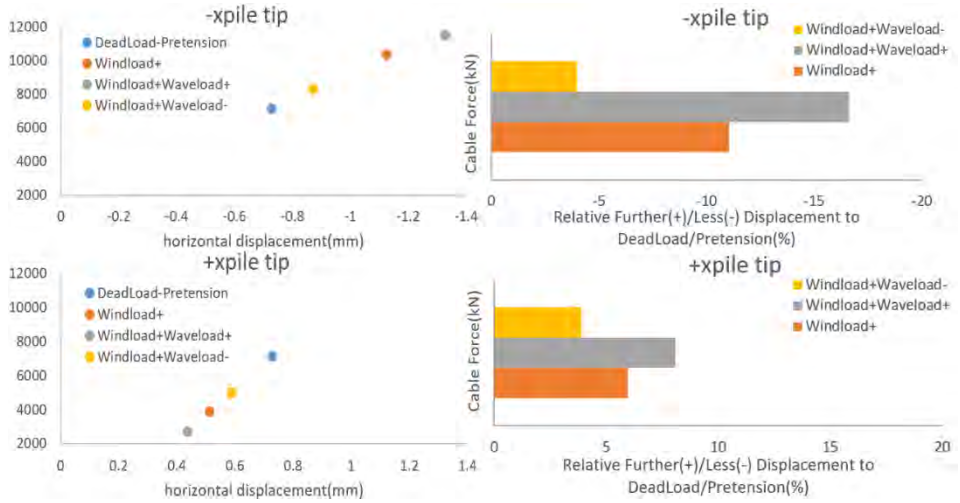

Figure 4.15 Lateral Tip Deflection of pair of opposite piles.

In order to clarify the response of the pile as a structural element, it is isolated and studied. The distribution of the shear forces (Fig. A.6) is a precise guide of the lateral earth pressure that it is opposed to(Fig. A.5), as they are linked by the following differential equation

$$\frac{dQ(x)}{dx} = q(x) \tag{31}$$

Q :shear force in position x [kN]

q :lateral pressure imposed by earth [kN/m]

The boundary condition on the top of the pile is directly derived from the horizontal component of the force imposed by the cable. The diagrams display the relieving interaction of the soil which fades the resultants to zero as the stresses are gradually transfer to the neighbor interface. Directly it is concluded that the actions in the region near the head of

the pile are the maximum (Fig. 4.16). Yet, there is another peak displayed at the position of rotation, characteristic of every short pile, which is due to the opposition of the lateral passive earth pressure, but in the current study it is negligible, by the time it's the 9% of the maximum (Fig. A.5). Continuing, particular interest is found on the start and the progress of the bending moment distribution (Fig. A.7).

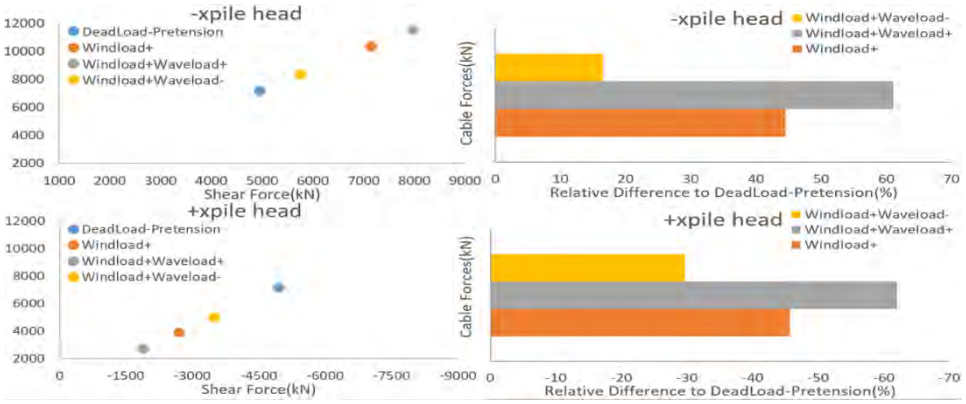

`Figure 4.16 Shear force at head of pair of opposite piles.

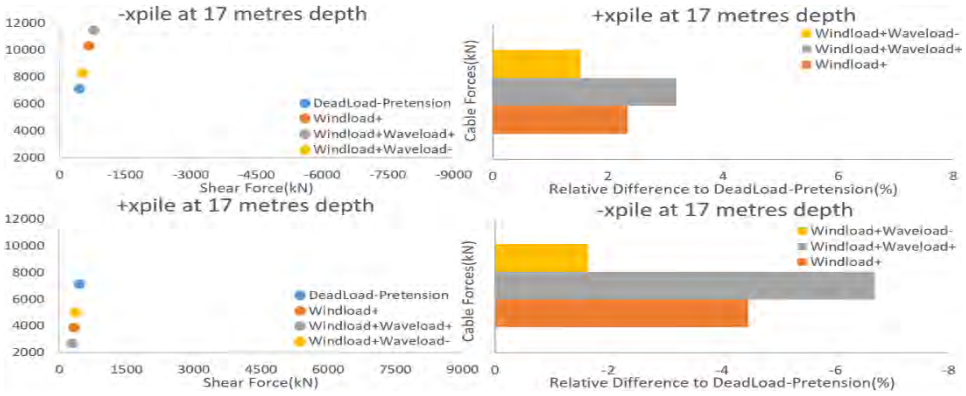

Figure 4.17 Shear force at level of rotation of pair of opposite piles.

The bending moment are linked to the shear forces through the fundamental differential equation of mechanics

$$\frac{dM(x)}{dx} = Q(x) \tag{32}$$

where

M : bending moment at position x [kN*m]
Q : shear force at position x [kN]

The difference and the outstanding in the current project is the application of the cantilever. By adding a cantilever at the head of the pile, automatically a reverse bending moment is created as the product of the vertical component of the cable force and the cantilever length

(Fig 4.18). In the project studied, the bending moment at the head of the pile is the maximum, followed by another at 13 meters depth, whose absolute value is the 11% of the maximum (Fig. 4.19). This maximum bending moment contributed by the cantilever beam is opposed to the action that tends to rotate the pile, consequently it moderates the kinematics of the pile, except from relieving the developed internal normal stresses.

In terms of interaction with soil, this pile rotation is important to be constraint in small strain sector, where elasticity modulus is high and there is still the possibility of return to initial state. Although plastification is expected, especially near the soil surface, it is essential to be constraint, else post-peak phenomena may occur which are accompanied with large displacements and unpredictable soil response, an irreversible situation that may become fatal for the stability of the system. The design has reserved very satisfying results in this matter, as the plastification zone doesn't exceed the limit of 5 meters depth, fact that in combination with small displacement, has granted a sufficient resistance against lateral loading (Fig A.5).

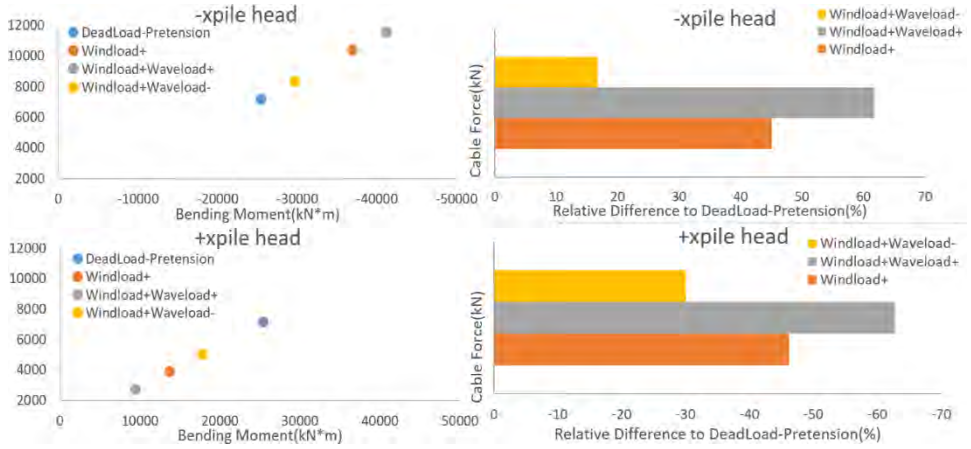

Figure 4.18 Bending moment at the head of pair of opposite piles.

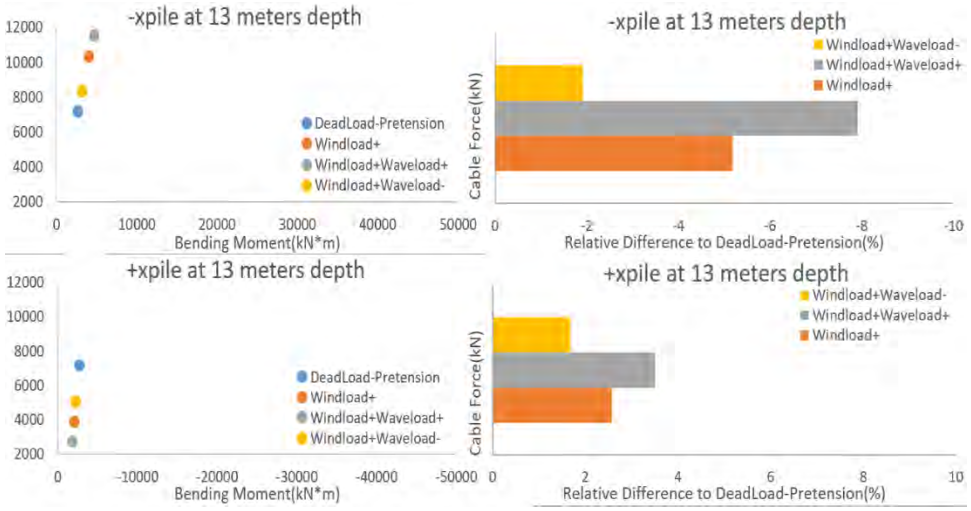

Figure 4.19 Bending moment at 13 meters depth of pair of opposite piles.

4.4. Axial Pile Response

The study of the vertical response of the pile is an order simpler than the lateral as the response is of single direction and of one dimension at the vertical axis. The piles are in constant state of extrusion, except one condition tracked at the relieved side when the wind and the wave act in the same direction (Fig. 4.20). The condition tracked is the one that the cable is least stressed among the rest of the cases, relieved in such degree that the pile's dead weight overwhelms the extracting force by 104%, by exact ratio of 2001 kN to 1921 kN. In correspondence with the lateral response, the shaft resistance provided by the interface between pile and soil defines the variation of the axial forces taking place in the element, linearly smoothing down the action along the pile, leading to zero at the tip region. To express the influence of the surrounding soil to the axial forces developed in the pile, the following differential equation is formed

$$\frac{dN(x)}{dx} = \tau(x) \tag{33}$$

where

$N(x)$: axial force in position x
$\tau(x)$: shaft resistance in position x

The value of the axial force on the top of the pile that defines the boundary value problem is given as the vertical component the cable force vector(Fig. 4.21). As it is displayed in the axial forces diagram (Fig. A.10), it is the maximum resultant along the length of the pile. According to elastic constitutive law, the concentration of axial forces provoke maximum strains at the same regions. Such strain may not be crucial for the pile as a structural element, yet they affect notably the activation of shaft resistance around pile's circumference (Fig. A.11). Specifically the strength to stress ratio of the surrounding soil doesn't vary linearly, as a rigid body pile movement would indicate, but it has a hyperbolic form for the first six meters of the pile (Fig. A.12). In extreme conditions of loading these ratios verge 80% to 90%, fact that implies partial slip of the upper zone. However, these ratios are limited at 28.5% of the total length of the pile indicating extra capacity of the pile against extrusion.

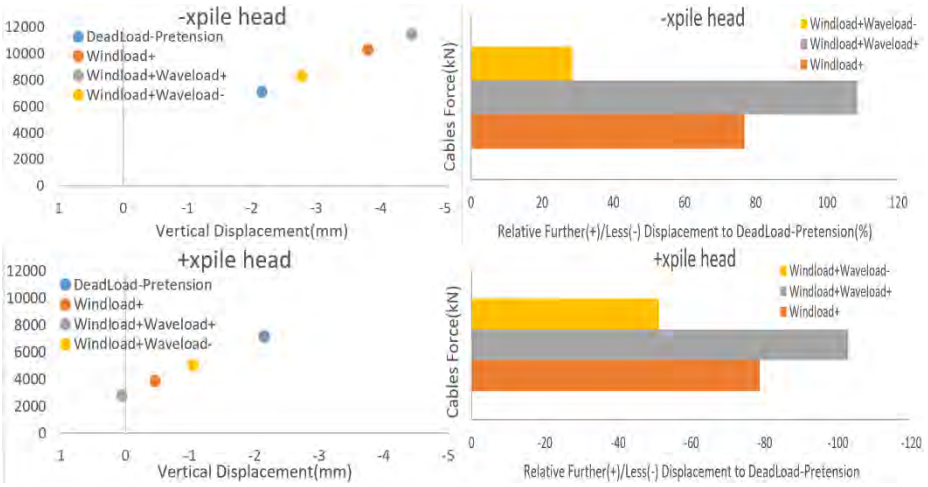

Figure 4.20 Vertical Head Deflection of pair of opposite piles.

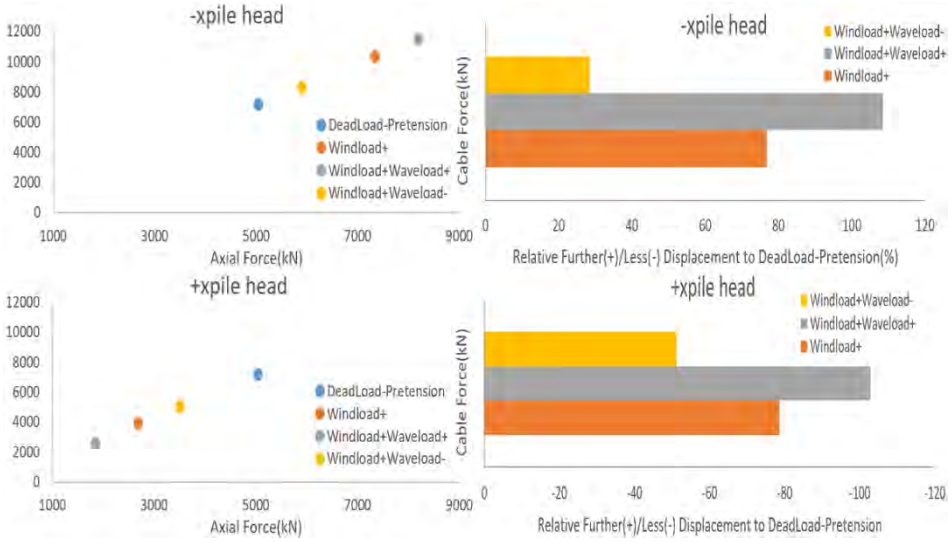

Figure 4.21 Axial Force at the head of pair of opposite piles.

4.5. Cantilever Influence

Cable Response

In order to highlight the contribution of the bending moment boundary condition applied by the cantilever addition, another analysis has been carried out where the cable attachment has been installed directly on the top of the pile(Fig. 4.22). Through the rest the thesis the condition of cooperation between pile and cantilever beam will be referred as **WC** (with cantilever), else the condition of absence of the cantilever will be referred as **NC** (no cantilever).

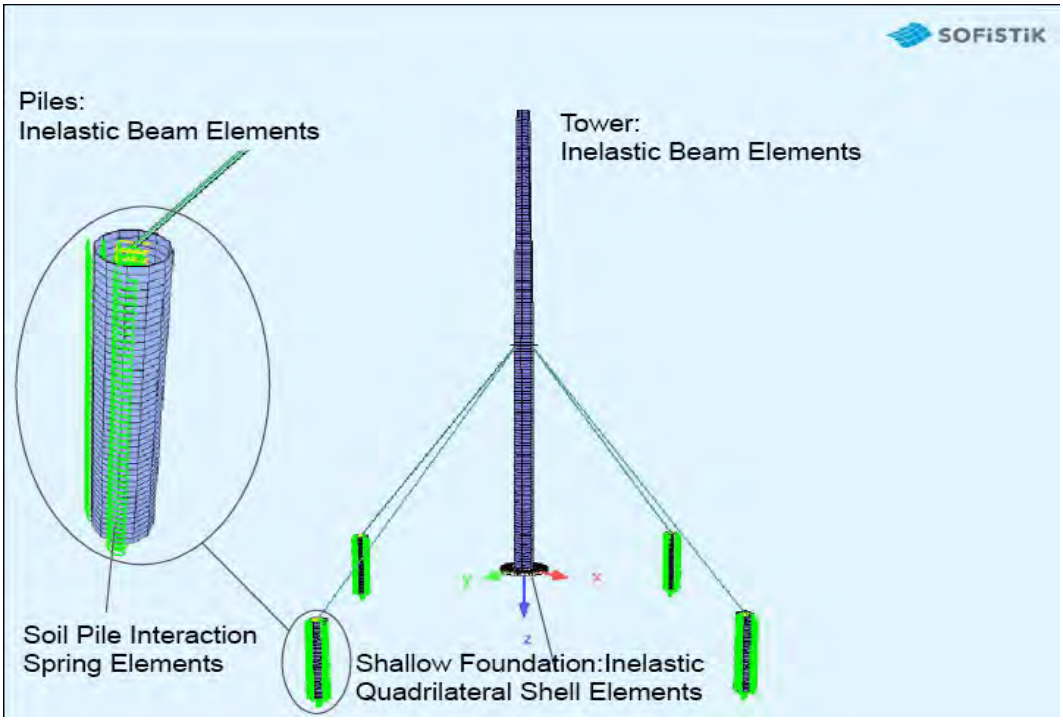

Figure 4.22 Overall aspect of the simulation model without cantilever prevention on reaction piles.

Despite the difference in pile head displacement due to the, the pretension carried by the cables is affected in minimal degree intervention as displayed in Fig. 4.23. The reduced displacement of the piles actually increases the axial forces that rule the cables about just 5% which corresponds to absolute value of 240kN (Fig. 4.23). This fact is enough to exempt from a new analysis of the superstructure, as the results would be very close to the ones already extracted.

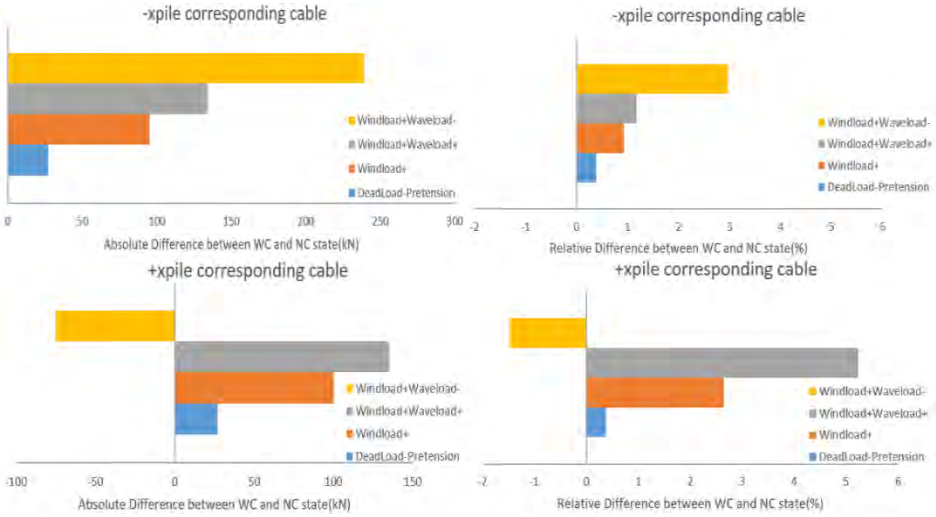

Figure 4.23 Difference in cables axial forces.

Pile Lateral Response

The absolute values of the lateral displacement at piles' heads without the cantilever beam intervention are displayed in Figs. 4.24 and 4.25 and the total response in Fig. A.14. There is difference in kinematics tracked, due to the additional freedom given to the body to rotate, which renders the pile of free headed conduct. Performing a relative comparison between the two versions of the pile which expresses the amount of relief taken place (Fig. A.24), it is revealed that the cantilever boundary limits the horizontal displacement

- at percentage of 54% compared to free head at the top of the pile (Fig. 5.25)
- at percentage of 21% compared to free head at the tip of the pile (Fig. 5.26)

The above values correspond to the case of the maximum cable force which arises from the combination of the wind and the wave acting in the same direction. Moreover, it is observed that the rotation position is transferred 4 meters higher, at 14 meters depth from the surface of the soil, defining new analogy of the bottom to top displacement which corresponds to value of 0.33. From the aspect of shear forces influence, the cantilever beam doesn't affect the starting point of their distribution, as it transfers the components of the cable force as they are. Still, it influences the lateral earth pressure which occurs in order to reach the kinematic equilibrium of the pile, especially in region where the pressure present peaks (Fig. A.15), which is indicated by the maximum of the horizontal displacement. Specifically, the head of the piles are disburdened about 20% to 30% of the lateral earth pressure that they are opposed to (Figs 4.26 and 4.27), providing a less steep gradient of shear degradation than that of the free headed state (Fig. A.16).

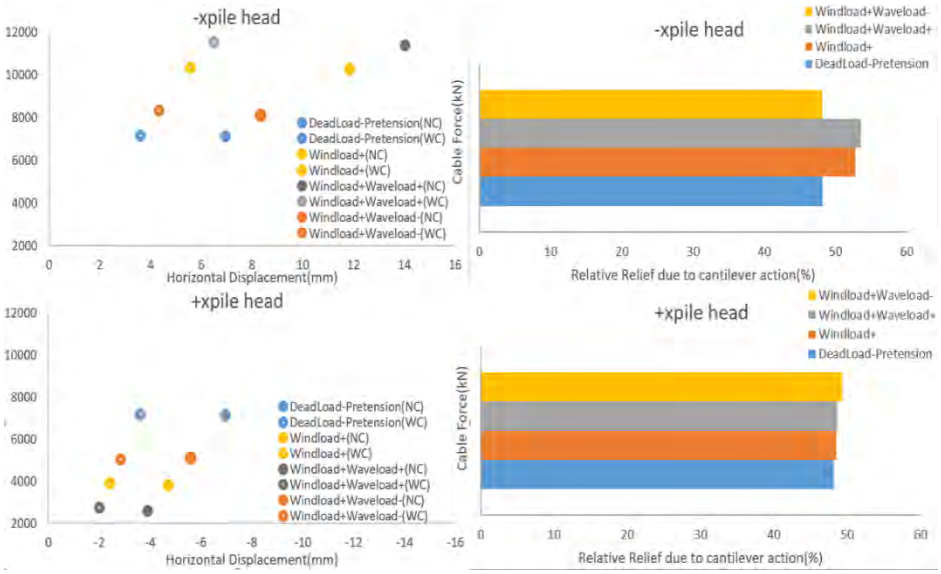

Figure 4.24 Head horizontal displacement of pair of piles.

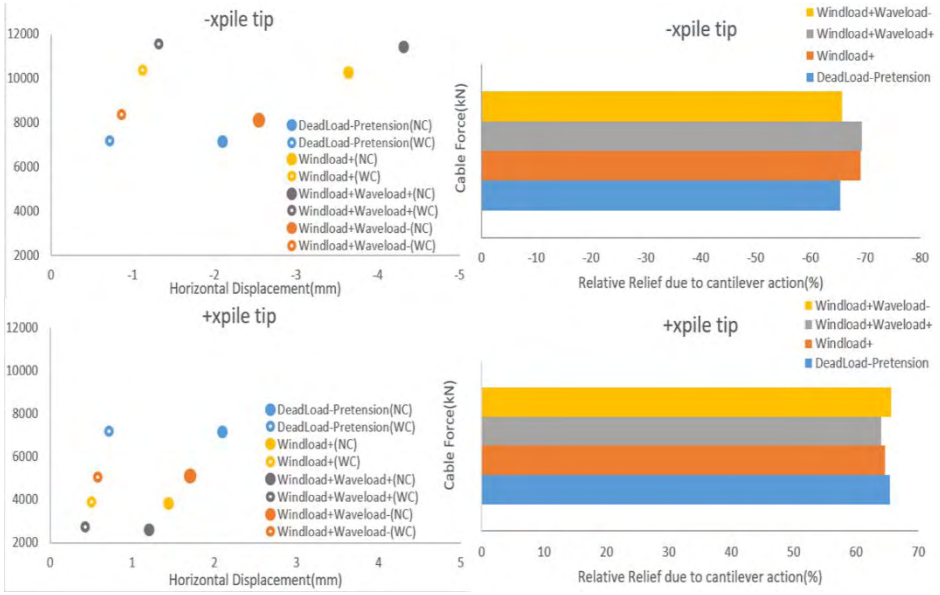

Figure 4.25 Tip horizontal displacement of pair of piles.

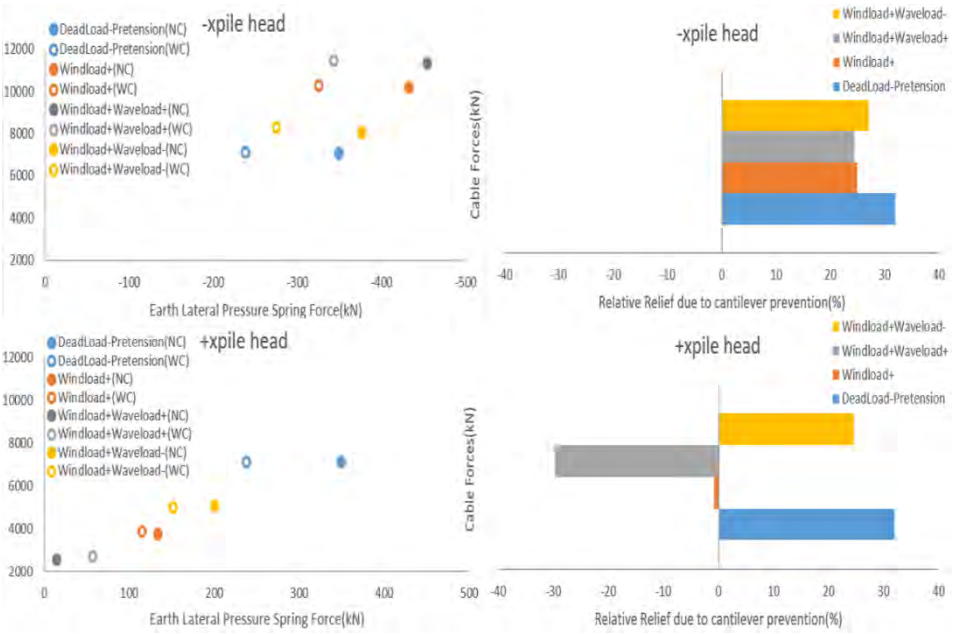

Figure 4.26 Head lateral earth pressure spring force of pair of piles.

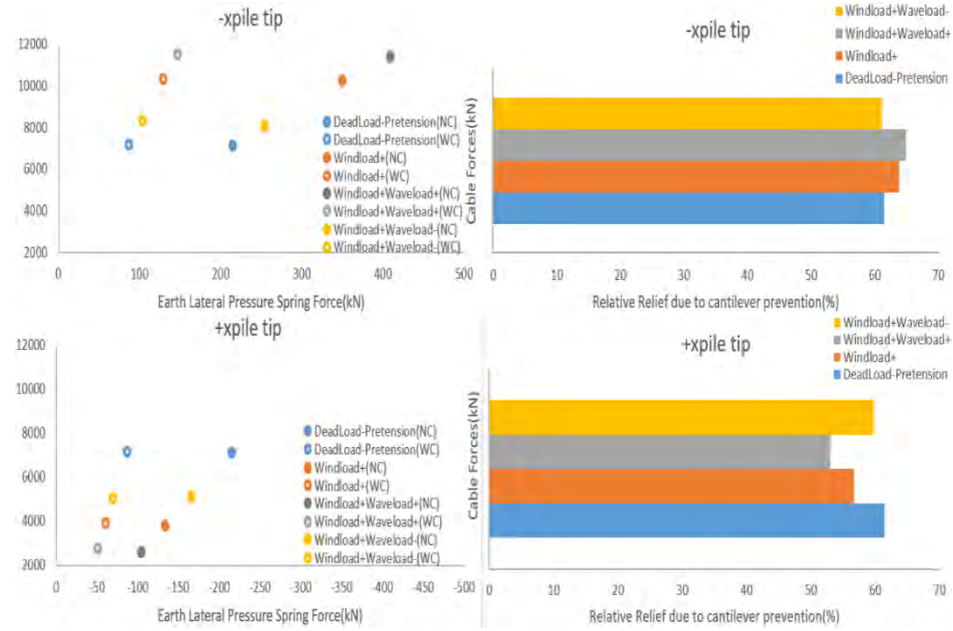

Figure 4.27 Tip lateral earth pressure spring force of pair of piles.

When examining the shear diagrams of the WC and NC states (Figs. A.6 and A.16), it is concluded that both of them resist the same lateral force at the top of the element, with the major difference that the pile of cantilever prevention shows smaller peaks. This is succeeded by exploiting vaster soil area in order to face the vertical force applied, rather than concentrating its resistance near the surface ,as implied by the level of sign alteration which is 8 m depth in NC and 14.5 m depth in WC. Due to the distortion of the curve that shows shear force distribution, there is no point at examining certain levels, but performing straight comparison between the maximum values indicated(Fig. 4.29).

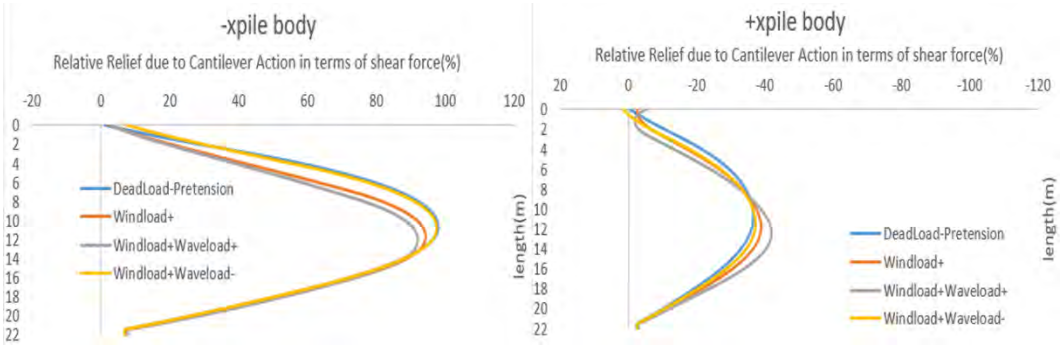

Figure 4.28 Relative Relief in terms of shear force of pair of opposite piles.

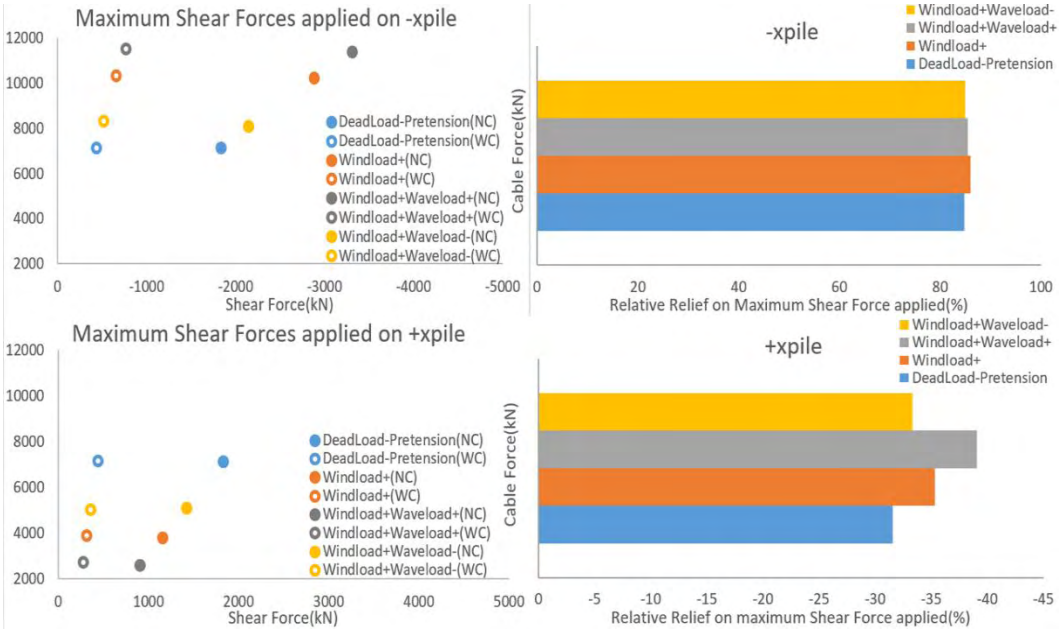

Figure 4.29 Relative relief in terms of shear force of pair of opposite piles.

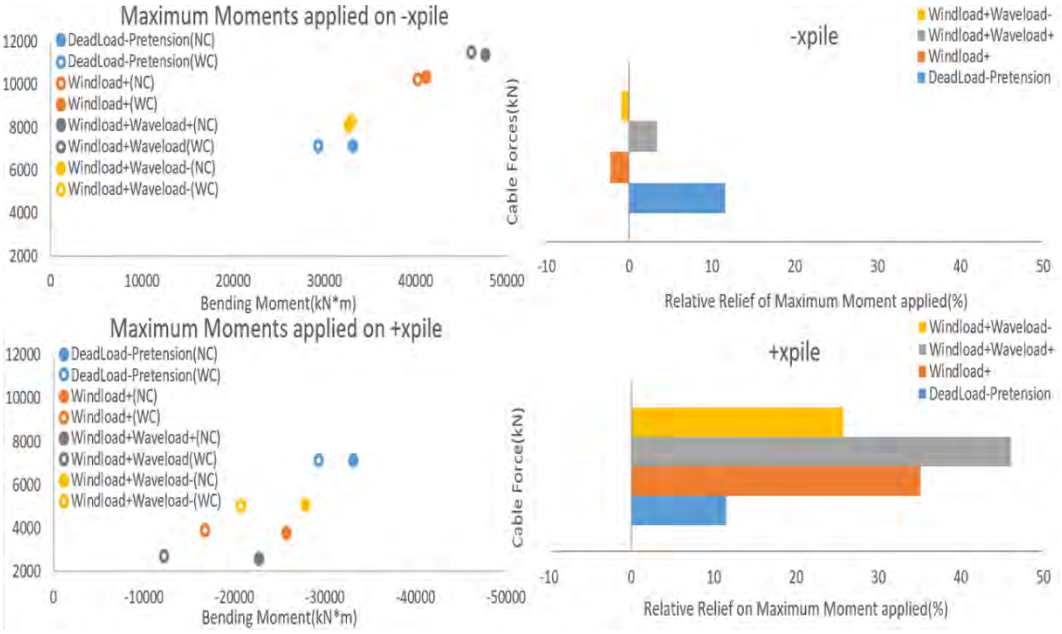

Figure 4.30 Relative Relief in terms of bending moment of pair of opposite piles.

According to the bending moment diagrams of the two states (Figs. A.7 and A.17), the boundary at the top of each pile changes radically the formation of the distribution curve, consequently there's no point at comparing the absolute values side to side. Indicatively, at the extreme case of wind and wave loading acting at the same direction, it is figured out that the variation of the ultimate magnitude is significantly reduced (Fig. 4.30).

The new boundary which is rendered by the cantilever may affect the shape of the distribution curves but overall it doesn't affect significantly the range where the values are varying. The limitation of the displacement focuses on keeping the surrounding soil in a fine condition in terms of plasticity. In the case where the pile responds as free headed and shows large displacements, the soil is plastified to deeper lengths down to 9 meters as well as at the tip of the pile (Fig. A.18). This situation may be proved problematic because the plastification implies irreversible strains and unexpected soil behavior leading to large displacements, which gradually downgrade the pretension that the cables are equipped with, along with the ability of the soil to receive superstructure loads.

Vertical Response

Studying the two version of the pile subject in terms of vertical kinematics and stress developed, the results extracted show negligible contribution thanks to the cantilever (Fig. 4.31). In contrast with the lateral response study, the vertical response is a one dimensional matter(without any rotations) along the vertical axis, as the phenomena along the body of the pile are relatively constant (Fig. A.19), concluding that the magnitude that takes place at the head of the pile is representative for the rest of the pile.

By the time, the vertical displacements of the pile are small enough to correspond to the linear elastic zone of the soil surrounding the pile, negligible variations to the displacement imply similarly negligible variations to the soil shaft resistance against extrusion (Fig A.28) and to the axial forces distribution (Fig. A.29). Yet, the soil substitution with springs is a numerical method that decouples fully the response of the soil at vertical and horizontal direction and cannot apprehend phenomena that distort the interface between the two elements, like possible detachment that would reduce the interacting surface.

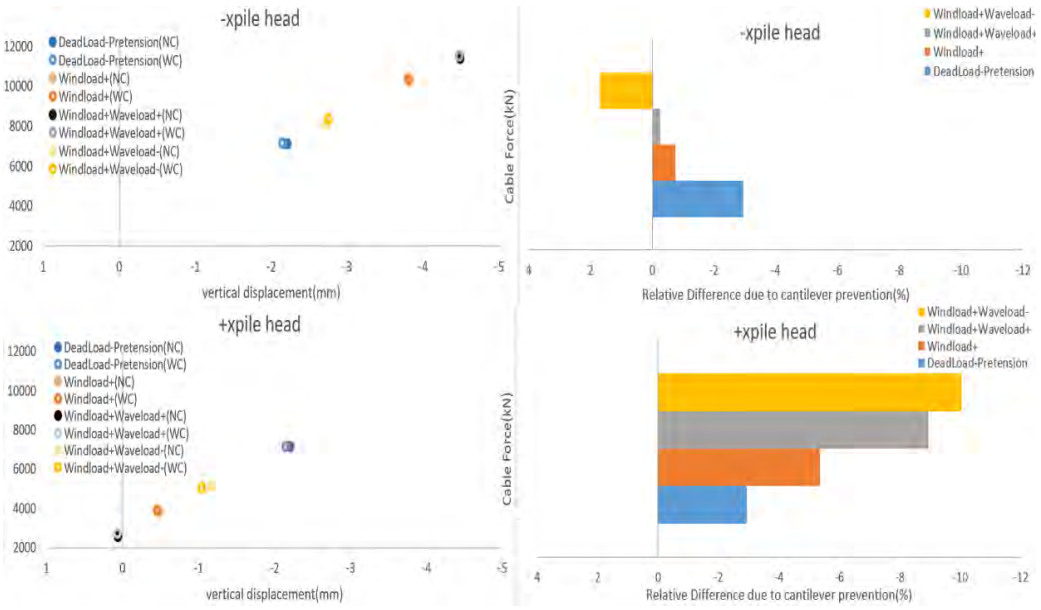

Figure 4.31 Relative reduction in terms of vertical displacement of pair of opposite piles.

4.6. Reaction piles: Mode of behavior

To avoid divergence due to the decouple of vertical and horizontal response and simulate the case better in such sensitive matters, a three dimensional analysis has been carried out in order to study the beneficial intervention of the cantilever beam addition to the interaction between the pile and soil exclusively. For this purpose, the commercial finite element code MARC Mentat by MSC Software has been utilized to simulate the interaction mechanism between soil and pile. The finite element model, which includes the pile under extrusion and the surrounding soil, targets on representing a concentrating output of the pile kinematics with or without cantilever intervention. The materials utilized are steel and clay (Table B.11) and the interaction between the contact bodies (Fig. 4.32) is under touching conditions, implying possible differential displacement(slip) and separation (Table B.12). Finally, the forces applied on the pile by the cables are directly taken from the SOFISTIK analysis.

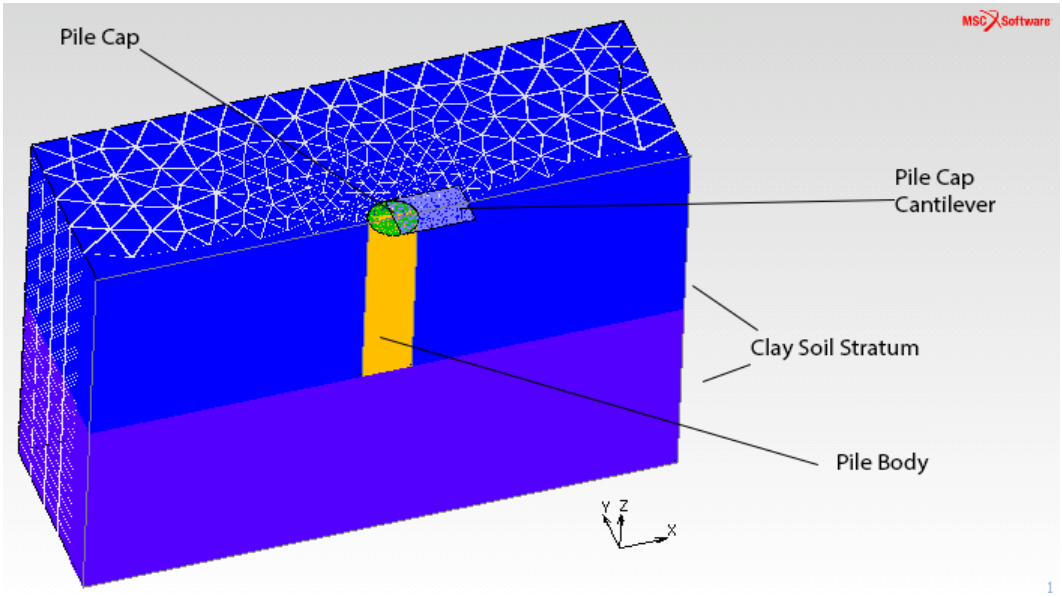

Figure 4.32 Three Dimensional Simulation of pile under extrusion.

In order to save computational time and resources, the two different states are applied to the same model by changing the position of force application.

Along with the several advantages given by the three dimensional analysis processing, there are many advanced options at the post processing stage and specifically at the presentation of the output. Particularly useful is the vector representation of the displacement in space, which shows the net influence of the cantilever to pile kinematics. By comparing the different version of pile loading (Figs 4.34 and 4.35), it concluded that the rotation of the pile body is severely constricted and its verticality is maintained, adopting the response of a fixed head pile. Moreover, the comparison between the displacement magnitude output reveals

great limitation thanks to the cantilever, especially at positions near the soil surface, that tend to be up to three times greater than the ones given by the SOFISTIK analysis (Fig A.30). Indicatively is cited the detailed comparison of the displacement taken place at the head of the pile. It is obvious that the relative difference between the two version is reduced as the imposed loads are augmented, as 60% of loading increase leads to 51% relative difference reduction (Fig. 4.33). Even if the gap between the absolute values remains large, such response to the loading increase implies that the fixed head condition is set for a range of imposed loading, surpass of which may cause the loss of pile's verticality. Therefore, in terms of safety, the design of the cantilever beam is sufficient.

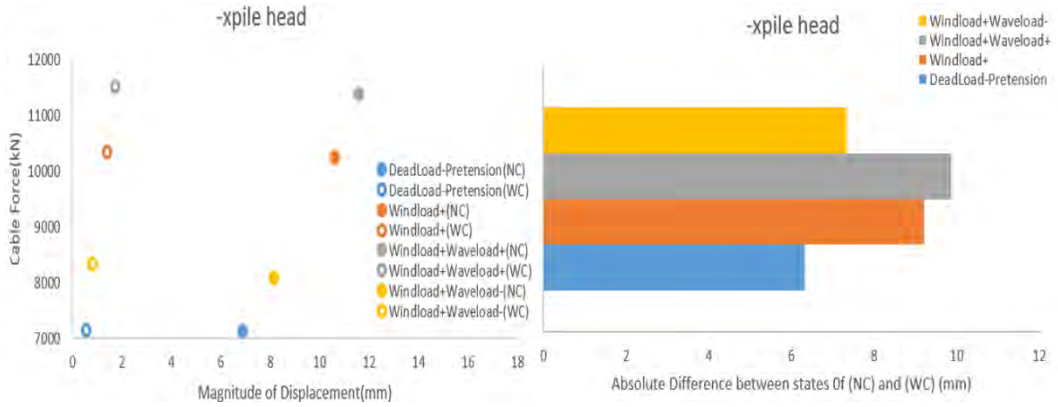

Figure 4.33 Variation of displacements at the pile head for the load cases imposed.

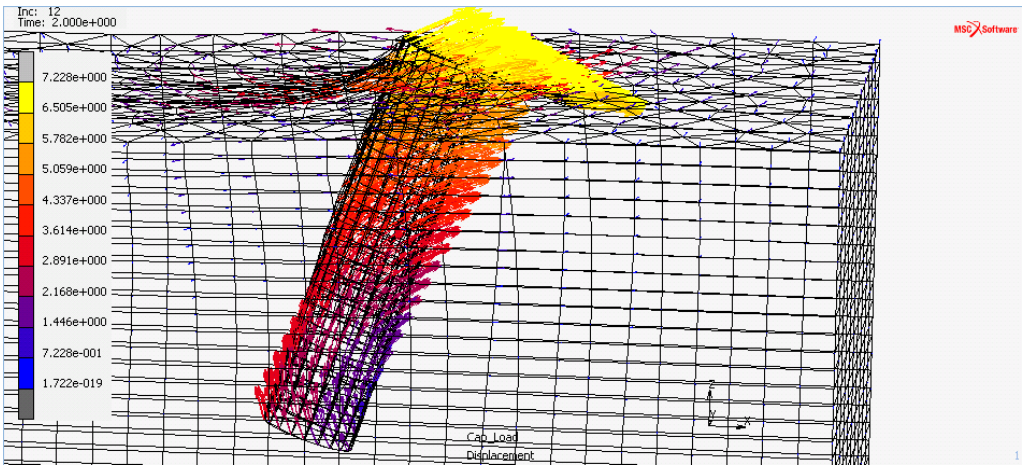

Figure 4.34a Three dimensional vector representation of pile displacement output at NC state(mm), at load case Dead Load-Pretension.

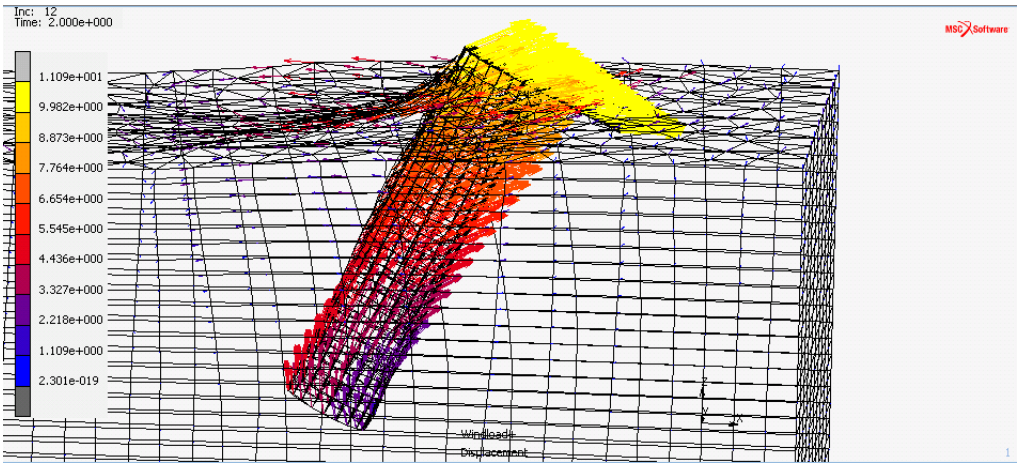

Figure 4.35b Three dimensional vector representation of pile displacement output at NC state(mm), at load case Windload+.

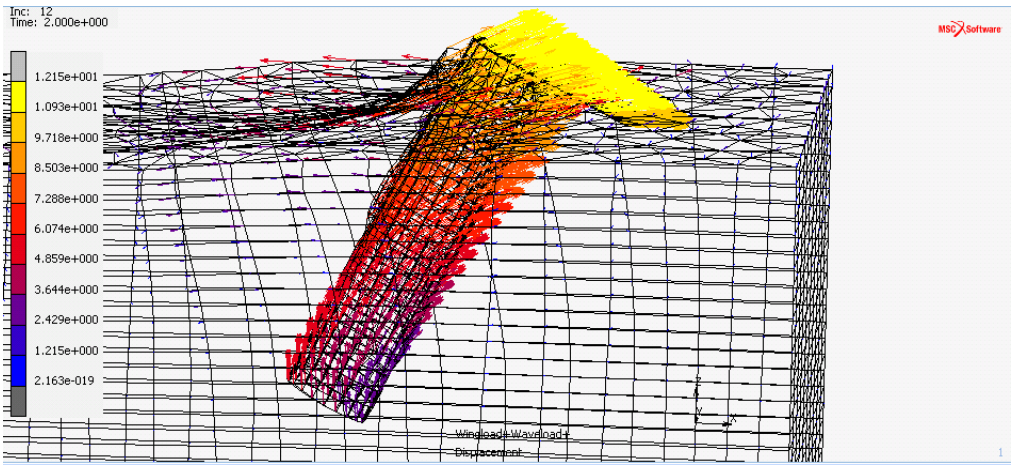

Figure 4.36c Three dimensional vector representation of pile displacement output at NC state(mm), at load case Windload+Waveload+.

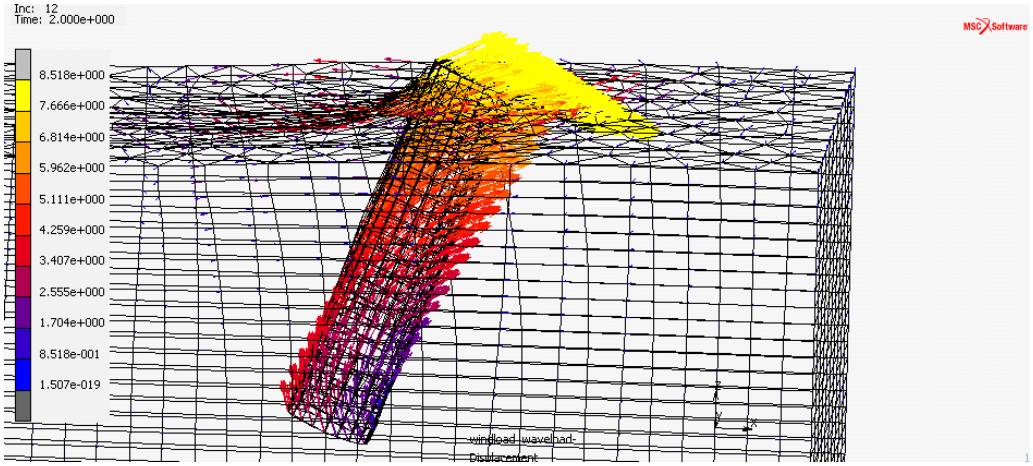

Figure 4.37d Three dimensional vector representation of pile displacement output at NC state(mm), at load case Windload+Waveload-.

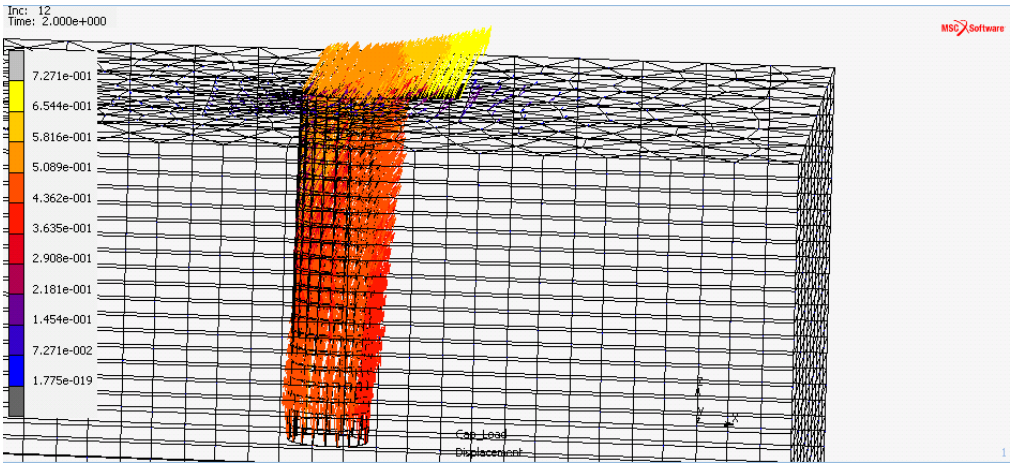

Figure 4.38a Three dimensional vector analysis of displacement output at WC state(mm), at load case Dead Load-Pretension.

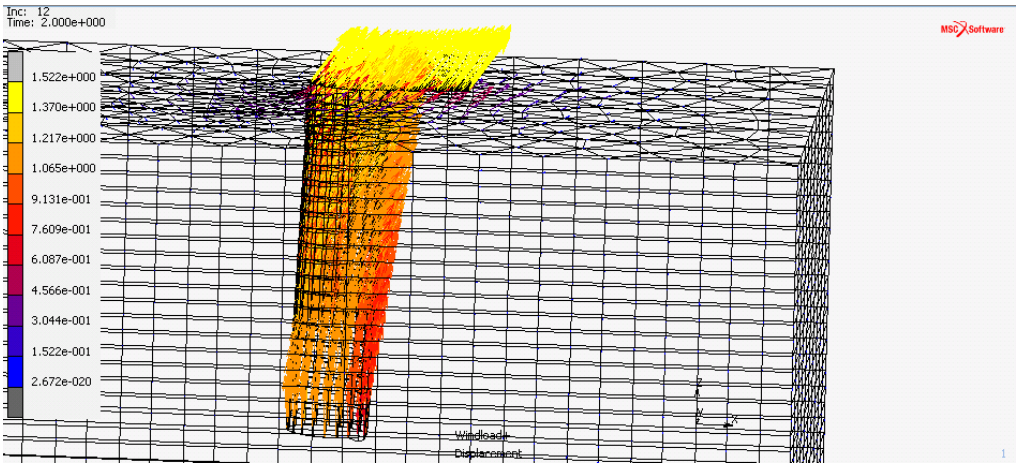

Figure 4.39b Three dimensional vector analysis of displacement output at WC state(mm), at load case Windload+.

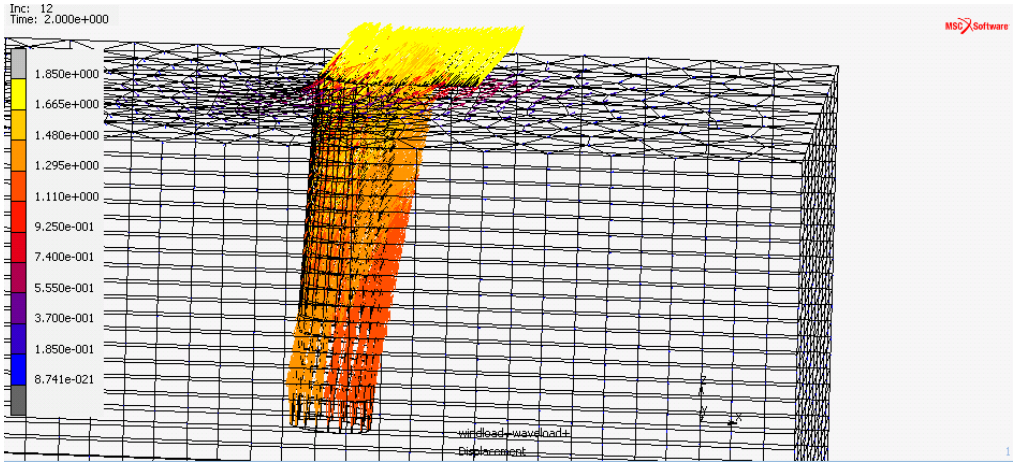

Figure 4.40c Three dimensional vector analysis of displacement output at WC state(mm), at load case Windload+Waveload+.

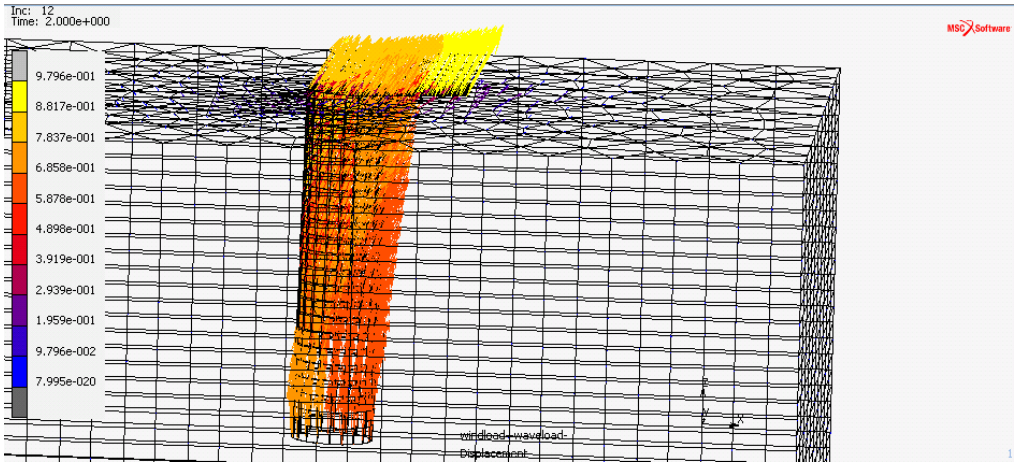

Figure 4.41d Three dimensional vector analysis of displacement output at WC state(mm), at load case Windload+Waveload-.

5. THREE DIMENSIONAL SOIL ANALYSIS

5.1. Simulation of Project

In order to get a simulation more credible and closer to the reality, a full three dimensional simulation of the project studied has been performed using the commercial finite difference code FLAC^{3D} by Itasca. Moreover, an identical model has been simulated in SOFISTIK in order to compare the results output side by side and test the credibility of the soil substitution method. The nature of this attempt differs from one presented at the previous chapter, as its goal is not to test the stability and safety of the structure, but to analyze the mechanisms that define the interaction between soil and structure. This alteration prohibits the engineer from making admissions and simplifications if possible, even if they are in favor of safety. Following this principle, no increment factor has been applied to the environmental loads.
The simulation takes advantage of the symmetry that characterizes the wind turbine structure. Practically, this indicates the simulation of the half project and the attachment of horizontal displacement constraints along the surface which corresponds to the missing half (Fig 5.1). Along with the model geometry, all environmental loading are diminished by half, as well as the cross sectional properties, except from the materials that are kept unedited. The soil is modelled by three dimensional hexahedral continuum inelastic elements, equipped with TRESCA constitutive model (Table C.1). The piles are also simulated with hexahedral elements which compose a solid body. By the time the pile is a mixed material cross section with expectations to reach the reality, several equivalent parameters are produced in order to display a realistic response to the imposed loads. Primarily, the specific weight of the elements must be calculated in order to give the actual dead weight that contributes to the resistance against extrusion. In order to unify the different specific weights of the plugged soil and structural steel that compose the cross section, an equivalent parameter has been calculated as weighted average, by the following equation

$$\gamma_{\mathrm{eq}} A_{\mathrm{total}} = \gamma_{\mathrm{steel}} A_{\mathrm{steel}} + \gamma_{\mathrm{soil}} A_{\mathrm{soil}} \tag{34}$$

$$\Rightarrow \gamma_{\mathrm{eq}} = 13.74\ \mathrm{kN/m^3}$$

where

A_{total} : surface area of total circular cross section,(19.635 m^2)
A_{steel} : surface area of steel, $(1.2566\ m^2)$
A_{soil} : surface section area of soil, $(18.398 m^2)$
γ_{steel} : specific weight of submerged steel, $(68.5\ \mathrm{kN}/m^3)$
γ_{steel} : specific weight of submerged clay studied, $(10\ \mathrm{kN}/m^3)$

Furthermore, already proven in the previous analysis, the pile is primarily exposed to bending, so its elastic parameters must be calculated to match its response to bending. By the time the clay has no tension capacity, the bending stiffness is exclusively provided by

steel and distributed to the solid pile elements through an equivalent modulus of elasticity estimated by the equation

$$E_{\mathrm{eq}}\mathrm{I}_{\mathrm{solid}} = E_{\mathrm{steel}}\mathrm{I}_{\mathrm{hollow}} \tag{35}$$

$$\Rightarrow E_{\mathrm{eq}} = 2.69\ 10^{7}\ \mathrm{kPa}$$

where

I_{solid} :moment of inertia of total circular pile cross section, 30.68 m^4
I_{hollow} :moment of inertia of hollow, 3.74m^4
E_{steel} : steel modulus of elasticity, 2.1 10^8 kPa

Finally, the piles are equipped with a steel cap on the top which is joined with the rest of the body. This technique is applied in order to transfer the stress carried by the cable to the total cross sectional area to avoid any local instabilities.

All of the structural members are simulated in terms of elasticity except from the cables that are additionally equipped with ultimate breaking force (Table C.2). The geometric properties are kept as they are declared in soil substitution analysis (Table B.1) and reduced to half as required by the half space analysis.

The interaction between the structure and the soil is implemented via interface elements that are installed:

- Along the circumference of the piles
- Along the bottom surface of the shallow foundation

These interfaces are adjusted so that they define the region of the different contact bodies, that they ensure the transfer of stresses from one body to another and track extreme phenomena such as differential displacement(slip) or loss of contact(separation). Specifically, the stiffness in normal and tangential direction declared is some order of magnitude amplified in relation to the elastic modulus of the soil, with purpose of ensuring that the differential displacement is not affected by possible displacement of the interaction elements. The possibility of detachment is given by the minimum tensile strength and the chance of slip may happen if the developed shear stress violates the limit of cohesion. Due to the disturbance of the initial soil frame structure the cohesion between pile and soil is reduced as nominated by API(2003).

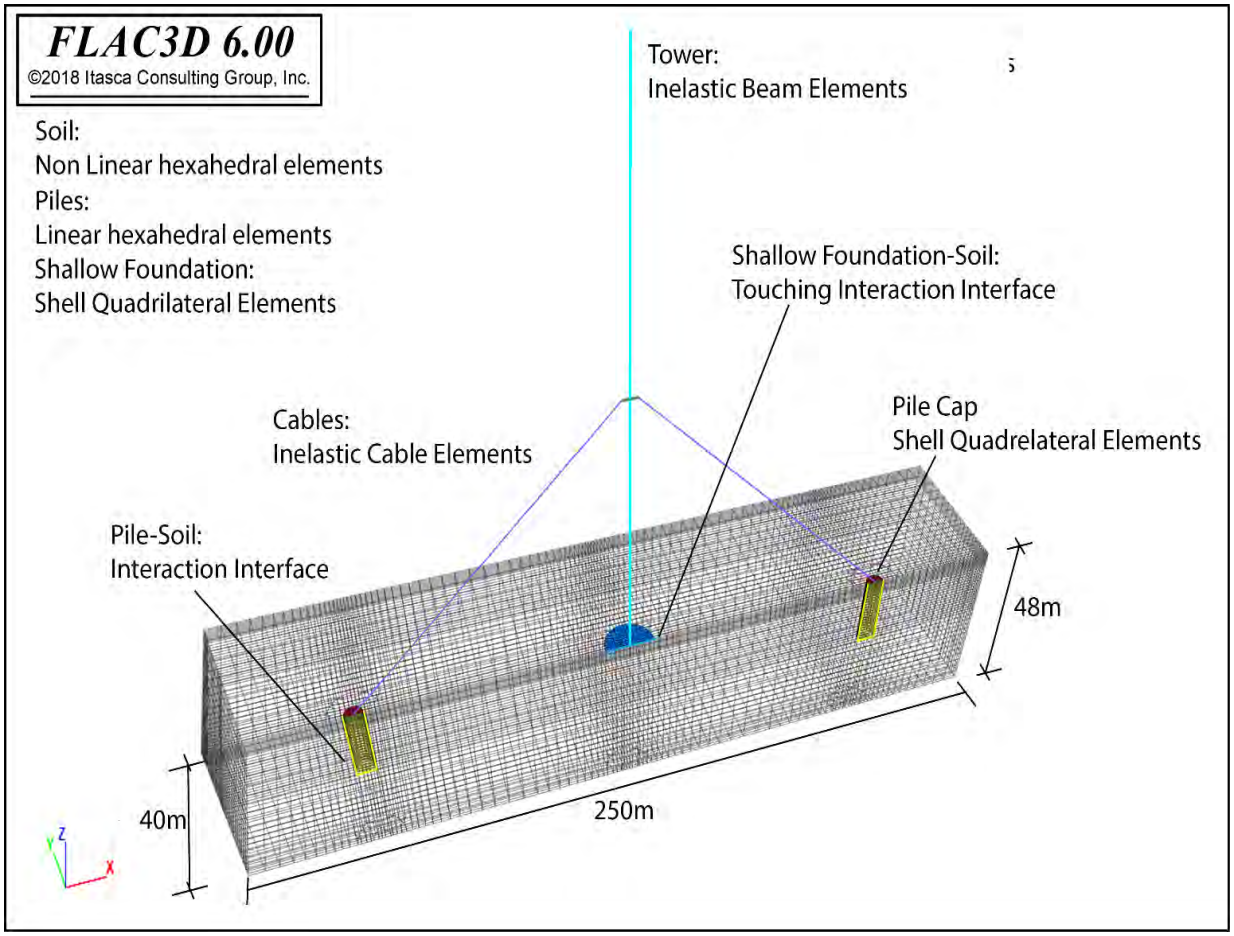

Figure 5.1 FLAC^{3D} Simulation Overview.

5.2. Superstructure Response

Tower

Studying the body of the tower imposed to the environmental loading, the form of the results extracted is in qualitative agreement with the simplified analysis accomplished with soil replacement. The formulation of the distribution diagrams (Fig. B.2) and the display of the deflection of the tower under environmental loading (Fig. B.1) is cited at the figure appendix, yet there is no interest of its exclusive commentary, as the conclusions would be similar to the one performed previously in chapter 4.2. On the other hand, the straight comparison between the output results derived from the two approaches of the problem is an enlightening procedure of investigating how the three dimensional analysis of the interaction between soil and structure finally affects the tower response.

Deflection

In terms of deflection, the straight comparison of the diagrams and the calculation of their relative difference figure out that the three dimensional analysis estimates slightly greater

horizontal deflection than the soil replacement, which is increased as the examined position goes higher reaching the ultimate relative difference of 0.27% (Fig C.1).
Specifically, the points where the interest is high are

- The base of the tower, at the level of soil surface
- The level where the cables set up is attached, at height of 75 meters
- The level of the rotor installation at the top level of the tower, at height of 150 meters

The first two points are representative of the resistance which is acquired from the soil by the shallow foundation and the piles anchoring, points where the lateral displacement is expected minimum, especially at the level of cables. Moreover, at the height of the rotor the horizontal displacement is also desired small, because any violation of the tilt limits would provoke second order additional bending phenomena caused by eccentricity.

Comparing side by side the deflection of the tower in each stage of loading separately, the general conclusion is that the three dimensional analysis gives away larger displacements than the soil replacement. Giving more attention to the crucial level of the lateral displacement constraint which is provided by the cable set up at height of 75 meters, it is presumed that the three dimensional analysis gives out larger displacements, up to 200 mm in the case of wind and wave force acting in the same direction (Figure 5.2). Continuing up to the height of 150 meters, again there is tracked additional displacement at the horizontal direction according to three dimensional analysis, which at the most extreme loading scenario corresponds to tilt of magnitude 0.0102, still within safety boundaries (Figure 5.3). Even if the estimation of the two analysis differs enough at the point of the cables attachment, still the deflection is kept in low levels in relation with the deflection taking place at the top (Fig. 5.4).

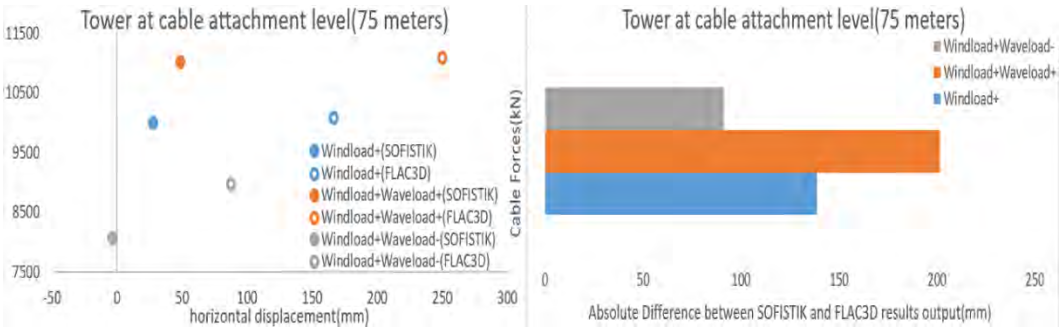

Figure 5.2 Simulation differences in terms of tower horizontal displacement at the cables attachment level.

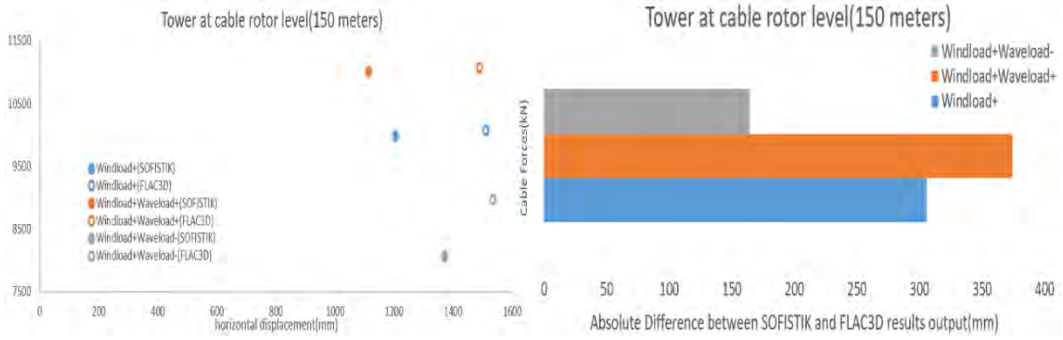

Figure 5.3 Simulation differences in terms of tower horizontal displacement at the rotor level.

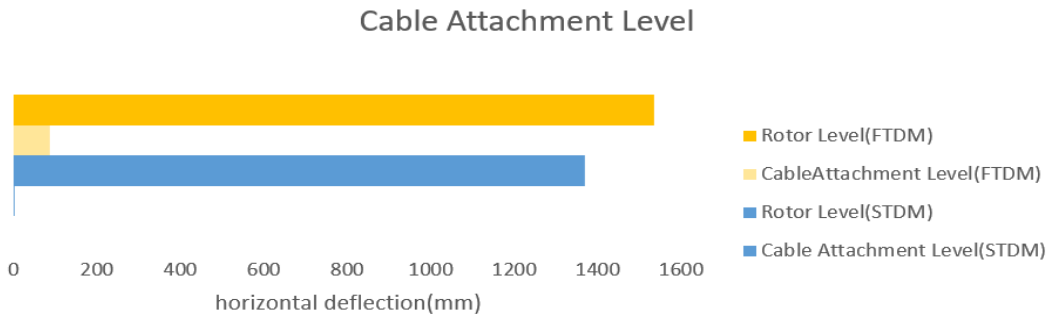

Figure 5.4 Simulation differences horizontal displacement at important tower points.

Finally, the lateral deflection of the shallow foundation is kept within very small vertical displacements in a manner that is doesn't affect the stability of the tower, for that reason any further investigation will be performed at separate study of the shallow foundation.

At the case of vertical displacement, there is a constant difference of 25mm, which is due to the settlement of the shallow foundation(Fig. C.2). Below the level of the cables attachment the inclination of the curve changes, with the three dimensional analysis giving a steeper one, which signifies a larger vertical component of the cable force.

Resultants

The formulation of the distribution curve of the axial, shear forces and bending moment resultants are in total qualitative agreement like the displacements, with some variations of the magnitude at the points where constraints are applied or loads are imposed. Primarily, the axial forces results are identical above the level of the cables attachment, which is expected by the time that part of the structure is isostatic (Fig. C.4). Any minimum divergence tracked, which doesn't exceed the ratio of 0.03, is due to the different solving algorithm utilized by each approach(Finite Element Method utilized by SOFISTIK and Finite Differences Method utilized by FLAC^{3D}). Under the point of cables attachment, slightly different gradient and starting value is figured out, both of them caused by the alternation in the value of cable forces. So does the diagram of the shear forces (Fig. C.5). Still, this small variation of the shear forces may be the cause of large divergence in the bending moment distribution, as the geometry of the structure is ruled by high distances. Indeed, as displayed

in the bending moment distribution diagram (Fig. C.6), there are two point where the divergence between the two analysis reaches its maximum, at the cables attachment level (Fig. 5.5) and at the base level (Fig. 5.6).

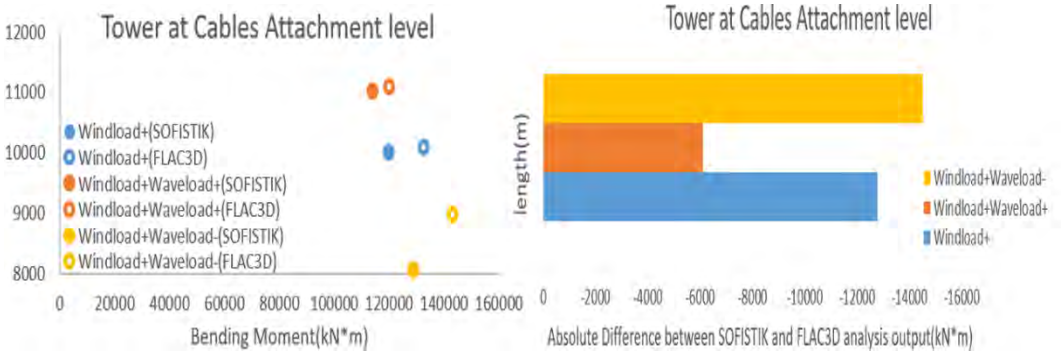

Figure 5.5 Bending moments at the base of the tower provided by the SOFISTK and by the FLAC^{3D} analysis.

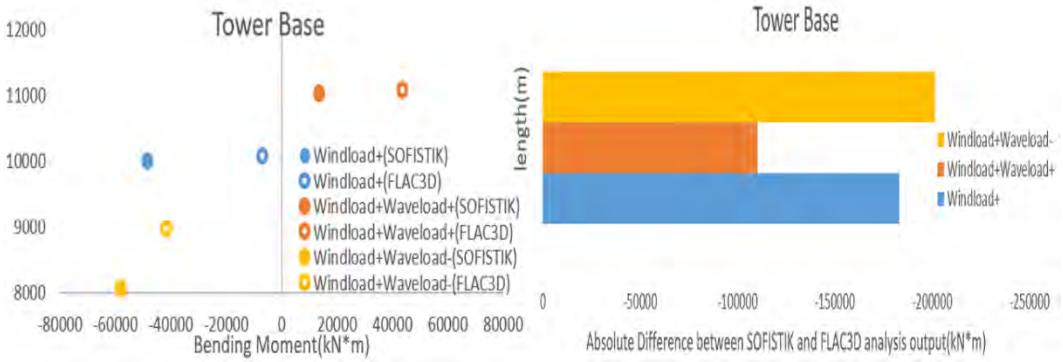

Figure 5.6 Simulation differences in terms of bending moments at the middle of the tower provided by the SOFISTIK and by the FLAC^{3D} analysis.

Cables

As mentioned previously, the cables are composed of cable elements that have the capacity of carrying solely axial forces. It is directly implied that the produced axial force is an exclusive result of the axial strain, which is derived by the differential displacement of the starting and ending node. According to the constitutive equation that defines axial forces and axial strain, high tension concludes larger tensile strain and vice versa.

Shown at the Figs C.7 and C.8 that correspond to the pair of cables at the plane of loading, the FLAC^{3D} analysis gives slightly higher values of cable axial forces at cases where there is tension added and considerably lower at cases of relief. This fact, in combination with the increased deflection of the point at the cables attachment, concludes greater magnitude of displacement of the piles head estimation by FLAC^{3D} than the one given by SOFISTIK.

5.3. Pile Response

Structural Element

This section concentrates on the pile which is in state of additional tension providing resistance against the dominant action of the wind. Obviously, this choice does not underestimate the importance of the pile in state of relief, which is essential to the stability of the structure, but is made under the reasonable thought that the study of the extreme condition of the tensioned pile covers sufficiently the phenomena that take place at the region of the relieved piles.

The kinematics of the piles are studied and presented separately in vertical and horizontal component (Figs. 5.7 and 5.8). Although the analysis performed by FLAC^{3D} takes into consideration the soil and pile interaction as a unified mechanism, without the need of decoupling the response in axial and lateral, this form of results presentation is kept the same as the one by SOFISTIK in order to be able to perform a straight and clear comparison between the results.

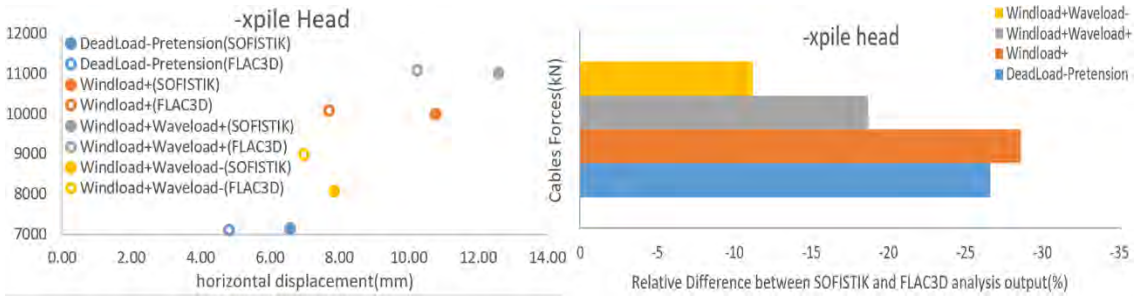

Figure 5.7 Simulation differences in terms of horizontal displacement at the head of the pile.

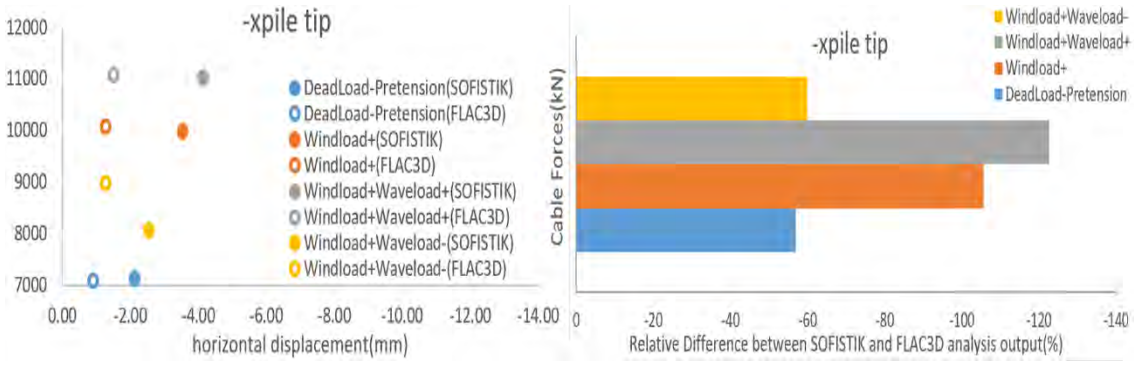

Figure 5.8 Simulation differences in terms of horizontal displacement at the tip of the pile.

The displayed output in Fig. C.9 points out that the full interaction of pile with soil gives out a slightly stiffer horizontal response at the top and bottom of the pile, accompanied with the relocation of the neutral point in lower level.

From the aspect of the surrounding soil, these displacement have an extended influence at the surrounding field kinematics. The horizontal displacement contour graph(Figure B.9) displays a resistance zone of soil that moves like a solid body with common displacement of its nodes, in agreement with the new position of the pile. The basic parameters that describe this zone are its width, depth and horizontal displacement and collected to the following bubble chart(Figure 5.9).

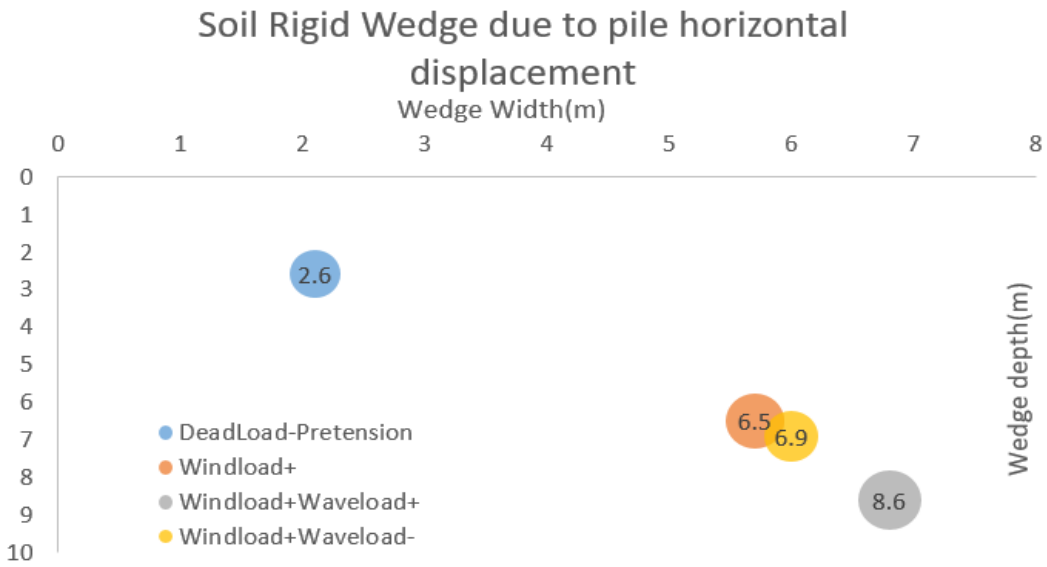

Figure 5.9 Soil rigid wedge characteristic.

As the displacement increases, the zone is expanded to greater area reaching an ultimate width of 6.8 meters and depth of 8.6 meters, figuring out a first estimation of the plastification taking place at the level next to the soil surface. Furthermore, the formation of the stress field at the surrounding soil define the influence of the pile which drags to greater depths the light stress contours at its back side, while at its front side drags stress of greater magnitude up to the soil surface (Fig. B.10). This difference of the magnitude of the horizontal stresses compared to the initial field stress leads to the increase of shear stresses that deform the shape of the elements and has the potential of creating plastification zones at these regions.

Reversing the procedure and focusing on the influence that the resisting soil has to the structural element of pile, the attention now is given to the resultants of axial, shear forces and bending moments. In order to extract and formulate these diagrams there has been made a procedure of converting the normal stresses of z direction to axial forces by integrating over the cross section area of the pile, the shear stresses of the xz plane to shear forces by integrating over the cross section area of the pile and the rotation of the piles by

multiplying them with the equivalent bending stiffness. These techniques are based on the following fundamental equation of continuum mechanics:

$$\iint \sigma_{zz} dA = N \tag{36}$$

$$\iint \sigma_{xz} dA = V_x \tag{37}$$

$$\frac{d^2x}{dz^2} = \frac{M}{EI} \tag{38}$$

The comparison between the shear forces distribution provided by FLAC^{3D} and SOFISTIK analysis provide curves in total qualitative agreement, with variation to the magnitude of their peaks. Specifically, the estimation by FLAC^{3D} is lower magnitudes at negative shear forces peaks, which is reasonable by the time the forces imposed by the cables are larger and the system stability requires larger positive shear surface(Figure B.7). Exactly the same is the difference at bending moments diagrams which are formed by the shear forces, as the geometry of piles defines zero value at starting and ending boundaries(Figure B.8).

Yet, the response at vertical axis is given considerably less stiffer by FLAC^{3D}. Specifically, there is a divergence of 2mm in favor of FLAC^{3D} that remains constant along the length of the piles, as they respond as rigid bodies with small strain expression (Fig. B.5). By examining the axial forces distribution diagram which reflects the resisting influence of the soil against pile extrusion, it is shown that the gradient of the axial force reduction is not constant but is expressed by two principal range of values (Fig. C.14), of small magnitude near the surface and of greater down to the rest of the body. As already mentioned, the theory behind the resistance against extrusion indicates that the action which absorbs the environmental forces and transfer them to the soil is the product of the modified cohesion at soil and pile interface(36.5kPa) and the surface of the interaction area. By the time the modified cohesion is relatively constant, no matter the depth, there is reduction of the interacting surface implied. Indeed, the interface output that displays the contact status between the pile and the soil gives away results that are in agreement with variation of the resistance against extrusion in sense of region reduction (Fig. B.12). Specifically, the zone of detachment of each loadcase matches the region where the small gradient of axial force reduction is applied.

On the other hand, such actions affect the vertical stress distribution by dragging large vertical stress to the soil surface at an annular region around the pile circumference (Fig. B.11), change that may provoke the formation of plastic zone. In addition, the sudden relief of the vertical overburden stress at the circular region right below the pile (Fig. B.11)is also a cause of great shear stresses, therefore of plastic zone.

Indeed, these potential plastified regions are displayed in the stress to strength ratio diagram (Fig. B.13). Judging from the contour provided, the dominant cause of plastification is the displacement of the top, as the areas behind the pile and under its tip remain of relatively constant volume through the different load cases.

5.4. Shallow Foundation Response

Structural Element

Defining its function, the foundation transfers all the actions which are indicated by the static analysis at the base level to the soil beneath. In order to express this interaction in terms compatible with the three dimensional nature of the soil, the axial forces and the bending moments are transposed to a unified action expressed by the volume changing normal stresses at the vertical z axis and the shear force is expressed by the shape changing shear stress of the xz plane.

Concerning the contact interaction, the foundation slab is in touching conditions with the soil beneath and interacts in direction parallel to its plane via Mohr Coulomb interface law, principle which exploits the cohesion as the resisting mechanism against potential horizontal relocation at the case of studied clay. Investigating the kinematic response of the element at the horizontal axis, there is movement tracked, which is limited between safety boundaries, as it doesn't show excessive slip. The maximum horizontal displacement tracked has magnitude of 9.3 mm, which is negligible in relation with the rest of the tower body, giving the shallow foundation the function of lateral deflection constraint (Fig. B.14). On the other hand, the vertical displacement is totally relied on the stiffness displayed by the soil and plays a key rule to the response of the rest of the structure.

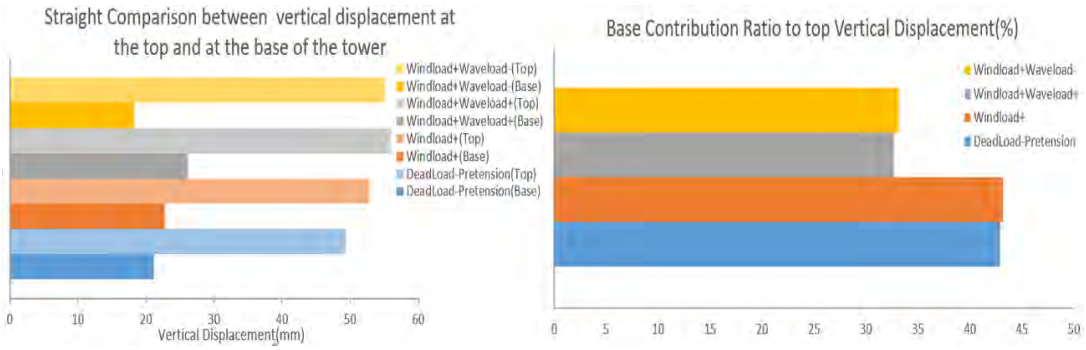

Figure 5.10 Settlement contribution ratio to the total vertical displacement the top level.

Estimating the ratio of the vertical displacement of the slab to that of the top of the tower (Fig. 5.10), which is the maximum tracked, it is figured out that the settlement is at least the 33% of the total displacement of the rotor. By the time the axial force is constant, the additional settlement that takes place is caused by the rotation of the slab(Figure 5.11). This rotation in sense of soil is a differential vertical displacement that creates stress concentration at specific small regions, combination which unavoidably leads to yielding. As indicated by the Mohr Coulomb constitutive model theory mentioned at the introduction, by the time a zone yield, its volumetric strain increases rapidly, a phenomenon that renders the foundation response sensitive to rotation due to the "collapse" of soil's capacity to maintain its stiffness after yielding point.

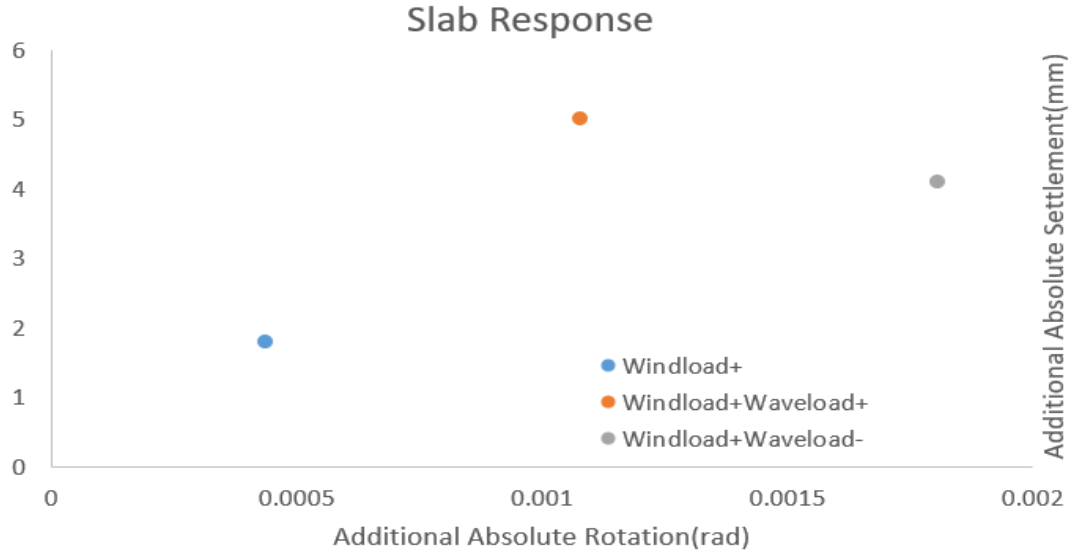

Figure 5.11 Slab Rotation and Settlement relationship.

Soil Beneath

Studying the matter from the position of the soil, it is spotted that at the region of great normal stress concentration, the soil expands in direction perpendicular to the vertical loading in order to deal with the compressive action of the vertical load transfer (Fig. B.16). This expansion, which is commonly known as Poisson effect, is intense near the surface and gradually fades as the depth increases, following the pace of the vertical normal stress distribution (Fig. B.18). Along with the vertical expansion, complementary vertical lifting of the soil around the slab takes place, a phenomenon also occurring due to the need of decompression. Such soil response under surface loading corresponds to general shear failure surface, characteristic of normally consolidated clays, as indicated at the introduction. Furthermore, in figure B.19 the estimation of the plastification zone is displayed. The depth

of these zones is in general kept unchanged, reaching a maximum 14m. In contrast, due to the differential settlement, the surface width of the zones is varying as displayed in Fig. 5.12.

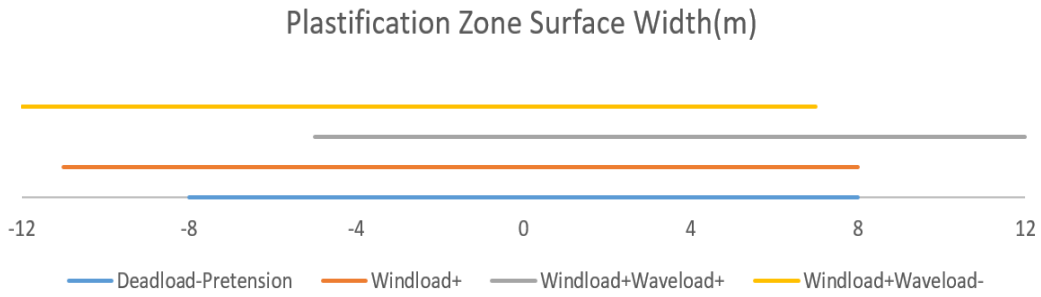

Figure 5.12 Plastification Zone Surface Width.

5.5. Structural Elements Interaction Through Soil

The interaction between different elements that are installed in small distance is a matter of great importance as the superposition of stresses may imply unexpected further strain of failure. Such matters can be investigated exclusively by three dimensional analysis and in the case studied such research has been made. In a sequence of importance, the first matter studied is the possibility of connection between the plastification zones created around the structural elements. As it proven in Fig. B.20, there is no interaction between the zones as the distance between their installation is sufficient to keep them isolated, providing a between neutral distance of 44 meters.

Following the sequence, the distribution of vertical normal stress is examined (Fig. B.21). Even if the contours seem to connect, the figure is misleading. The stressed influence by the elements is absorbed by the soil and is embraced in such that it is fitted to the initial stress field. So does the distribution of the horizontal stresses (Fig. B.22).

Finally, the distribution of shear stress is examined, the action that changes the shape of the imposed zones, and the result differs from the previous. Shown in Fig. B.23, there is vast superposition zone which connects the shallow foundation with the pile that is imposed to additional extrusion force. The result is a range of zones that are under shape distortion due to significant difference between the vertical and horizontal stresses. Nevertheless, by the time such action doesn't cause plastification or an unstable situation due to excessive displacement, it is not a matter of importance related to the stability of the superstructure.

6. SUMMARY AND CONCLUSIONS

6.1. Importance of Subject Studied

One of the most urgent issues of the present to the nations of Europe is the establish of their power efficiency and independence. Due to political and environmental matters that have risen the last decades, the solution indicated is the renewable energy sources, field where the wind power attracts more and more attention. In order to construct wind turbines that reach higher level of performance and surpass civil restrictions that complicate their realization, relocation has been suggested from land or coastal areas to open sea, a proposal that requires stability solutions in deep water settlement. Such stability relies on a foundation concept which would be sufficient to deal with massive overturning moments and lateral loads, while its actualization would be compatible with economic criteria indicating that foundation cost should not exceed a certain percentage of the total cost of the project.

The requirements proposed are demanding and their fulfillment is based on advanced structural and geotechnical analysis and design. The technology of bottom fixity, such as monopile or gravity based models, that refers to offshore structure settlement may cover the need of existing OWT at shallow waters but cannot be applied in transient or deep waters as it exceeds the realizable economic planning. Furthermore, installation concepts applied in existing structures settled at deep waters are relied on floating, whose capacity of providing stability to an OWT of the scale asked is questionable. Combining the interaction with sea bottom and the lateral cable support system that characterizes each of the mentioned technologies, a hybrid foundation concept has been developed(Fig. 3.1). The tower is settled on a shallow foundation that interact with the soil in touching conditions, transferring the vertical loads and acquiring shear resistance via friction. Additionally, the OWT is supported by a cross set up system of four prestressed cables that are attached to the tower body and anchored at the sea bottom, providing resistance against lateral loading and overturning moments, without the development of great displacements.

6.2. Research Target and Results

The analysis of soil and structure interaction which is required to estimate the response of the structure against environmental loading and the resisting mechanisms activated can be conducted in two major simulation procedures:

- The simplified three dimensional numerical method (STDM),
- The full three dimensional numerical method (FTDM).

The simplified three dimensional numerical method is a simulation technique that replaces the resisting action provided by the soil with springs equipped with nonlinear stress-strain constitutive laws reflecting the highly nonlinear soil mechanical behavior. This method is totally focused on the aspect of structural elements response, providing sufficient information about developed displacements and stress condition, yet it cannot give any clue of the structural influence to the soil. Although this approach relies on simplifying assumptions not fully covering the gap between simulation and reality, plus it requires solid theoretical background and experience in terms of geotechnical engineering, it is perfectly fitted to the present requirements and necessities of the structural design procedure which requires fast, economic and reliable analysis. In terms of preprocessing, the declaration of input is simple as, apart from the elastic parameters of the soil, which are studied and registered in vast bibliography, the post elastic behavior is defined by a perfectly plastic law activated by excessive displacement, therefore no complicated laboratory tests are needed, such as triaxial tests, to figure out the nature of the soil studied. Continuing to processing, the calculation procedure is a matter of minutes in terms of time and the results output is a matter of megabytes in terms of memory. Despite the evolution that has brought in computational power and memory storage, these sources are still limited. In addition, in order to perform economic valid design, a parametric study is required, implying a great number of analyses in relatively short time. Finally, the results output is easily manipulated as there is close focus to the structural elements, with the interference additional elements of the simulation. Obviously, the admissions made and the simplification applied lead to results with divergence from reality. Nevertheless, such divergence is close enough to the reality that can be covered by the application of increment factors.

The other option of studying the project is the full three dimensional method, which aims to model the reality the most credible way possible. The soil is modelled by three dimensional elements which are equipped with constitutive law defining yielding due to an excessive stress condition and with flow rule that defines the transition from the elastic to the plastic phase. This finite multitude of elements compose a meshing body that is able to figure the distribution of stresses, strains and displacements through the soil body, along with the display of plastification zones. Additionally, the simulated soil interacts with the structure via

interface elements, which are equipped with parameters that correspond to real interface properties, allowing the tracking of nonlinear phenomena, such as separation or slipping. Due to the superiority of the results credibility, the analysis carried out corresponds to a serviceability limit state (SLS), where no increment factor are applied to the characteristic values, as they would distort the actual display of the mechanisms that activate. Even if this option provides vaster and more reliable out of the case studied, it is accompanied with a number of major demands that renders its use rather inconvenient. Initially, in order to exploit the capacity of simulating the nonlinear nature of soil at its full, reliable evidence of that nature is needed, collection of which is a funds and time consuming procedure. Afterwards, the solving process is matter of days or even weeks with large memory demands as the output results reach the size of Gigabytes, parameters that not only allow the perform of parametric investigation, but don't let any mistakes or error in data declaration. Finally, the extract of the results consists by itself a difficult procedure, as the produced output is so vast that it can't manipulated without data analysis routines, which require programming knowledge and experience.

After performing both of the analysis at the studied OWT, the results are encouraging for the reliability of the simplified soil approach, besides the safety and the serviceability of the tower. Focusing on the guyed cable system contribution to the tower stiffness, the response of the piles is examined at the loadcase which tends to impose the highest extracting force. Although the mechanism that provide the required resistance demand extended analysis, as well as the kinematics developed, the contribution to the guyed support system can be expressed sufficiently by the displacement at the pile head. It is proven that the divergence of the displacement estimation by the STDM to the one made by FTDM at the highest tension value is 3.17mm(Fig. 6.1), implying that the '*t-z*' and '*p-y*' curve adoption is an excellent choice of soil replacement. Along with the relative difference of axial forces that gives a divergence ratio of 0.05% it is concluded that the STDM captures the stiffness of the guyed support system close enough. Focusing on the cable attachment level, where there is strong demand of lateral deflection constraint, the STDM indicates an overall displacement of 45 mm, while FTDM indicated a worse scenario of 250 mm. Although the difference is vast, the absolute magnitude in relation with the one expressed at the top are an order of magnitude lower, therefore the lateral constraint function of the cables is valid by both analysis. Continuing to the top of the tower where the rotor is installed, the maximum displacement given is 1534 mm by STDM, which corresponds to tilt of 0,01 rad, while FTDM estimates it about 1340mm, forming a divergence ratio of 12%.

On the other hand, investigating the stiffness of the tower in terms of vertical displacement, the divergence is increased. Even if the STDM achieves to track correctly the rotation of the slab and the additional settlement that takes place due to it, the estimation of the equivalent vertical displacement taking place at the attachment point between the shallow footing and the tower differs about 66% (Fig. 6.2)because the elastic perfectly plastic spring that replace the soil cannot take into account phenomena like volume decompression and Poisson effect that accompany soil yielding under compression at a limited area of application(Fig. 6.3). Such data imply the need of developing curves of response that estimate the nonlinear behavior of soil under large compressive loads including the influence of possible side movement.

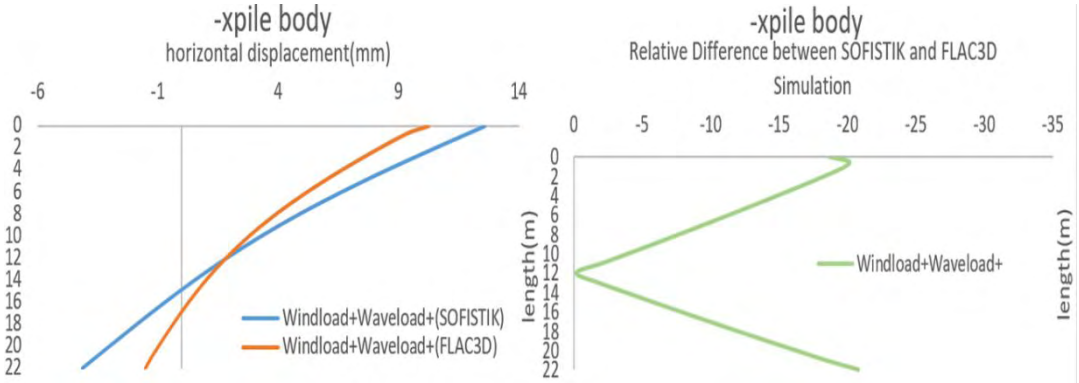

Figure 6.1 Divergence Between STDM and FTDM estimation of maximum horizontal displacement of piles.

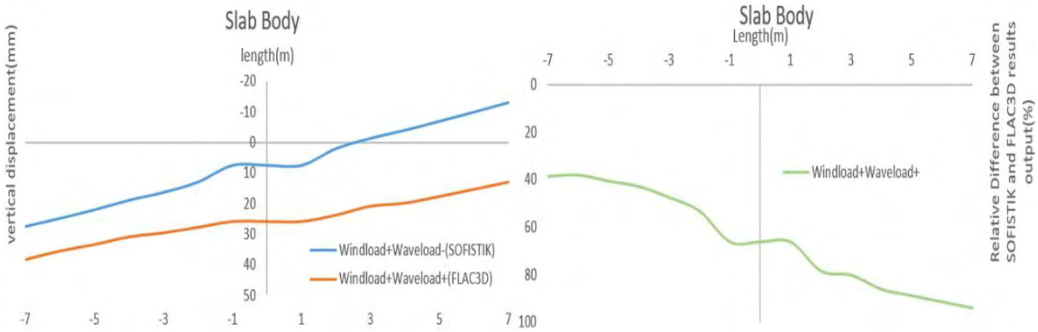

Figure 6.2 Divergence Between STDM and FTDM estimation of maximum vertical displacement of shallow foundation.

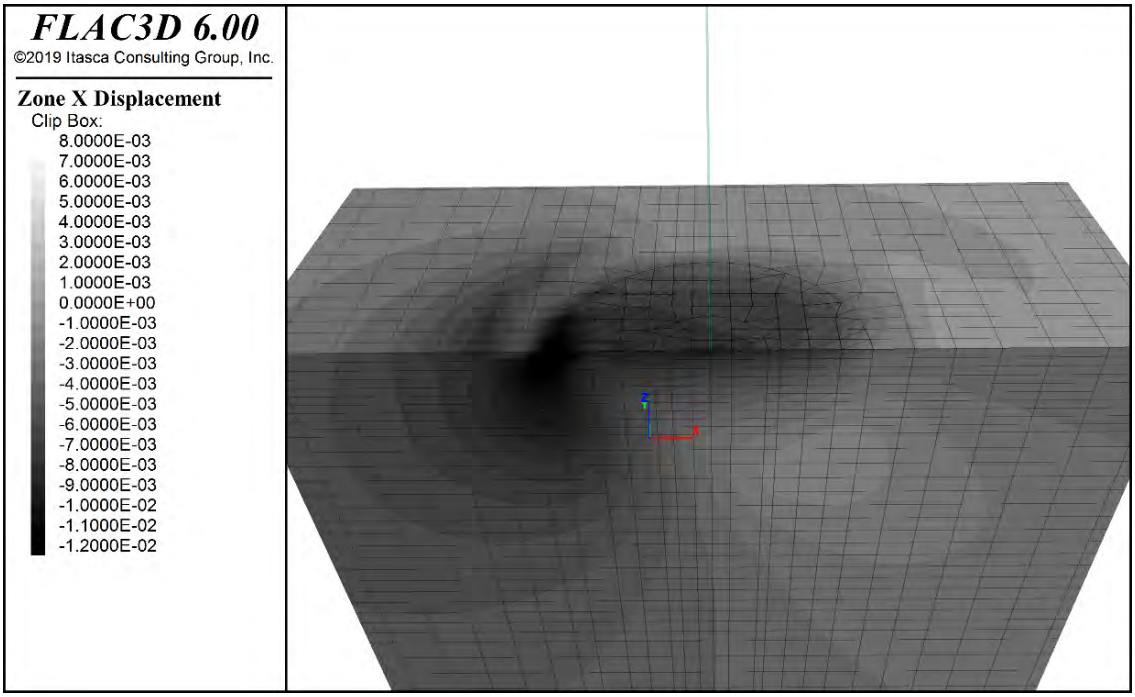

Figure 6.3 Horizontal Displacement of soil beneath the shallow foundation.

Along with the previous procedure of comparing the available methods of estimating the response of the structure studied, which eventually validates the results output of the STDM, there has been a complementary analysis conducted, which is performed choosing the STDM, that focuses on the influence of the following intervention at the geometry of the pile. This intervention is the separation between the head of the pile and the point of the attachment of the cable by the addition of a cantilever beam. This additive structural element exploits the distance created to generate a beneficial moment which opposes to the action which tends to rotate and extract the pile. According to the comparison between the versions of the pile geometry, merge of the pile head with the point of cable attachment (NC) or separation between them (WC), this intervention has significant contribution at the restriction of the displacements of the piles, especially at the level of their head. Specifically, the beneficial action of the moment restricts up to 50% and 21% the lateral displacement of the pile at the level of its head and its tip respectively, changing its kinematics from free headed to fixed headed (Fig. 6.4). The study of the influence of such restrictions to the superstructure actually implies that the overall stiffness of the tower isn't significantly changed. What is radically changed is the conditions of interaction between soil and pile. The NC state gives a plastification zone that reaches depth of 9 meters, while the WC state limits it down to 5 meters. The importance lying at this change is the fact that extended yielding zones provokes interaction conditions that are very sensitive to further displacements. According to stress and strain relations at post elastic phase, relatively small variation of imposed loading may lead to incommensurate large displacement. Such

displacement could be a threat to the resistance provided by the guy cable system due to possible axial relief of the cables, implying loss of pretension force. In addition, such situation is irreversible, which practically means that there are not options of fixing that would bring back to the system its initial stiffness. Therefore, the addition of the beam element is vital to reserve the standard function of the tower.

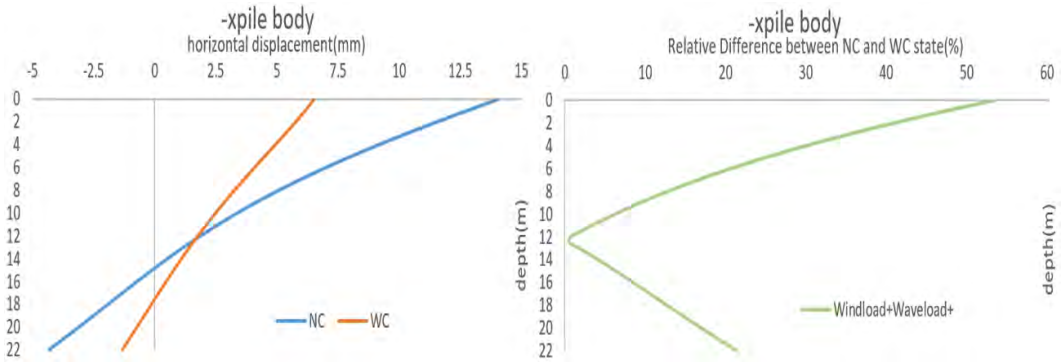

Figure 6.4 Divergence Between NC and WC states estimation of lateral displacement

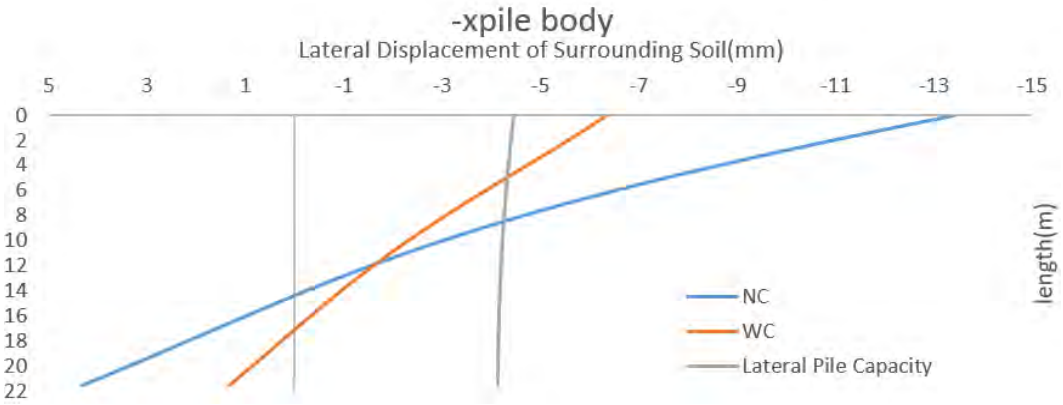

Figure 6.5 Divergence Between NC and WC states estimation of plastification zone.

FIGURE APPENDIX

SOFiSTiK Output

FLAC^{3D} Output

Comparison between SOFISTIK and FLALC3D analysis output

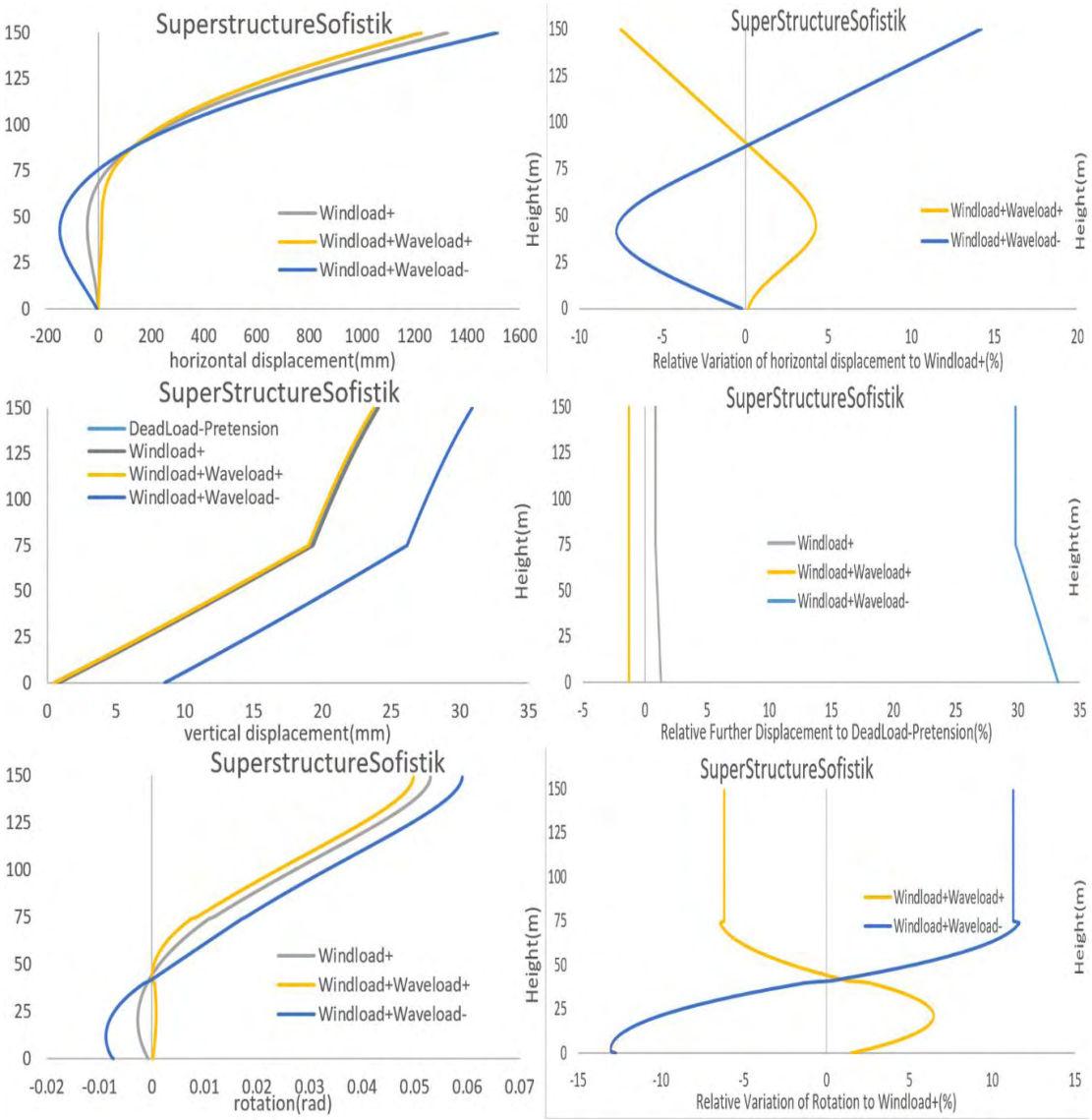

Figure A. 1 SOFiSTiK Tower Deflection Output.

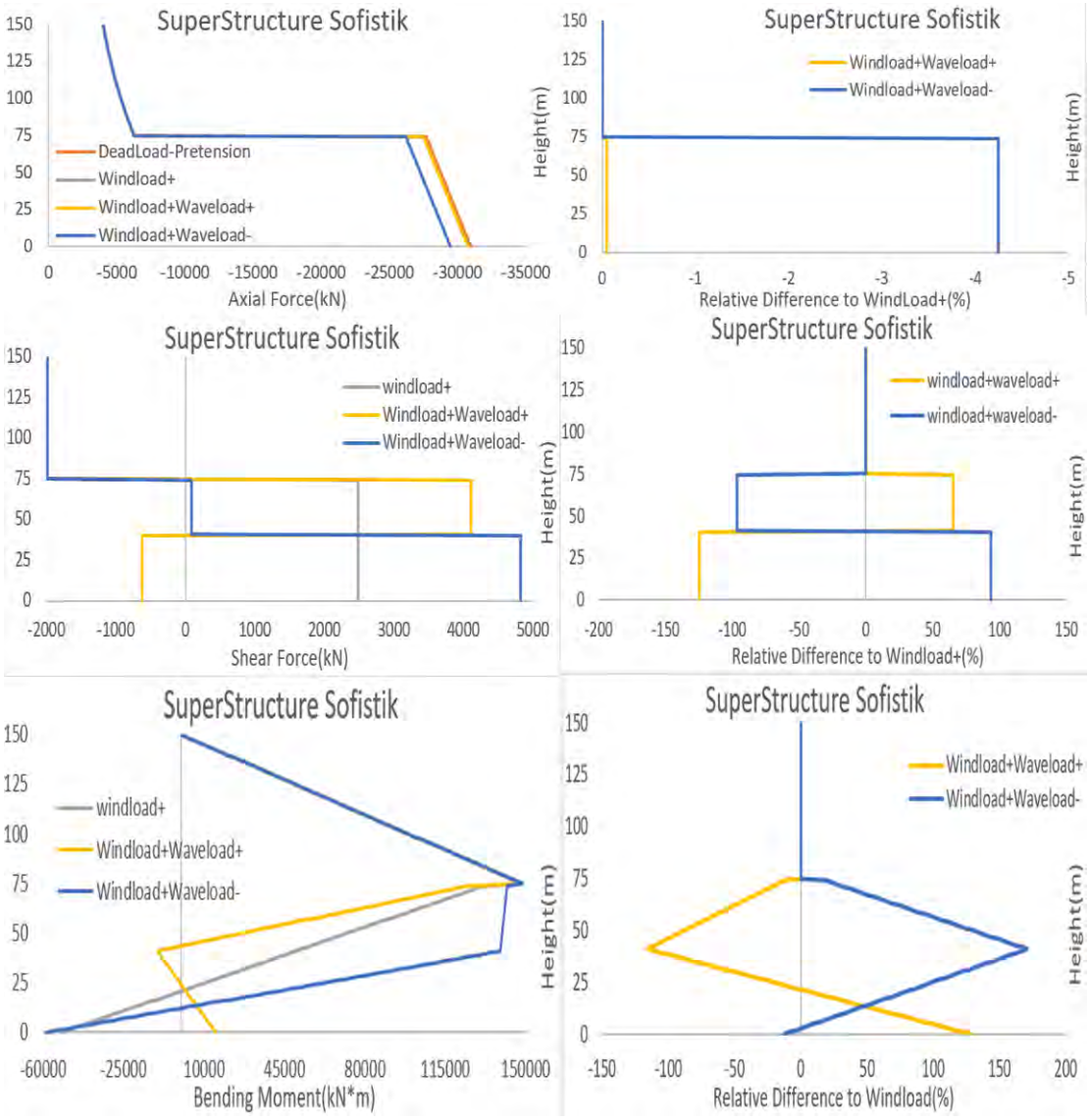

Figure A. 2 SOFiSTiK Tower Resultants Output.

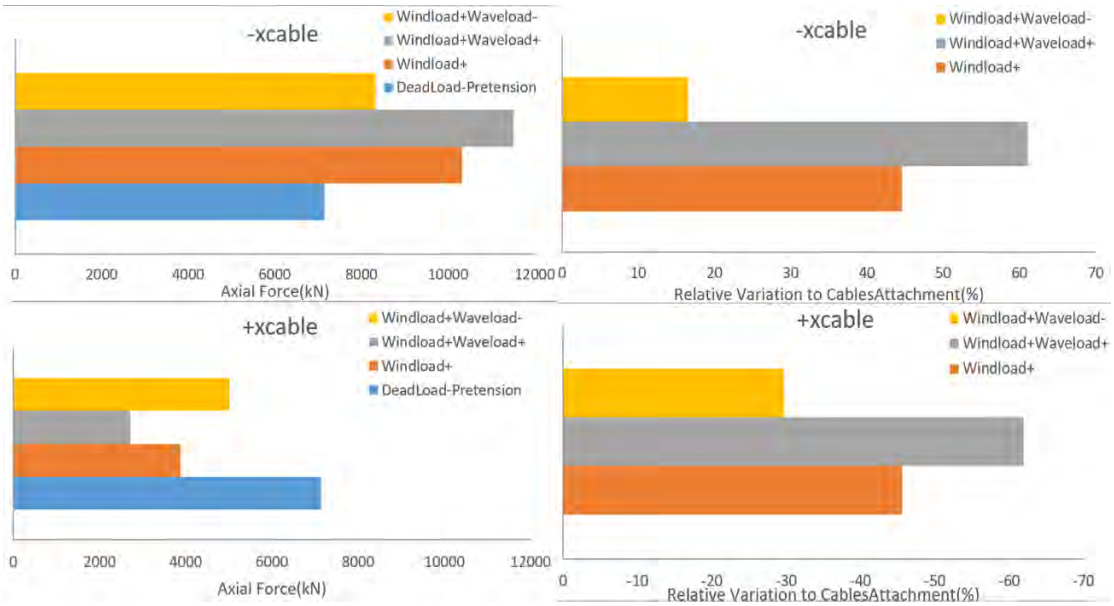

Figure A. 3 SOFiSTiK Cable Axial Forces Output(WC State).

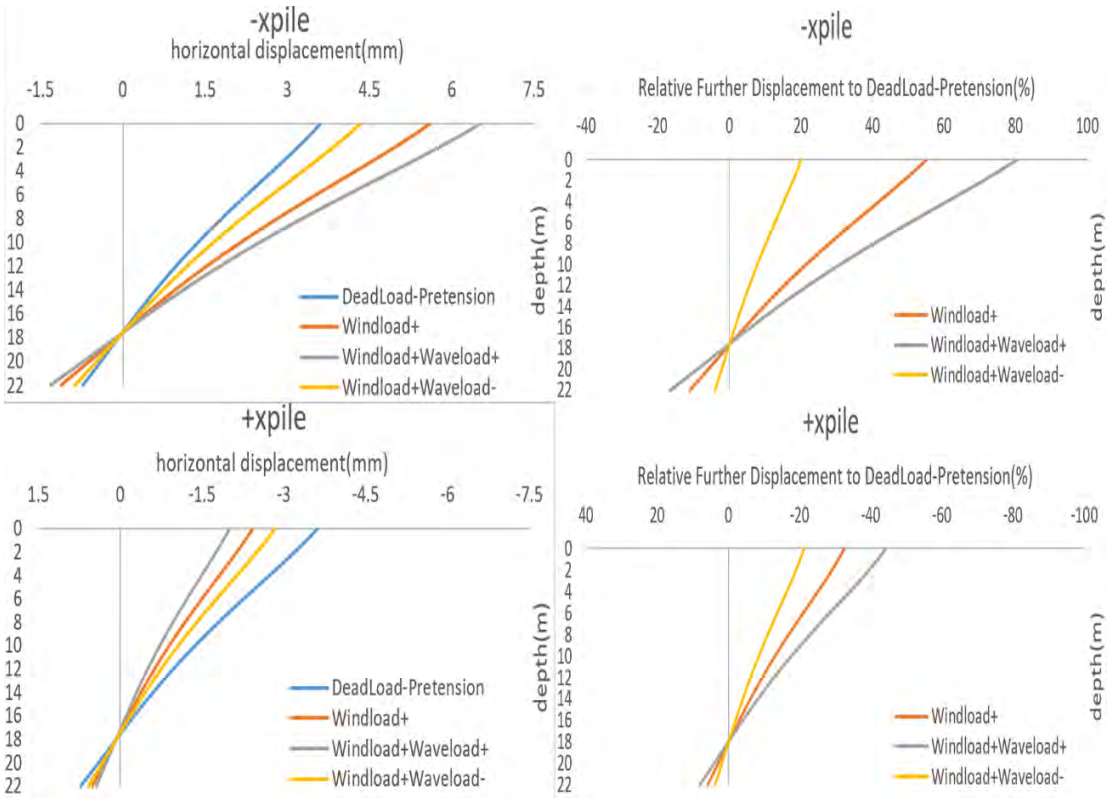

Figure A. 4 SOFiSTiK Lateral Deflection of pair of opposite piles Output(WC State).

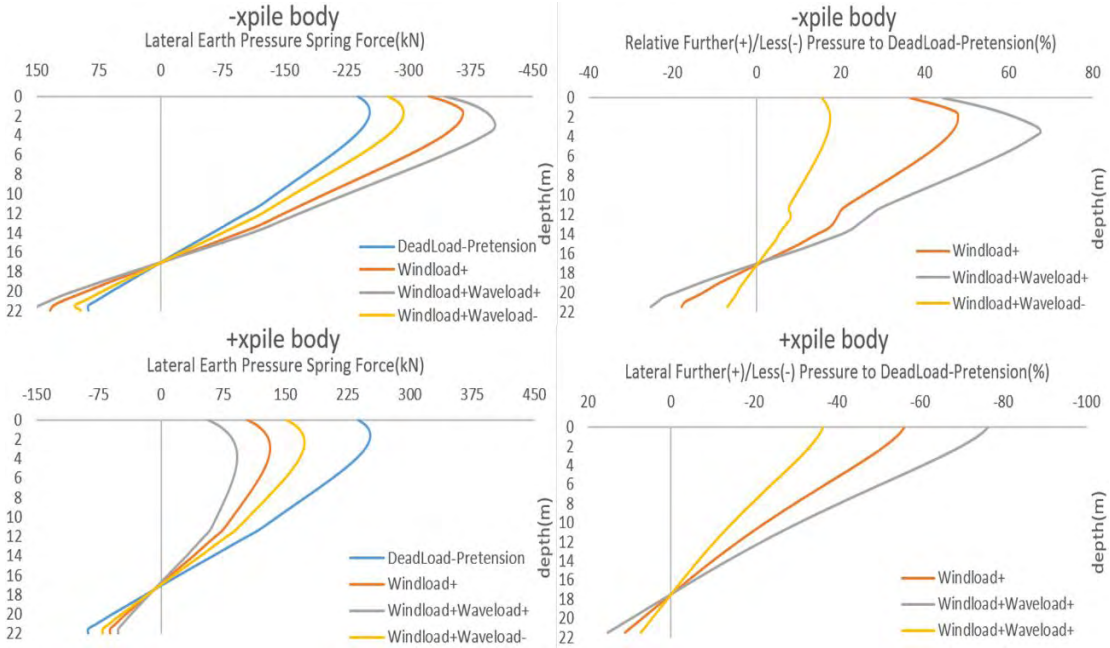

Figure A. 5 SOFiSTiK Lateral Earth Pressure Spring Force of pair of opposite piles Output(WC State).

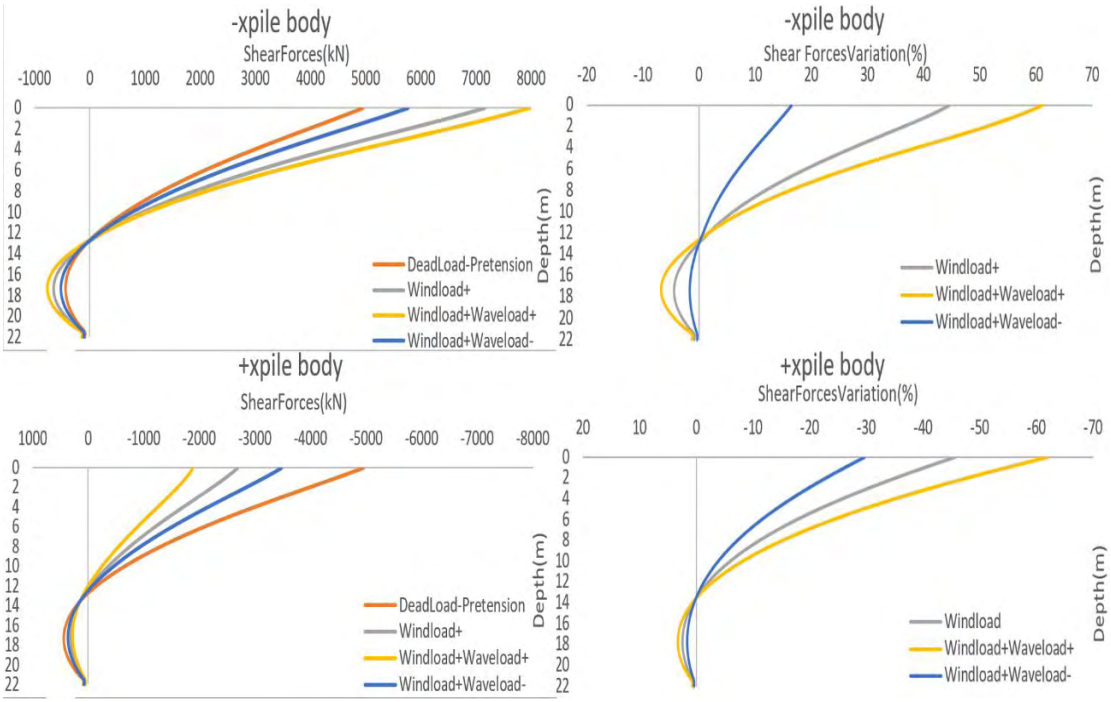

Figure A. 6 SOFiSTiK Shear Force Distribution of pair of opposite piles Output(WC State).

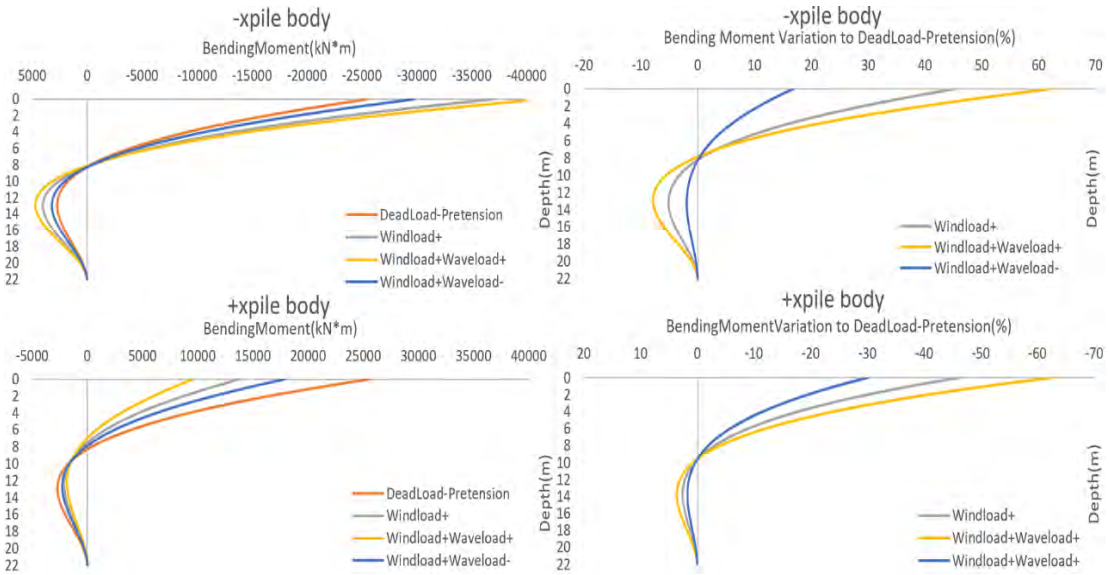

Figure A. 7 SOFiSTiK Bending Moment Distribution of pair of opposite piles Output(WC State).

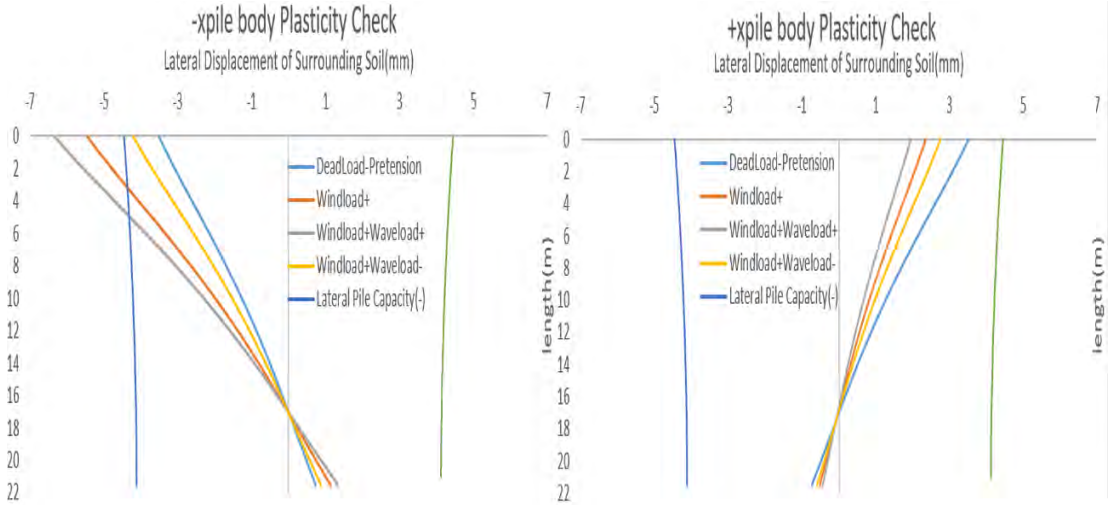

Figure A. 8 SOFiSTiK Plastification Zone of pair of opposite piles Output(WC State).

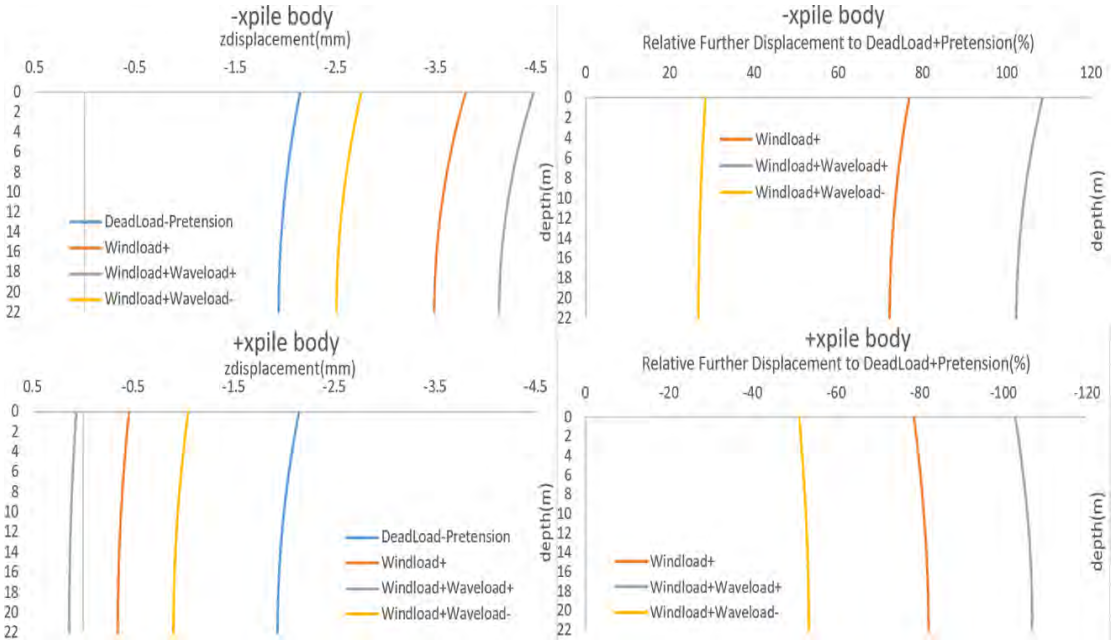

Figure A. 9 SOFiSTiK Vertical Deflection of pair of opposite piles Output(WC State).

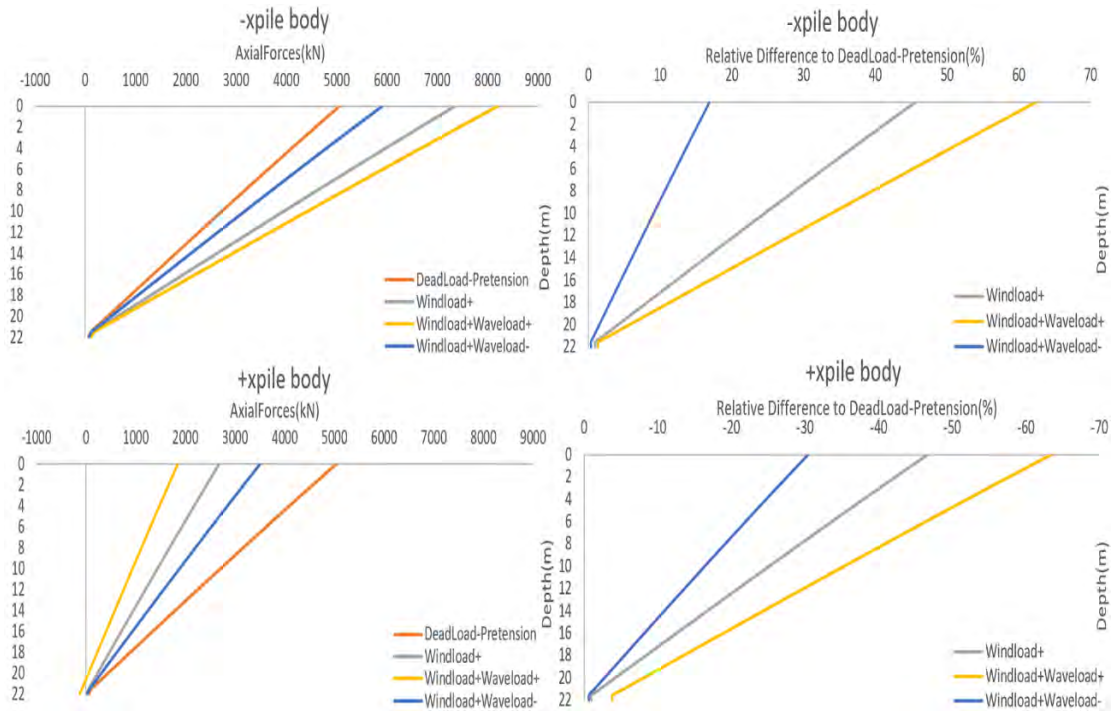

Figure A. 10 SOFiSTiK Axial Force Distribution of pair of opposite piles Output(WC State).

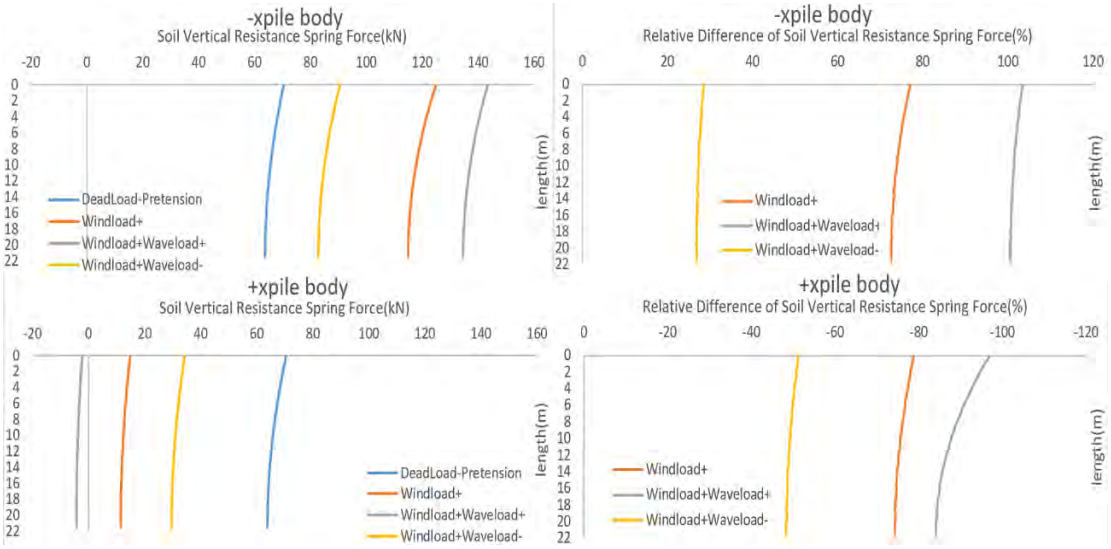

Figure A. 11 SOFiSTiK Earth Shaft Resistance Spring Force of pair of opposite piles Output(WC State).

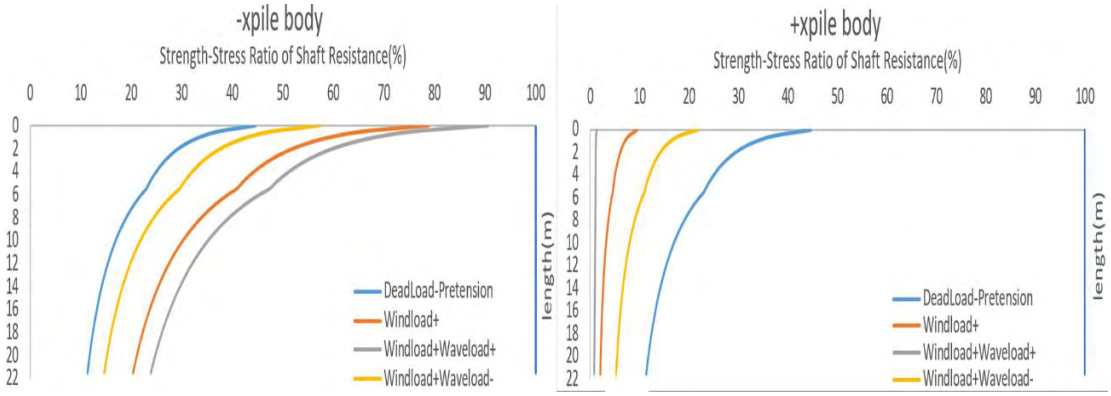

Figure A. 12 SOFiSTiK Stress Strength Ratio in terms of capacity against extrusion of pair of opposite piles Output(WC State).

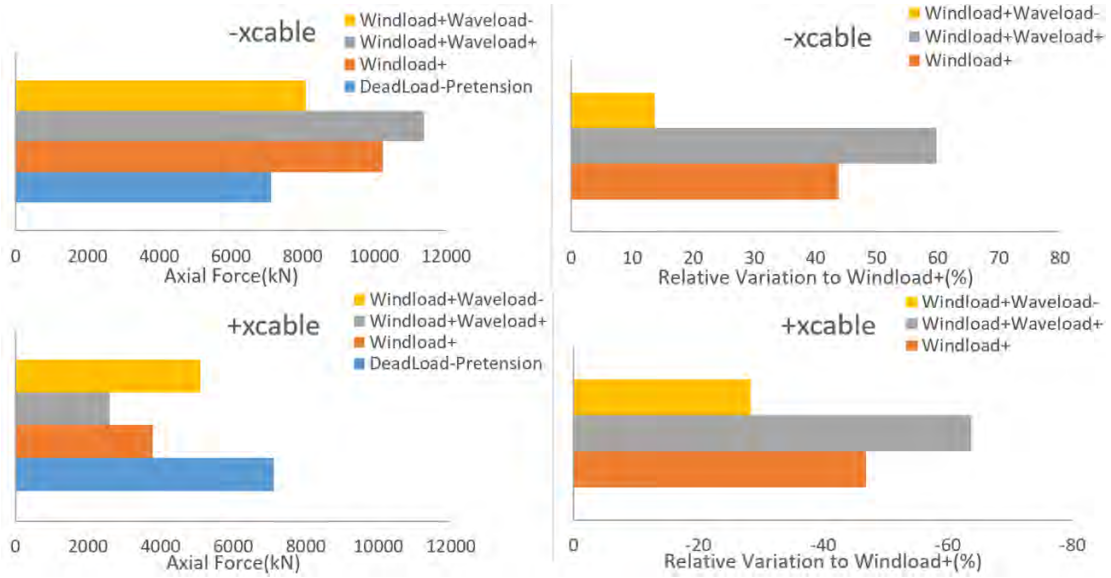

Figure A. 13 SOFiSTiK Cable Axial Forces Output(NC State).

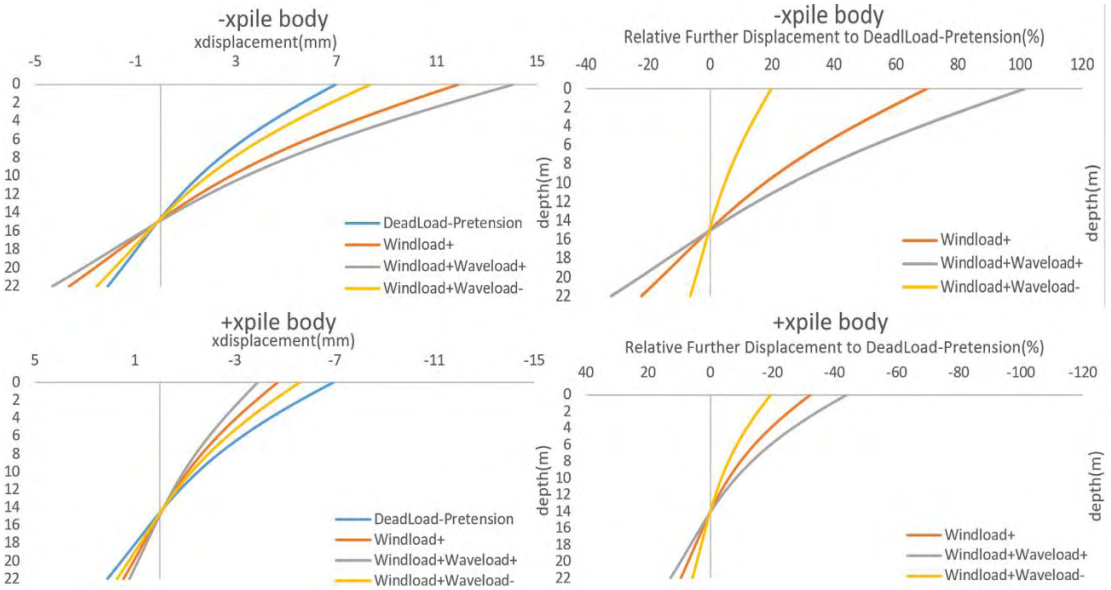

Figure A. 14 SOFiSTiK Horizontal Displacement of opposite pair of piles Output(NC State).

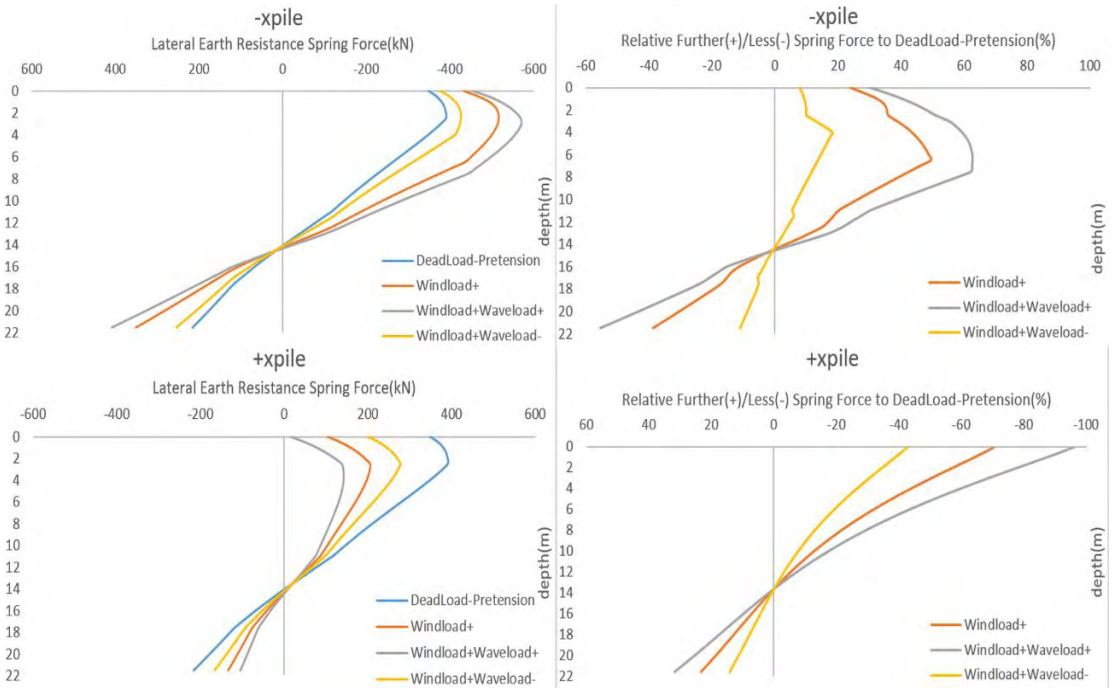

Figure A. 15 SOFiSTiK Lateral Earth Pressure Spring Force of opposite pair of piles Output(NC State).

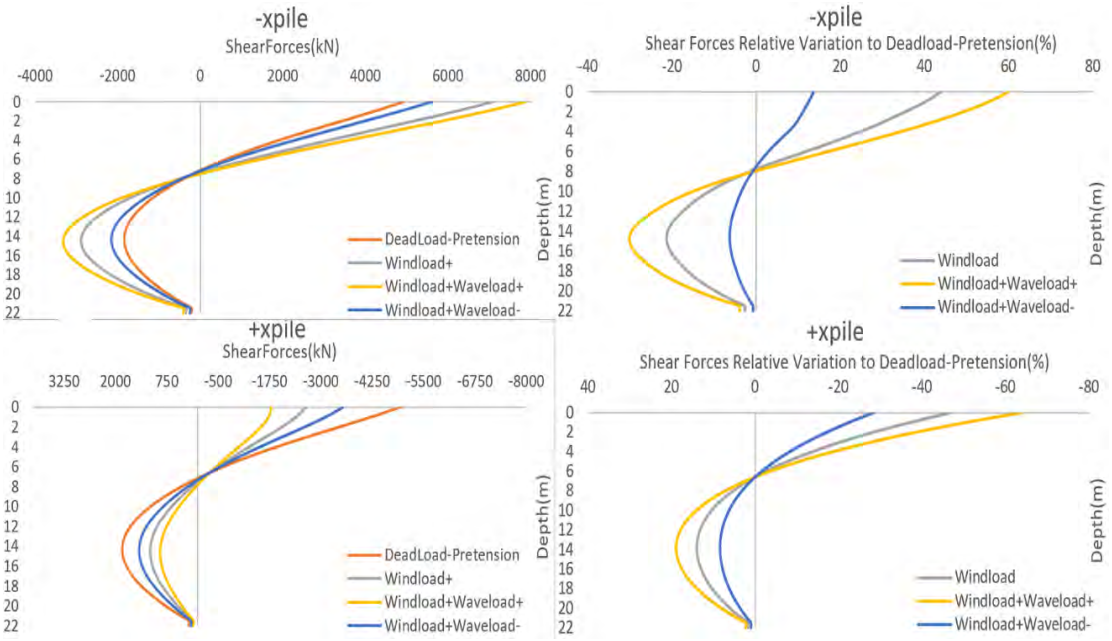

Figure A. 16 SOFiSTiK Shear Force Distribution of opposite pair of piles Output(NC State).

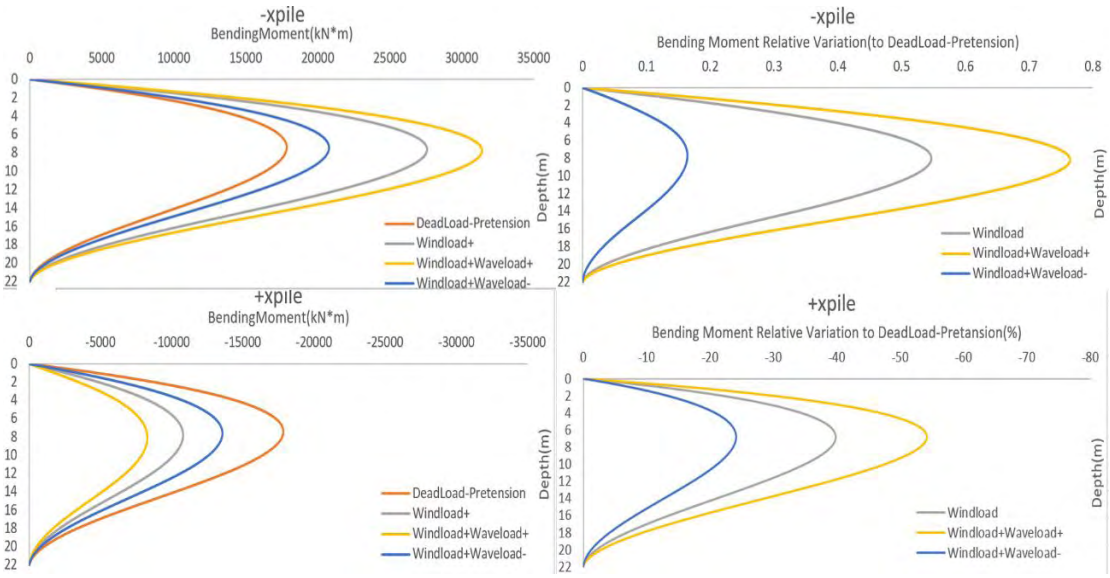

Figure A. 17 SOFiSTiK Bending Moment Distribution of opposite pair of piles Output(NC State).

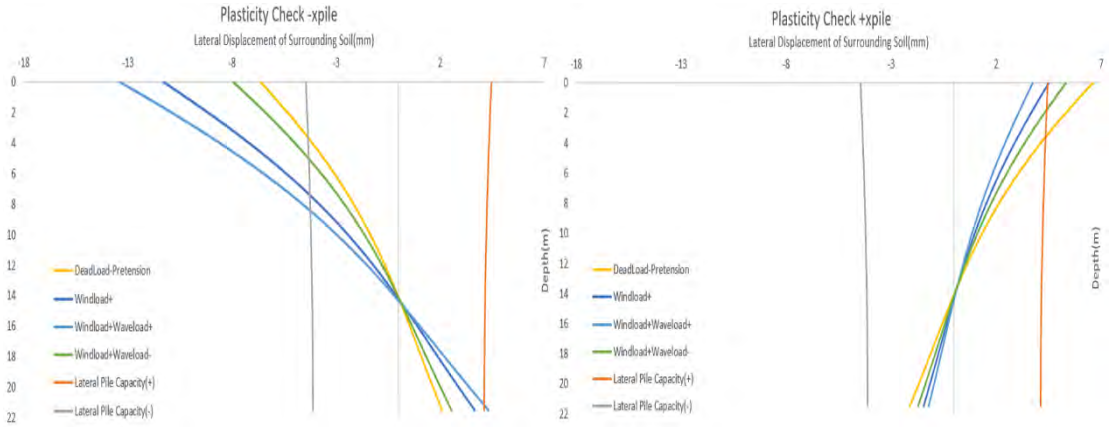

Figure A. 18 SOFiSTiK Plastification Zone estimation of opposite pair of piles Output(NC State).

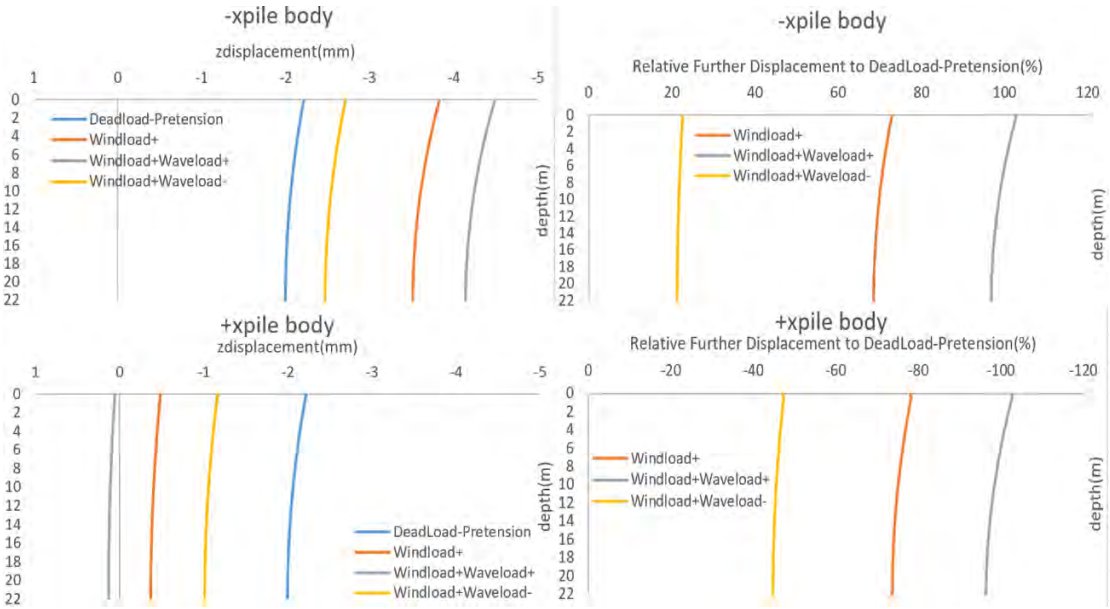

Figure A. 19 SOFiSTiK Vertical Displacement of opposite pair of piles Output(NC State).

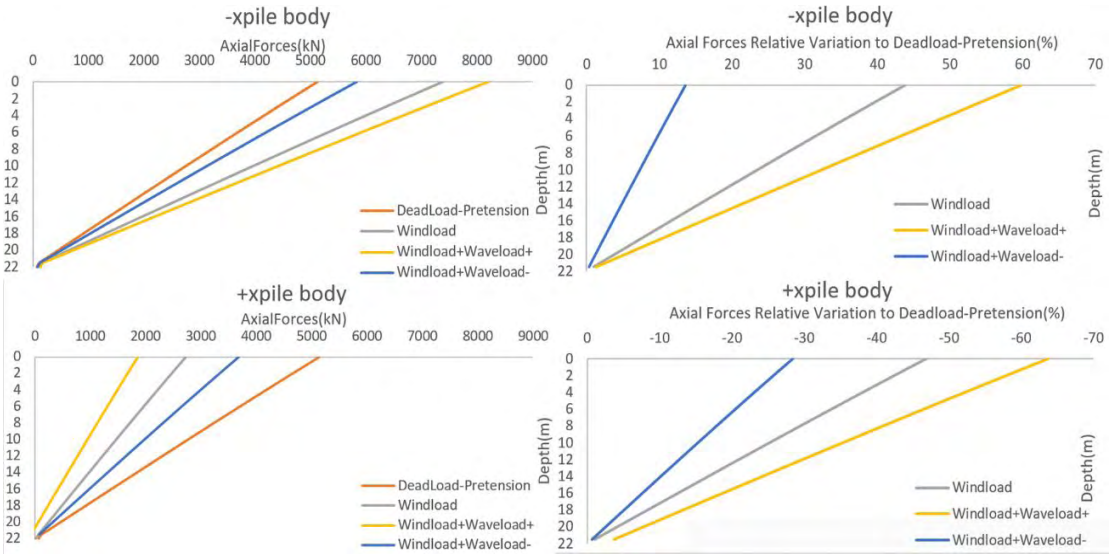

Figure A. 20 SOFiSTiK Axial Force Distribution of opposite pair of piles Output(NC State).

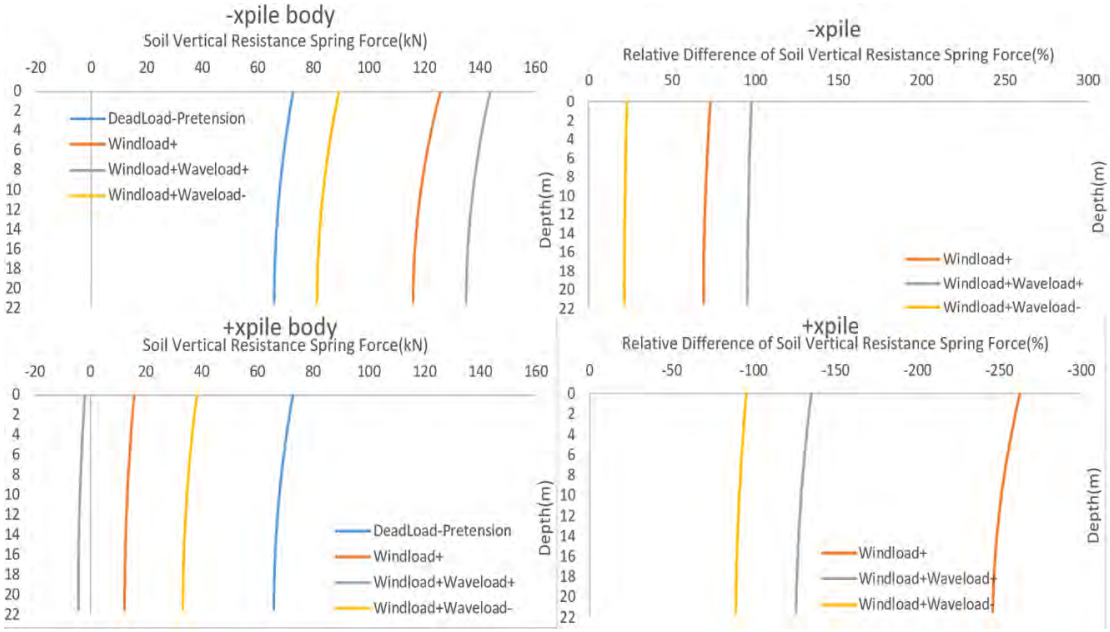

Figure A. 21 SOFiSTiK Earth Shaft Resistance Spring Force of opposite pair of piles Output(NC State).

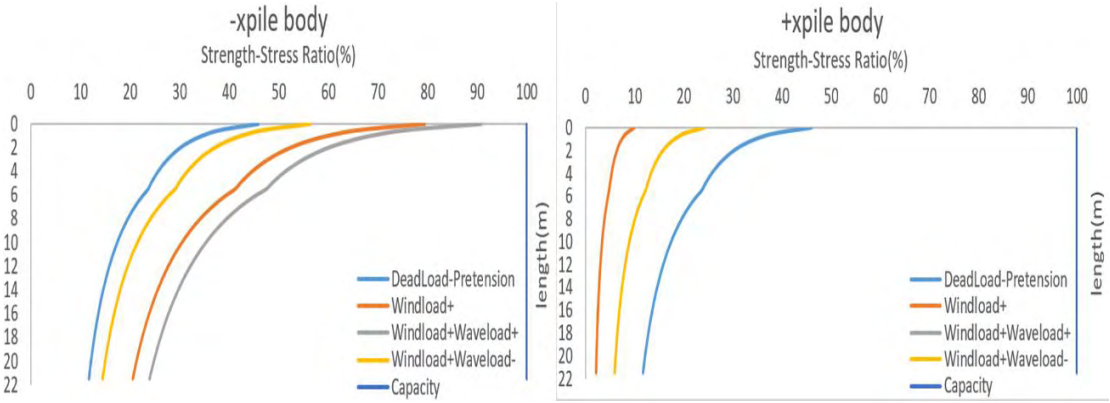

Figure A. 22 SOFiSTiK Stress Strength Ratio in terms of capacity against extrusion of opposite pair of piles Output(NC State).

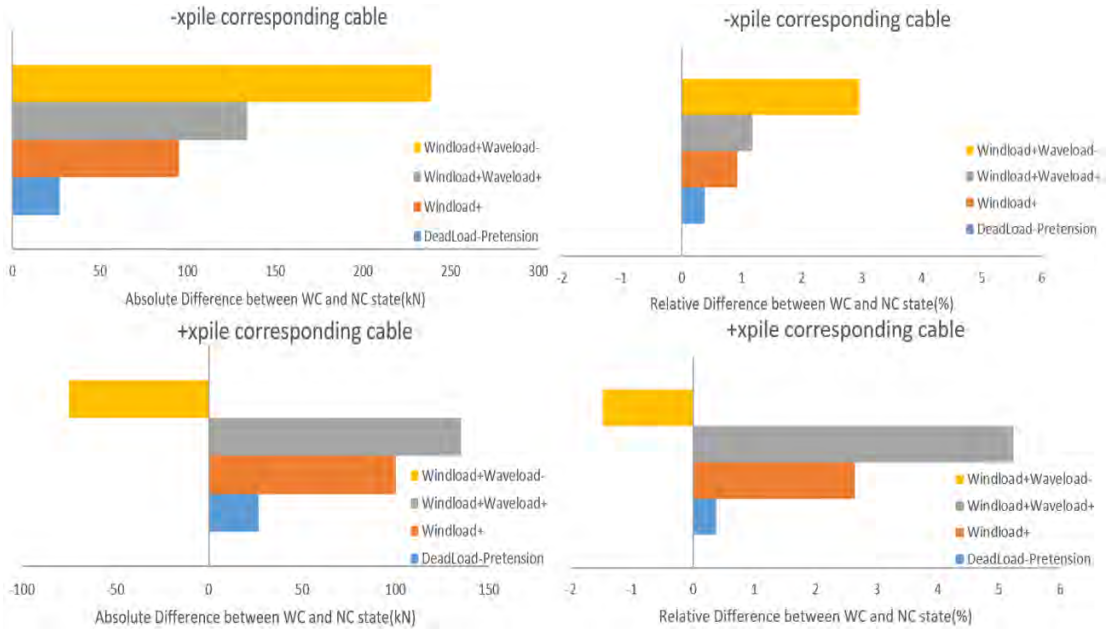

Figure A. 23 SOFiSTiK Divergence of Cable Axial Forces between NC and WC state Output.

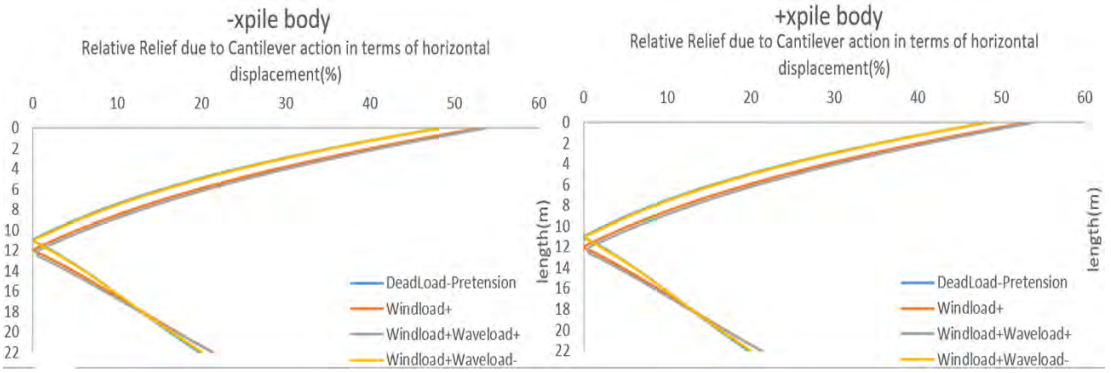

Figure A. 24 SOFiSTiK Relative relief in terms of horizontal displacement due to cantilever influence.

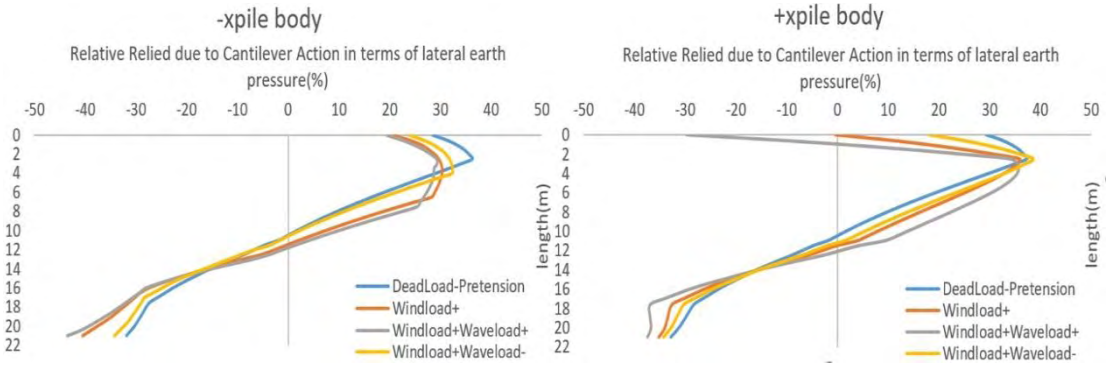

Figure A. 25 SOFiSTiK Relative relief in terms of lateral earth pressure due to cantilever influence.

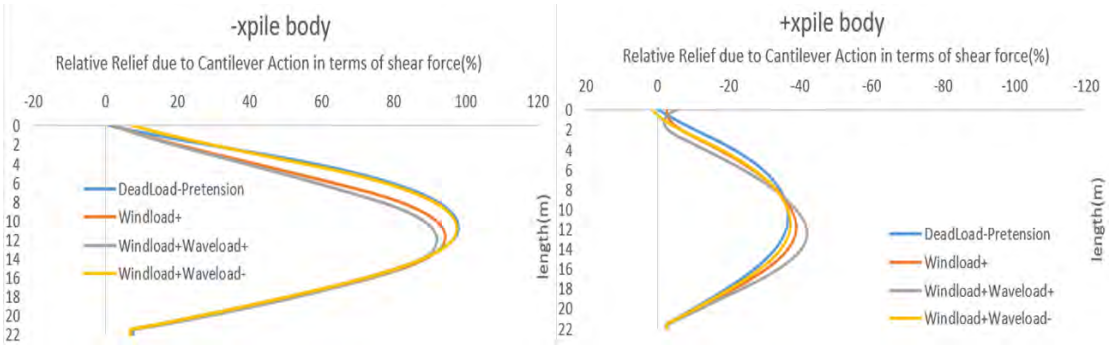

Figure A. 26 SOFiSTiK Relative relief in terms of shear force distribution due to cantilever influence.

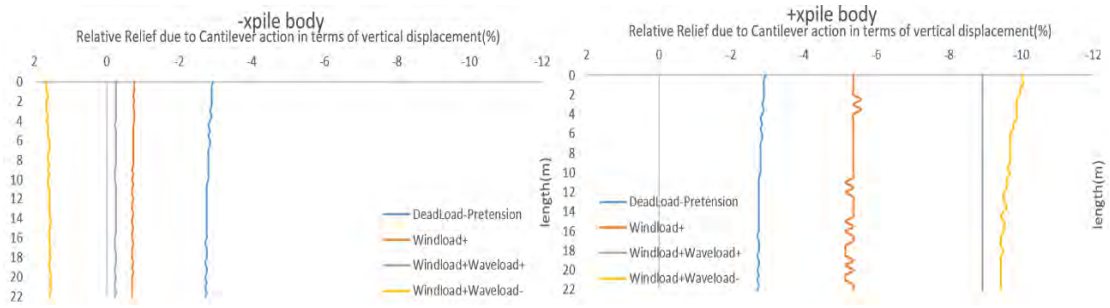

Figure A. 27 SOFiSTiK Relative relief in terms of vertical displacement due to cantilever influence.

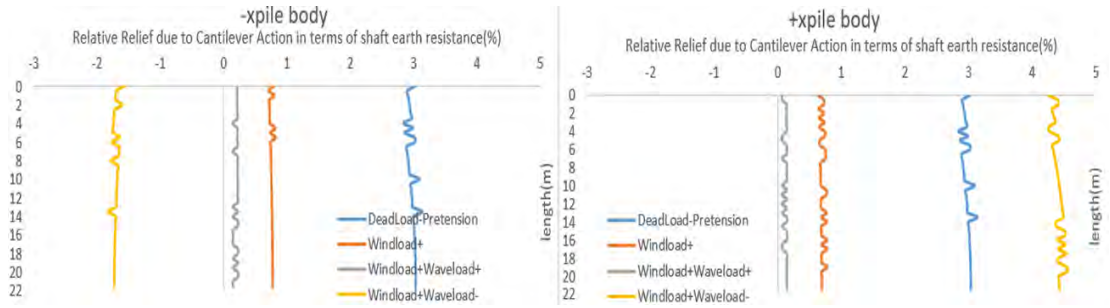

Figure A. 28 SOFiSTiK Relative relief in terms of shaft earth resistance due to cantilever influence.

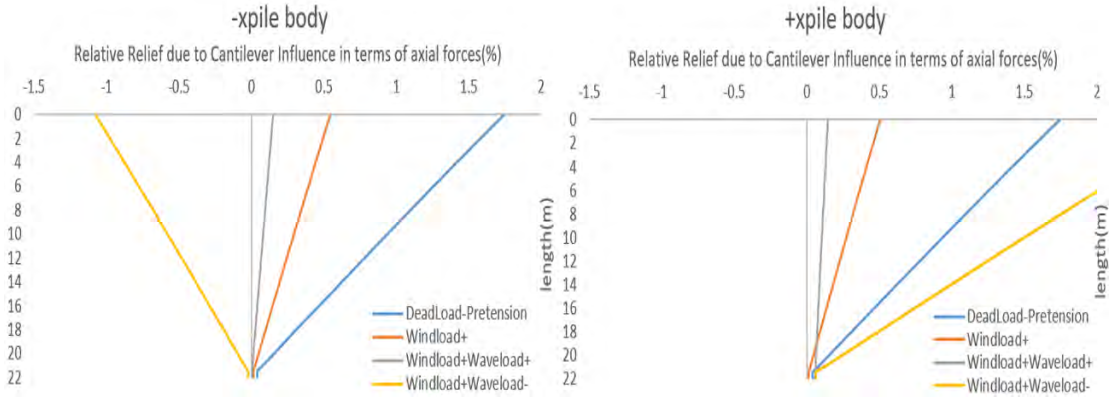

Figure A. 29 SOFiSTiK Relative relief in terms of axial force distribution due to cantilever influence.

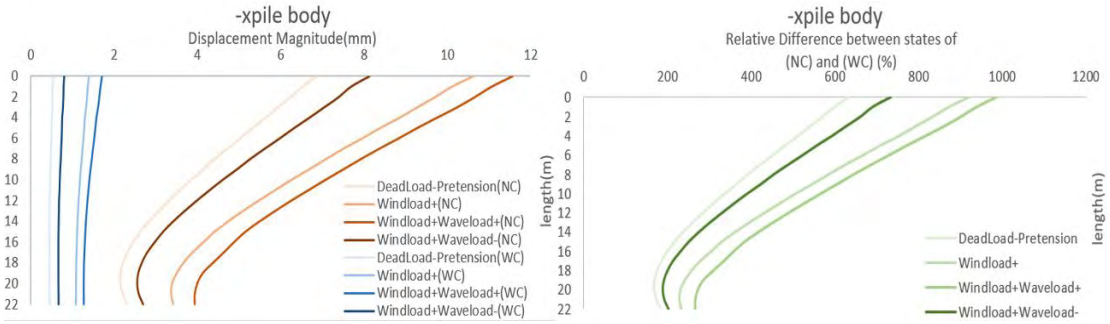

Figure A. 30 Relative Reduction of the axial force thanks to the addition of the cantilever element according to MARC Mentat.

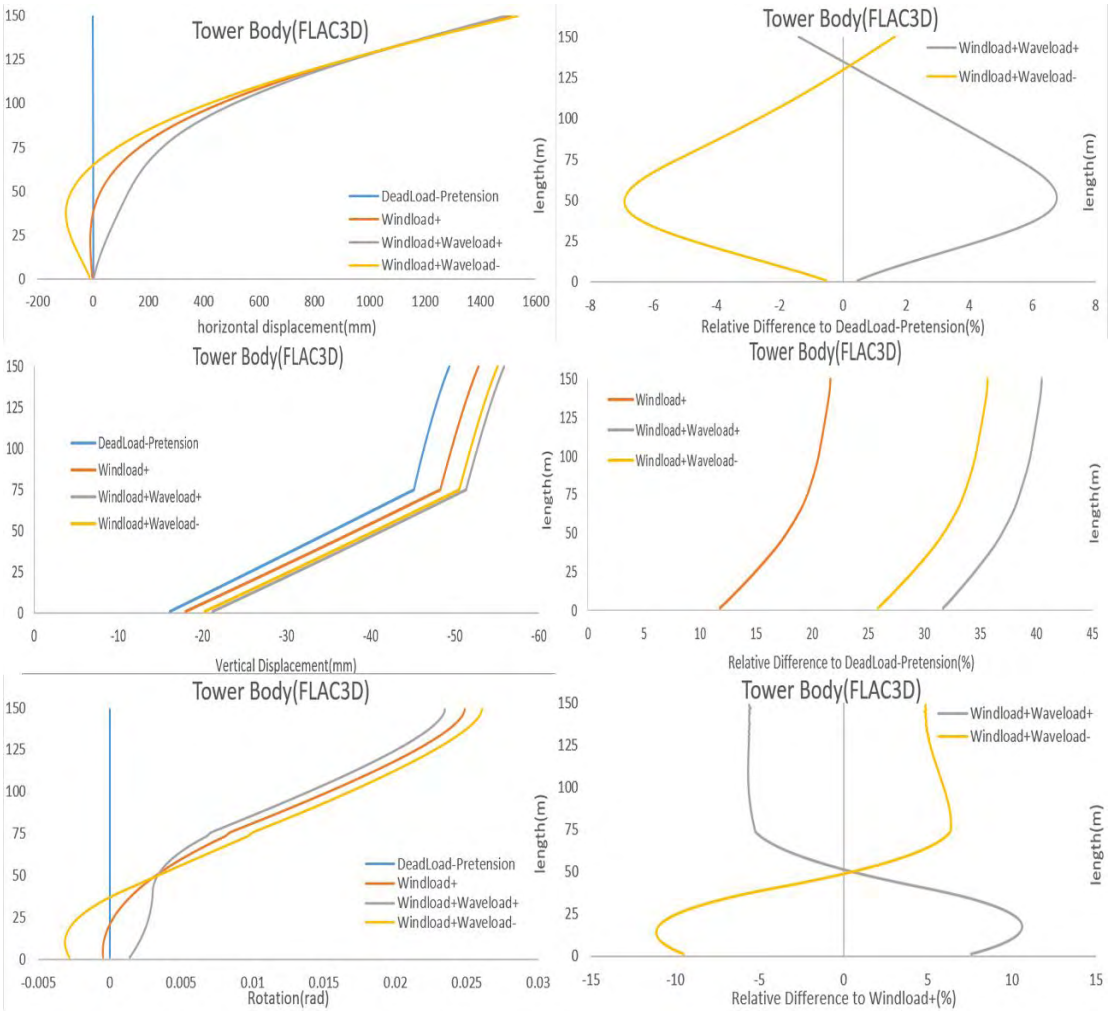

Figure B. 1 FLAC^{3D} Tower Deflection Output.

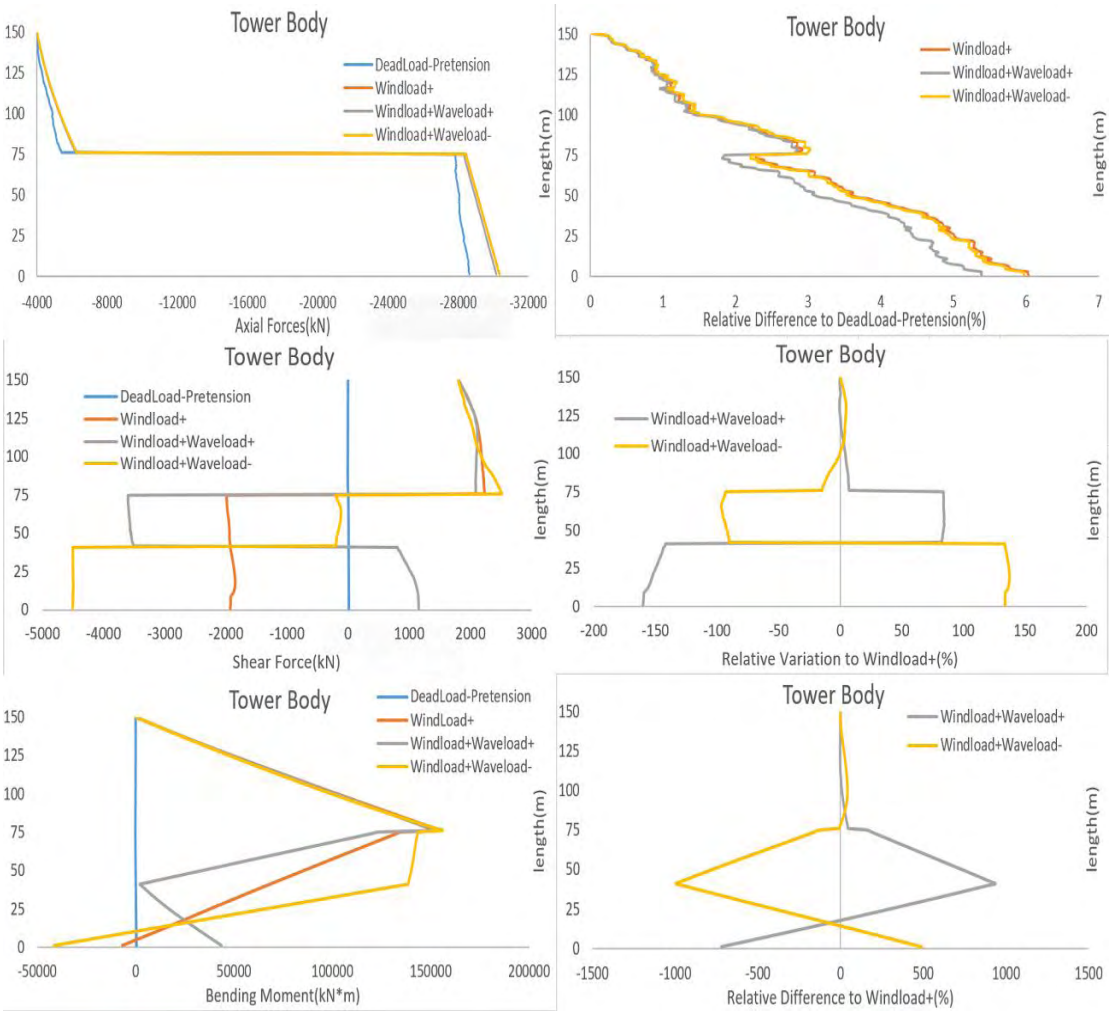

Figure B. 2 FLAC^{3D} Tower Resultants Output.

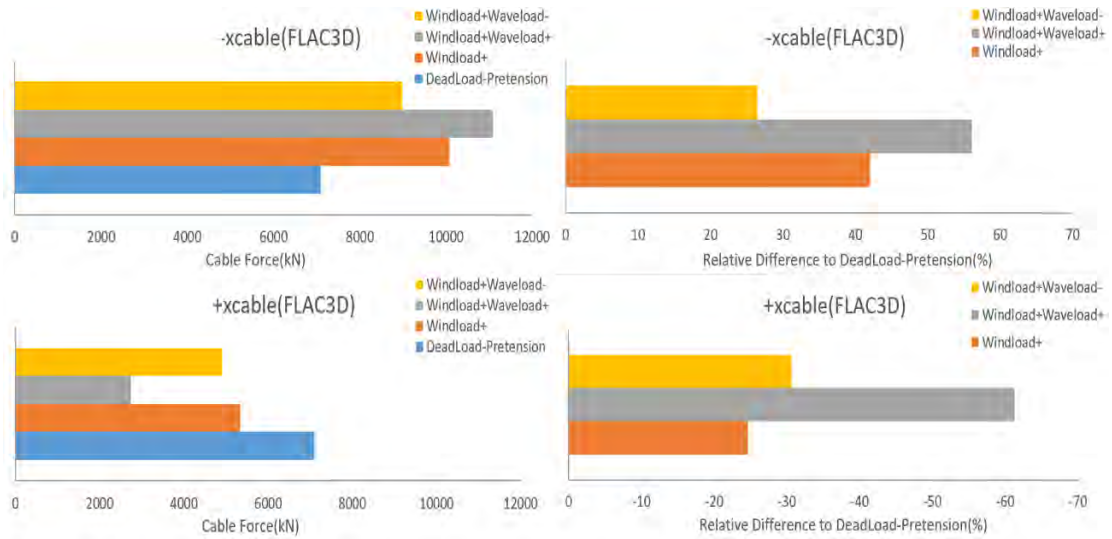

Figure B. 3 FLAC^{3D} Cable Forces Resultants Output.

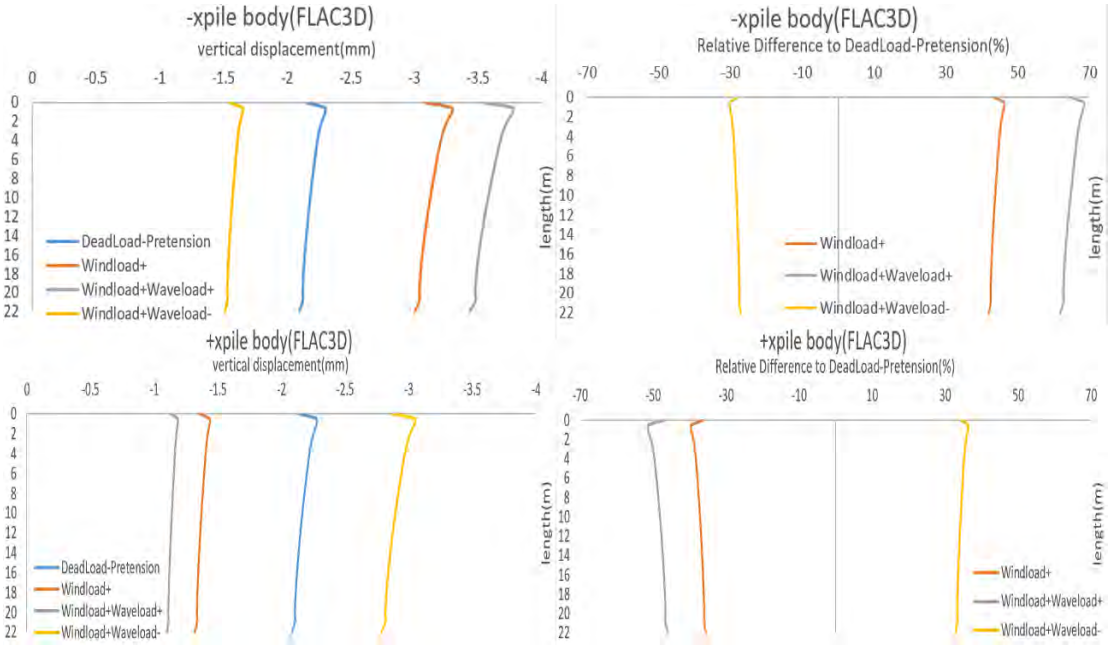

Figure B. 4 FLAC^{3D} horizontal displacement of pair of opposite piles Output.

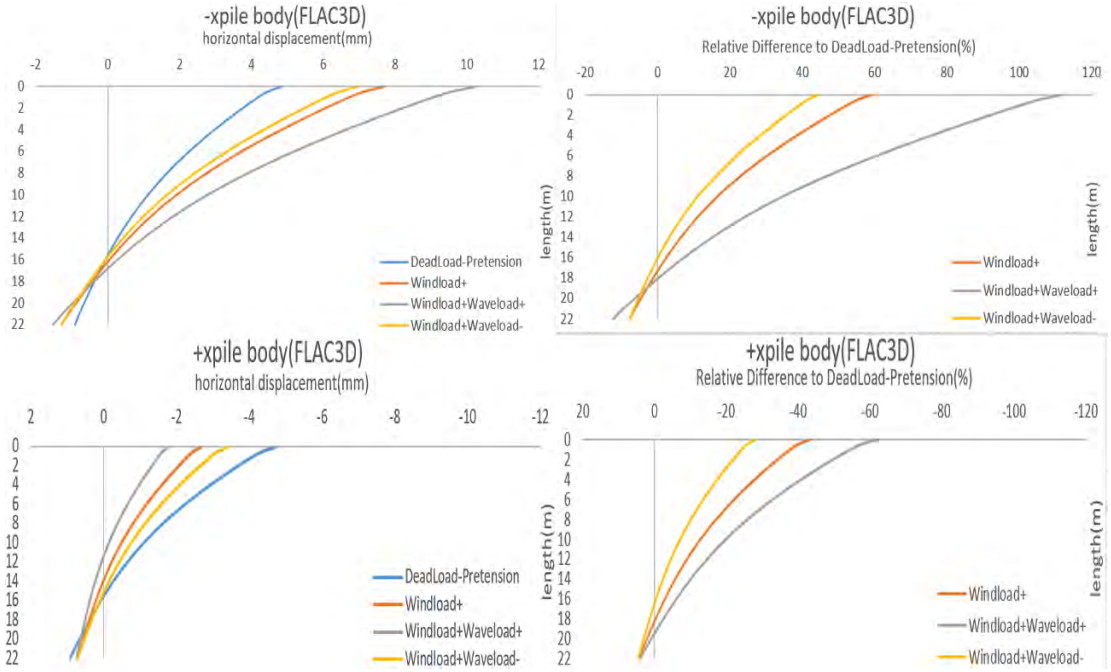

Figure B. 5 FLAC^{3D} vertical displacement of pair of opposite piles Output.

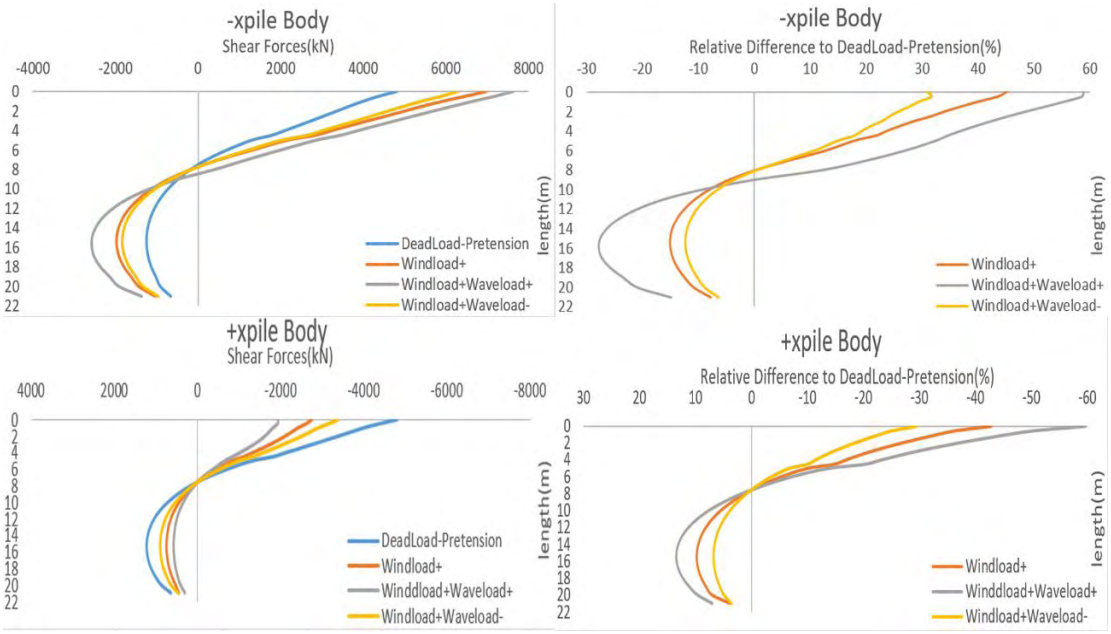

Figure B. 6 FLAC^{3D} axial force distribution of pair of opposite piles Output.

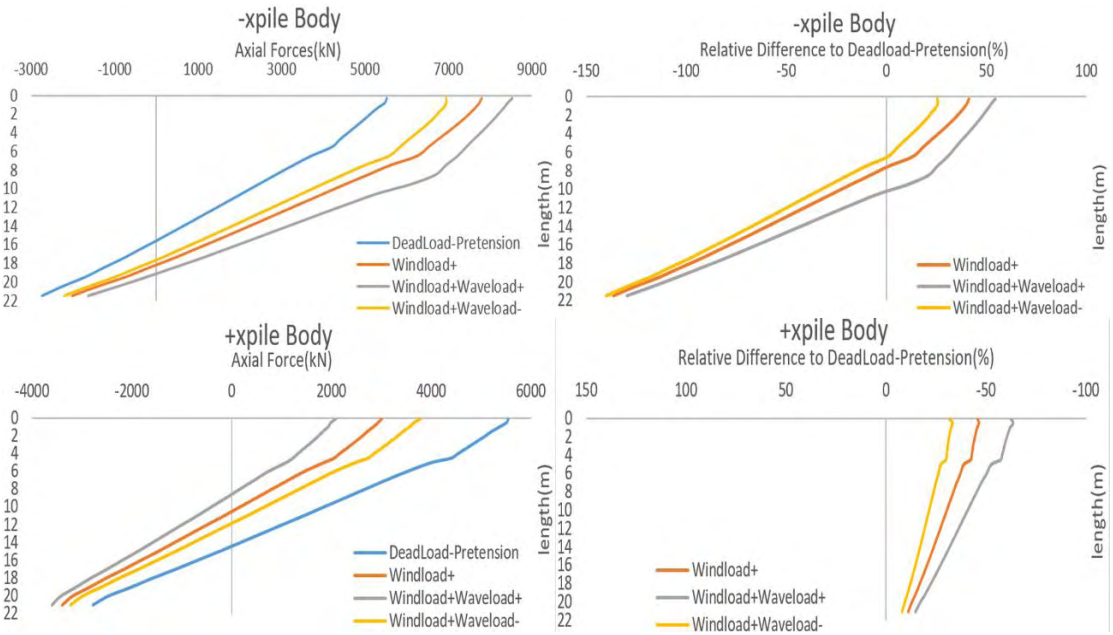

Figure B. 7 FLAC^{3D} shear force distribution of pair of opposite piles Output.

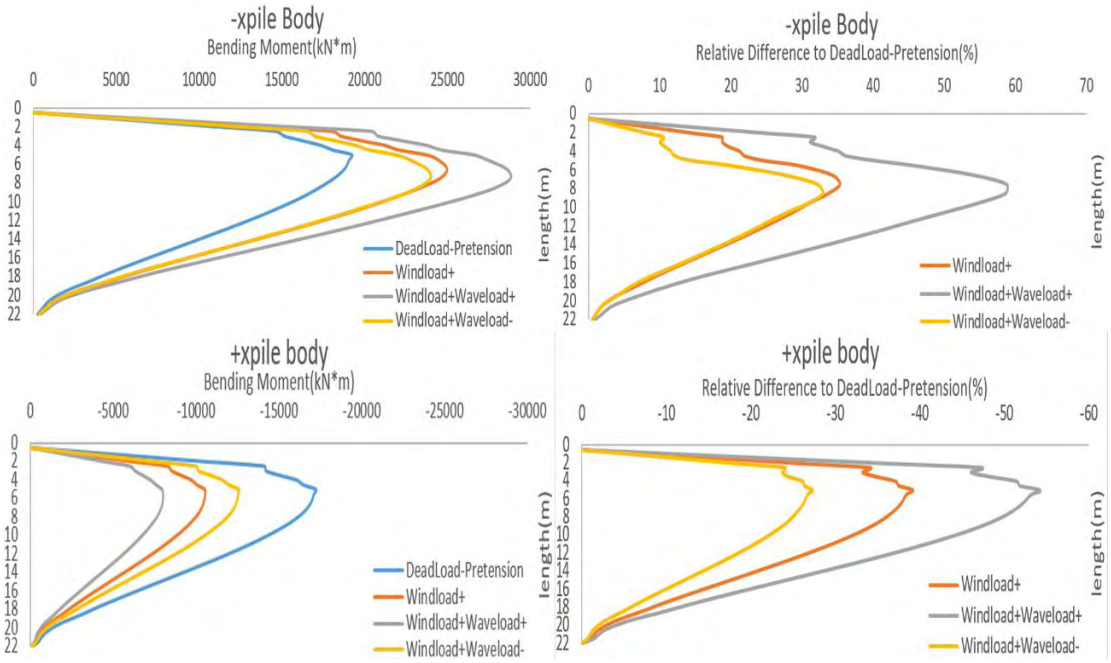

Figure B. 8 FLAC^{3D} bending moments distribution of pair of opposite piles Output.

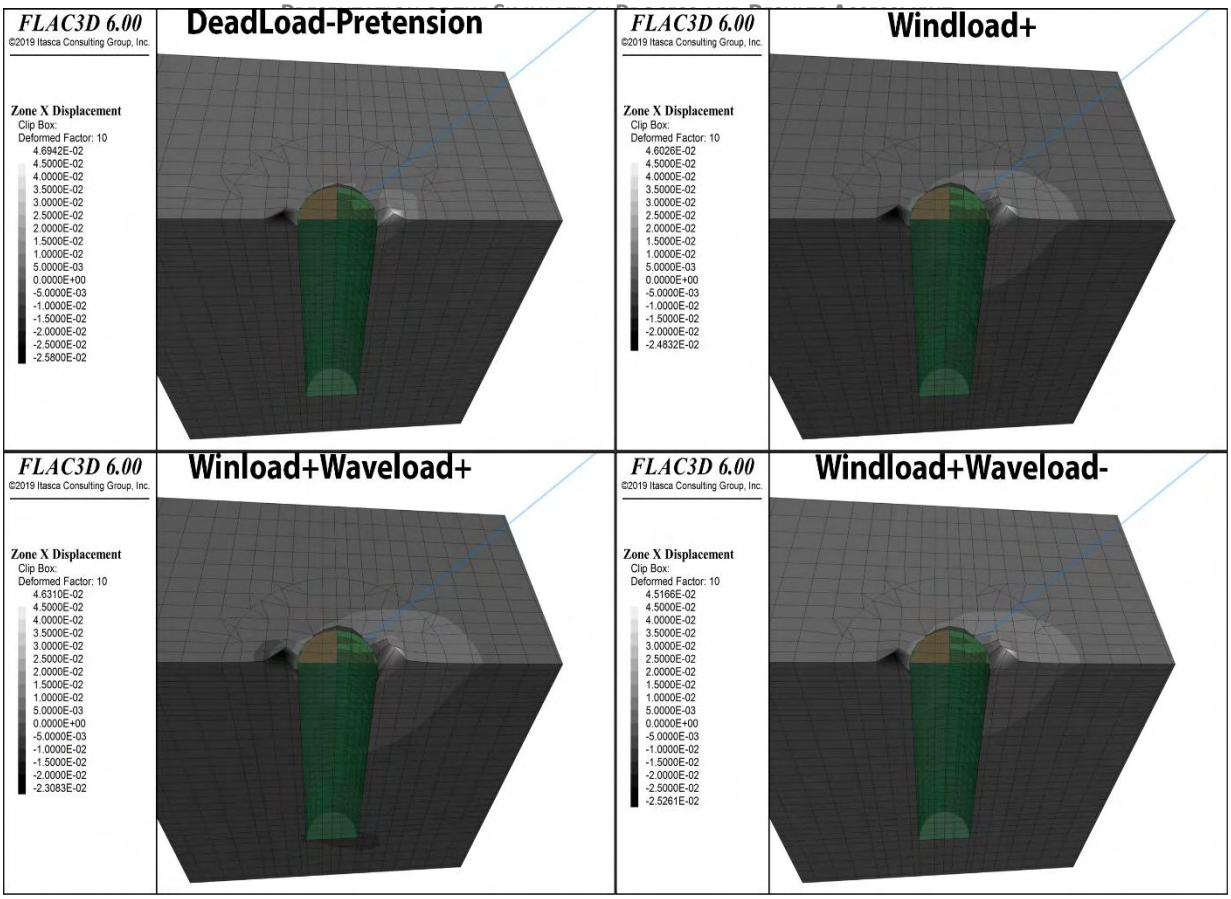

Figure B. 9 FLAC^{3D} pile surrounding soil horizontal kinematics.

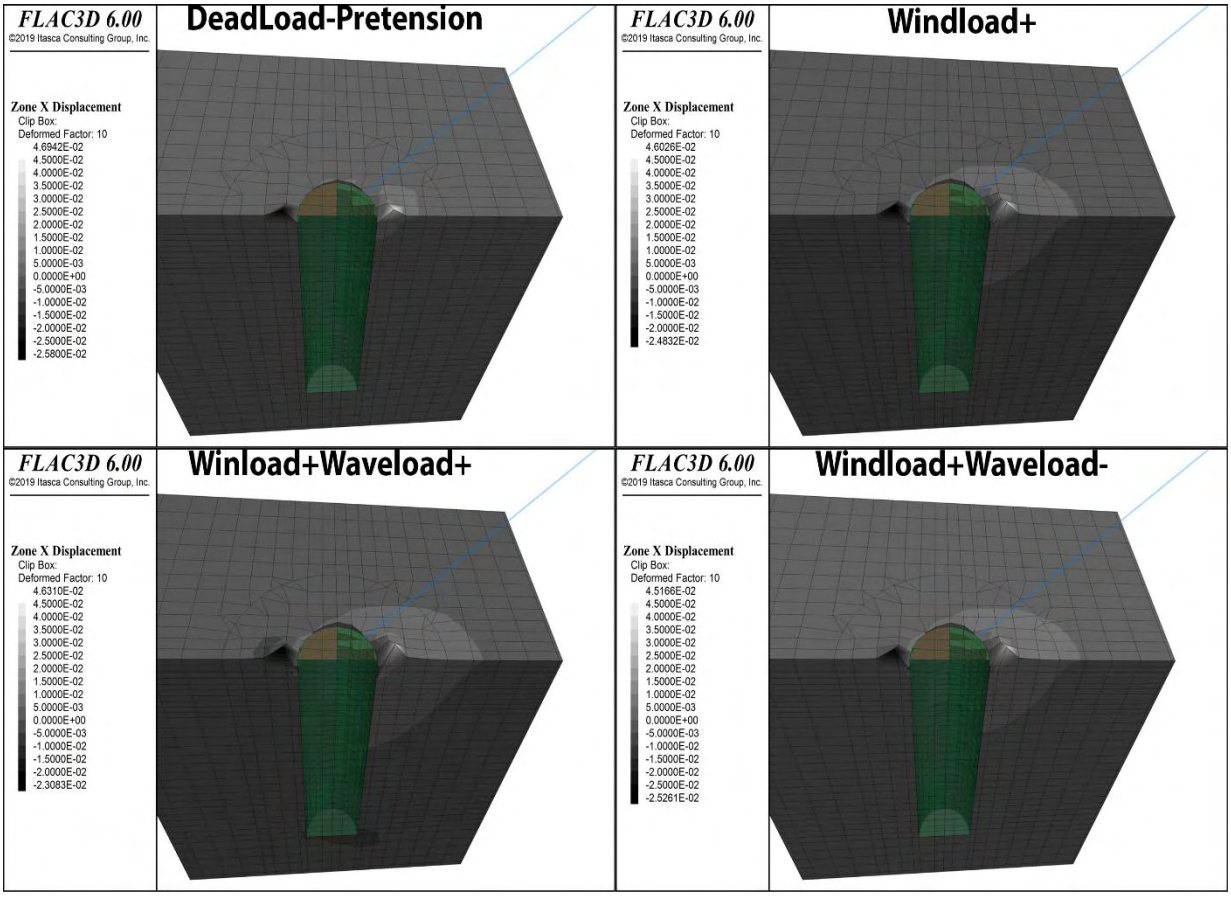

Figure B. 10 FLAC^{3D} pile surrounding soil horizontal(xx) stress field.

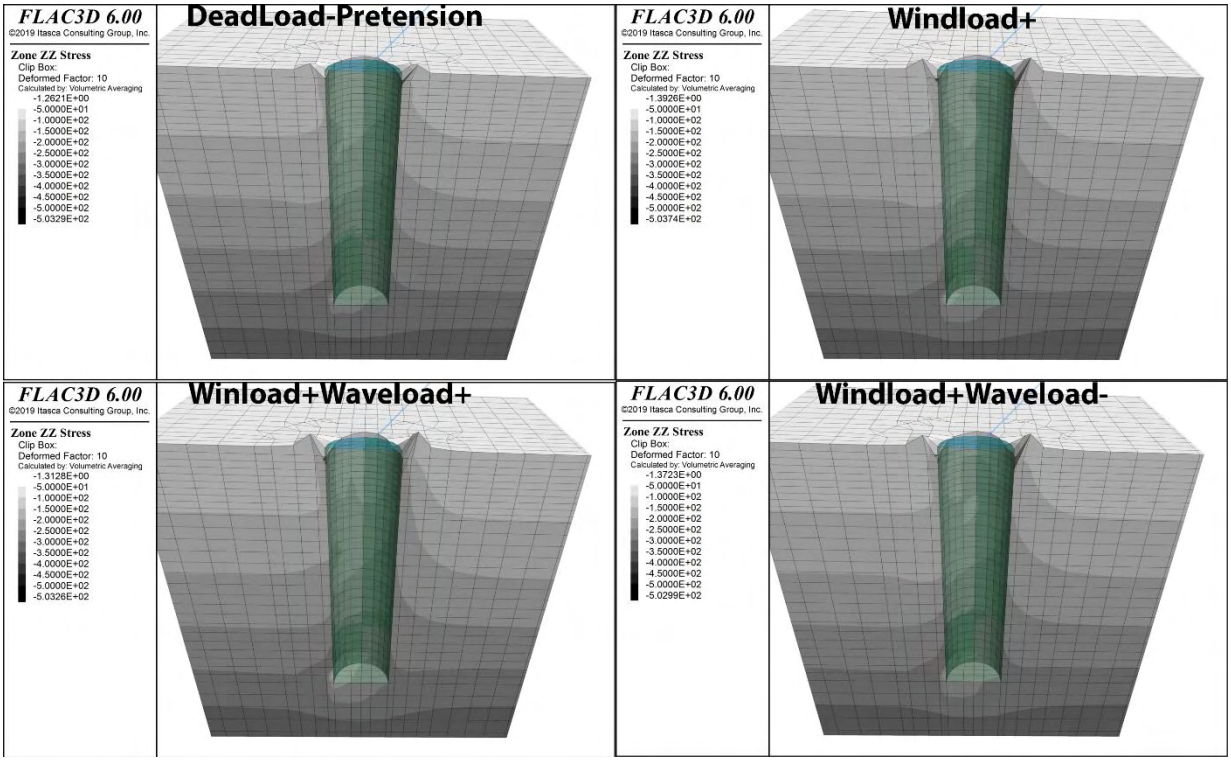

Figure B. 11 FLAC^{3D} pile surrounding soil vertical(zz) stress field.

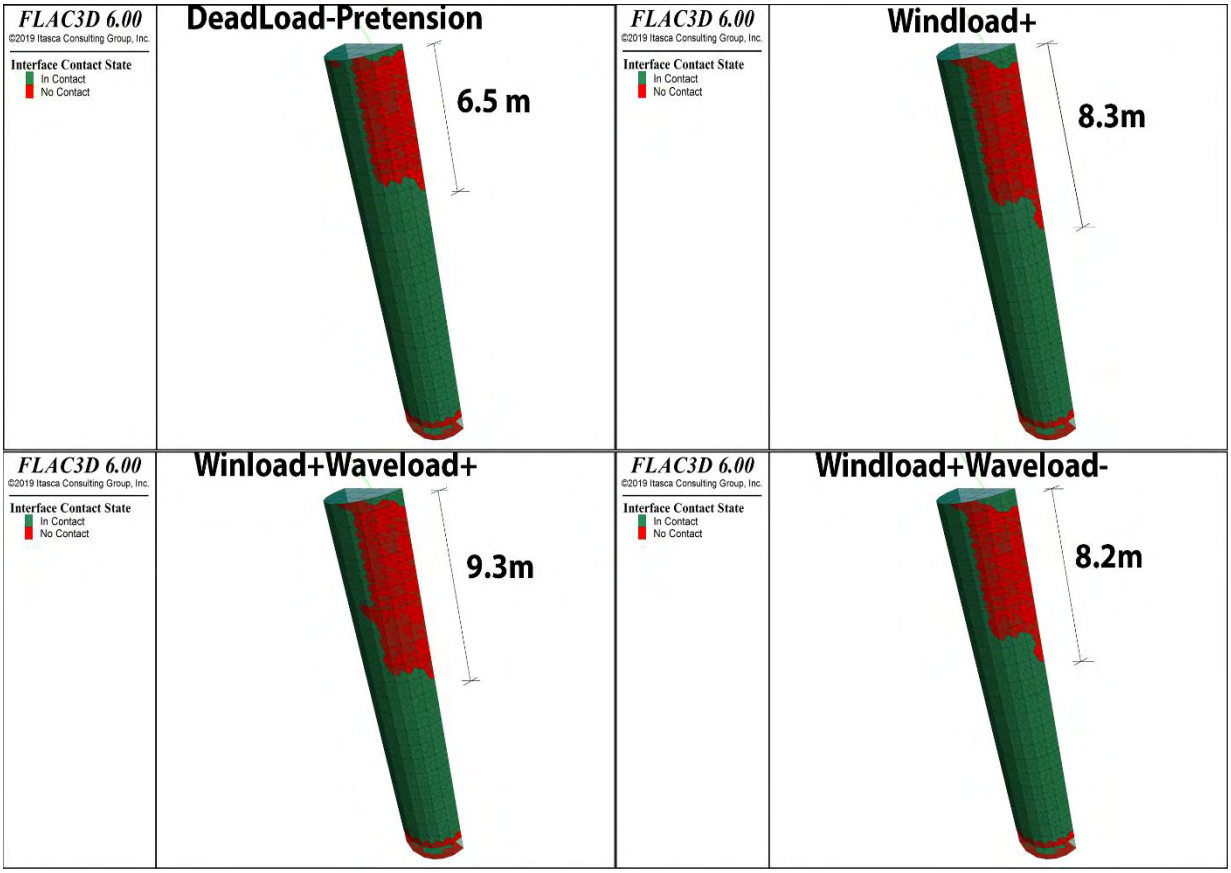

Figure B. 12 FLAC^{3D} pile interface contact status.

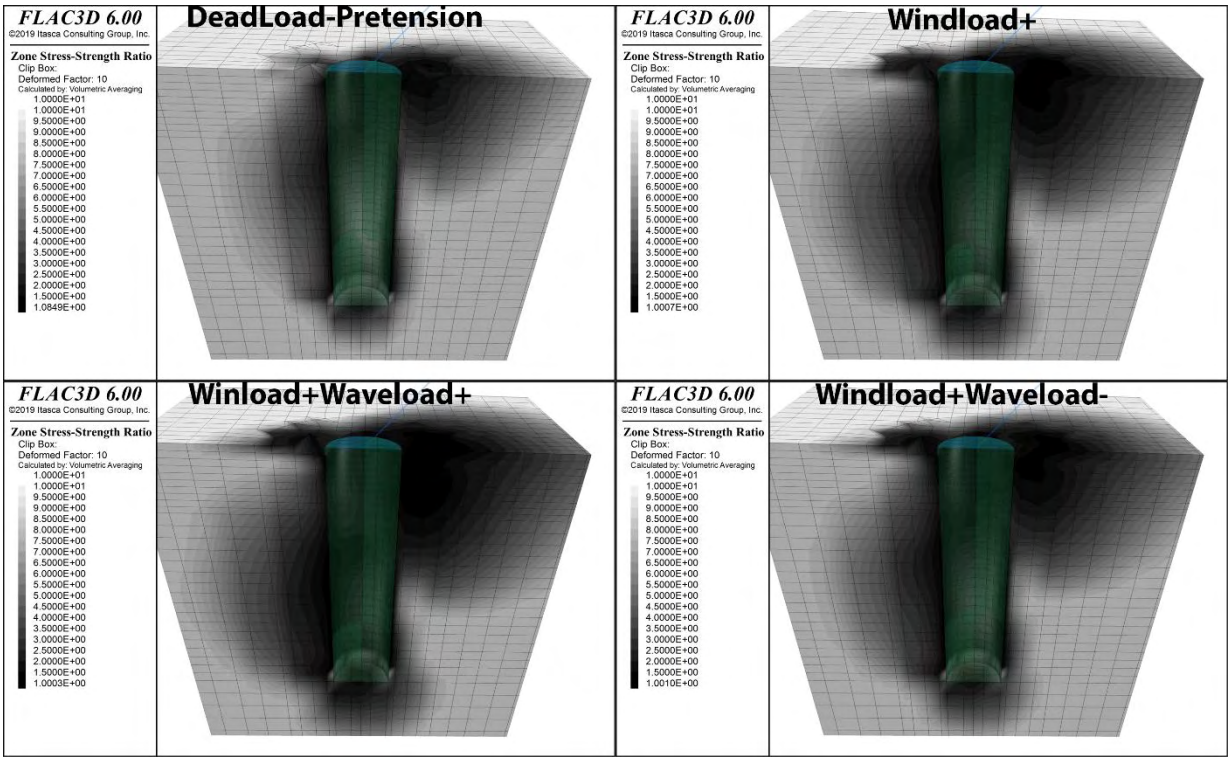

Figure B. 13 FLAC^{3D} Stress Strength ratio status of soil near piles.

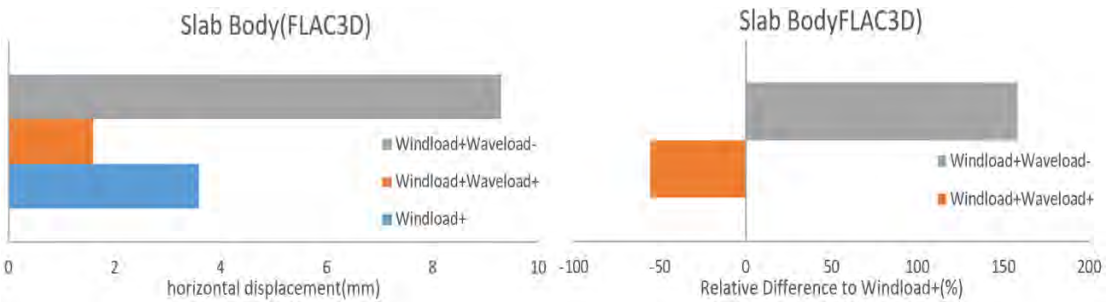

Figure B. 14 FLAC^{3D} Foundation Slab horizontal displacement output.

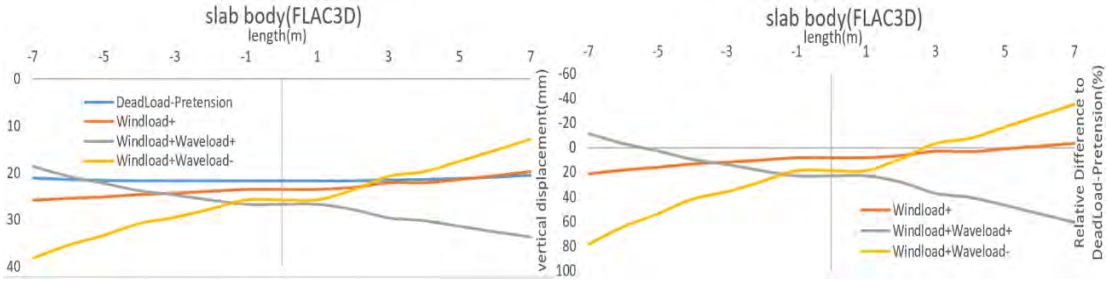

Figure B. 15 FLAC^{3D} Foundation Slab vertical displacement output.

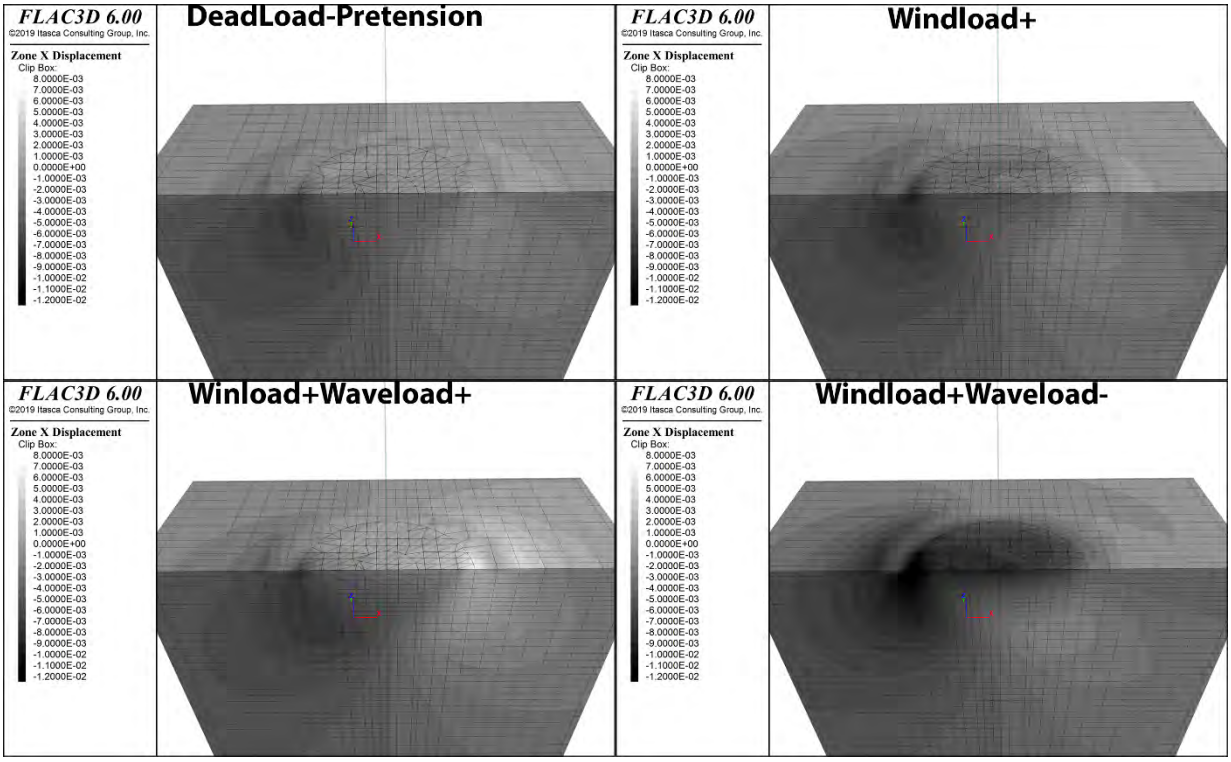

Figure B. 16 FLAC^{3D} soil beneath shallow foundation horizontal displacement output.

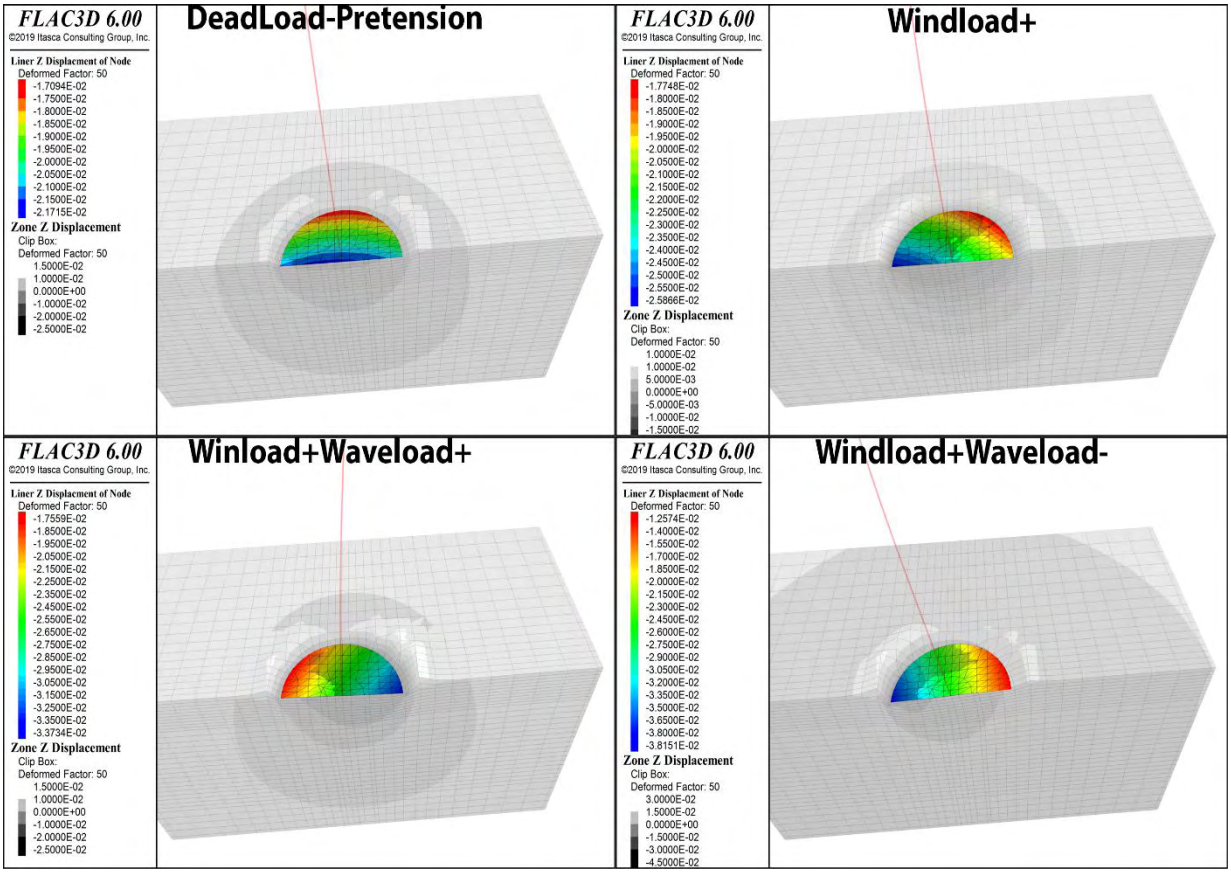

Figure B. 17 FLAC^{3D} soil beneath shallow foundation vertical displacement output.

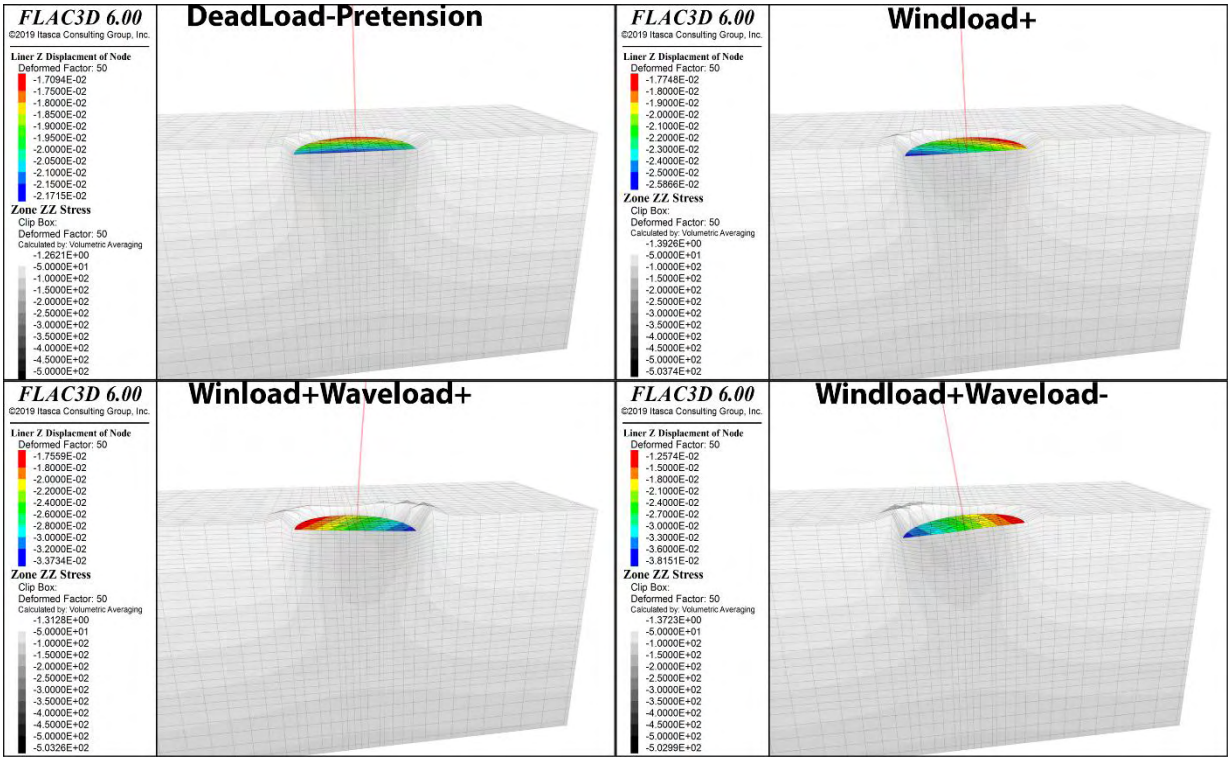

Figure B. 18 FLAC^{3D} soil beneath shallow foundation vertical (zz) stress filed output.

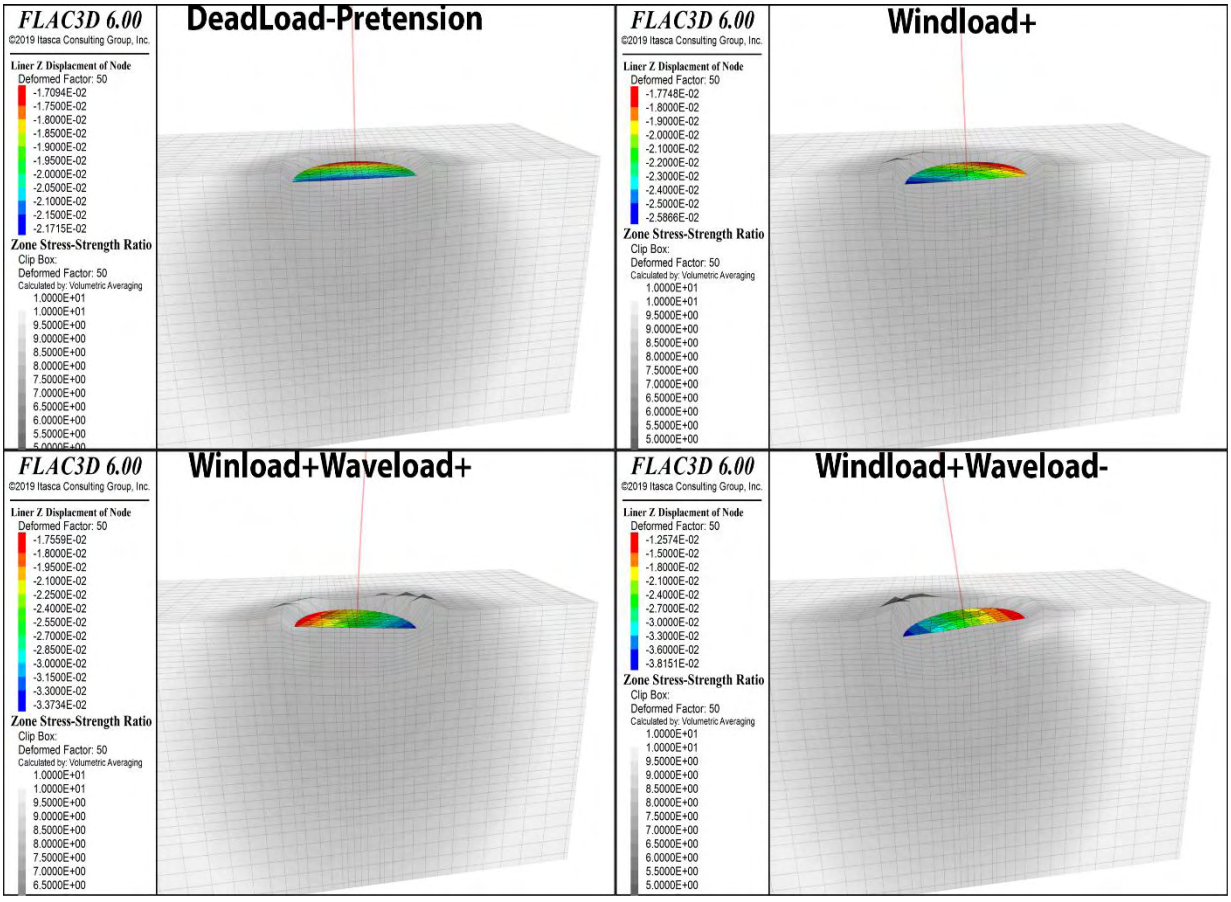

Figure B. 19 FLAC^{3D} soil beneath shallow foundation plastic zone estimation output.

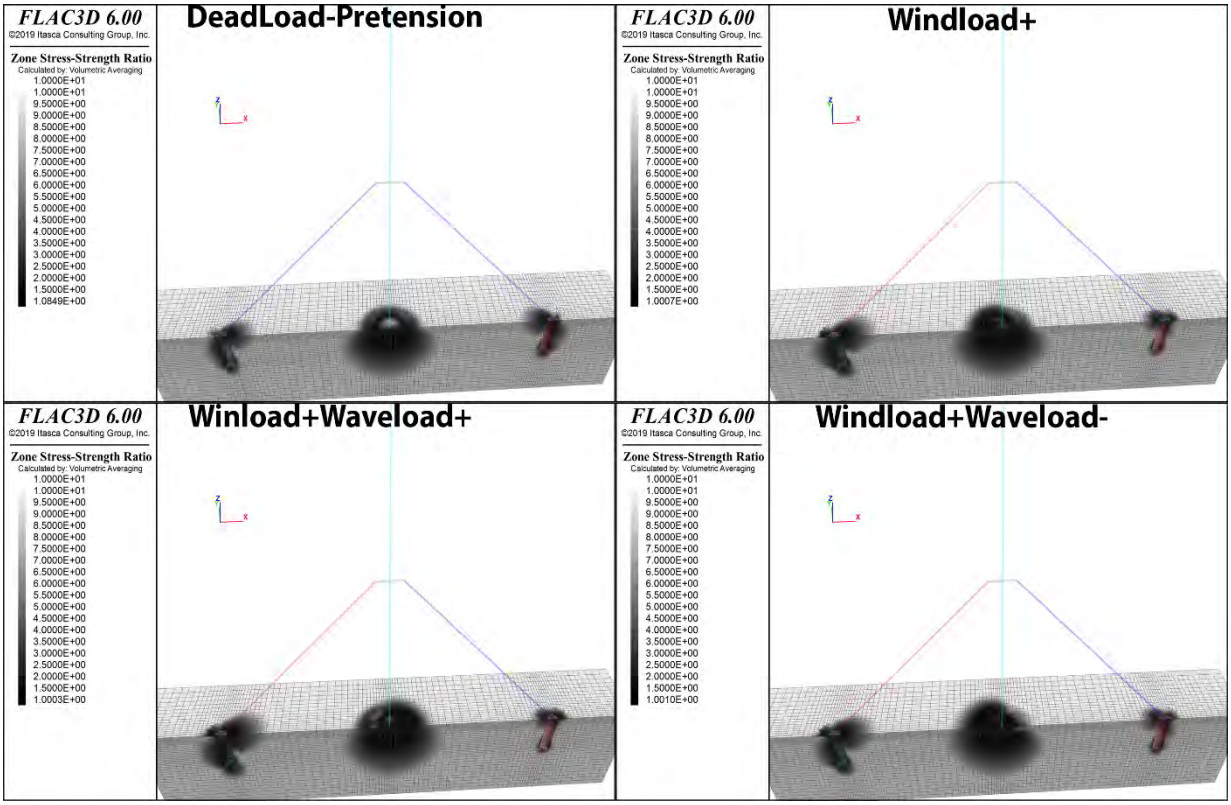

Figure B. 20 FLAC^{3D} plastification zone ranges in global aspect.

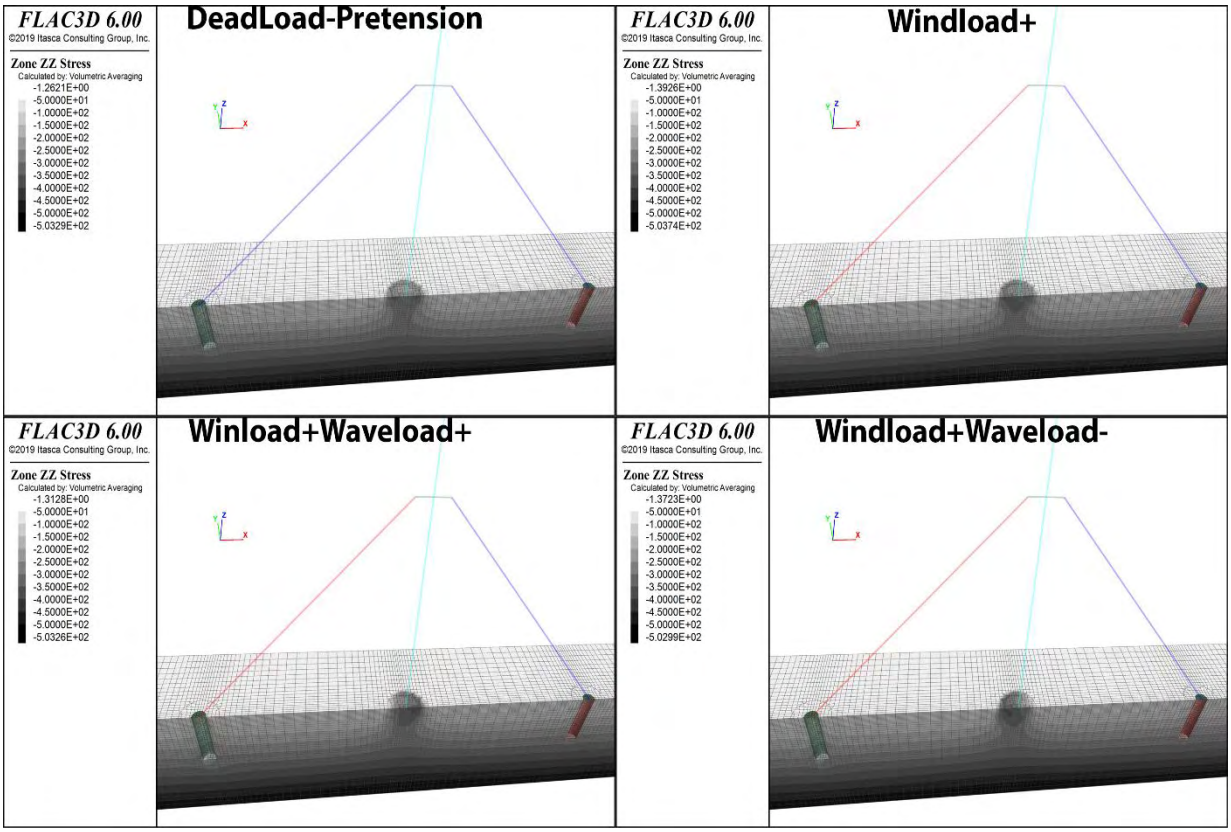

.

Figure B. 21 FLAC^{3D} zzstress distribution in global aspect.

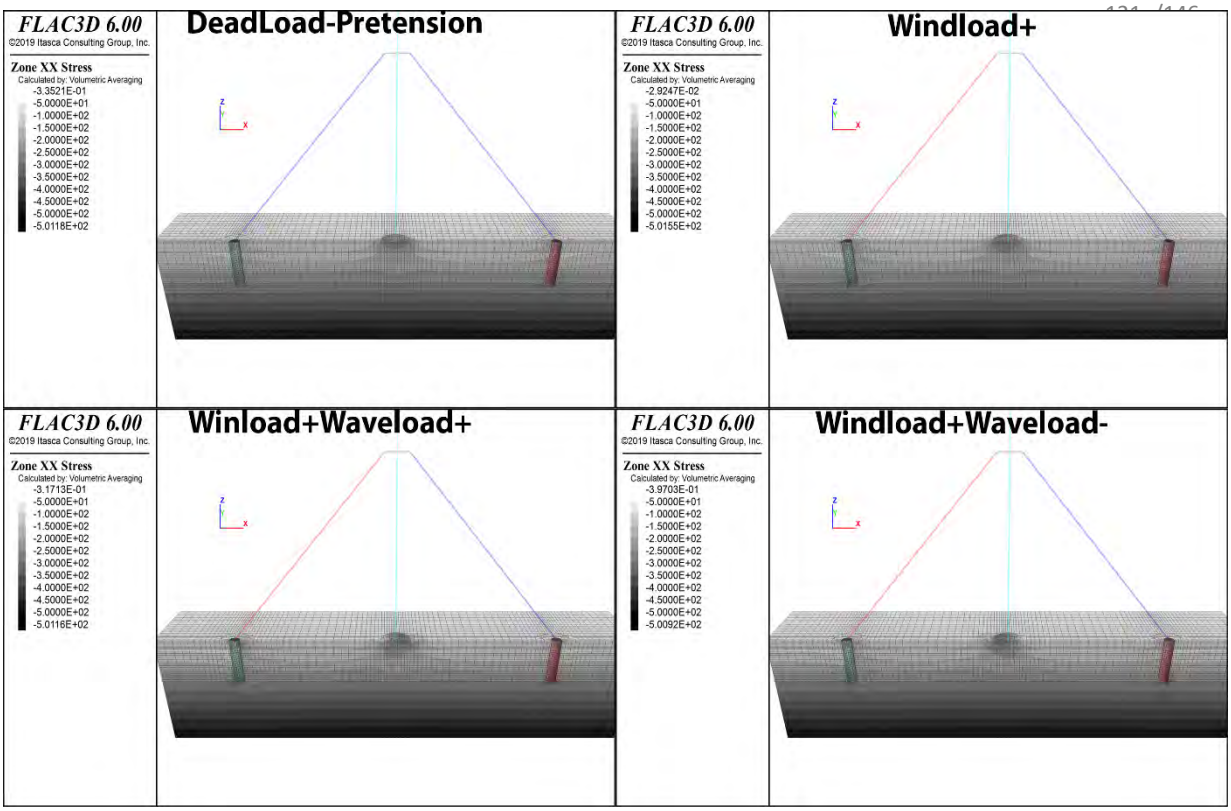

Figure B. 22 FLAC^{3D} xxstress distribution in global aspect.

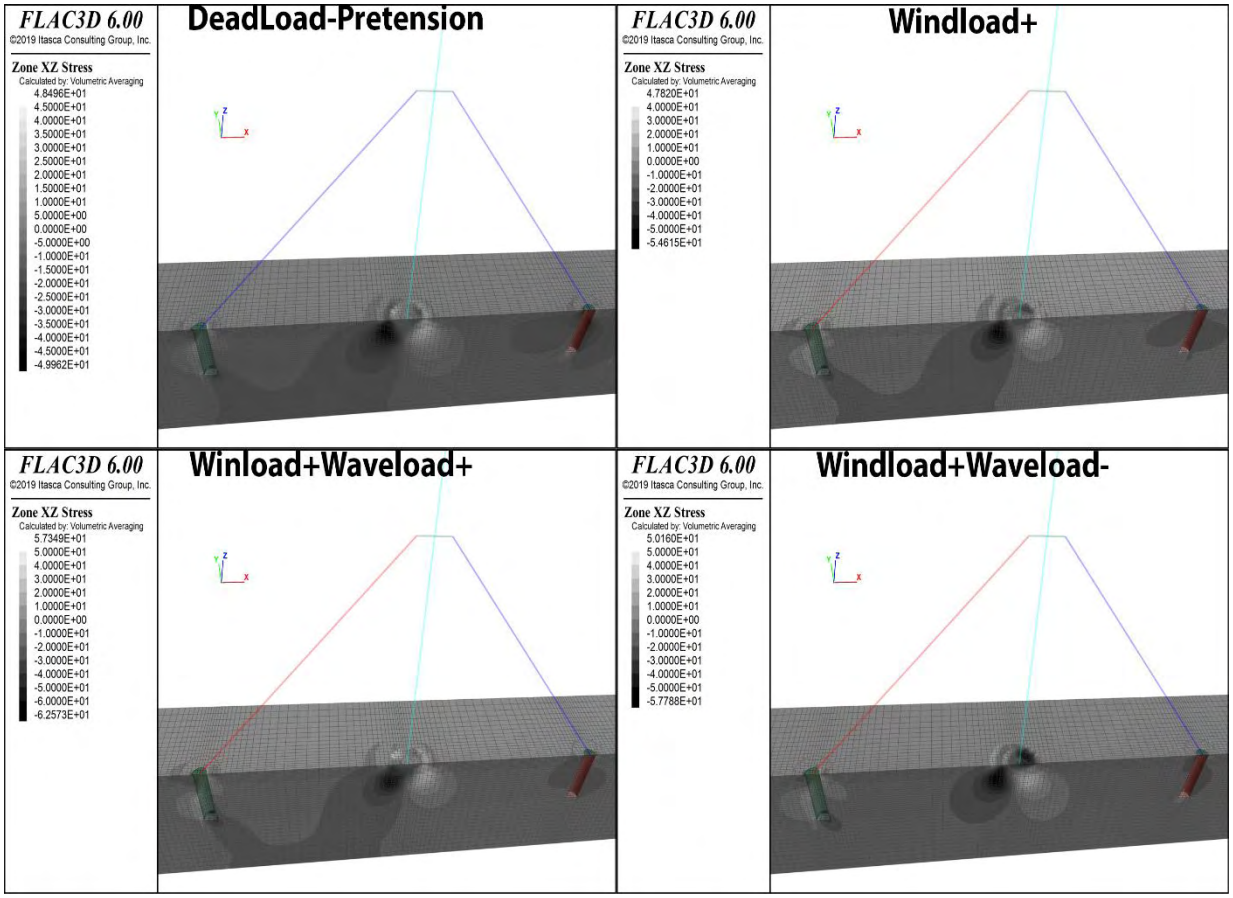

Figure B. 23 FLAC^{3D} xzstress distribution in global aspect.

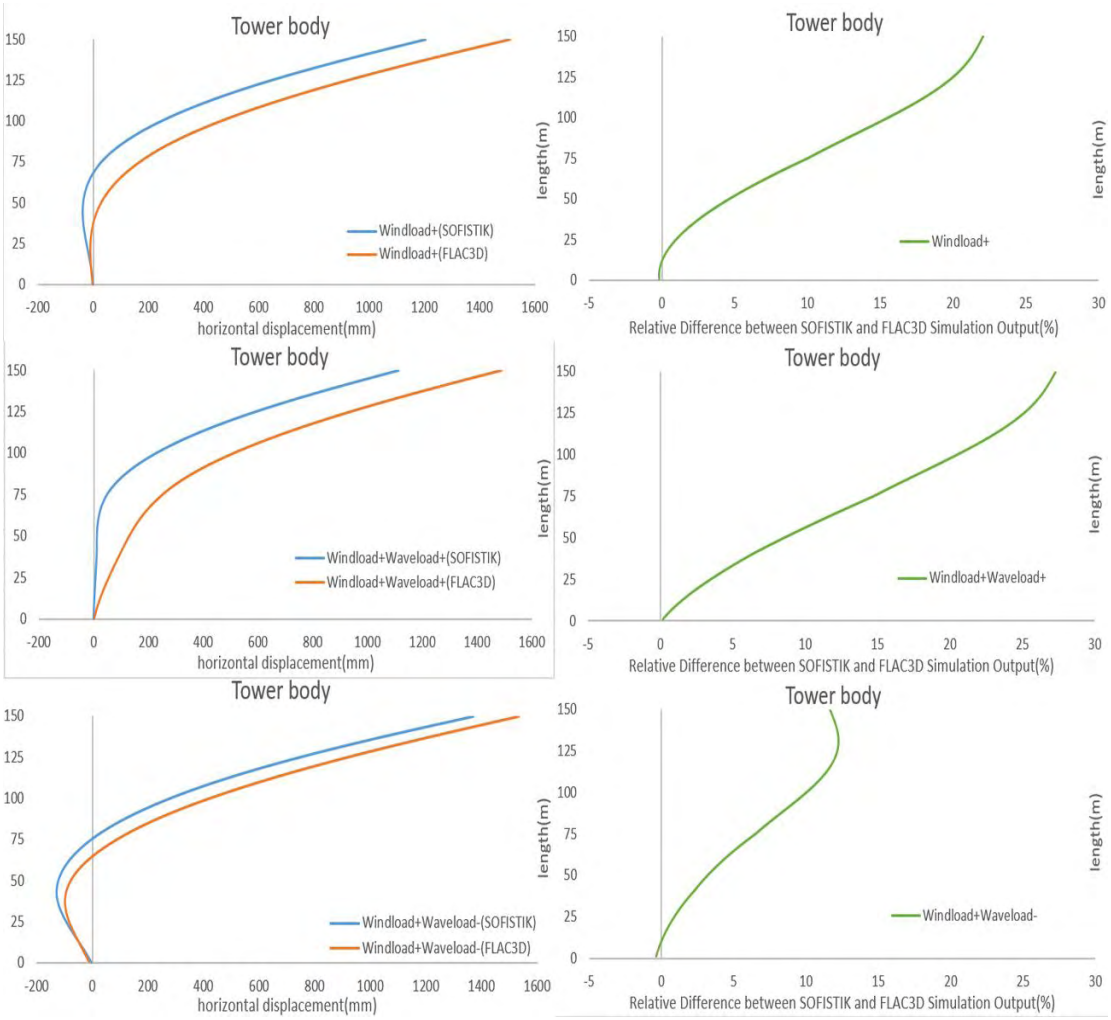

Figure C. 1 STDM and FTDM Simulation differences in terms of tower horizontal deflection.

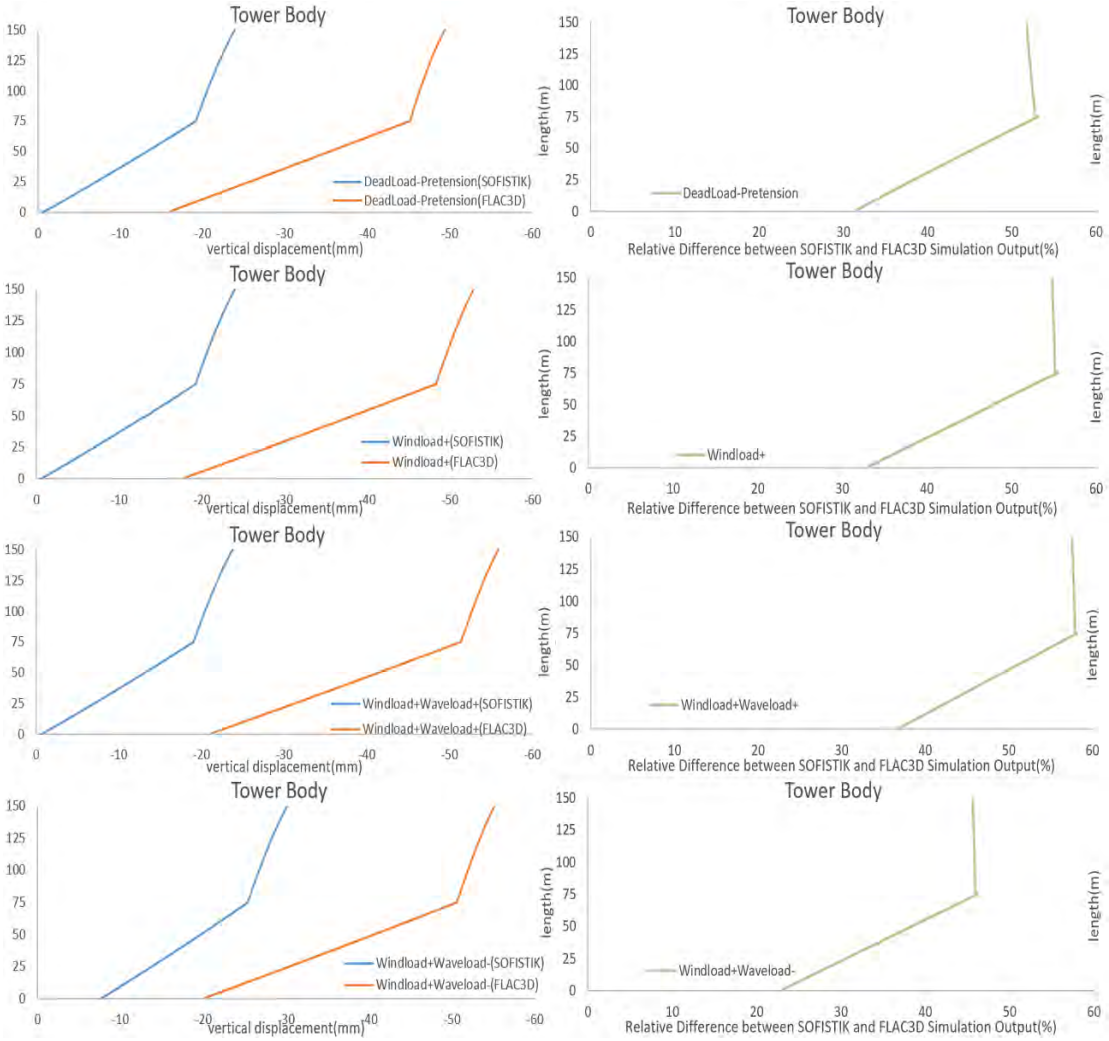

Figure C. 2 STDM and FTDM Simulation differences in terms of tower vertical deflection.

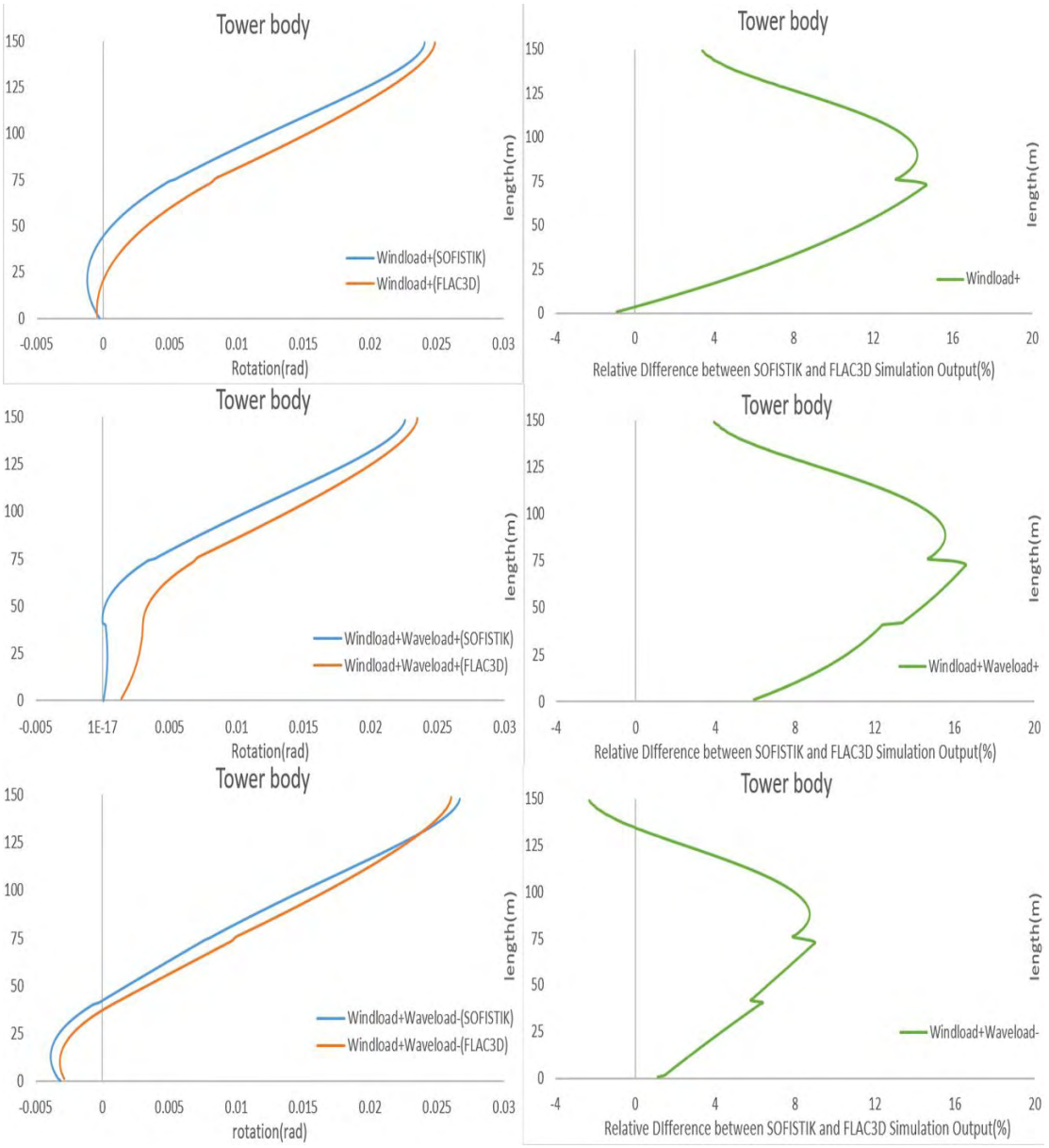

Figure C. 3 STDM and FTDM Simulation differences in terms of tower rotation.

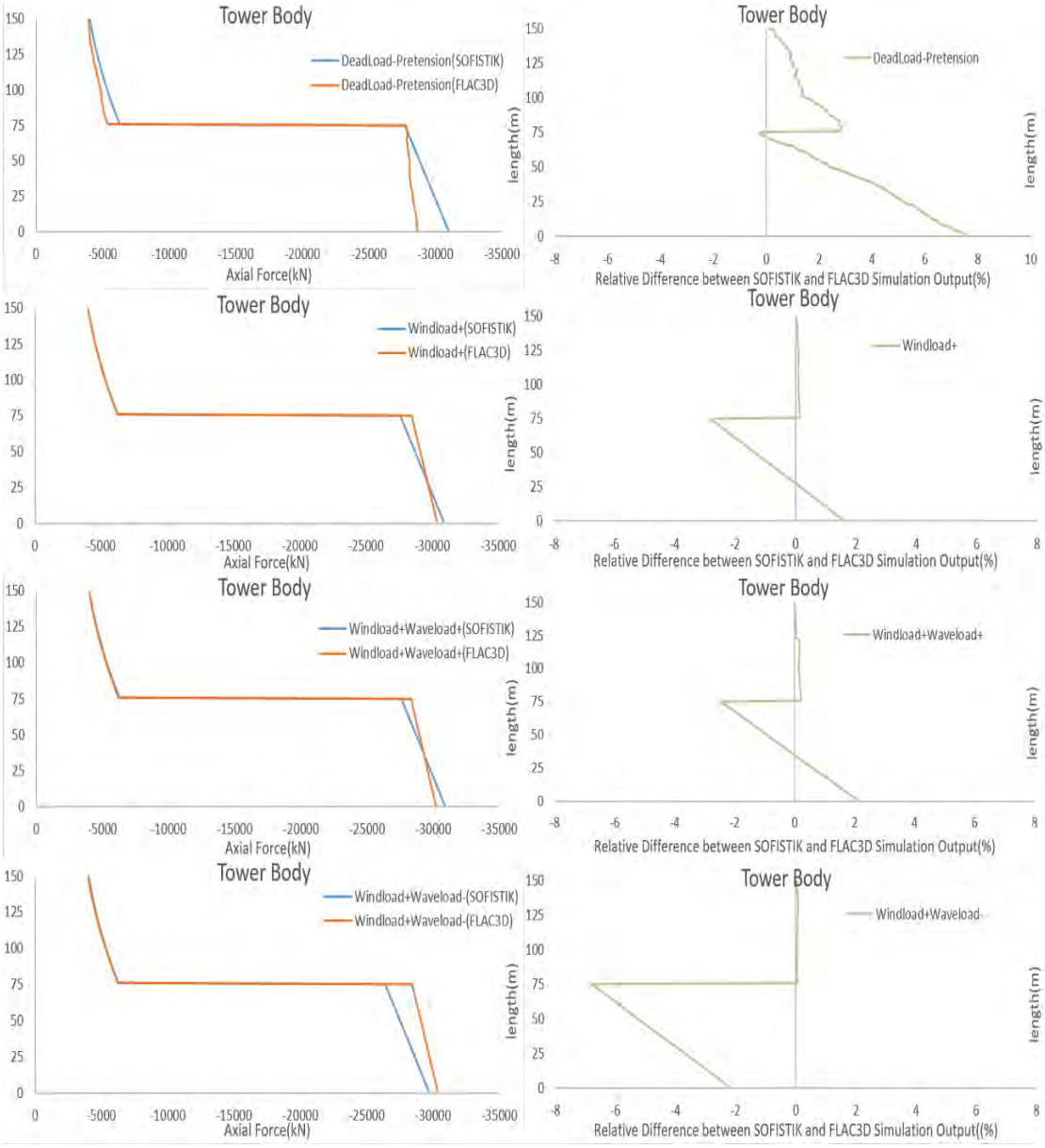

Figure C. 4 STDM and FTDM Simulation differences in terms of tower axial forces.

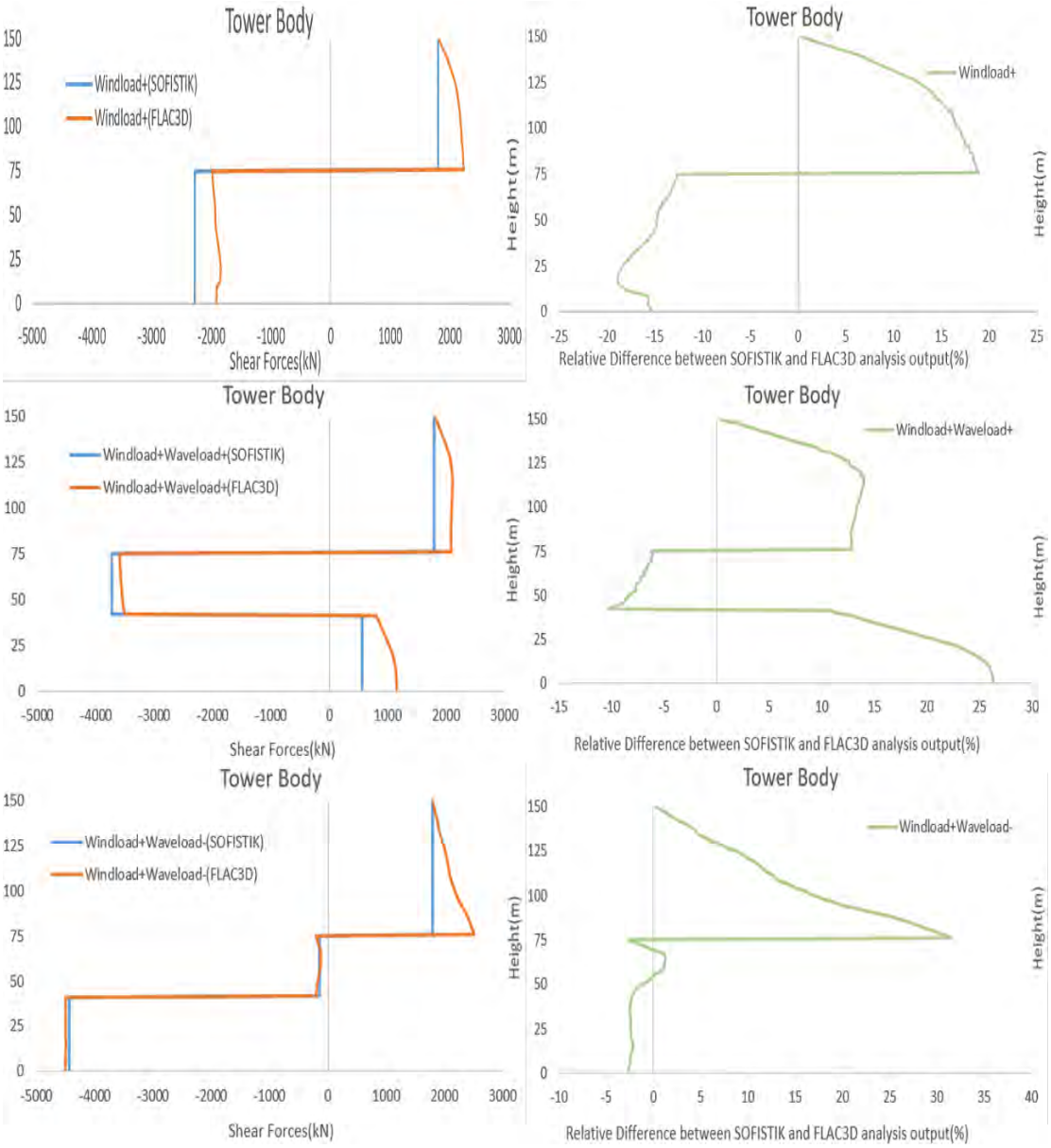

Figure C. 5 STDM and FTDM Simulation differences in terms of tower shear forces.

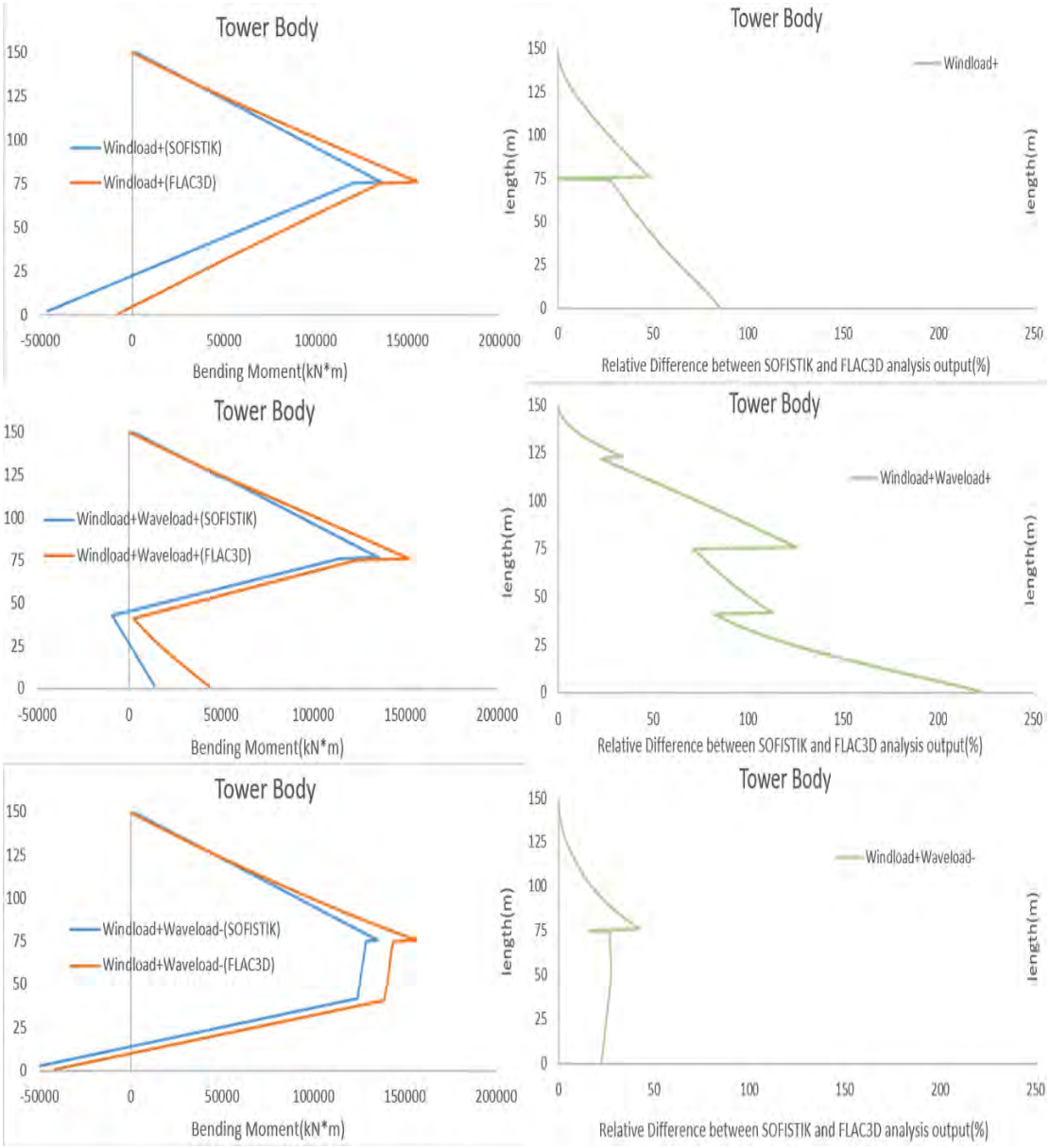

Figure C. 6 STDM and FTDM Simulation differences in terms of tower bending moments.

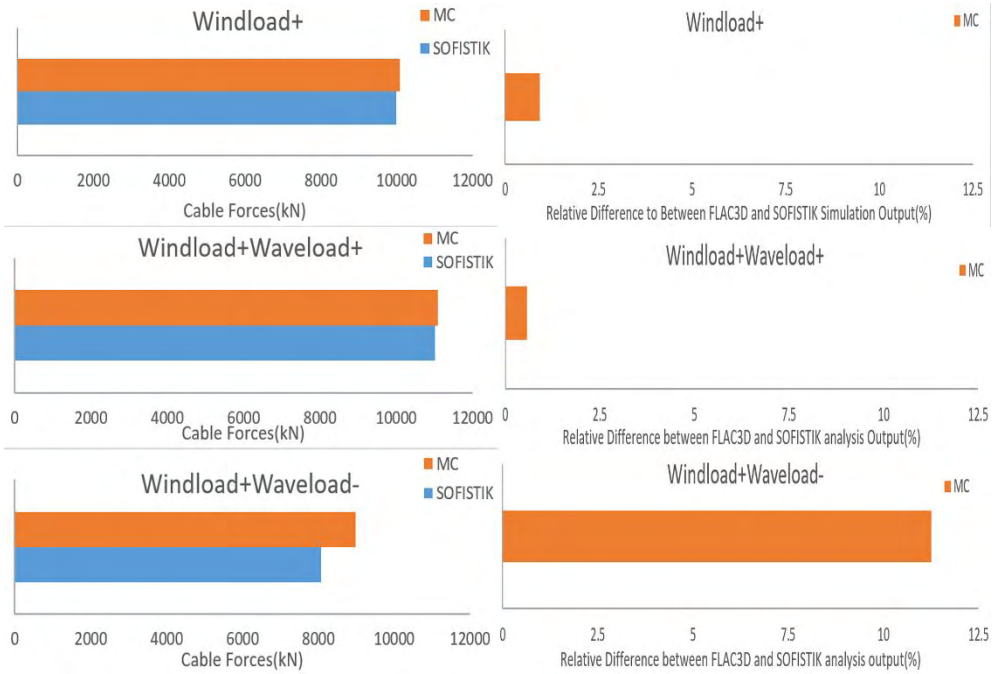

Figure C. 7 STDM and FTDM Simulation differences in terms of –xcable axial force.

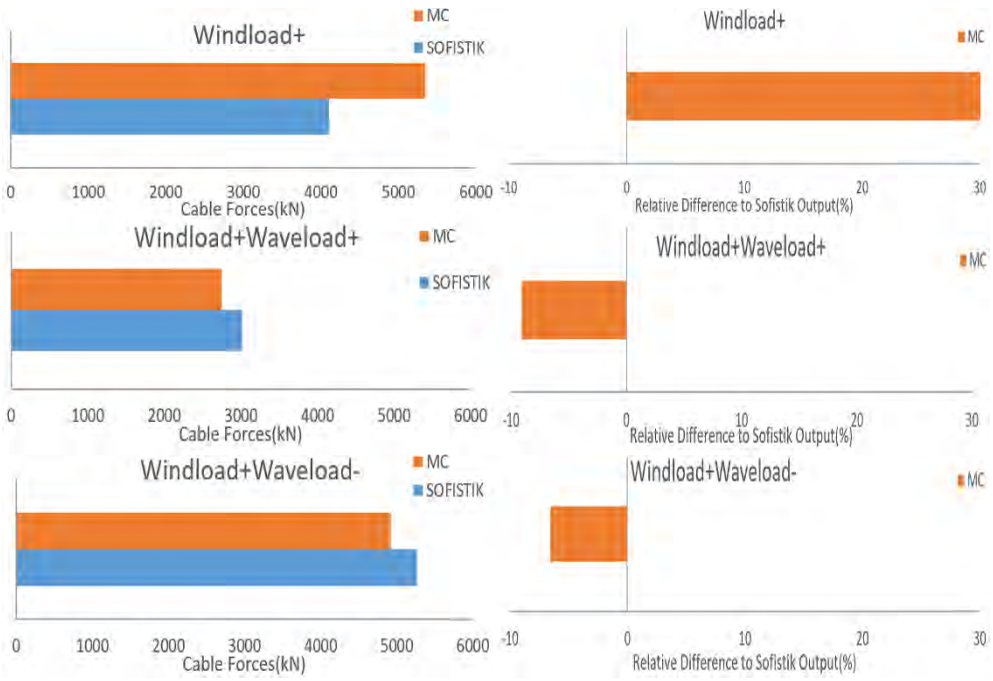

Figure C. 8 STDM and FTDM Simulation differences in terms of +xcable axial force.

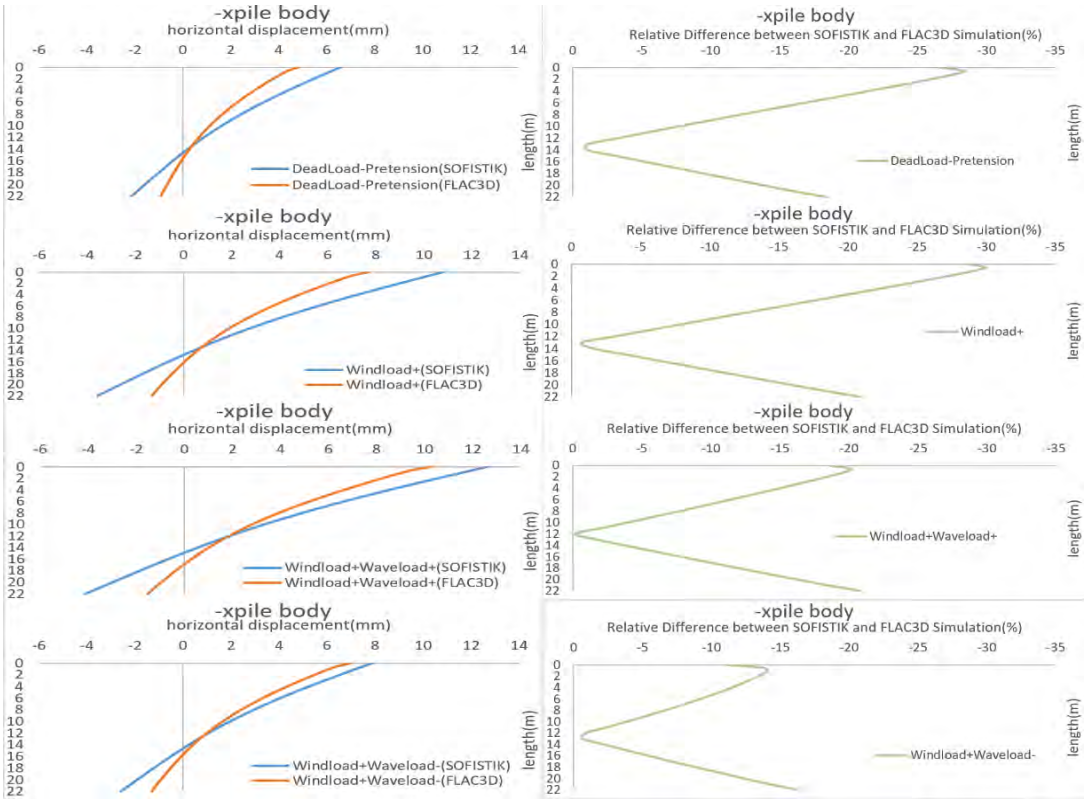

Figure C. 9 STDM and FTDM Simulation differences in terms of -xpile horizontal displacement.

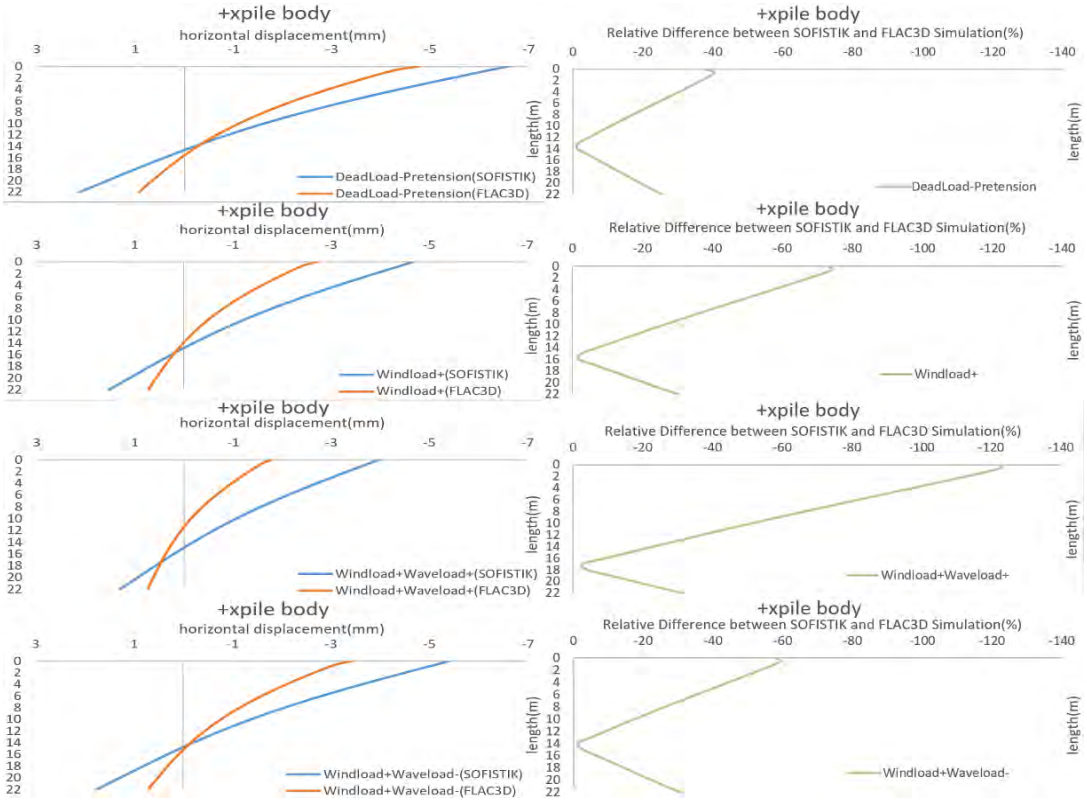

Figure C. 10 STDM and FTDM Simulation differences in terms of +xpile horizontal displacement.

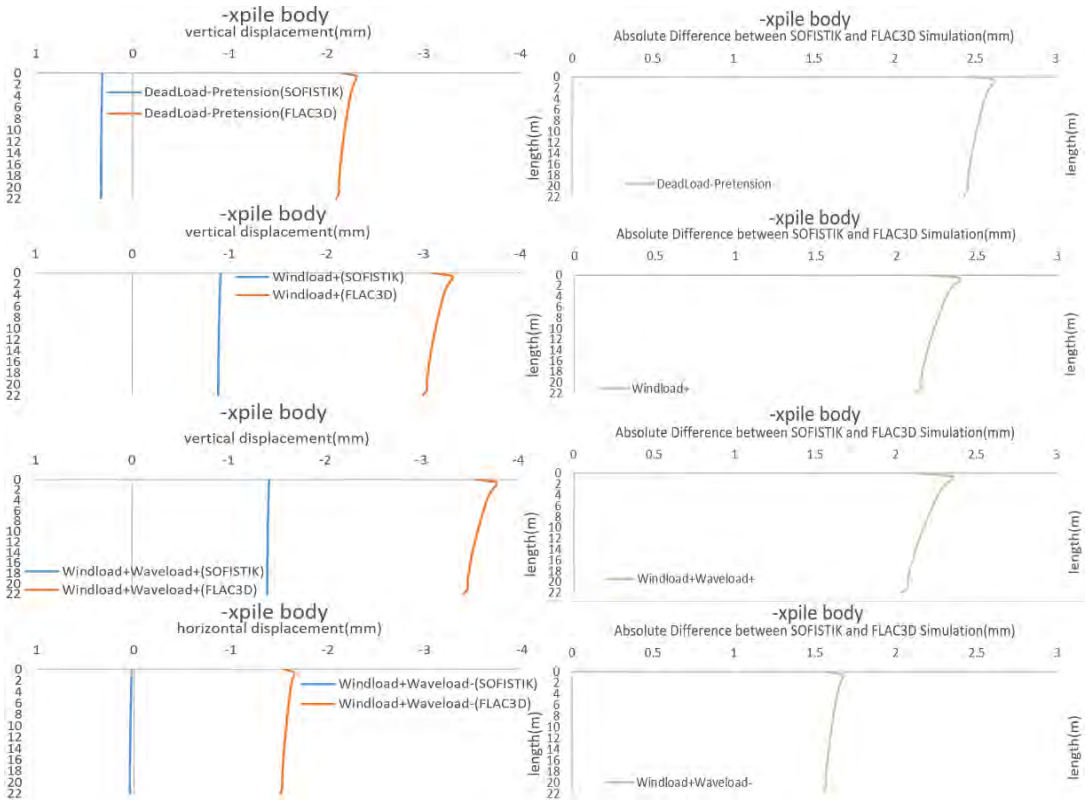

Figure C. 11 STDM and FTDM Simulation differences in terms of -xpile vertical displacement.

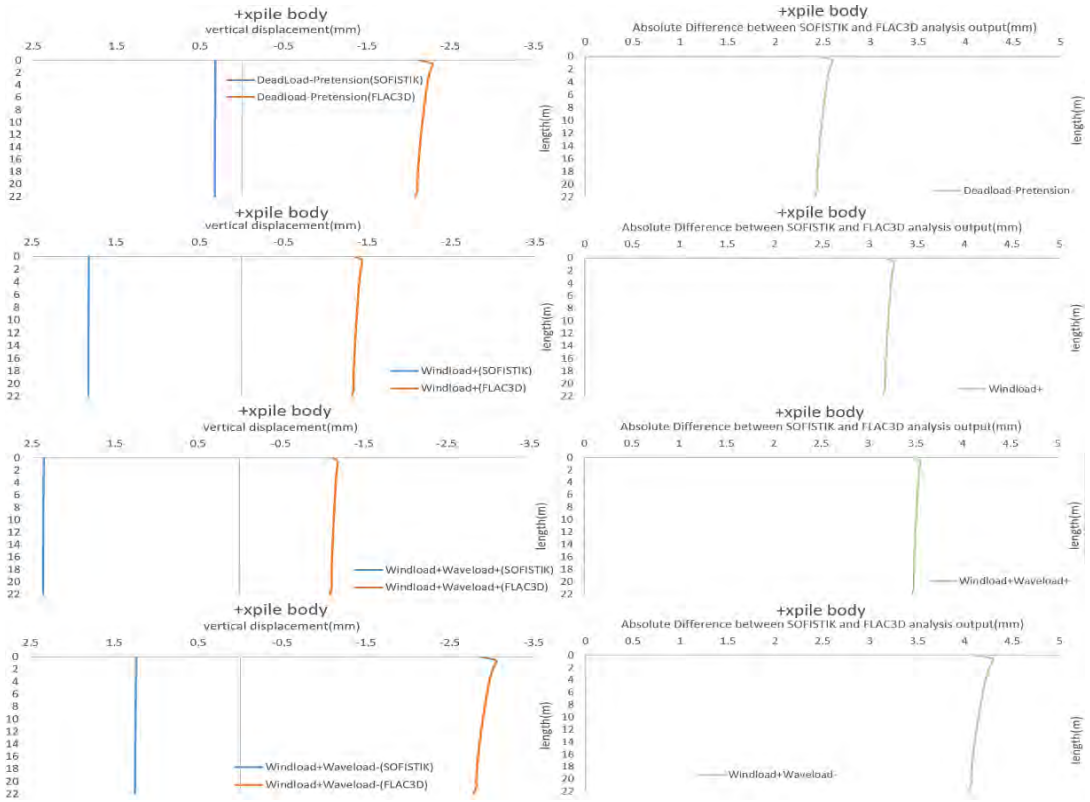

Figure C. 12 STDM and FTDM Simulation differences in terms of +xpile vertical displacement.

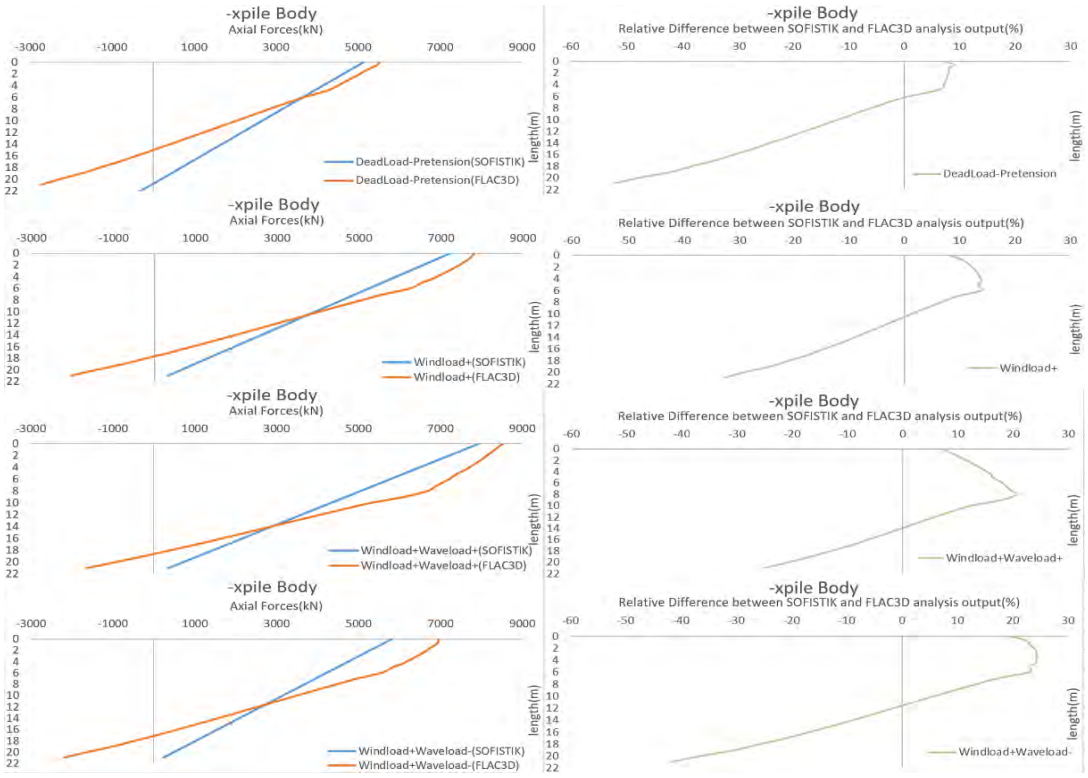

Figure C. 13 STDM and FTDM Simulation differences in terms of -xpile axial force distribution.

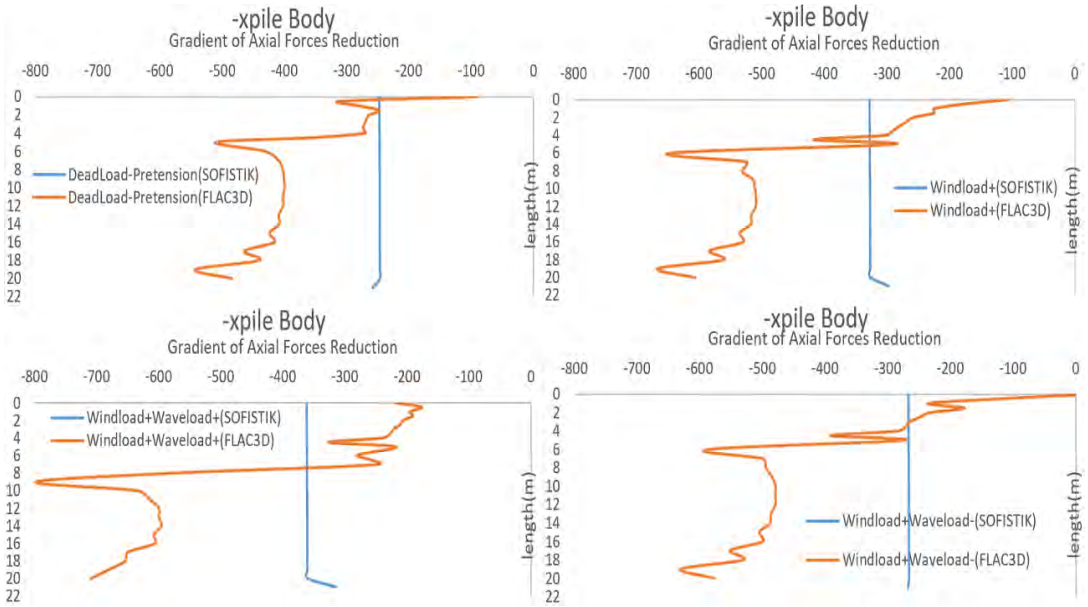

Figure C. 14 STDM and FTDM Simulation differences in terms of -xpile gradient of axial force reduction.

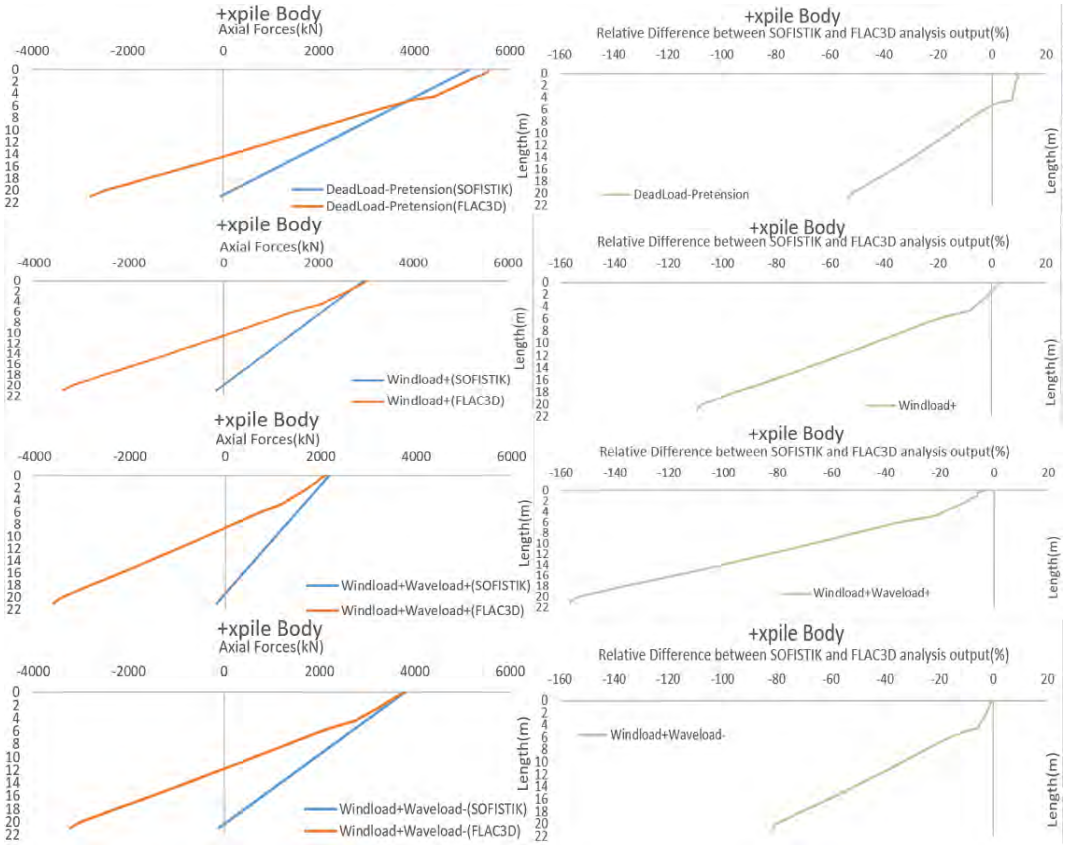

Figure C. 15 STDM and FTDM Simulation differences in terms of +xpile axial force distribution.

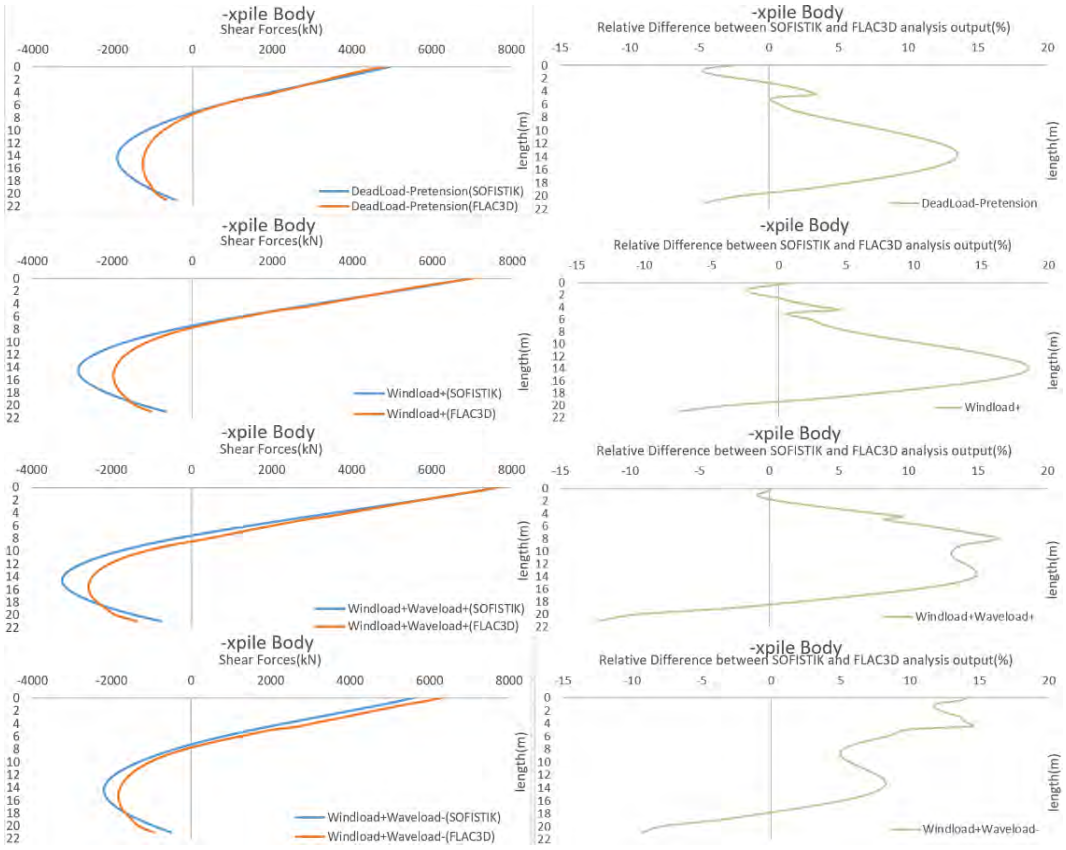

Figure C. 16 STDM and FTDM Simulation differences in terms of -xpile shear force distribution.

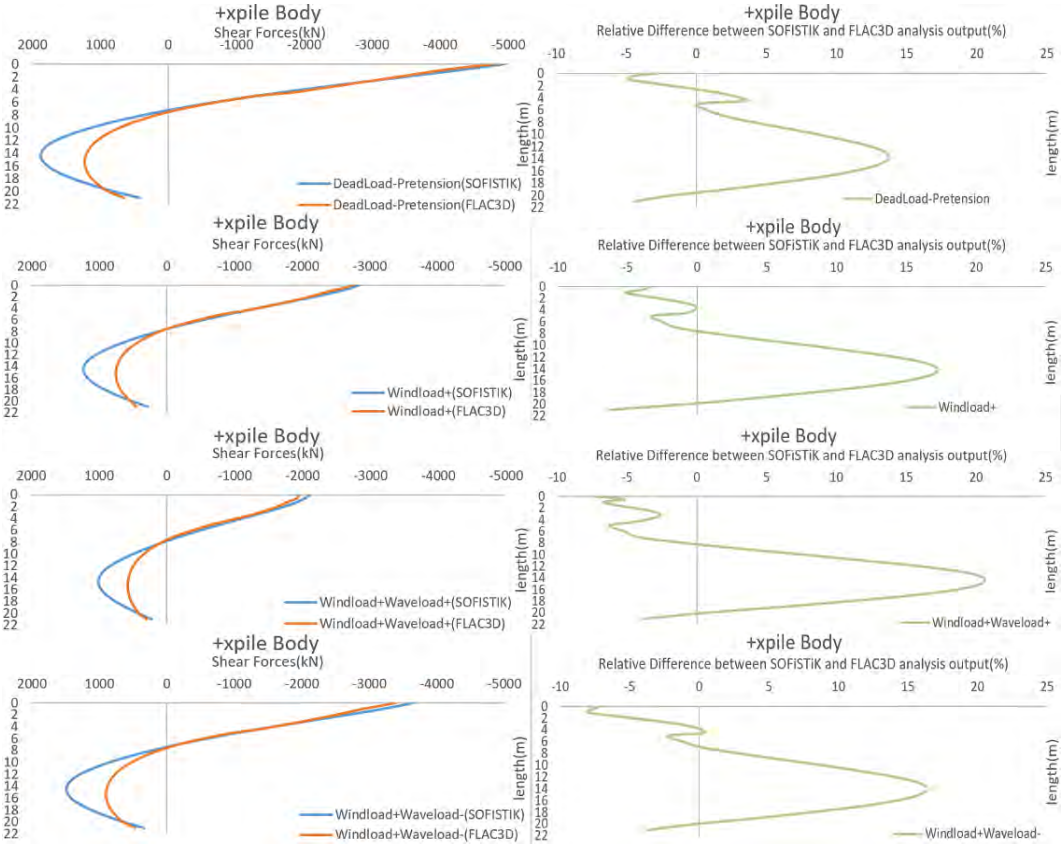

Figure C. 17 STDM and FTDM Simulation differences in terms of +xpile shear force distribution.

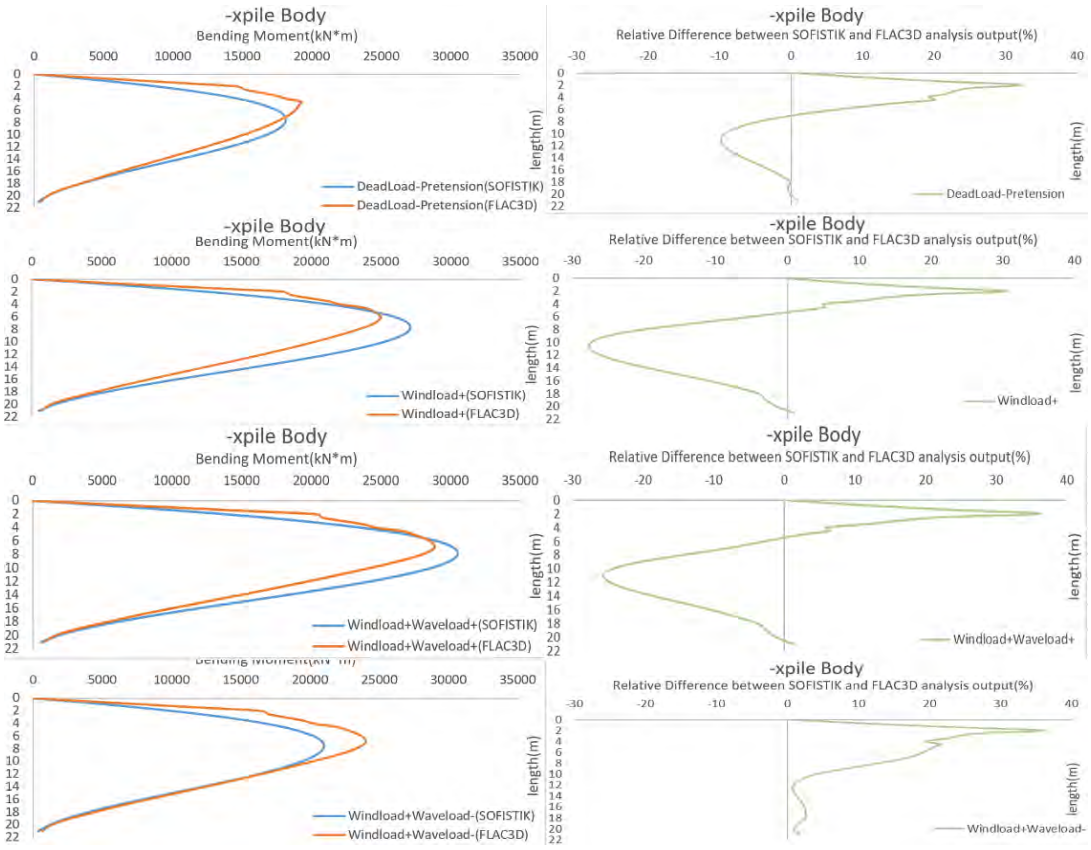

Figure C. 18 STDM and FTDM Simulation differences in terms of -xpile bending moment distribution.

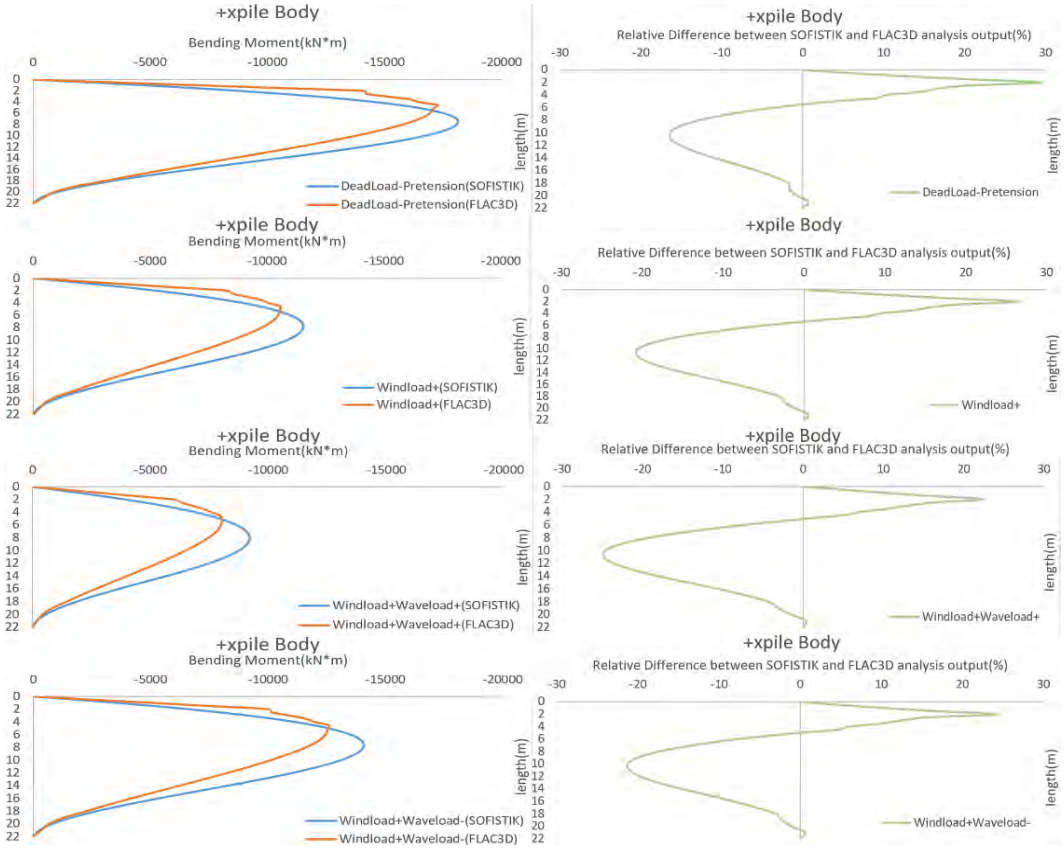

Figure C. 19 STDM and FTDM Simulation differences in terms of +xpile bending moment distribution.

TABLE APPENDIX

Structure Overview

SOFiSTiK/ Marc Mentat/ FLAC^{3D} Simulation

Rotor's Functional Characteristics

Number of Blades	**3**
Rotor Diameter, D_r	140.4 m
Hub Height, H_b	100.0 m
Cut in, Cut out Wind Speed	4 m/s, 25m/s
Cut-in, Cut Out Rated Rotor Speed	5.27 rpm,12.19 rpm
Rotor and Nacelle Mass, m_{NR}	400tn

Table A. 1 Rotor's Functional Characteristic.

Tower Cross Section Review

Tower Height ,H_t	**150m**
Tower Diameter ,D_b/	6.0 m/
thickness, t_b(up to 75 m height)	30 mm
Tower Diameter, D_t/	3.6 m/
thickness, t_t (top)	21 mm
Modulus of Elasticity, E	240 Gpa
Material Specific Weight, γ	78.5 kN/m^3
Tower mass, m_t	578 tn

Table A. 2 Tower Cross Section Review.

Structural Properties of single strand

Material	Steel
Modulus of Elasticity(MPa)	1700
Poisson's Ratio	0.2
Specific Weight(kN/m^3)	78.5
Cross Sectional Area (mm^2)	11677.4
Strand Ultimate Breaking Strength(kN)	17516

Table A. 3 Structure Properties of prestressed cables.

Soil's Estimated Properties

Granulometry Entry	Clay
Submerged Specific Weight [kN/m^3]	10
Undrained Shear Strength [kPa]	60
Poisson's Ratio[-]	0.49
Initial Elastic Modulus[kPa]	108000
Internal Friction Angle [◦]	0
Tensile Strength [kPa]	0

Table A. 4 Soil's Estimated Properties.

Shallow Foundation Vertical Capacity

Total Interacting Surface(m$^{2)}$	**Soil's Ultimate Vertical Stress Capacity(kPa)**	**Ultimate Foundation Vertical Capacity(kN)**
154	308.4	47474

Table A. 5 Shallow Foundation Vertical Capacity.

Pile Cross Section Properties

Material	Steel
Cross Section	Circular Hollow
Area (m^2)	0.1568
Bending Stiffness (kN*m^2)	1.024e8

Table A. 6 Pile Cross Section Properties.

Pile Shaft Resistance Properties

Clay Cohesion(kPa)	**Reductive Factor(API)**	**Interface Shear Resistance(kPa)**	**Shaft Surface(m^2)**	**Total Friction Force (kN)**
36	0.875	31.5	7.854	11133.01897

Table A. 7 Pile Shaft Resistance Properties.

Dead load of allocation of piles

Material	Cross Sectional Area(m^2)	Total Volume(m^3)	Total Weight(kN)	Contribute at Total Weight(%)
Steel	1.23	27.20	1905.8	31.52
Encased Clay	18.85	414.86	4139.6	68.48
Total	20.09	442.06	6045.44	100

Table A. 8 Dead Load Allocation of Piles.

Geometrical Properties(SOFiSTiK Simulation)

Piles					
Shape	Diameter (m)	Thickness (m)	Area (m^2)	Moment of Inertia (m^4)	
Tubular	5	0.08	1.2365	3.742	
Tower (bottom to middle height)					
Shape	Diameter (m)	Thickness (m)	Area (m^2)	Moment of Inertia (m^4)	
Tubular	6	0.03	0.56266	1.2628	
Tower (top)					
Shape	Diameter (m)	Thickness (m)	Area (m^2)	Moment of Inertia (m^4)	
Tubular	3.6	0.021	0.23612	0.19070	
Cable					
Shape	Diameter (m)	Thickness (m)	Area (m^2)	Moment of Inertia (m^4)	
Circular	14	-	0.0467	-	
Shallow Foundation (inner circle)					
Shape	Diameter(m)	Thickness(m)	Area (m^2)	Volume (m^3)	
Cylinder	6	2	28.274	56.549	
Shallow Foundation (external annular)					
Shape	Casing Diameter(m)	Tubing Diameter(m)	Thickness(m)	Area(m^2)	Volume(m^3)
Annular	14	6	1	125.66	125.66

Table B. 1 SOFiSTiK Simulation declared structural geometrical properties.

Material Properties(SOFISTIK Simulation)

Structural Element	**Elastic Modulus (kPa)**	**Poisson Ratio (-)**	**Yielding Stress (kPa)**	**Specific Weight (kN/m^3)**	**Pretension (kPa)**
Pile	2.1e8	0.2	15e5	68.5	-
Tower	2.1e8	0.2	15e5	78.5	-
Cable	1.7e8	0.2	15e5	78.5	7100
Shallow Foundation	2.1e8	0.2	15e5	68.5	-

Table B. 2 SOFiSTiK Simulation declared material properties.

Shallow Foundation Elastic Support

Elastic Constant normal to surface (Kn/m^3)	602578
Elastic Constant Tangential to Surface (Kn/m^3)	10000
Maximum Tensile stress of interface (kPa)	0
Maximum Compression stress of interface (kPa)	308.4

Table B. 3 SOFiSTiK Simulation Shallow Foundation Bedding Elastic Support.

Windload+

Height(m)	Horizontal displacement(mm)	Vertical displacement(mm)	rotation(rad)	tilt(-)
0	-1.825	0.843	-0.000656	-0.0121667e-03
41	-42.373	11.201	-0.000832	-0.832e-3
75	30.897	19.318	0.010924	-0.279713e-3
150	1325.858	24.061	0.053034	8.662273e-3

Table B. 4 Windload+ Tower Deflection SOFiSTiK Analysis Output.

Windload+

Height(m)	Axial Forces(kN)	Shear Forces(kN)	Bending Moments(kN*m)
0	-30771.1	2488.09	-52019.54
41	-28961.1	2488.09	49942.27
75	-6272.3	-1980	148500
150	-4000	-1980	0

Table B. 5 Windload+ Tower Resultants SOFiSTiK Analysis Output.

Windload+Waveload+

Height(m)	xdisplacement(mm)	zdisplacement(mm)	rotation(rad)	Tilt(-)
0	0.404	0.538	0.000128	0.00269333e-03
41	13.069	10.891	0.000494	0.494e-03
75	53.915	19.004	0.007512	0.08548e-03
150	1225.857	23.747	0.049754	8.006533e-3

Table B. 6 Windload+Waveload+ Tower Deflection SOFiSTiK Analysis Output.

Windload+Waveload+

Height(m)	Axial Forces(kN)	Shear Forces(kN)	Bending Moments(kN*m)
0	-30756.9	-619.02	15059.82
41	-28946.9	4110.98	-10307.62
75	-6272.3	-1980	148500
150	-4000	-1980	0

Table B. 7 Windload+Waveload+ Tower Resultants SOFiSTiK Analysis Output.

Windload+Waveload-

Height(m)	xdisplacement(mm)	zdisplacement(mm)	rotation(rad)	Tilt(-)
0	-4.37	8.539	-0.007398	-0.0291e-03
41	-145.338	18.444	-0.001452	-1.452e-3
75	-4.857	26.186	0.0171	-0.96408e-03
150	1514.423	30.929	0.059016	9.899433e-03

Table B. 8 Windload+Waveload- Tower Deflection SOFiSTiK Analysis Output.

Windload+Waveload-

Height(m)	Axial Forces(kN)	Shear Forces(kN)	Bending Moments(kN*m)
0	-29464.6	4821.02	-58632.28
41	-27654.5	91.02	138933.25
75	-6272.3	-1980	148500
150	-4000	-1980	0

Table B. 9 Windload+Waveload- Tower Resultants SOFiSTiK Analysis Output.

Geometric Properties(MARC MENTAT Simulation)

	Element Type	Thickness(m)
Soil	Three Dimensional Solid Element	-
Pile Cap	Three Dimensional Shell Element	1
Pile Cantilever Beam	Three Dimensional Shell Element	1
Pile Hollow Cylinder	Three Dimensional Shell Element	0.08

Table B. 10 MARC Mentat Simulation declared geometric properties.

Material Properties(MARC MENTAT Simulation)

Structural Element	Material	Specific Weight(kN/m³)	Elastic Modulus(kPa)	Poisson Ration(-)	Plasticity Yield Stress (kPa)
Soil	Clay	10	108000	0.49	60
Pile Cap	Structural Steel	78.5	2.1e8	0.2	-
Pile Cantilever Beam	Structural Steel	78.5	2.1e8	0.2	-
Pile Hollow Cylinder	Structural Steel	78.5	2.1e8	0.2	-

Table B. 11 MARC Mentat Simulation declared material properties.

Clay and Steel Interface Parameters(Touching Conditions)*

Normal Stiffness(kN/m³)*	Shear Stiffness(kN/m³)	Ultimate Tension Limit(kPa)*	Ultimate Slip Limit(kPa)
∞	1000	0	36

Table B. 12 MARC Mentat Simulation declared interface properties.

Material Properties of three dimensional elements(FLAC^{3D} Simulation)

	Modulus Elasticity (kPa)	Poisson Ratio (-)	Specific Weight (kN/m³)	Cohesion (kPa)	Friction angle (◦)	Tension (kPa)
Clay	1.08e5	0.49	10	60	0	0
Structural Steel	2.69e7	0.20	13.74	-	-	-

Table B. 13 FLAC^{3D} Simulation declared material properties of three dimensional elements.

Material Properties of superstructure elements(FLAC^{3D} Simulation)

Structural Element	Elastic Modulus (kPa)	Poisson Ratio (-)	Specific Weight (kN/m³)	Ultimate Breaking Force (kN)
Tower	2.1e8	0.2	78.5	-
Cables	1.7e8	0.2	78.5	70064
Shallow Foundation	2.1e8	0.2	65	-

Table B. 14 FLAC^{3D} Simulation declared material properties of superstructure elements.

Interface Elements Parameters

Normal Stiffness(kN/m^3)	Normal Detachment Stress(kPa)	Shear Stiffness(kN/m^3)	Cohesion (kPa)
1e7	1	1e7	60

Table B. 15 FLAC^{3D} Simulation declared interaction parameters of interfaces.

References

American Petroleum Institute (API). (2002). Recommended practice for planning designing and constructing fixed offshore platforms-Working stresses design (ACI 318-05) and Commentary (ACI 318R-05), Washington.

Antoniou, M. (2014). Numerical Analysis of a Guyed Support Structure for Next Generation Offshore Wind Turbines in Deep Waters, MSc Thesis, Division of Civil Engineering, University of Dundee

Anastasopoulos I., Theofilou M.(2015), Hybrid foundation for offshore wind turbines: Environmental and seismic loading. Soil Dynamics and Earthquake Engineering. Vol 80,pp 192-209.

Bowles, J.E.(1996). *Foundation Analysis and Design*. Fifth edition, McGraw-Hill, NY.

Broms, B. B. (1964). Lateral resistance of piles in cohesive soils. *ASCE Journal of Soil Mechanics and Foundations Division*, Vol. 90(SM3), pp. 123-156.

Comodromos, E.M. και Papadopoulou, M.C.(2012a) Response evaluation of horizontally loaded pile groups in clayey soils, *Geotechnique*, 62, αρ. 4, 329-39

Comodromos, E.M. και Papadopoulou, M.C.(2013) Explicit extension of the p-y method to pile groups in cohesive soils, *Computers & Geotechnics* 47, 28-41.

Comodromos, E.M., Papadopoulou, M.C. και Laloui, L. (2016) "Contribution to the design methodologies of piled raft foundations under combined loadings", *Canadian Geotechnical Journal*, doi: 10.1139/cgj-2015-0251.

Coulomb, C.A. (1776). Essais sur une application des règles de maximis et minimis à quelques problèmes de statique à l' architecture . *Mem. Acad. des Sciences* 3, 38.

DNV GL AS(2016). *Loads and site conditions for wind turbines*. Available online at www.dnvgl.com

Danish Wind Industry Association(2003). *Offshore Wind Conditions*. Available online at www.windpower.org

DIN 4014. (1990). *Bored piles; construction procedure, design and bearing behaviour*. German code; Berlin.

DIN 1054 (1990). *Bearing capacity of most commonly used types of piles*. German code; Berlin.

DIN 1054 (2005). *Ground – Verification of the safety of earthworks and foundations*. German code; Berlin.

Drucker, D.C. (1984). From Limited Experimental Information to Appropriately Idealized Stress-Strain Relations. *In Mechanics of Engineering Materials*, Desai, C.S. και Gallagher, R.H. (Editors), John Wiley, London, 231-252.

EIA(2018). *International Energy Outlook 2018 Executive Summary.* Available online at www.eia.gov

IEA(2013). *Technology Roadmap, Wind Energy.* Available online at www.iea.org

Hetenyi, M. (1946). *Beams on elastic foundations*. Univ. of Michigan Press: Michigan.

Itasca Consulting Group (2014). *FLAC, Fast Lagrangian analysis of continua user's and theory manuals*, Version 7.0, Minneapolis.

Itasca Consulting Group (2005, 2009, 2012. 2017). *FLAC^{3D}, Fast Lagrangian analysis of continua user's and theory manuals*, Version 6.0, Minneapolis.

Kondner, R.L.(1963) Hyperbolic stress-strain response: Cohesive soils. J. Soil Mech. & Found., ASCE-89. Αρ. 1, 115–143.

Kurian V.J., Narayanan S.P. and Ganapathy C. (2010). Towers for Offshore Wind Turbines. *In 10th Asian International Conference on Fluid Machinery.* Kuala Lumpur, Malaisia

Lombardi, D., Bhattacharya, S. and Muir Wood, D., 2013. Dynamic soil–structure interaction of monopile supported wind turbines in cohesive soil. *Soil Dynamics and Earthquake Engineering*, Vol. 49, pp. 165–180.

Matlock, H., and Reese, L.C., 1960. Generalized solutions for laterally loaded piles. *ASCE Journal of Soil Mechanics and Foundations Division*, Vol. 86(SM5), pp. 63-91

Matlock, H. και Reese, L.C. (1970). Generalized solutions for the laterally loaded piles. *J. Soil Mech. Found. ASCE* 86, SM5, 63-91.

Meyerhof, G.G., 1951. The ultimate bearing capacity of foundations. *Géotechnique*, Vol. 2(4), pp.301 – 332.

MSC Software Corporation and licensors (2016). *MARC Mentat, User's Guide*, Version 2016

Natarajan, A., Hansen, M. H., & Wang, S. (2016). Design Load Basis for Offshore Wind turbines: DTU Wind Energy Report No. E-0133.

National Renewable Energy Laboratory(2012).*Renewable Electricity Study*. Vol 2. Available online at www.globalccsinstitute.com

Papadopoulou, MC and Comodromos, EM (2014) "Explicit extension of the p-y method to pile groups in sandy soils", Acta Geotechnica, Vol. 9 (3), pp. 485-497.

Passon P., Kühn1 M., Butterfield S., Jonkman J., Camp T., Larsen T.J.(2007). OC3 – Benchmark Exercise of Aero-Elastic Offshore Wind Turbine Codes. *In EAWE Special Topic Conference: The Science of Making Torque from Wind.Lyngby, Denmark*

Poulos, H. G. (1971). Behaviour of laterally loaded piles: II-Pile groups. *J. Eng. Mech. Div., ASCE* 97, SM5, 733-751.

Poulos, H. G. (1989). Pile behaviour – theory and application. *Géotechnique* 39, Αρ. 3, 366-415.

Prager, W. (1955). The Theory of Plasticity: A Survey of Recent Achievements (James Clayton Lecture). *In Proc. Inst. Mech. Eng*. 41, 3-19.

Randolph, M.F. (1981). The response of flexible piles to lateral loading. *Géotechnique*, 31(2), 247-259.

Randolph, M. F. (1986). *Ratz – Load transfer analysis of axially loaded piles*. Research report no 86003, University of Western Australia 1986.

Randolph, M.F. και Gourvenec S. (2011). *Offshore geotechnical engineering*. Spon Press, New York.

SOFiSTiK AG(2014).*SOFiMSHA Manual*,Version 2014.4, Oberschleissheim, Germany.

SOFiSTiK AG(2014).*SOFiMSHC Manual*,Version 2014.4, Oberschleissheim, Germany.

Terzaghi, K. (1943). *Theoretical soil mechanics*. New York: J. Wiley.

Terzaghi, K. και Peck, R.B. (1967). *Soil mechanics in engineering practice*. New York: J. Wiley.

Timoshenko, S.P. και Goodman J.N. (1971). *Theory of elasticity*. 3nd edition McGraw-Hill, New York.

Vesic, A.S. (1967). A study of Bearing Capacity of Deep Foundations. *Final Rep., Proj. B-189*, School of Civil Eng., Georgia Inst. Tech., Atlanta.

Vesic, A.S. (1973). Analysis of ultimate loads of shallow foundations. *J. Soil Mech Found. Engng ASCE* 99, Αρ. 1, 45-73.